

8-2019

A Study of Protein and Peptide-directed Nanoparticle Synthesis for Catalytic Materials

Abdollah Mosleh
University of Arkansas, Fayetteville

Follow this and additional works at: <https://scholarworks.uark.edu/etd>



Part of the [Biological Engineering Commons](#), [Catalysis and Reaction Engineering Commons](#), [Molecular, Cellular, and Tissue Engineering Commons](#), [Nanoscience and Nanotechnology Commons](#), and the [Polymer and Organic Materials Commons](#)

Citation

Mosleh, A. (2019). A Study of Protein and Peptide-directed Nanoparticle Synthesis for Catalytic Materials. *Graduate Theses and Dissertations* Retrieved from <https://scholarworks.uark.edu/etd/4248>

This Dissertation is brought to you for free and open access by ScholarWorks@UARK. It has been accepted for inclusion in Graduate Theses and Dissertations by an authorized administrator of ScholarWorks@UARK. For more information, please contact uarepos@uark.edu.

A Study of Protein and Peptide-directed Nanoparticle Synthesis for Catalytic Materials

A dissertation submitted in partial fulfillment
of the requirements for the degree of
Doctor of Philosophy in Engineering, with a concentration in Chemical Engineering

by

Imann Mosleh
Shahid Bahonar University of Kerman
Bachelor of Science in Materials Science and Engineering, 2012
Tarbiat Modares University
Master of Science in Nanotechnology/Nanomaterials Engineering, 2014
University of Arkansas
Master of Science in Microelectronics and Photonics, 2016

August 2019
University of Arkansas

This dissertation is approved for recommendation to the Graduate Council.

Robert Beitle Jr., Ph.D.
Dissertation Director

Christa Hestekin, Ph.D.
Committee Member

Lauren Greenlee, Ph.D.
Committee Member

M. Hassan Beyzavi, Ph.D.
Committee Member

David Ford, Ph.D.
Committee Member

Abstract

Nanoparticles have received much attentions due to their unique properties that makes them suitable candidates for a broad range of applications. As the size of particles decreases, their surface area-to-volume ratio would increase which is the main cause of much attention. In addition to the size, their morphologies and compositions may also play important roles for defining unique properties. Nanoparticle synthesis include both bottom-up and top-down strategies. To control the process of inorganic nanoparticles synthesis one could follow the bottom-up approach to have atom-level control over their compositions, morphologies, phases, and sizes which is the subject of this work. Due to their specific sequence of amino acids, proteins and peptides has been demonstrated to be used for nanoparticle synthesis. The main obstacle to widespread development and commercialization of protein and peptide-directed nanoparticle synthesis platforms is their high cost when the peptide is obtained by traditional chemical synthesis. A promising approach for the cost-effective production of nanoparticles using protein/peptide derives from our effort to develop *Escherichia coli* into an expression platform. In contrast to most biochemical engineering applications, the purity of the fusion proteins and peptides may be less stringent for nanoparticle synthesis, demonstrating the fact that crude bacterial lysates containing fusion peptides may be used in lieu of expensive, pure peptide in nanoparticles synthesis while the nucleation and growth mechanism is consistent with traditional systems. Indeed, it is conceivable that simply concentrating the protein/peptide may be the only purification step necessary for nanoparticle synthesis. Additionally, catalytic activities of the fusion protein-directed nanoparticles were evaluated using the most popular and efficient routes for the formation of carbon– carbon bonds, Suzuki-Miyaura coupling and Stille coupling reactions. The unpurified fusion protein-directed nanoparticles showed slightly higher

catalytic activity comparing to the chemically synthesized peptide counterparts. Moreover, fusion protein-directed nanoparticles presented high catalytic activities in green solvents as well as high stability and recyclability. They also could be utilized efficiently for the synthesis of Lapatinib precursor, an oral active anti breast cancer drug. The excel catalytic activity of the fusion protein-directed nanoparticles make them an excellent candidate for catalytic applications in the future.

Acknowledgements

Firstly, I would like to express my sincere gratitude to my advisor, Dr. Bob Beitle, for the continuous support of my Ph.D. study, for his patience, motivation, trust, and immense knowledge. His guidance helped me in the research and writing of this dissertation. I could not have imagined having a better advisor for my Ph.D. study. His advice and supports on research as well as my life have made me a better person. Secondly, I am thankful to Dr. M. Hassan Beyzavi who let me enable my research ability in a new field that I have never experienced before. He helped me to be a great presenter, researcher, and hard-working person. I also would like to thank the rest of my dissertation committee: Dr. Lauren Greenlee, Dr. David Ford, and Dr. Christa Hestekin, for serving as my committee members and for their insightful comments and encouragement that helped me to develop as a researcher.

I would like to thank Dr. Ahmed El-Masheiti and Dr. Hazim Aljewari for their help to support a plebeian in the molecular biology lab work. Their continuous help during my research made me confident that impossible is impossible.

I want to express my deep appreciation to Sayed Omid Sayedaghaee for being a great classmate and wonderful friend, and for all the fun we have had in the past five years. More than other things, I would like to thank Omid for his priceless support in the last year.

Last but not the least, I would like to thank my family: my parents, my brother, Salman and my sisters, Somayyeh and Leila, for supporting me spiritually throughout the hard situations and hopeless moments of my life. I would like to thank all of you for your sleepless nights you were warming my heart with the hope of being reunited with my family again. Your prayer for me was what sustained me thus far. At the end, I would like to express appreciation to my beloved wife, Negin, who spent sleepless nights with me and supported me during writing this

dissertation and was always my support in the moments when there was no one to answer my queries. Having you again is a great miracle and present from the one who is the greatest and sees us.

Dedication

To my parents and my wife.

آنانکه محیط فضل و آداب شدند
در جمع علوم شمع اصحاب شدند

ره زین شب تاریک نبردند بروز
گفتند فسانه ای و در خواب شدند

حکیم عمر خیام

Scientists are like the candles of the way,
They light the path for the travelers on the way,
Yet, could never light the night like a day,
They just tell a story and pass away.

Omar Khayyam

The great Persian scientist, philosopher and poet,

(AD 1048 –1131)

Table of Contents

Chapter 1. Overview	1
Chapter 2. Background	2
2.1. Nanoparticles and synthesis strategies	2
2.2. Protein and peptide for nanoparticle preparation	3
2.3. Recombinant production of peptides and proteins	5
2.4. <i>Escherichia coli</i> as expression host	7
2.5. Fermentation	8
2.6. Protein and peptide expression in host cell and Green Fluorescent Protein (GFPuv)	9
2.7. Purification	10
2.7.1. Chromatography	10
2.7.2. Nanoparticle purification	10
2.8. Heterogenous catalysis	11
2.9. Coupling reactions	12
2.9.1. Suzuki-Miyaura coupling reaction	13
2.9.2. Stille coupling reaction	15
2.10. Need	17
2.11. Significance	18
2.12. References	19
Chapter 3. Properties-controlled synthesis of recombinant peptide fusion protein-templated palladium nanoparticles	24
3.1. Recombinant construction of fusion protein	25
3.1.1. Design of primers	26

3.1.2. Recombinant expression vector construction of fusion proteins	27
3.2. Purification of fusion proteins	32
3.2.1. Purification through diethylaminoethyl chromatography (DEAE).....	32
3.3. Properties-controlled parameters in nanoparticle synthesis.....	32
3.3.1. Reducing agent type.....	33
3.3.2. Reducing agent concentration.....	37
3.3.3. pH of the medium	39
3.3.4. Temperature	40
3.3.5. GFPuv fusion protein type.....	42
3.3.6. Palladium salt.....	45
3.3.7. Conclusion	46
3.4. References.....	48
Chapter 4. Recombinant peptide fusion proteins enable palladium nanoparticle growth	50
4.1. Introduction.....	53
4.2. Experimental Methods.....	53
4.2.1. Fusion Protein Preparation.....	53
4.2.2. Palladium Nanoparticle Synthesis	54
4.3. Results and Discussion.	54
4.4. Conclusion	58
4.5. References.....	59
4.6. Supporting Information.....	61
Chapter 5. Recombinant peptide fusion protein-templated palladium nanoparticles for Suzuki- Miyaura coupling and Stille coupling reactions	66

5.1. Introduction.....	70
5.2.1. Preparation of strain used to express (Pd ₄) ₃ -GFPuv.....	72
5.2.2. Expression of the recombinant protein	74
5.2.3. Lysate preparation.....	75
5.2.4. Enrichment.....	75
5.2.5. Nanoparticle synthesis and characterization.....	76
5.3. Results and Discussion	76
5.3.1. Application as catalyst in coupling reactions.....	83
5.3.1.1. Suzuki-Miyaura coupling.....	83
5.3.1.2. General applicability using Suzuki-Miyaura coupling reaction	86
5.3.1.3. Stille coupling	88
5.3.1.4. General applicability using Stille coupling reaction.....	90
5.3.2. Stability and recyclability	91
5.3.3. Kinetic study of coupling reactions	93
5.3.3.1. Suzuki-Miyaura coupling reaction rate study	94
5.3.3.2. Stille coupling reaction rate study.....	96
5.3.4. Fusion protein-templated Pd NPs for anticancer drug precursor synthesis	98
5.4. Conclusion	101
5.5. References.....	103
5.5. Supporting Information.....	106
Inductively coupled plasma mass spectroscopy (ICP-MS)	107
A Procedures for Catalytic Processes and Compound Characterization	108
GC mass spectrometry spectra of the compounds	113

ESI high resolution mass spectrometry spectra of the compounds.....	115
NMR spectra of the compounds	123
Chapter 6. Summary and future works	158
6.1. Summary	158
6.2. Future work.....	159
6.2.1. Fusion protein purification.....	159
6.2.2. Coupling product purification.....	160
6.2.3. Fabrication of precious and non-precious nanoparticles	160
Appendix (I).....	161
Appendix (II)	162
Appendix (III)	164
Appendix (IV).....	167

List of Figures

Figure 1. Schematic of Suzuki-Miyaura coupling reaction.	14
Figure 2. Schematic of Stille coupling reaction using Pd ⁰ as catalyst.	16
Figure 3. Schematic illustration of plasmid construction containing MBP-GFP.	28
Figure 4. Agarose electrophoresis gel run for recovered Addgene-plasmid-51559.	28
Figure 5. Successful fusion protein genes construction and plasmid	31
Figure 6. TEM image of recombinant fusion protein-directed palladium nanoparticles.....	37
Figure 7. TEM image of protein-directed palladium nanoparticles using different ratios.	38
Figure 8. TEM image of fusion protein-directed palladium nanoparticles using different pH.....	40
Figure 9. TEM image of palladium nanoparticles prepared at different temperatures.....	41
Figure 10. TEM image of palladium nanoparticles prepared using GFPuv fusion proteins.	44
Figure 11. TEM image of palladium nanoparticles prepared using different palladium salt.	46
Figure 12. Overview of plasmid construction.....	73
Figure 13. Gel electrophoresis indicating successful gene construction.	77
Figure 14. a. Ion exchange chromatography for enrichment of (Pd ₄) ₃ -GFPuv.....	78
Figure 15. TEM of particles (a) lysate,(b) GFPuv (c) (Pd ₄) ₃ -GFPuv, (d) pure (Pd ₄) ₃ -GFPuv....	79
Figure 16. XPS spectrum of and XRD pattern of (Pd ₄) ₃ -GFPuv fusion protein.....	81
Figure 17. Elemental analysis of prepared nanoparticles from cell lysate..	82
Figure 18. Recyclability of (Pd ₄) ₃ -GFPuv fusion protein-templated Pd NPs.	92
Figure 19. (Pd ₄) ₃ -GFPuv fusion protein-templated Pd NPs catalyst after five cycles.	93
Figure 20. TOF determination for the Suzuki-Miyaura coupling model reaction.....	95
Figure 21. Reaction rate determination for the Suzuki-Miyaura coupling.	96
Figure 22. TOF determination for the Stille coupling model reaction.	97

Figure 23. Stille coupling model reaction rate analysis.....	98
Figure 24. Lapatinib route of synthesis.....	99

List of Tables

Table 1. Protein and peptides examples for nanoparticle synthesis.....	4
Table 2. A list of recombinant peptides approved by FDA or EMA.....	6
Table 3. A list of selected coupling reaction.....	12
Table 4. Associated costs for pharmaceutical-grade peptides and polypeptide.....	17
Table 5. Peptide sequences and properties of synthesized palladium nanoparticles	26
Table 6. Primers and their sequences for fusion protein construction.....	26
Table 7. Master mix and primer preparation for primers for fusion protein construction.....	29
Table 8. Steps and conditions of thermal cycling for PCR.....	29
Table 9. The effect of reducing agent change on nanoparticle size.....	34
Table 10. The effect of type and concentration of reducing agent on nanoparticle size.	37
Table 11. The effect of pH change on nanoparticle size.....	39
Table 12. The effect of temperature on nanoparticle size.....	41
Table 13. The effect of fusion protein types on nanoparticle size.	43
Table 14. The effect of palladium salt on nanoparticle size.	45
Table 15. List of primers used for plasmid construction.	74
Table 16. Catalyst survey for Suzuki-Miyaura coupling reaction	83
Table 17. Optimized condition via coupling reaction Solvent, base, and temperature.	85
Table 18. Substrate scope for Suzuki-Miyaura coupling reaction.....	87
Table 19. Catalyst survey for Stille coupling reaction.....	88
Table 20. Optimized condition via coupling reaction Solvent, base, and temperature.	89
Table 21. Substrate scope for Stille coupling reaction	91

List of Published papers

Paper 1. I. Mosleh, M. Benamara, L. Greenlee, M.H. Beyzavi, R. Beitle, Recombinant peptide fusion proteins enable palladium nanoparticle growth, Mater. Lett. 252 (2019) 68-71. doi: 10.1016/j.matlet.2019.05.080. (Chapter 4)

Chapter 1. Overview

This dissertation describes the development of a novel method for recombinant production of peptides used for precious catalytic nanoparticles synthesis implies *E.coli* doing catalysis. Chapter 2 describes a brief introduction to nanoparticle characteristics and synthetic strategies toward their preparation. The latest studies on employing biomaterials for nanoparticles have been introduced. Also, the current recombinant protein production platform is reviewed in order to remove the roadblock for inexpensive precious nanoparticles preparation. Lately, different types of coupling reactions used to study the catalytic activity of nanoparticles are described. In Chapter 3, recombinant construction of fusion proteins as well as properties-controlled parameters in nanoparticles synthesis is described. Chapter 4 describes the nucleation and growth of palladium nanoparticles using recombinant peptide fusion proteins in an unpurified mixture. In Chapter 5, the catalytic activity of synthesized, fusion protein templated nanoparticles is investigated using Suzuki-Miyaura coupling and Stille coupling reactions. Also, kinetic studies of Suzuki-Miyaura coupling and Stille coupling reactions is discussed. Finally, to conclude, the impact of the work is discussed with recommended improvements and future work can be taken up to further improve the process.

Chapter 2. Background

2.1. Nanoparticles and synthesis strategies

Nanostructured materials have sizes on the nanoscale in at least one dimension which is typically in the range of 10^{-9} - 10^{-7} m. The size of nanomaterials is larger than molecules but much smaller than bulk materials. For example, a nanoparticle with 1-2 nm diameter has roughly 10-250 atoms [1]. The materials at nanosize often show different physical and mechanical properties due to dramatic changes in their crystallinity, phase, morphology and structure which make them unique candidates for a broad range of applications in electronics, catalysis, composite design, drug delivery, and biopharmaceuticals. Due to their small sizes, nanoparticles have large surface area-to-volume ratio (aspect ratio) which is the main reason for their unique properties. Large surface area of nanoparticles is of high importance in the context of catalysis, adsorption, and active sites and it is important to control the size and morphology of nanoparticles to attain desired properties.

Nanoparticles can be prepared by two basic strategies, classified as “top-down” and “bottom-up”. In a top-down strategy, the nanoparticles are made from bulk materials using mostly physical and lithographic methods. The control over morphology and size of obtained nanoparticles are not simple. On the other hand, ionic, atomic, and molecular units are the building blocks of nanostructured materials in a bottom-up approach. This approach allows researchers to design, control and produce nanoparticles with desired properties, sizes, morphologies, and compositions mostly using chemical synthesis. The body of this work focuses on bottom-up strategy due to the use of peptides during synthesis that bind/act at the atomic level.

2.2. Protein and peptide for nanoparticle preparation

Living organisms produce intriguing materials by using structures like peptides or proteins and inorganic materials in order to assemble uniform nanostructured materials. Researchers and scientists are inspired by these naturally controlled systems to adopt efficient and controllable methods for nanoparticle fabrication [2–4]. Due to their unique sequence-specific properties, proteins and peptides can direct the assembly, composition, and structure of variety of inorganic nanoparticles. These amino acids within protein/peptide can recognize and bind to the desired inorganic ions and make a substrate for nucleation and growth of that specific materials. The unique recognition properties of generated nanoparticles can be better encoded by a peptide as it is simpler as compared to a protein. Having less complex structure is the main reason that researchers mostly use peptides for nanoparticle production rather than proteins. In fact, proteins and peptides have played significant roles in the preparation of various inorganic nanoparticles. It is important to note that by combining molecular biology and material science, a broad range of metal binding biomaterials have been synthesized and been exploited [5,6]. Some of these proteins/peptides are listed in Table 1 adapted from Chen et al. [7].

Being easily prepared through chemical synthesis or genetic engineering, peptides and proteins are remarkable candidates as tools for the fabrication of inorganic nanostructured materials. The subject of this research is preparation of nanoparticles using bottom-up strategy which nanoparticles can be built from atoms and ions known as the building blocks of nanostructured materials. The presence of proteins/peptides in a solvent free, aqueous environment can impart precise, atom-level control over nanoparticle composition, morphology, and phase [8–10].

Table 1. Protein and peptides examples for nanoparticle synthesis [7].

Protein name or peptide sequence	Inorganic materials	Salt
AYSSGAPPMPPF	Ag	AgNO ₃
AYSSGAPPMPPF	Au	HAuCl ₄
NPSSLFRYLPSD	Ag	AgNO ₃
AHHAHHAAD	Au	ClAuPMe ₃
HGGGHGHHGGGHG	Cu	CuCl ₂
HGGGHGHHGGGHG	Ni	NiCl ₂
HYPTLPLGSSTY	CoPt	(NH ₄) ₂ PtCl ₄ + Co-(CH ₃ COO) ₂
HNKHLPTQPLA	FePt	FeCl ₂ and H ₂ PtCl ₆
GDVHHHGRHGAEHADI	CdS	CdCl ₂ + Na ₂ S
VCATCEQIADSQHRSHRQMV	ZnS	zinc 2,9,16,23-tetrakis (phenylthio)- 29H,31Hphtanlocyanine + Na ₂ S
NNPMHQN	ZnS	ZnCl ₂ + Na ₂ S
SLKMPHWPHLLP	GeO ₂	tetramethoxygermanium
TGHQSPGAYAAH		
SSKKSYSYSGSKGSKRRIL	TiO ₂ nanoparticles	titanium bis(ammonium lactato) dihydroxide tetramethoxysilane triisopropylsilane
SSKKSYSYSGSKGSKRRIL	Titanium phosphate spheres	titanium bis (ammonium lactato) dihydroxide tetramethoxysilane triisopropylsilane
SSKKSYSYSGSKGSKRRIL	Silica nanostructures	titanium bis(ammonium lactato) dihydroxide tetramethoxysilane triisopropylsilane
EAHVMHKVAPRPGGGSC	ZnO	Zn(OH) ₂

Table 2. Protein and peptides examples for nanoparticle synthesis. Cont.

Protein name or peptide sequence	Inorganic materials	Salt
HQPANDPSWYTG	BaTiO ₃ nanoparticles	Ba(CH ₃ COO) ₂ +
NTISGLRYAPHM		K ₂ [TiO- (C ₂ O ₄) ₂]
PDFDFDFDFDFDP	Calcium phosphate	CaCl ₂ + K ₂ HPO ₄
FDFDFDFD	CaCO ₃	CaCl ₂ + (NH ₄) ₂ CO ₃
AAPNSPWYAYEY	CaMoO ₄	calcium acetate + ammonium
SWSPAFFMQNMP		paramolybdate
GLRSKSKKFRRPDIQYDPDATDEDITSHM	Hydroxyapatite (HA)	KH ₂ PO ₄ + CaCl ₂
AYSSGAPMPPF	Au	HAuCl ₄
BP-AYSS-PEP _{Au}	Au	HAuCl ₄
C ₆ -AA-PEPAu	Au	HAuCl ₄
C ₁₂ -AA-PEPAu	Au	HAuCl ₄
C12H23O-AYSSGAPMPP	Au	HAuCl ₄
Stable protein 1	Ag, Au, Cu	AgClO ₄ , HAuCl ₄ , CuSO ₄
TSNAVHPTLRHL (Pd4)	Pd	K ₂ PdCl ₄
SSKKSYSYSGKSKRRIL (R5)	PdAu	K ₂ PdCl ₄ , HAuCl ₄
WAGAKRHPTLRHL	PdAu	K ₂ PdCl ₄ , HAuCl ₄
SSKKSYSYSGKSKRRIL (R5)	PdPt	K ₂ PdCl ₄ , K ₂ PtCl ₄
6his-SP1	Pd	Na ₂ PdCl ₄
denatured BSA (dBSA)	Mn-doped Zns	Mn(Ac) ₂ , ZnAc ₂
Consensus tetratricopeptide repeat protein (CTPR3) and ¹⁵ N-CTPR	Au	HAuCl ₄

2.3. Recombinant production of peptides and proteins

In 1982, a revolutionary change took place in the manufacturing of essential products when Eli Lilly corporation received FDA approval for the first recombinantly produced pharmaceutical product called human insulin [11]. Since it was a big change in the large-scale

manufacturing of biological products, researchers became excited to develop biological products with higher performance compared to the naturally occurring ones. They were successful in exploiting recombinant platforms for developing a wide range of drugs for commercial use. Some of these products are tabulated in Table 2, adapted from Schmidt et al. [12].

In order to recombinantly produce a desired therapeutic protein, living organisms such as bacteria, yeast, mammalian cells, molds, and insect cells can be used as expression platforms [12,13]. Using this method, the host cell produces heterologous proteins and peptides using biological processes occurring inside the cell. It is important to note that using molecular biology modifications, the genetic information of the DNA is manipulated and eventually, mRNA is fabricated. The process of mRNA synthesis is called transcription which prepares mRNA to be used as a template for protein synthesis. The process of protein fabrication is called translation. As of 2014, FDA regulations for approving therapeutic peptides are limited to those which used *Escherichia coli* (Calcitonin, Insulin and its variants), *Staphylococcus cerevisiae* (Insulin and its variants, Lepirudin, Liraglutide) and *Pseudomonas pastoris* (Ecallantide) as their expression host cells [14]. Although each expression host has its own advantages and disadvantages, *E. coli* is known as the most widely used host [15,16], where in 2009, 40% of recombinant pharmaceuticals used mammalian cells followed by *E. coli* as expression host [16].

Table 3. A list of recombinant peptides approved by FDA or EMA [12].

Year	Generic name	Company	Length (aa)
1983	Insulin	Eli Lilly	51
1991	Insulin	Novolin	51
1996	Insulin lispro	Eli Lilly	51
1997	Desirudin	Canyon Pharmaceuticals	65
1998	Lepirudin	Hoechst Marion Roussel	65

Table 4. A list of recombinant peptides approved by FDA or EMA. Cont.

Year	Generic name	Company	Length (aa)
1998	Glucagon	Novo Nordisk	29
2000	Insulin glargine	Physicians Total Care	53
2001	Nesiritide	Scios	32
2001	Insulin aspart	Novo Nordisk	51
2002	Teriparatide	Eli Lilly	34
2004	Insulin glulisine	Sanofi Aventis	51
2005	Insulin detemir	Novo Nordisk	50
2005	Calcitonin	Upsher-Smith Laboratories	32
2005	Mecasermin	Tercica	70
2009	Liraglutide	Novo Nordisk	31
2009	Ecallantide	Dyax	60
2012	Teduglutide	NPS Pharmaceuticals	33

2.4. *Escherichia coli* as expression host

Similar to the other expression systems that have been used in lab and industry, *E. coli* has its own advantages and disadvantages. One of the most important advantages of an *E. coli* expression system is that it has been widely used in research labs and industry, its molecular genetics are well known which has resulted in various engineered plasmids [17,18]. The simple structure of *E. coli* and its cheap path of production have encouraged researchers to seek fast and high volume cultivation methods which could be appropriate for lab scale as well as industrial scale processes [17,18]. On the other hand, the inability to perform post translational modifications could be named as the main disadvantage of *E. coli*. Glycosylation is an example of post translational modifications that *E. coli* is not able to perform. The production of endotoxins, the formation of inactive inclusions, and having a different codon frequency than the

human genome can be included in the list of its disadvantages [13,19,20]. Nowadays, a broad range of *E. coli* strains has been developed by researchers to overcome the disadvantages.

Campylobacter jejuni has been used for transferring the N-linked glycosylation mechanism to prepare glycosylated proteins in *E. coli*. Furthermore, In order to correct the different codon frequency, BL21 Codon Plus™ and Rosetta™ are used while Origami™ and Rosetta-gami™ promote disulfide bond formation [21]. At the end, since the large scale production of recombinant proteins and peptides without glycosylation is of high demand, *E. coli* is still the best choice and its advantages outweigh the disadvantages.

2.5. Fermentation

It is important for any process to achieve the maximum yield of protein with minimal expenses in a short time. This can be done by large scale manufacturing when the researchers are certain about the process. In the other words, the aim of most biochemical engineering research is to reach to the maximum productivity in minimum time from any given cell culture [15].

There are two different methods of fermentation; shaker process and bioreactor process. In the shaker process, all the raw materials are added at the beginning, and growth conditions cannot be controlled. Since the oxygen concentration and pH may decrease with time, the rate of bacterial growth would be lowered. On the other hand, this process is very simple and inexpensive so that it can be used to check if the expression is doable or not [22]. In order to obtain high cell density and optimize, bioreactor processes are used. These processes can be categorized as simple batch, fed-batch, and continuous processes. Fed-batch fermentation process has been reported to be successful in obtaining orders of magnitude more dry cell weight over a simple batch process [23,24]. This process may take more preparation time, but the quantity of target protein could be

high. In addition, the growth rate is controllable and undesired effects such as substrate inhibition, acetate formation, and heat dissipation are minimized [25,26]. In the context of this body of work, shaker and fed-batch processes will be used.

2.6. Protein and peptide expression in host cell and Green Fluorescent Protein (GFPuv)

The main challenge faced during expression of peptide is the small number of amino acids in the sequence of peptide structure because they are prone to degradation within the cell [27]. Within this context, this dissertation focused upon Pd4 (palladium binding sequence) peptide [28] which has only 12 amino acids in its structure for nanoparticle preparation. Also, linking the peptide to the reporter protein GFPuv as a fusion partner was chosen to stabilize and protect the peptide within the host cell. Since the reporter protein GFPuv is fluorescent, upstream and downstream processing can be monitored easily [29]. It also facilitates the process of purification via Ion Exchange, Immobilized Metal Affinity Chromatography and Aqueous Two-Phase Extraction [30]. To ensure against inhibited cell growth, it is important to differentiate the growth phase from protein production phase by using an inducible thermal or chemical promoter [31]. Different chemical promoters such as lactose, isopropyl- β -D-thiogalactopyranoside (IPTG), arabinose or thermal promoters such as PR and PL can be used. Some of the promoters, specially IPTG, could be toxic to the cells in high concentrations while they can be effective in controlling expression systems. In this study, the constructs are expressed in different fusion forms employing pBAD systems. Also, this system is inducible by arabinose as chemical promoter.

2.7. Purification

One of the most important steps in any chemical or biochemical processes is purification. In this research, there are two distinctive roles for purification: proteins/peptides from the cell content, and nanoparticles from the synthesis mix.

2.7.1. Chromatography

A variety of purification strategies can be employed for proteins/peptides depending on the cloning strategy. One of the purification methods is fast protein liquid chromatography (FPLC) which is widely used for protein purification. In this method, the target protein, which is also called the protein of interest (POI) is purified using a difference in affinity. Proteins are in the mobile phase which bind ligands attached to the stationary phase (beads). The POI would be displaced and eluted using a mobile phase that attenuates adsorption. Otherwise, the POI cannot be purified from others attached content on resin. Since the purification in large scale is very complex, the body of this work focuses on minimizing the purification steps of the Pd4 fusion protein. Since major drawbacks of large scale production using a chromatography column are the resin cost and time, minimizing the number of purification steps would be extremely attractive [23].

2.7.2. Nanoparticle purification

In order to prepare the synthesized nanoparticles for characterization and enhance their yield for catalytic applications, it may be necessary to isolate the nanoparticles from the proteins/peptides. One of the purification methods is mild acid treatment with hydrochloric acid. Since the nucleation of nanoparticles is initiated from the amino acids that are negatively charged

such as histidine and cystine, nanoparticles are likely linked to them after formation. A simple acid treatment drops the pH to 5.0 and will cause the protonation of these amino acids. As a result, synthesized nanoparticles will be separated from the scaffold protein/peptide. Since the purpose of this work is to produce metallic nanoparticles, some of them such as palladium nanoparticles have been reported to be ferromagnetic when the particle diameter is smaller than 10 nm, possessing magnetic moments due to their surface atoms [32]. As a result, in order to recover the nanoparticles, acid treatment combined with the use of centrifugation and magnetic separation could cause the separation of nanoparticles from lysate [32].

2.8. Heterogenous catalysis

Catalyst is a substance used to boost and accelerate the rate of chemical reaction by providing an alternative route and remaining intact and unchanged during the process [1]. The catalytic reactions have lower activation energies and their cycle is usually made of three major steps. First, reactants are adsorbed to the unoccupied active site of the catalyst to form activated complexes. Subsequently, the products will be obtained through chemical conversion of activated complexes. Finally, the catalyst will undergo the desorption from active sites. This cycle continues until one of the reactants is fully consumed.

Catalysts can be categorized based on their physical properties into two major types; homogeneous catalysts and heterogeneous catalysts. Although homogeneous catalysts are great candidates with high yield of selectivity and conversion, their complicated separation and non-recyclability have made them less favorable in industrial uses. On the other hand, heterogeneous catalysts due to their low metal contaminations, ease of recyclability, and reasonable conversion yields have attracted many attentions and been used widely in industries specially

pharmaceuticals. Heterogeneous catalysts usually contain transition-metals, immobilized on a substrate of alumina, carbon, silica, or organic frameworks [33–38]. Recently, researchers have developed heterogeneous catalysts that are supported on biological materials such as peptides and proteins[3,28,39].

2.9. Coupling reactions

One series of catalytic reactions proceed through carbon-carbon bond formation called coupling reaction. In order to obtain coupling products, the presence of metal catalysts and bases plays an important role [40,41]. Preparation of not only basic organic molecules but complex compounds has made the coupling reaction a desired path to manufacture new products for chemical, pharmaceutical and agricultural industries. There are different types of coupling reactions which a selected set of reactions is reported on Table 5.

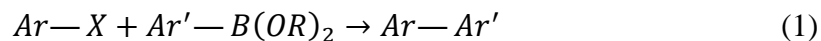
Table 5. A list of selected coupling reaction.

Reaction	Year	Catalyst	Base requirement
Wurtz Reaction [42]	1855	Sodium	No
Glaser Reaction [43]	1869	Copper	Yes
Ullmann Reaction [44]	1901	Copper	Yes
Gomberg-Bachmann Reaction [45]	1924	—	Yes
Cadiot-Chodkiewicz Coupling [46]	1956	Copper	No
Kumada Coupling [47,48]	1972	Nickel, Palladium	No
Heck Reaction [49,50]	1972	Palladium	Yes
Sonogashira Reaction [51]	1973	Palladium, Copper	Yes
Stille Reaction [52]	1977	Palladium	Yes
Suzuki-Miyaura Coupling [53]	1979	Palladium	Yes
Hiyama Coupling [54]	1988	Palladium	Yes

The first coupling reactions was reported by Charles A. Wurtz and the coupling reaction was named after him in the middle of the nineteenth century [42]. After him, a wide variety of coupling reactions under diverse conditions have been developed which a few of the most commonly used reaction in industry are listed in Table 5. In early 1970s, palladium was introduced and used as catalyst in coupling reactions resulted in new compounds with excellent catalytic activities. As listed in Table 5, these reaction includes Kumada reactions [47,48], Heck reactions [49,50], Sonogashira reactions [51], Stille reactions [52] and Suzuki-Miyaura couplings (1979) [53]. The most popular coupling reactions are Suzuki-Miyaura coupling and Stille coupling that have a wide variety of applications specially in pharmaceutical industries.

2.9.1. Suzuki-Miyaura coupling reaction

In a Suzuki-Miyaura coupling reaction, an organohalide and a boronic acid are the coupling partners and the catalysis occurs using palladium complex [53]. This reaction was named after Akira Suzuki who primarily published it and finally shared the 2010 Noble Prize in Chemistry with Richard Heck, and Ei-ichi Negishi for their successes in discovery of palladium-catalyzed coupling reactions [55]. The general reaction for Suzuki-Miyaura coupling reaction is given as



Where Ar and Ar' are aryl groups, X is halide, $B(OR)_2$ is boronic group, and $Ar-Ar'$ is the coupled product. Using a palladium complex as catalyst and base, an aryl halide ($Ar-X$) is coupled by a carbon-carbon single bond to an organoboronic species ($Ar'-B(OR)_2$) and the coupling product ($Ar-Ar'$) is synthesized. The Suzuki-Miyaura coupling reaction mechanism is shown in Figure 1. First, the palladium as a catalyst is oxidatively added to the halide in order

to form the organopalladium compound ($\text{Ar—Pd}^{\text{II}}\text{—X}$). Subsequently, the base is reacted with organopalladium compound leading to intermediate ($\text{Ar—Pd}^{\text{II}}\text{—CO}_3^-$). The organopalladium compound ($\text{Ar—Pd}^{\text{II}}\text{—Ar}'$) is obtained via transmetalation of the intermediate with boronated complex. Eventually, the desired product ($\text{Ar—Ar}'$) is formed and the original palladium catalyst restores to the catalytic cycle.

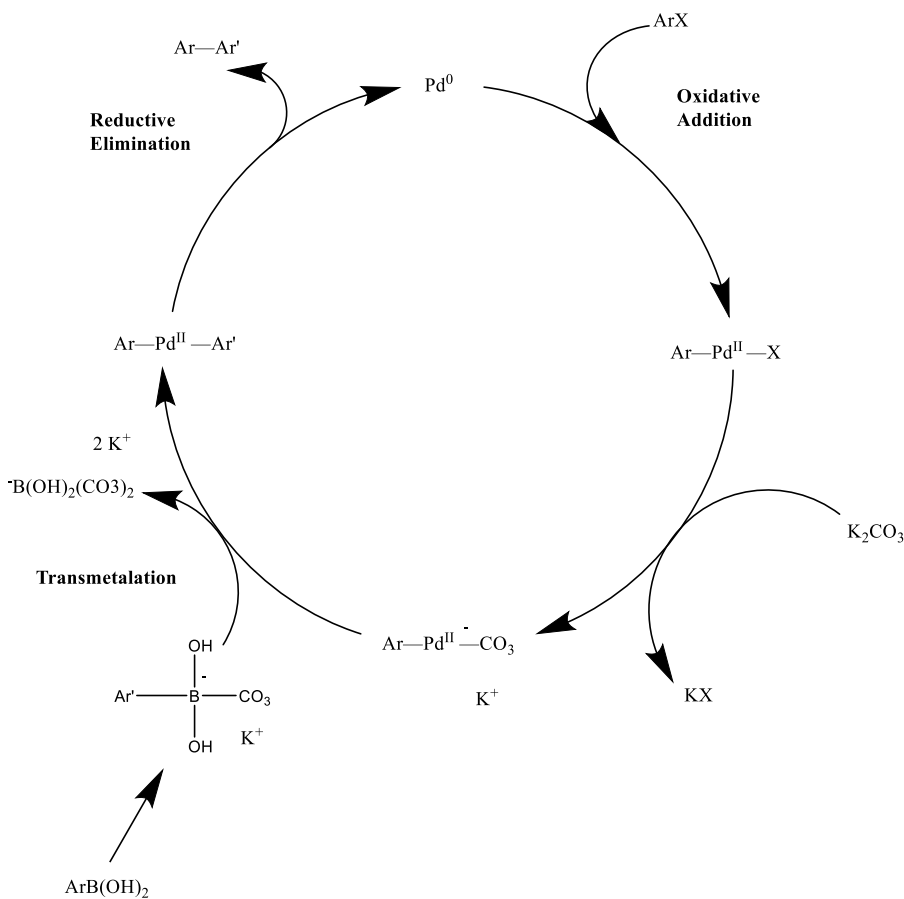
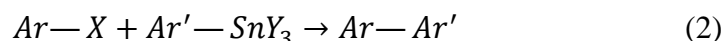


Figure 1. Schematic of Suzuki-Miyaura coupling reaction using Pd^0 and K_2CO_3 as catalyst and base, respectively.

2.9.2. Stille coupling reaction

The Stille coupling reaction which is also known as Migita-Kosugi-Stille coupling reaction, is the well-known and one of the most extensively studied pathways for palladium-catalyzed coupling reactions in which an organotin (organostannanes) compound and organohalide are the coupling partner [39,52]. The general reaction for Stille coupling reaction is given as



Where Ar and Ar' are aryl groups, X is halide, SnY_3 is stannane group, Y can be alkyl groups or halides such as Cl, and $Ar-Ar'$ is the coupled product. An aryl halide ($Ar-X$) is coupled by a carbon-carbon single bond to an organostannane species ($Ar'-SnY_3$) using a palladium catalyst and base to obtain the coupling product ($Ar-Ar'$). The schematic of the Stille coupling reaction mechanism of aryl halide group and phenyltin trichloride ($PhSnCl_3$) is shown in Figure 2. The first step is oxidative addition of the palladium catalyst to the halide in order to form the organopalladium compound ($Ar-Pd^{II}-X$) using palladium ions. Subsequently, the part of the catalyst that remained intact does not participate in the reaction but the organopalladium compound ($Ar-Pd^{II}-Ar'$) is obtained via transmetalation of the intermediate with tin complex. Finally, the coupling product ($Ar-Ar'$) is formed in reductive elimination step and the original palladium catalyst restores to the catalytic cycle to join the unreacted part.

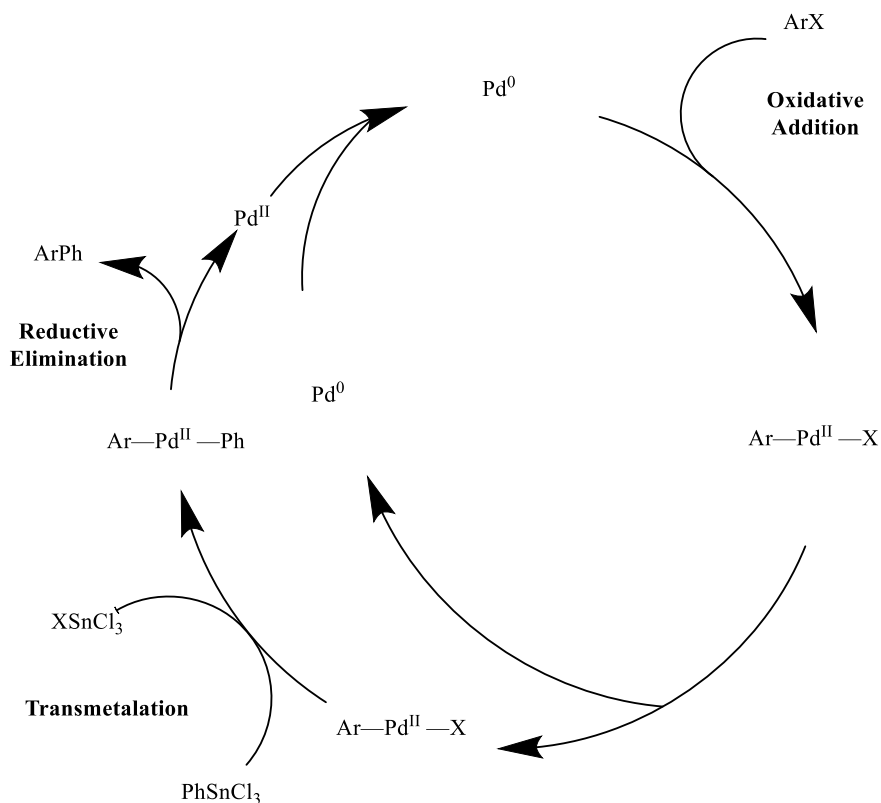


Figure 2. Schematic of Stille coupling reaction using Pd^0 as catalyst.

Most of pharmaceutical products can be made using these two coupling reactions. These coupling reactions can tolerate a broad range of organic functionality and simplify the preparation of complex compounds as well as novel chemicals as they can be performed in the presence of water. For instance, anti-tumor-growth drug called antiangiogenic tyrosine kinase for [56], phosphodiesterase IV inhibitors for the intervention of arthritis, asthma, and colitis [57] can be prepared through these coupling reactions.

In addition, Suzuki and Stille couplings are versatile reactions, as they can be proceeded using a minute amount of palladium in various types of catalyst [39,58], while in many coupling reactions, higher catalyst loading might needed to obtain a desired yield [59].

2.10. Need

The main roadblock to widespread development and commercialization of peptide-directed nanoparticle synthesis for applications that include catalysis is the high cost of peptide. For example, it would be cost prohibitive to manufacture platinum or palladium nanoparticles, valued at \$200 - \$2,000 per gram, when peptide costs exceed \$10,000 per gram. Such a differential is even more exacerbating for a nonprecious nanoparticle, or when the peptide length grows to incorporate multiple functional domains. The costs for pharmaceutical-grade polypeptides are listed in Table 6 [60]. Using *E. coli* as expression host to recombinantly produce many copies of desired peptide and enhancing the amount of potential nanoparticle nucleation sites by increasing the concentration of peptides may result in a money saving strategy for producing catalytic nanoparticles.

Table 6. Associated costs for pharmaceutical-grade peptides and polypeptide [60].

Product	Human insulin	Monoclonal antibody
Scale (kg / y)	18,000	6.5
Location of product	intracellular	secreted
Chemical reactions (yes / no) in bioprocess	yes, polypeptide cleavage	no
Total capital investment	\$78 million	\$16.3 million
NPV at 7% interest	\$216 million	\$32.5 million
Upstream number of unit operations (a)	5	6
Recovery number of unit operations (b)	26	11
Unit product cost (\$ / gram)	42	908

(a) does not include master cell bank storage

(b) includes CnBr cleavage steps

2.11. Significance

The significance of this research is to overcome the money-consuming traditional means for preparing bio-templated nanoparticles. By proposing a cost-effective approach for the production of nanoparticles using protein/peptide derived from *E. coli*, the cost of solid phase synthesis and purification will be circumvented.

The broad goals of this work are to provide proof of concept that Pd4 peptide can be produced recombinantly, and finally, to assess their use in cross-coupling reactions following a bottom-up strategy. The other broad goal of this experimental research is to synthesize precious inorganic nanoparticles including palladium and identify the main parameters affecting their size, morphology, and compositions. It is important to note that the synthesized nanoparticles due to their high efficiency coming from being built using bottom-up strategy, have high potential to be used as catalysis for cross-coupling reactions.

2.12. References

- [1] Y. Xia, X. Xia, Y. Wang, S. Xie, Shape-controlled synthesis of metal nanocrystals, *MRS Bull.* 38 (2013) 335–344. doi:10.1557/mrs.2013.84.
- [2] S. Weiner, L. Addadi, Design strategies in mineralized biological materials, *J. Mater. Chem.* 7 (1997) 689–702.
- [3] M.B. Dickerson, K.H. Sandhage, R.R. Naik, Protein-and peptide-directed syntheses of inorganic materials, *Chem. Rev.* 108 (2008) 4935–4978.
- [4] A.-W. Xu, Y. Ma, H. Cölfen, Biomimetic mineralization, *J. Mater. Chem.* 17 (2007) 415–449.
- [5] M. Sarikaya, C. Tamerler, A.K.-Y. Jen, K. Schulten, F. Baneyx, Molecular biomimetics: nanotechnology through biology, *Nat. Mater.* 2 (2003) 577.
- [6] S.R. Whaley, D.S. English, E.L. Hu, P.F. Barbara, A.M. Belcher, Selection of peptides with semiconductor binding specificity for directed nanocrystal assembly, *Nature.* 405 (2000) 665.
- [7] C.-L. Chen, N.L. Rosi, Peptide-based methods for the preparation of nanostructured inorganic materials, *Angew. Chem. Int. Ed.* 49 (2010) 1924–1942.
- [8] N.M. Bedford, A.R. Showalter, T.J. Woehl, Z.E. Hughes, S. Lee, B. Reinhart, S.P. Ertem, E.B. Coughlin, Y. Ren, T.R. Walsh, B.A. Bunker, Peptide-Directed PdAu Nanoscale Surface Segregation: Toward Controlled Bimetallic Architecture for Catalytic Materials, (2016). doi:10.1021/acsnano.6b03963.
- [9] C.-Y. Chiu, Y. Li, L. Ruan, X. Ye, C.B. Murray, Y. Huang, Platinum nanocrystals selectively shaped using facet-specific peptide sequences, *Nat. Chem.* 3 (2011) 393.
- [10] S. Papst, S. Cheong, M.J. Banholzer, M.A. Brimble, D.E. Williams, R.D. Tilley, One-pot synthesis of water soluble iron nanoparticles using rationally-designed peptides and ligand release, *Chem. Commun.* 49 (2013) 4540–4542.
- [11] L. Sanchez-Garcia, L. Martín, R. Mangues, N. Ferrer-Miralles, E. Vázquez, A. Villaverde, Recombinant pharmaceuticals from microbial cells: a 2015 update, *Microb. Cell Factories.* 15 (2016) 33.
- [12] F.R. Schmidt, Recombinant expression systems in the pharmaceutical industry, *Appl. Microbiol. Biotechnol.* 65 (2004) 363–372. doi:10.1007/s00253-004-1656-9.
- [13] A.L. Demain, P. Vaishnav, Production of recombinant proteins by microbes and higher organisms, *Biotechnol. Adv.* 27 (2009) 297–306.

- [14] S. Wegmuller, S. Schmid, Recombinant peptide production in microbial cells, *Curr. Org. Chem.* 18 (2014) 1005–1019.
- [15] N.K. Tripathi, High yield production of heterologous proteins with *Escherichia coli*, *Def. Sci. J.* 59 (2009) 137–146.
- [16] L. Yee, H.W. Blanch, Recombinant protein expression in high cell density fed-batch cultures of *Escherichia coli*, *Bio/Technology.* 10 (1992) 1550.
- [17] N. Ferrer-Miralles, J. Domingo-Espín, J.L. Corchero, E. Vázquez, A. Villaverde, Microbial factories for recombinant pharmaceuticals, *Microb. Cell Factories.* 8 (2009) 17. doi:10.1186/1475-2859-8-17.
- [18] H.P. Sørensen, K.K. Mortensen, Advanced genetic strategies for recombinant protein expression in *Escherichia coli*, *J. Biotechnol.* 115 (2005) 113–128.
- [19] K. Terpe, Overview of bacterial expression systems for heterologous protein production: from molecular and biochemical fundamentals to commercial systems, *Appl. Microbiol. Biotechnol.* 72 (2006) 211. doi:10.1007/s00253-006-0465-8.
- [20] S.C. Makrides, Strategies for achieving high-level expression of genes in *Escherichia coli*., *Microbiol Mol Biol Rev.* 60 (1996) 512–538.
- [21] M. Wacker, D. Linton, P.G. Hitchen, M. Nita-Lazar, S.M. Haslam, S.J. North, M. Panico, H.R. Morris, A. Dell, B.W. Wren, N-linked glycosylation in *Campylobacter jejuni* and its functional transfer into *E. coli*, *Science.* 298 (2002) 1790–1793.
- [22] J.R. Lloyd, A.W. Bunch, The physiological state of an ethylenogenic *Escherichia coli* immobilized in hollow-fiber bioreactors, *Enzyme Microb. Technol.* 18 (1996) 113–120.
- [23] M.S. Fruchtl, Expression, Production, and Purification of Novel Therapeutic Proteins, (n.d.) 235.
- [24] J. Lee, S.Y. Lee, S. Park, Fed-batch culture of *Escherichia coli* W by exponential feeding of sucrose as a carbon source, *Biotechnol. Tech.* 11 (1997) 59.
- [25] P.-H. Wu, G.R. Nair, I.-M. Chu, W.-T. Wu, High cell density cultivation of *Escherichia coli* with surface anchored transglucosidase for use as whole-cell biocatalyst for α -arbutin synthesis, *J. Ind. Microbiol. Biotechnol.* 35 (2008) 95.
- [26] S.Y. Lee, High cell-density culture of *Escherichia coli*, *Trends Biotechnol.* 14 (1996) 98–105.
- [27] J. Svenson, W. Stensen, B.-O. Brandsdal, B.E. Haug, J. Monrad, J.S. Svendsen, Antimicrobial peptides with stability toward tryptic degradation, *Biochemistry.* 47 (2008) 3777–3788.

- [28] N.M. Bedford, H. Ramezani-Dakhel, J.M. Slocik, B.D. Briggs, Y. Ren, A.I. Frenkel, V. Petkov, H. Heinz, R.R. Naik, M.R. Knecht, Elucidation of peptide-directed palladium surface structure for biologically tunable nanocatalysts, *ACS Nano*. 9 (2015) 5082–5092.
- [29] R.P. Mukherjee, R. Beitle, S. Jayanthi, T.K.S. Kumar, D.S. McNabb, Production of an anti-*Candida* peptide via fed batch and ion exchange chromatography, *Biotechnol. Prog.* 32 (2016) 865–871.
- [30] Y. Li, R.R. Beitle, Protein Purification via Aqueous Two-Phase Extraction (ATPE) and Immobilized Metal Affinity Chromatography. Effectiveness of Salt Addition To Enhance Selectivity and Yield of GFPuv, *Biotechnol. Prog.* 18 (2002) 1054–1059.
- [31] M.G. Aucoin, V. McMurray-Beaulieu, F. Poulin, E.B. Boivin, J. Chen, F.M. Ardelean, M. Cloutier, Y.J. Choi, C.B. Miguez, M. Jolicoeur, Identifying conditions for inducible protein production in *E. coli*: combining a fed-batch and multiple induction approach, *Microb. Cell Factories*. 5 (2006) 27. doi:10.1186/1475-2859-5-27.
- [32] T. Taniyama, E. Ohta, T. Sato, Observation of 4d ferromagnetism in free-standing Pd fine particles, *EPL Europhys. Lett.* 38 (1997) 195.
- [33] C.N. Satterfield, *Heterogeneous catalysis in industrial practice*, (1991).
- [34] L. Chen, Z. Gao, Y. Li, Immobilization of Pd(II) on MOFs as a highly active heterogeneous catalyst for Suzuki–Miyaura and Ullmann-type coupling reactions, *Catal. Today*. 245 (2015) 122–128. doi:10.1016/j.cattod.2014.03.074.
- [35] L. Zhang, Z. Su, F. Jiang, Y. Zhou, W. Xu, M. Hong, Catalytic palladium nanoparticles supported on nanoscale MOFs: a highly active catalyst for Suzuki–Miyaura cross-coupling reaction, *Tetrahedron*. 69 (2013) 9237–9244. doi:10.1016/j.tet.2013.08.059.
- [36] W. Dong, C. Feng, L. Zhang, N. Shang, S. Gao, C. Wang, Z. Wang, Pd@UiO-66: An Efficient Catalyst for Suzuki–Miyaura Coupling Reaction at Mild Condition, *Catal. Lett.* 146 (2016) 117–125. doi:10.1007/s10562-015-1659-4.
- [37] Z. Chen, Z.-M. Cui, F. Niu, L. Jiang, W.-G. Song, Pd nanoparticles in silica hollow spheres with mesoporous walls: a nanoreactor with extremely high activity, *Chem. Commun.* 46 (2010) 6524–6526. doi:10.1039/C0CC01786H.
- [38] R. Li, P. Zhang, Y. Huang, C. Chen, Q. Chen, Facile Approach to Prepare Pd Nanoarray Catalysts within Porous Alumina Templates on Macroscopic Scales, *ACS Appl. Mater. Interfaces*. 5 (2013) 12695–12700. doi:10.1021/am4040762.
- [39] D.B. Pacardo, M. Sethi, S.E. Jones, R.R. Naik, M.R. Knecht, Biomimetic Synthesis of Pd Nanocatalysts for the Stille Coupling Reaction, (2009). doi:10.1021/nn9002709.

- [40] J. Hassan, M. Sevignon, C. Gozzi, E. Schulz, M. Lemaire, Aryl-aryl bond formation one century after the discovery of the Ullmann reaction, *Chem. Rev.* 102 (2002) 1359–1470.
- [41] R. Chinchilla, C. Nájera, The Sonogashira reaction: a booming methodology in synthetic organic chemistry, *Chem. Rev.* 107 (2007) 874–922.
- [42] A. Wurtz, Sur une nouvelle classe de radicaux organiques, *Ann Chim Phys.* 44 (1855) 275–312.
- [43] C. Glaser, Beiträge zur Kenntniss des Acetylnbenzols, *Berichte Dtsch. Chem. Ges.* 2 (1869) 422–424.
- [44] F. Ullmann, J. Bielecki, Ueber synthesen in der biphenylreihe, *Berichte Dtsch. Chem. Ges.* 34 (1901) 2174–2185.
- [45] M. Gomberg, W.E. Bachmann, The synthesis of biaryl compounds by means of the diazo reaction, *J. Am. Chem. Soc.* 46 (1924) 2339–2343.
- [46] W. Chodkiewicz, Synthesis of acetylenic compounds, *Ann ChimParis.* 2 (1957) 819.
- [47] K. Tamao, K. Sumitani, M. Kumada, Selective carbon-carbon bond formation by cross-coupling of Grignard reagents with organic halides. Catalysis by nickel-phosphine complexes, *J. Am. Chem. Soc.* 94 (1972) 4374–4376.
- [48] M. Yamamura, I. Moritani, S.-I. Murahashi, The reaction of σ -vinylpalladium complexes with alkyllithiums. Stereospecific syntheses of olefins from vinyl halides and alkyllithiums, *J. Organomet. Chem.* 91 (1975) C39–C42.
- [49] R.F. Heck, J.P. Nolley Jr, Palladium-catalyzed vinylic hydrogen substitution reactions with aryl, benzyl, and styryl halides, *J. Org. Chem.* 37 (1972) 2320–2322.
- [50] T. Mizoroki, K. Mori, A. Ozaki, Arylation of olefin with aryl iodide catalyzed by palladium, *Bull. Chem. Soc. Jpn.* 44 (1971) 581–581.
- [51] K. Sonogashira, Y. Tohda, N. Hagihara, A convenient synthesis of acetylenes: catalytic substitutions of acetylenic hydrogen with bromoalkenes, iodoarenes and bromopyridines, *Tetrahedron Lett.* 16 (1975) 4467–4470.
- [52] D. Milstein, J.K. Stille, A general, selective, and facile method for ketone synthesis from acid chlorides and organotin compounds catalyzed by palladium, *J. Am. Chem. Soc.* 100 (1978) 3636–3638.
- [53] N. Miyaura, A. Suzuki, Stereoselective synthesis of arylated (E)-alkenes by the reaction of alk-1-enylboranes with aryl halides in the presence of palladium catalyst, *J. Chem. Soc. Chem. Commun.* (1979) 866–867.

- [54] Y. Hatanaka, T. Hiyama, Cross-coupling of organosilanes with organic halides mediated by a palladium catalyst and tris (diethylamino) sulfonium difluorotrimethylsilicate, *J. Org. Chem.* 53 (1988) 918–920.
- [55] The Nobel Prize in Chemistry 2010, NobelPrize.Org. (n.d.).
<https://www.nobelprize.org/prizes/chemistry/2010/summary> .
- [56] M. Feuerstein, H. Doucet, M. Santelli, Efficient coupling of heteroaryl bromides with arylboronic acids in the presence of a palladium–tetraphosphine catalyst, *Tetrahedron Lett.* 42 (2001) 5659–5662.
- [57] O.V. Gozhina, Design, Synthesis and Biological Activity of Small α -Aminoboron Containing Peptidomimetics, (2013).
- [58] M. Ghotbinejad, A.R. Khosropour, I. Mohammadpoor-Baltork, M. Moghadam, S. Tangestaninejad, V. Mirkhani, SPIONs-bis (NHC)-palladium (II): A novel, powerful and efficient catalyst for Mizoroki–Heck and Suzuki–Miyaura C–C coupling reactions, *J. Mol. Catal. Chem.* 385 (2014) 78–84.
- [59] N.T.S. Phan, v. d. Sluys, M.; Jones, CW Ad V, *Synth Catal.* 348 (2006) 609.
- [60] D. Petrides, Bioprocess design and economics, *Biosepar. Sci. Eng.* (2000).

Chapter 3. Properties-controlled synthesis of recombinant peptide fusion protein-templated palladium nanoparticles

In this chapter, the recombinant construction of fusion proteins and peptides has been explored. The prepared fusion proteins and peptides have been used for palladium nanoparticle synthesis. Subsequently, the parameters that may control the size, morphology, composition, and properties of nanoparticles have identified. The NPs with different properties have been synthesized and characterized.

3.1. Recombinant construction of fusion protein

The first step which is primarily the base of this research is to demonstrate that peptides and small proteins may be produced recombinantly. In order to investigate the recombinant production of peptides choosing the peptide sequence is required. Since the focus of this work is on using peptides and proteins that can direct the nanoparticles, the presence of amino acids that can help the peptides to anchor to the nanoparticles is inevitable. The peptide used to illustrate nanoparticle synthesis, commonly referred to as Pd4 (TSNAVHPTLRHL) has been described previously to non-covalently bind to Pd [1–5]. This classic Pd4 peptide was derived from M13 phage display adsorption on bulk polycrystalline palladium and has histidine residues at its sixth and eleventh position in the peptide structure [6,7]. The peptide can anchor to the surface of palladium nanoparticle surfaces through histidine residues. In order to study the effect of histidine residue on the properties of synthesized Pd NPs, four different peptides reported by Bedford *et al.* were constructed as fusion proteins [6]. As provided in Table 7, they have reported that using different peptide sequences resulted in nanoparticles with different sizes and catalytic properties. The design of first substitute for Pd4 is based on substituting histidine with alanine in the sixth position. This peptide sequence is called A6. Consequently, the final fusion protein would be (A6)₁-GFPuv. The next peptide, A11, has alanine in the eleventh position and after fusion to GFP, (A11)₁-GFPuv protein would be generated. In the structure of the fourth peptide, histidine residues are replaced with alanine, resulting in a new mutant called A6,11. Based on the data provided by Bedford *et al.*, substitution of histidine with alanine does not affect significantly on the nanoparticles size, while their catalytic activities altered as measured by their turnover frequency in Stille coupling reaction. This change is mainly due to the effect of altering the sequence which affects the morphology, roughness, and chemisorption sites of NPs surfaces.

Table 7. Peptide sequences and properties of synthesized palladium nanoparticles (adopted from [6]).

Peptide	Sequence	Size (nm)	Stille Coupling TOF (h ⁻¹)
Pd4	TSNAVHPTLRHL	2.1 ± 0.4	2200 ± 100
A6	TSNAVAPTLRHL	2.2 ± 0.7	5200 ± 400
A11	TSNAVHPTLRAL	2.6 ± 0.4	1300 ± 10
A6,11	TSNAVAPTLRAL	2.8 ± 0.7	360 ± 20

3.1.1. Design of primers

The design of primers and plasmid construction for four different peptides sequence have been successfully performed. As provided in Table 8, sequences of fusion proteins were designed using SnapGene® software and were purchased from addgene®. As each peptide used in this work has only twelve amino acids in its structure, the forward primers contain amino acid sequences pertaining to designed peptides which make it easier to fuse them using forward primer to the reporter protein.

Table 8. Primers and their sequences for fusion protein construction

Primer	Sequence
(Pd4) ₁ GFP forward	5'-ACGGAATTCATGACTTCCAATGCTGTTTCATCCAACCTTAA GACACCTAGCTCGAGCCCGG-3'
(Pd4) ₁ GFP reverse	5'-GACTCTAGACCTTTGTACAGTTCATCCATACCATGCGTGA TGCCCG-3'
(A6) ₁ GFP forward	5'-CGGAATTCATGACTTCCAATGCTGTTGCCAACTTTAAGAC ACCTAGCTCGAGCCCGG-3'
(A6) ₁ GFP reverse	5'-CTCTAGACCTTTGTACAGTTCATCCATACCATGCGTGATG CCCGC-3'

Table 9. Primers and their sequences for fusion protein construction. Cont.

Primer	Sequence
(A11) ₁ GFP forward	5'-CGGAATTCATGACAAGTAATGCTGTACATCCAACCTTTAA GAGCTTTAGCTCGAGCCCGG-3'
(A11) ₁ GFP reverse	5'-GACTCTAGACCTTTGTACAGTTCATCCATACCATGCGTG-3'
(A6,11) ₁ GFP forward	5'-CGGGAATTCATGACTTCCAATGCTGTTGCGCCAACCTTTA AGAGCGCTAGCTCGAGCCC-3'
(A6,11) ₁ GFP reverse	5'-CTCTAGACCTTTGTACAGTTCATCCATACCATGCGTGATG CCCGC-3'

3.1.2. Recombinant expression vector construction of fusion proteins

The schematic of plasmid construction containing GFPuv fusion proteins and required steps for replacing an arabinose-inducible GFPuv gene with one extended by DNA of the proposed mutants are illustrated in Figure 3. First, to prepare the new plasmid, addgene-plasmid-51559 were digested with *EcoRI* and *XbaI* restriction enzymes before the ligation. Finally, the designed DNA containing desired peptides were ligated to the DNA to construct four pIMA plasmids containing GFPuv fusion proteins.

The plasmid containing GFPuv codon (Addgene-plasmid-51559) was purchased from Addgene® and received in *E. coli*. In order to use the plasmid for recombinant construction of fusion proteins, it was recovered from *E. coli* cell. A loop of *E. coli* containing plasmid was taken from the delivered tube and the cells were spread on agar plate. A single colony of cells was taken after 24 hours of growth and placed in 5 mL LB broth containing 5 µL of 10g/mL Ampicillin. After 24 hours, plasmid recovery process was proceeded following E.Z.N.A.® Plasmid DNA Mini Kit I Spin Protocol. As shown in Figure 4, the strong band belongs to the Addgene-plasmid-51559 which indicated successfully recover of the plasmid from *E. coli* cells.

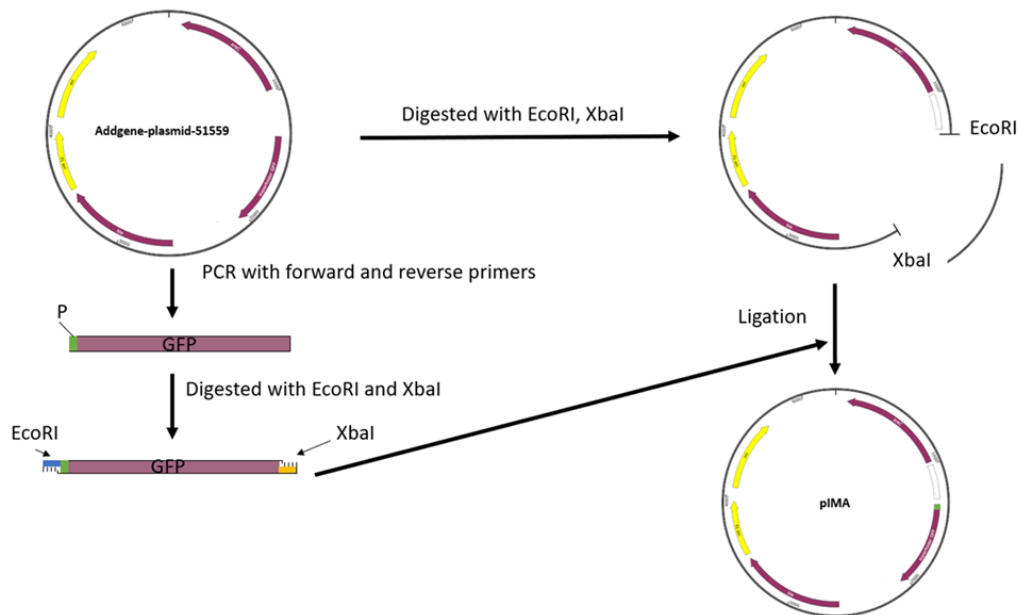


Figure 3. Schematic illustration of plasmid construction containing peptide fused to GFPuv.

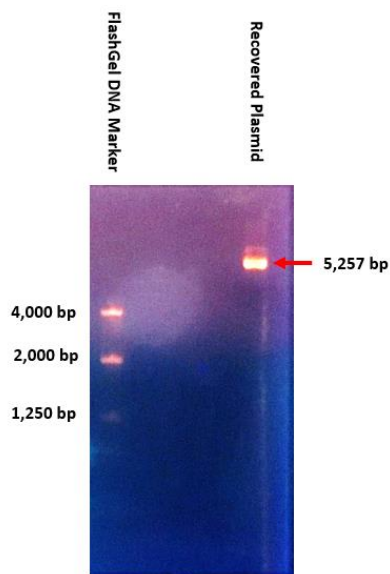


Figure 4. Agarose electrophoresis gel run for recovered Addgene-plasmid-51559.

DNA for the designed peptides was fused to the 5' end of GFPuv DNA using primers during PCR. As the designated primers were recovered from lyophilizer, primer tubes were vortexed three times for 30 seconds. Subsequently, primer tubes were centrifuged for 10 seconds and according to the amount of each primer provided in Table 10, the primers were used to prepare

their exclusive master stock solutions. For example, for (Pd4)₁GFP forward primer, 256 μ L of Tris-EDTA (TE) buffer was added to the solid primers. Subsequently, 15 μ L of the prepared mixture was added to 135 μ L of deionized water and the working sample was obtained. Eventually, 1.25-1.5 μ L of working sample (both for forward and reverse primers) containing 5-7 pico mole of primers was added to 10 μ L of deionized water and 5-7 μ L of recovered plasmid in order to prepare the master mix. The remaining working samples were stored under -20 °C. Finally, the tubes containing master mixes were placed in PCR machine for 135-165 minutes following the specifications provided in

Table 11.

Table 10. Master mix and primer solution preparation for primers needed for fusion protein construction.

Primer	Amount of primer (nmol)	Master stock Molar concentration(nmol/ μ L)	Needed volume for PCR mix (μ L)
(Pd4) ₁ GFP forward	25.6	256	1.792
(Pd4) ₁ GFP reverse	28.2	282	1.974
(A6) ₁ GFP forward	23.3	233	1.631
(A6) ₁ GFP reverse	33.7	337	2.359
(A11) ₁ GFP forward	27.7	277	1.939
(A11) ₁ GFP reverse	29.1	291	2.037
(A6,11) ₁ GFP forward	27.6	276	1.932
(A6,11) ₁ GFP reverse	30.0	300	2.100

Table 11. Steps and conditions of thermal cycling for PCR.

Steps	Temperature (°C)	Time	Cycles
Initial denaturation	94	5 min	1
Final denaturation	94	5 min	35

Annealing	63	45 sec	
Extension	72	1 min	
Final Extension	72	5 min	1

Consequently, the DNA for the final fusion proteins were attained after PCR (Figure 5). According to SnapGene® software analysis, (Pd4)₁-GFPuv, (A6)₁-GFPuv, (A11)₁-GFPuv, (A6,11)₁-GFPuv has 788, 782, 784, and 783 base pairs in their structures, respectively. Also, the presence of digested plasmid using *EcoRI* and *XbaI* restriction enzymes on N-terminus and C-terminus, respectively, was confirmed by agarose electrophoresis gel run (Figure 5).

The GFPuv fusion proteins were then digested from the parent plasmid using *EcoRI* and *XbaI* restriction enzymes on N-terminus and C-terminus, respectively in order to obtain cohesive ends. A mixture of one μL of each restriction enzyme, ten μL of gene, and 2.5 μL of 10X concentrated Smart-cut buffer was incubated at 37 °C for an hour. The same procedure was carried out for opening the parent plasmid before ligation.

In order to ligate the constructed gene with opened plasmid, a mixture containing two μL of the opened plasmid, two μL of constructed gene, two μL of 10X buffer, one μL of ligase enzyme, and 13 μL of deionized water was prepared and incubated at 16 °C for overnight (16 hours). Eventually, GFPuv fusion proteins was recovered through agarose electrophoresis gel run.

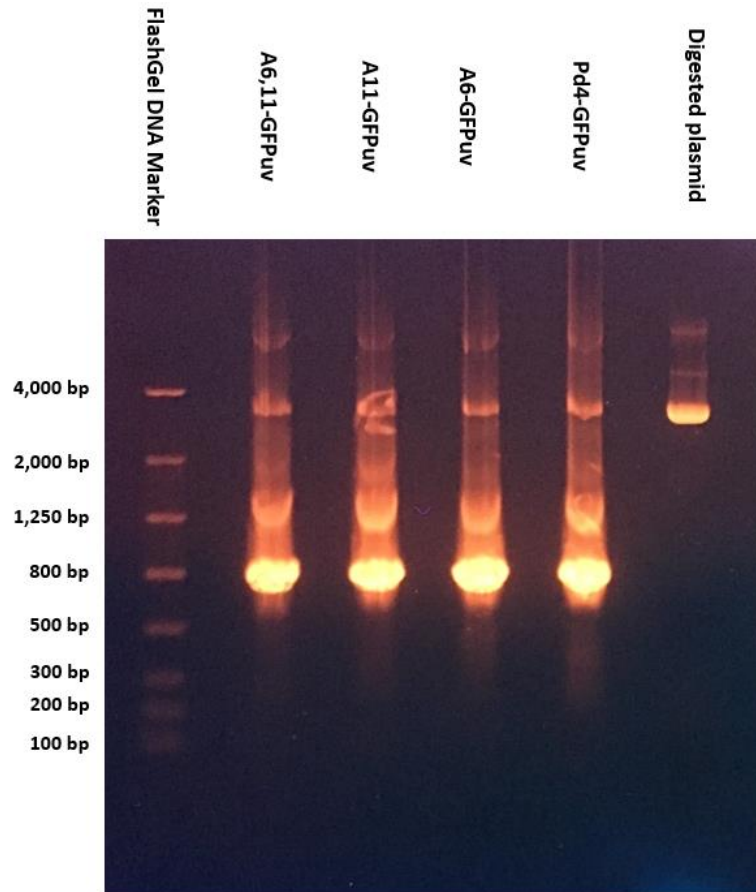


Figure 5. Successful fusion protein genes construction and plasmid digestion confirmed by agarose electrophoresis gel.

A tube of BL21(DE3) Competent *E. coli* cells (store at -80°C) were thawed in ice for 10 minutes and the amount of $5\ \mu\text{l}$ containing 100 ng of desired plasmid DNA was added to it. The tube will be flicked for 5 times in order to mix the cells. After placing the mixture on ice for 30 minutes, the mixture was heat shocked for 10 seconds at 42°C . $950\ \mu\text{l}$ of room temperature SOC was pipetted into the mixture and the mixture was placed at 37°C for 60 minutes. Subsequently, the tube containing the mixture was shaken vigorously (250 rpm) or was rotated. The selection plates were warmed to 37°C and after mixing the cells thoroughly by flicking the tube and inverting, it was 10-fold diluted serially in SOC. Consequently, $50\text{-}100\ \mu\text{l}$ of each dilution was spread onto a selection plate and was incubated overnight at 37°C .

A single colony of the transformed cells was inoculated into 5 ml of LB media containing 5 µl of ampicillin and incubated overnight in a shaker at 37°C. Then, this 5 ml was added to 500 ml LB containing 0.5 ml ampicillin in a shake flask. Induction with 10mM L-arabinose was conducted when the OD₆₀₀ reached to 0.3. Samples were collected every hour after induction for 16 hours and the fermentation was stopped, and the harvested cells were collected by centrifugation at 5000×g at 3°C and were frozen at -80°C.

3.2. Purification of fusion proteins

Since it is necessary to increase the amount of fusion protein in the sample with enrichment of peptide content in medium, purification from the lysate is inevitable. Fusion proteins could be purified through ion exchange chromatography of DEAE.

3.2.1. Purification through diethylaminoethyl chromatography (DEAE)

In DEAE purification approach, the lysate was purified using a 3.5 kDa MWCO dialysis membranes. The lysate was processed using an ÄKTA FPLC System. A HiTrap® DEAE FF column was equilibrated with IEX DEAE Buffer A (25 mM Tris-HCl, pH=8) and be prepared to load the lysate. The column was washed with 20 column volumes (CV) of the Buffer A. After washing the column and loading the lysate, enrichment was proceeded via a stepwise elution with IEX DEAE Buffer B (25 mM Tris-HCl, 1 M NaCl, pH=8). Fractions was collected and analyzed using SDS-PAGE gel and a fluorimeter.

3.3. Properties-controlled parameters in nanoparticle synthesis

Nanoparticles (NPs) receive attentions due to their unique chemical, physical, and mechanical properties arising from their crystallinity, phase, morphology, structure, and high

surface to area aspect ratio. These properties which are distinct from those of bulk materials (possessing lower surface to area aspect ratio) enable them for a diverse set of applications especially catalysis [8–12]. Palladium has been widely used due to its catalytic performance which makes it an inevitable element for various applications including hydrogen evolution, carbon dioxide reduction, and organic coupling reaction[12–14]. However, its applications have been hindered due to its high cost and limited supply and the development of cost-effective catalytic system is highly needed. Meanwhile, identifying the parameters that control the size, morphology, composition, and properties of nanoparticles is of high importance toward the development of cost-effective catalytic systems.

There are many factors affecting nanoparticle properties synthesized in aqueous media using chemical reduction. Following factors including type of reducing agent, concentration of the reducing agents, pH of the medium, temperature, type of palladium salt, and fusion protein type used for nanoparticle synthesis were investigated in this work.

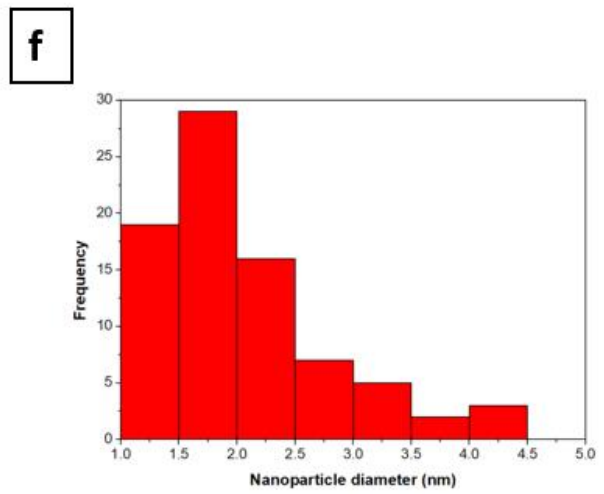
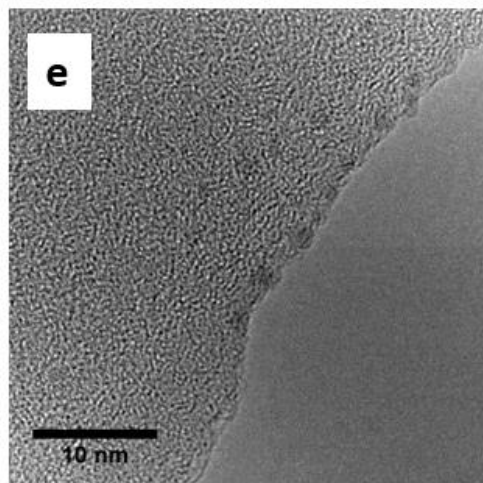
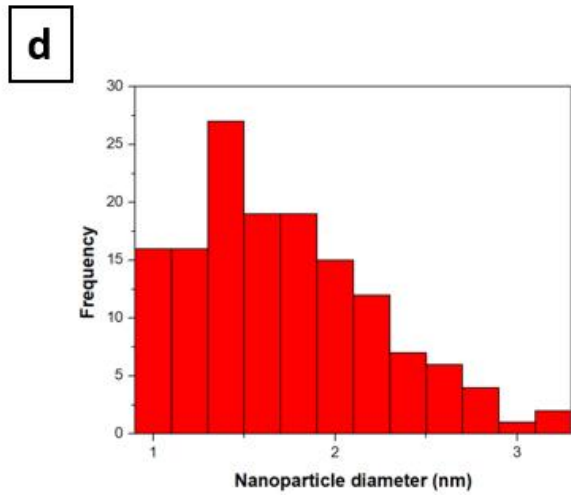
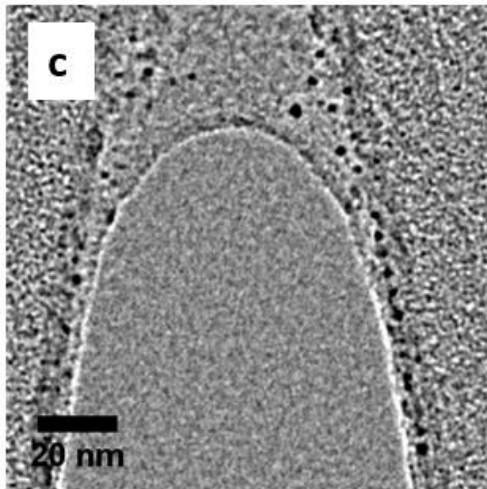
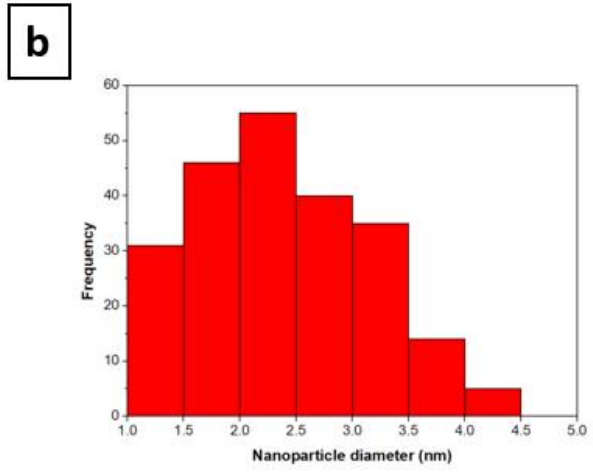
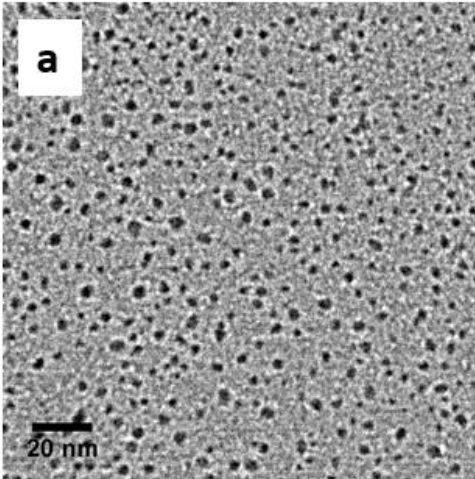
3.3.1. Reducing agent type

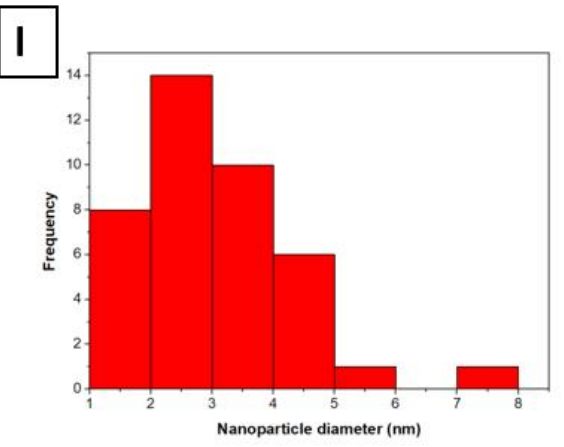
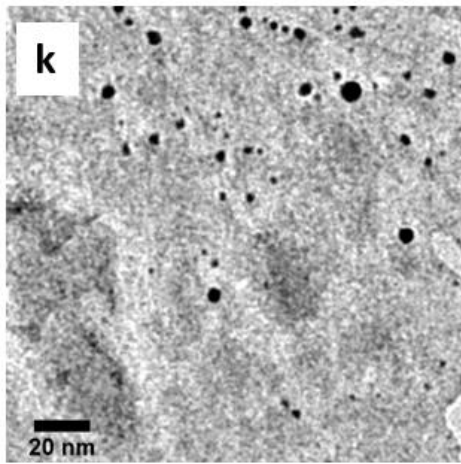
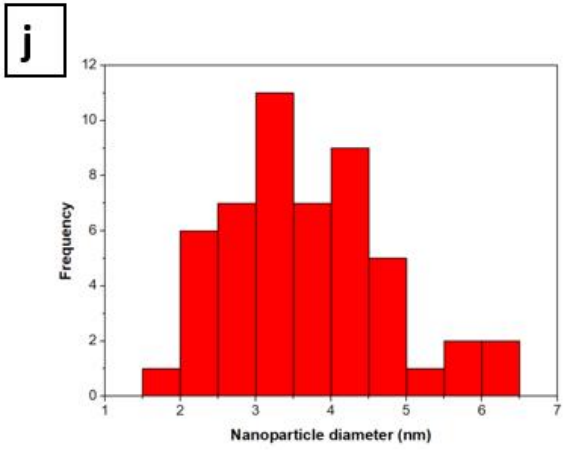
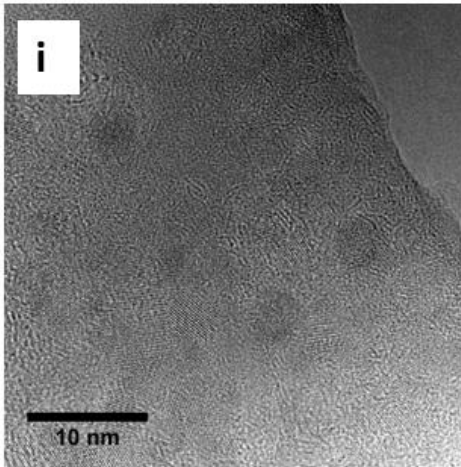
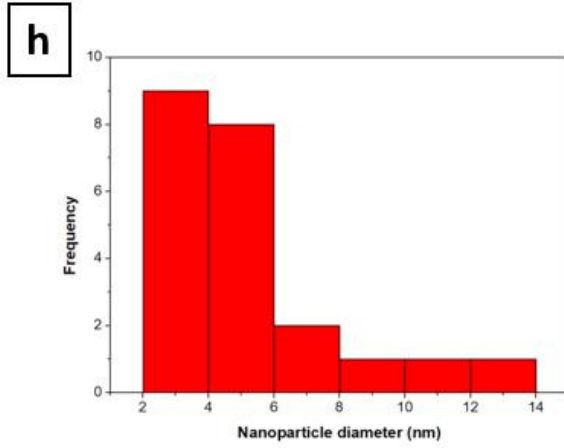
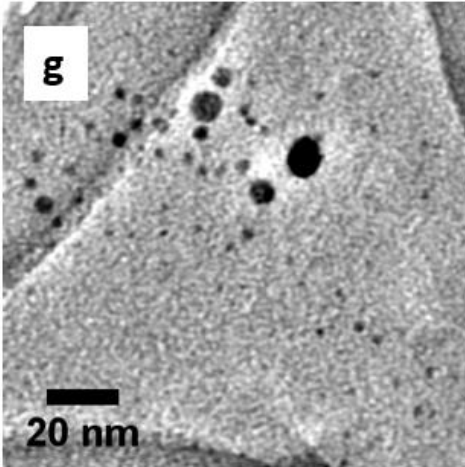
The first parameter needed to be investigated was the type of reducing agent. Most researchers use sodium borohydride (NaBH_4) as a reducing agent while there are more than 150 different reducing agents that can be used to reduce the metallic ions to synthesize metallic nanoparticles [15]. Seven distinctive types of reducing agents were examined in this study. The results of different types of reducing agents for the sample prepared at pH of 7.0 with K_2PdCl_4 salt at room temperature with salt to reducing agent ratio of 1/40 equivalent is provided in Table 12. Spherical nanoparticles were prepared using listed reducing agents in Table 12 with their size histograms are shown in Figure 6. Well-dispersed palladium nanoparticles were synthesized in

the range of 1.8-5.7 nm using different reducing agents while no aggregation observed. The disadvantages associated with reducing agents except NaBH₄ and NaCNBH₃ are their low yield of nanoparticle formation and slow rate of the reaction while using NaBH₄ and NaCNBH₃, palladium nanoparticles were formed relatively with higher rate. As toxicity of NaCNBH₃ has made it less favorable for the scientist, NaBH₄ can be named as the best reducing agent among those studied.

Table 12. The effect of reducing agent change on nanoparticle size.

Entry	Reducing agent	Nanoparticle diameter (nm)
1	NaBH ₄	2.4 ± 0.3
2	Ascorbic Acid(C ₆ H ₈ O ₆)	1.8 ± 0.2
3	NaHSO ₃	2.0 ± 0.2
4	PPh ₃	5.7 ± 0.5
5	NaCNBH ₃	3.5 ± 0.4
6	Formic Acid (CH ₂ O ₂)	3.1 ± 0.9
7	B ₂ pin ₂	2.9 ± 0.8





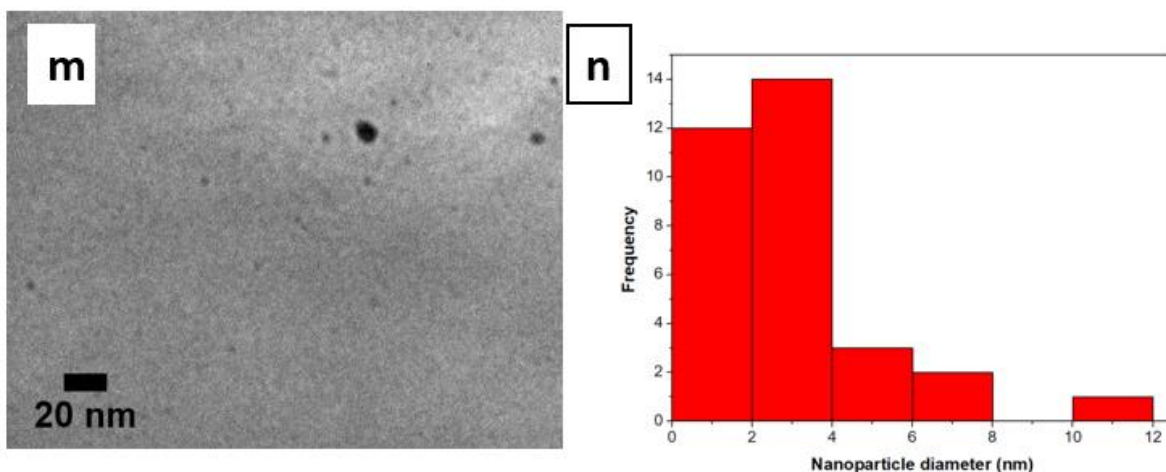


Figure 6. TEM image of recombinant fusion protein-directed palladium nanoparticles using (a)NaBH₄, (c) Ascorbic Acid, (e) NaHSO₃, (g) PPh₃, (i) NaCNBH₃, (k) Formic Acid, and (m) B₂pin₂ as reducing agents. Size histogram of synthesized palladium nanoparticles using (b)NaBH₄, (d) Ascorbic Acid, (f) NaHSO₃, (h) PPh₃, (j) NaCNBH₃, (l) Formic Acid, and (n) B₂pin₂ as reducing agents.

3.3.2. Reducing agent concentration

The other studied parameter was the ratio of metal salt to reducing agent (salt: reducing agent). These ratios that were studied included 1/4, 1/40, and 1/400. The results of different ratios of reducing agents for the sample prepared at pH of 7.0 with K₂PdCl₄ salt at 25°C is provided in Table 13.

Table 13. The effect of type and concentration of reducing agent on nanoparticle size.

Reducing agent	Salt: reducing agent		
	1/4	1/40	1/400
NaBH ₄	1.5 ± 0.2	2.4 ± 0.3	1.6 ± 0.2

Confirmed by TEM images (Figure 7a), well-dispersed and spherical palladium nanoparticles were synthesized even using ratio of 1/4 and the average diameter of 1.5 ± 0.2 nm was achieved (Figure 7b). Due to low concentration of reducing agent present in the nanoparticle synthesis process, many metallic ions might not get the chance to reduce and contribute to

nanoparticle production. Also, they did not get the chance to make bigger nanoparticles through nanoparticle-nanoparticle interactions as the process of growth was stopped by consumption of reducing agent in the medium. On the other hand, adding a great amount of reducing agent (1/400 ratio) has lowered the efficiency of the nanoparticle formation process as many nanoparticles were synthesized but their average diameter was 1.6 ± 0.2 nm. This can be attributed to the excess amount of the reducing agents which had increased the nanoparticles formation rate (Figure 7 c and d). Employing the 1/40 ratio, nanoparticles can be formed with average diameter of 2.4 ± 0.3 nm as the amount of reducing agent in the medium was adequate.

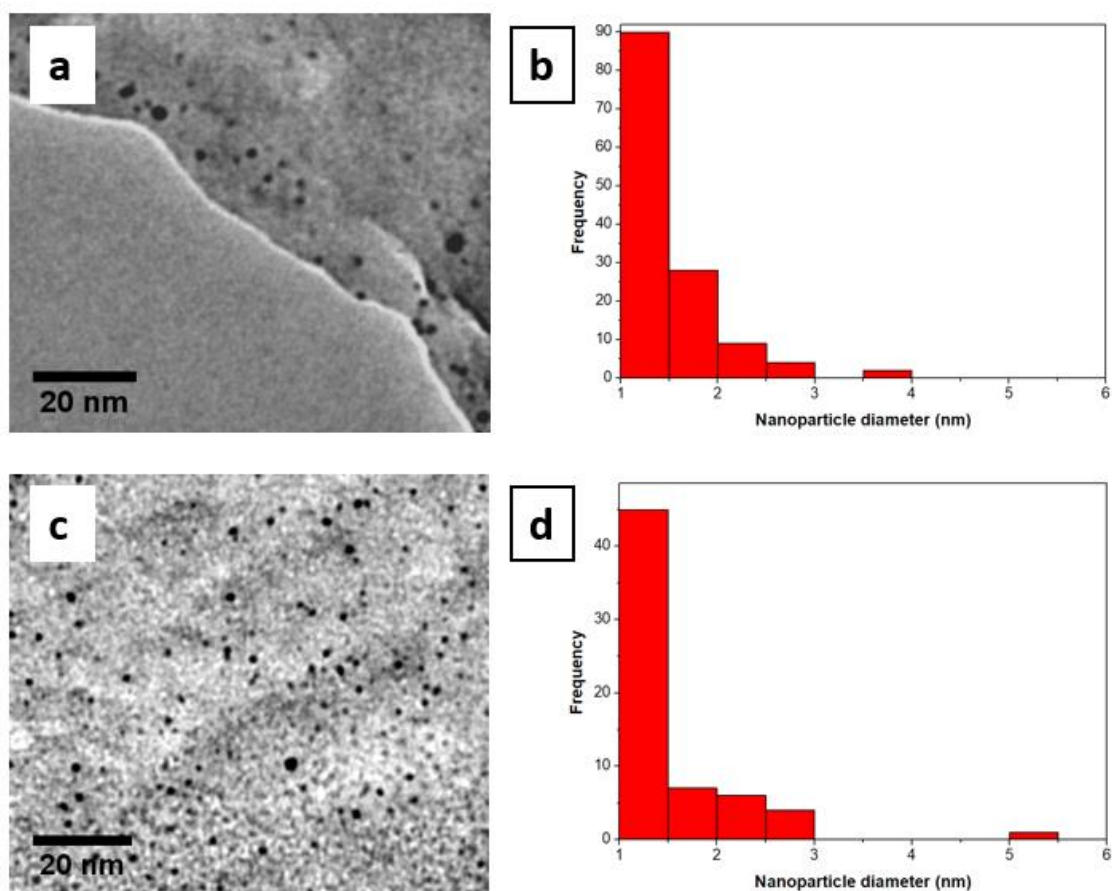


Figure 7. TEM image of recombinant fusion protein-directed palladium nanoparticles using (a) 1/4 ratio and (c) 1/400 ratio. Size histogram of synthesized palladium nanoparticles using (b) 1/4 ratio and (d) 1/400 ratio.

In addition, nanoparticle formation rate was suitable so that they can be grown through Ostwald ripening and nanoparticle-nanoparticle interaction [16,17].

3.3.3. pH of the medium

In chemical reductions approaches, size, morphology, and stability of synthesized nanoparticles highly depend on the pH of the medium. Three sets of experiments were examined in media with different pH of 5.0, 7.0, and 9.0. The results of changing the pH for the sample prepared with K_2PdCl_4 salt and $NaBH_4$ as reducing agent at $25^\circ C$ with salt to reducing agent ratio of 1/40 equivalent is provided in Table 14.

Table 14. The effect of pH change on nanoparticle size.

pH	5.0	7.0	9.0
Nanoparticle diameter(nm)	3 ± 0.4 nm	2.4 ± 0.3 nm	2.0 ± 0.3 nm

The TEM images of prepared palladium nanoparticles using different pH of media are shown in Figure 8. The nanoparticles prepared in the medium with lower pH were found to be larger in size. It can be argued that decreasing the pH caused the anchoring amino acids to be protonated and weaken the bonds between the protein and nanoparticle nuclei. Consequently, the nanoparticles had more chance to grow after the nucleation was initiated and nanoparticle with larger size can be obtained (Figure 8a). On the other hand, increasing the pH of the medium, nanoparticle nuclei were surrounded with fusion proteins and their growth were inhibited (Figure 8c). Also, the reducing agents are pH sensitive and changing the pH affects their yield in the process of nanoparticle formation.

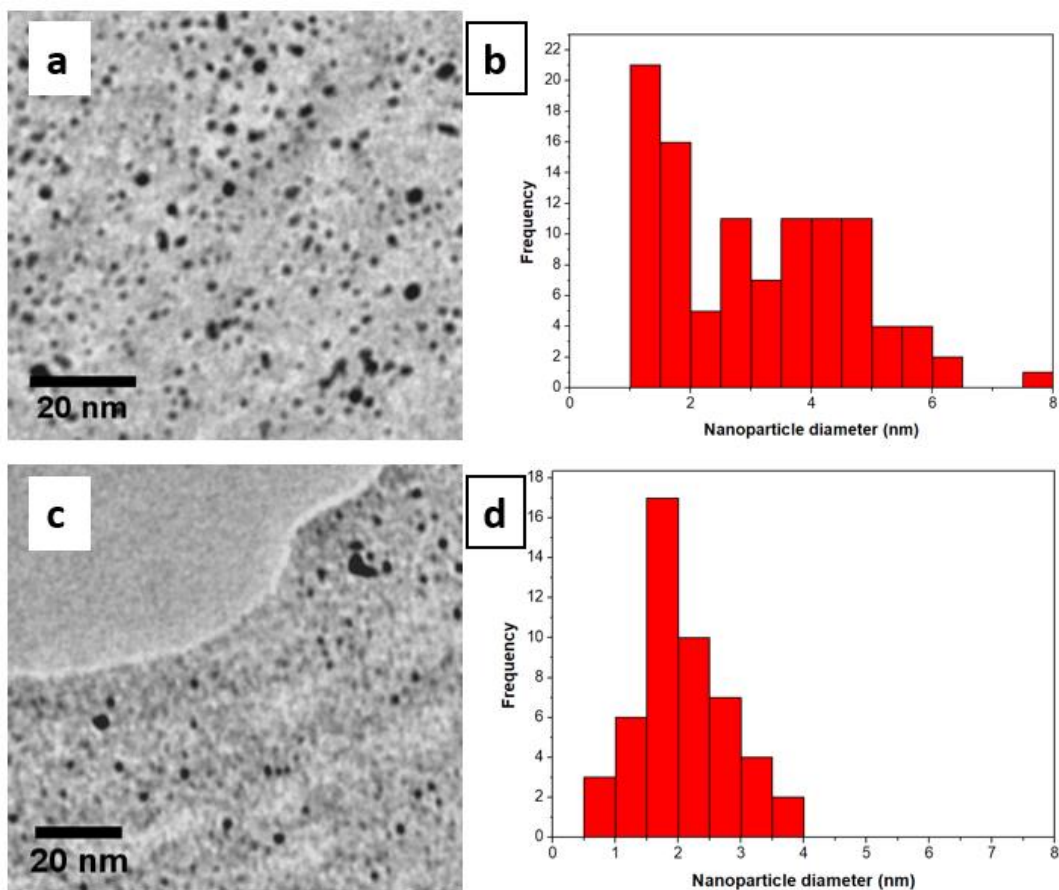


Figure 8. TEM image of recombinant fusion protein-directed palladium nanoparticles using (a)pH of 5.0 and (c) pH of 9.0. Size histogram of synthesized palladium nanoparticles using (b)pH of 5.0 and (d) pH of 9.0.

3.3.4. Temperature

The other parameter that can affect nanoparticle properties is the temperature. Changing the temperature could affect the reactions kinetics and may result in differences in uniformity and properties of nanoparticles. The nanoparticle formation reaction was proceeded under four different temperatures (4°C, 15°C, 20°C and 50°C). The results of different temperature for the sample prepared at pH of 7.0 with K_2PdCl_4 salt with salt to reducing agent ratio of 1/40 equivalent is provided in Table 15.

Table 15. The effect of temperature on nanoparticle size.

Temperature	4 °C	15 °C	25 °C	50 °C
Nanoparticle diameter(nm)	9.4 ± 1.7	5.2 ± 1.3	2.4 ± 0.3	2.0 ± 0.6

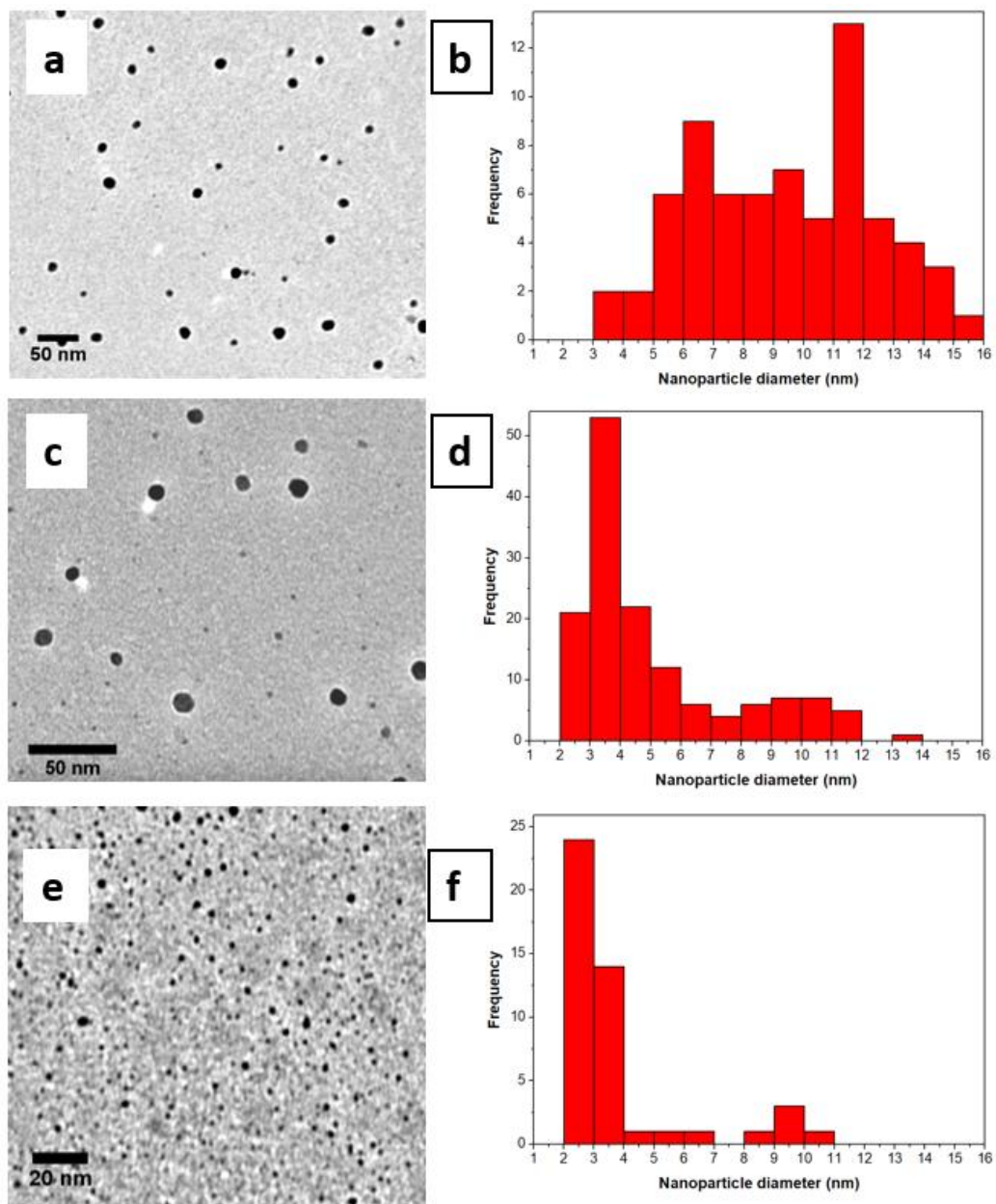


Figure 9. TEM image of palladium nanoparticles prepared at (a) 4 °C, (c) 15 °C, and (e) 50 °C. Size histogram of synthesized palladium nanoparticles prepared at (b) 4 °C, (d) 15 °C, and (f) 50 °C.

The average diameter size of nanoparticles prepared at 4 °C was 9.4 ± 1.7 nm showing that performing the reaction at low temperature caused the lower rate of the reaction including slower consumption of reducing agent and slower rate of nucleation resulted in extending the nanoparticle growth time range. As palladium nanoparticle had more time to grow following Ostwald ripening as well as nanoparticle-nanoparticle interactions, spherical nanoparticles with no aggregation were obtained (Figure 9a). Increasing the temperature of the nanoparticle formation reaction to 15 °C resulted in discrete spherical nanoparticles with average diameter size of 5.2 ± 1.3 nm indicating that consumption rate of reducing agent was increased (Figure 9c). Eventually, well-dispersed spherical nanoparticles with average diameter size of 2.0 ± 0.6 nm were attained as the reaction was performed at 50 °C (Figure 9e).

3.3.5. GFPuv fusion protein type

Different types of protein can be an effective parameter to be investigated as properties-controlled parameter in nanoparticle synthesis. Five different recombinant fusion proteins prepared using *E. coli* as expression host were studied in this work. (Pd4)₃-GFPuv, (Pd4)₁-GFPuv, (A6)₁-GFPuv, (A11)₁-GFPuv, and (A6,11)₁-GFPuv were employed for nanoparticle synthesis. Except (Pd4)₃-GFPuv containing three copies of palladium directed peptide called Pd4, the rest of the proteins contained one copy of peptide fused to the reported protein. Pd4, A6, A11, and A6,11 peptides had 12 amino acids in their structures while their difference is the quantity and position of histidine in their structures. As histidine can anchor to positively charged metallic ions through its imidazole ring, the histidine amino acids in Pd4 structure which exist in 6th and 11th positions were substituted with alanine and A6, A11, and A6,11 peptides were constructed [6]. The other amino acid that can anchor to positively charged metallic ions is

cysteine [18]. As cysteine can be easily oxidized to form a dimer containing disulfide bridge between two cysteines, it is less favorable to be investigated [19]. Thus, four fusion proteins called (Pd4)₁-GFPuv, (A6)₁-GFPuv, (A11)₁-GFPuv, and (A6,11)₁-GFPuv were constructed and used for this experiment. The results of different fusion protein type for the sample prepared at pH of 7.0 with K₂PdCl₄ salt with salt to reducing agent ratio of 1/40 equivalent at room temperature is provided in Table 16. The average nanoparticle size using different fusion proteins remained almost the same while their chemical activities needed be studied for more explanation of the role of fusion proteins on nanoparticles properties.

Table 16. The effect of fusion protein types on nanoparticle size.

Fusion protein type	(Pd4) ₃ - GFPuv	(Pd4) ₁ - GFPuv	(A6) ₁ - GFPuv	(A11) ₁ - GFPuv	(A6,11) ₁ - GFPuv
Nanoparticle diameter(nm)	2.4 ± 0.3	2.6 ± 0.5	2.7 ± 0.7	2.6 ± 0.4	2.8 ± 0.3

A theoretical catalytic study was performed on Pd4, A6, A11, A6,11 showing that prepared palladium nanoparticles with the same size have different catalytic activities. Although peptide-directed nanoparticles using different peptides have almost the same average diameter size, nanoparticle shapes and catalytic sites on the surface of nanoparticles prepared using different peptides are different. Thus, synthesized palladium nanoparticles possessed different catalytic activities [1,6]. The catalytic activity of synthesized palladium nanoparticles was attributed to the total free energy of the peptide due to its different conformation in the medium [6].

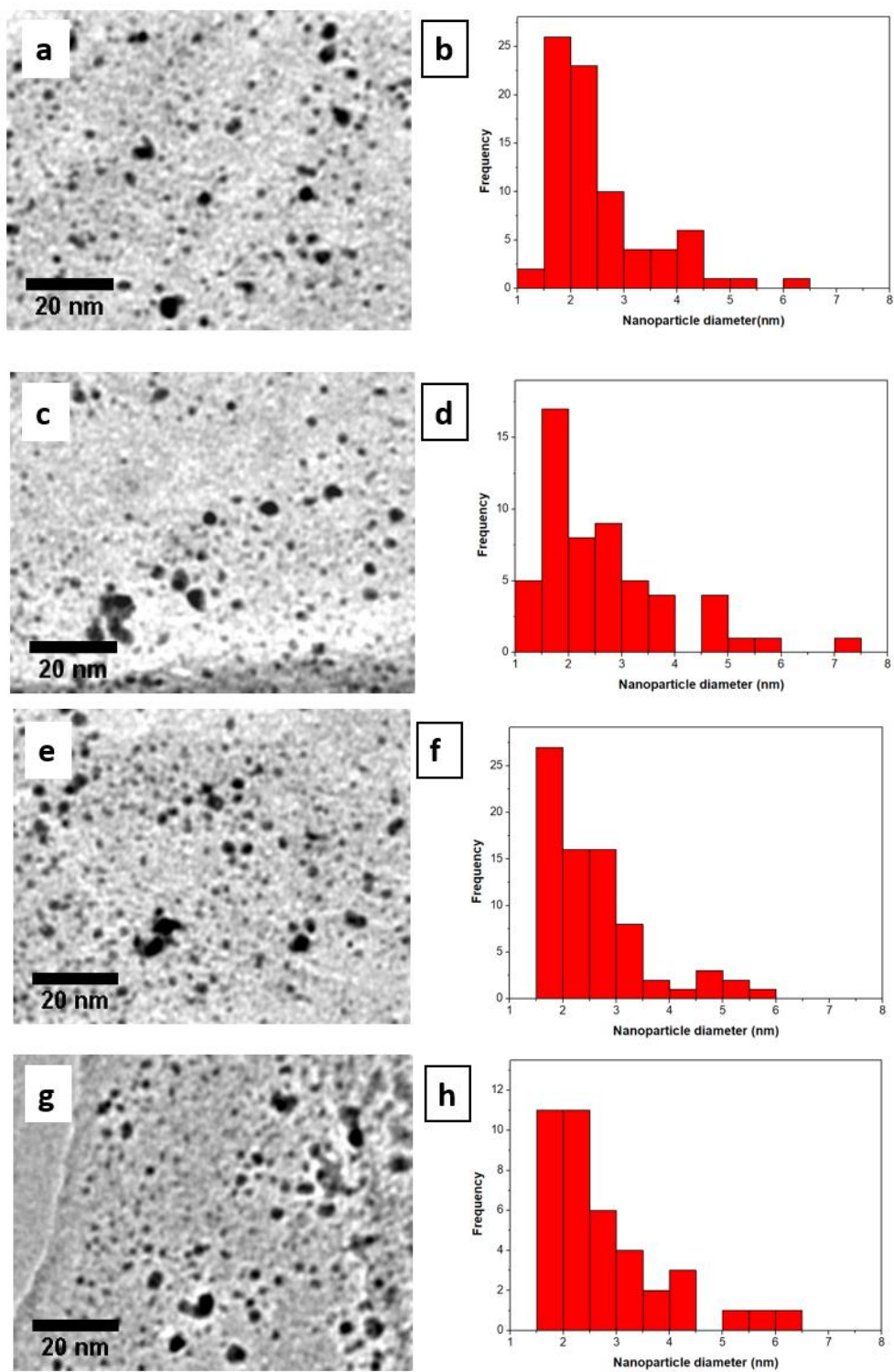


Figure 10. TEM image of palladium nanoparticles prepared using (a) $(Pd_4)_1$ -GFPuv, (c) $(A_6)_1$ -GFPuv, (e) $(A_{11})_1$ -GFPuv, and (g) $(A_6,11)_1$ -GFPuv fusion proteins. Size histogram of synthesized palladium nanoparticles prepared using (b) $(Pd_4)_1$ -GFPuv, (d) $(A_6)_1$ -GFPuv, (f) $(A_{11})_1$ -GFPuv, and (h) $(A_6,11)_1$ -GFPuv fusion proteins.

It is important to note that by fusing peptide containing 12 amino acid to the GFPuv reporter protein containing 238 amino acids, the conformation of the prepared fusion protein could not changes comparing to the peptide holding 12 amino acids. Thus, the peptides free energies are decreased after fusion, yet their catalytic activities should be studied for further analysis. The TEM images and their related size distributions of prepared nanoparticles using different fusion proteins are shown in Figure 10.

3.3.6. Palladium salt

The last parameter that was investigated is the type of palladium salt. Five different types of palladium salt were used for palladium nanoparticle synthesis. The results of using different types of palladium salt for the sample prepared at pH of 7 and NaBH₄ as reducing agent at 25°C with salt to reducing agent ratio of 1/40 equivalent is provided in the Table 17.

Table 17. The effect of palladium salt on nanoparticle size.

Pd salt	K ₂ PdCl ₄	Na ₂ PdCl ₄	PdI ₂	Pd (TFA) ₂
Nanoparticle diameter(nm)	2.4 ± 0.3	2.2 ± 0.3	2.6 ± 0.3	2.4 ± 0.3

The TEM images and their related size distributions of prepared nanoparticles using different palladium are shown in Figure 11. The peptide-directed nanoparticles were spherical and discrete with almost same average diameter size. It can be concluded that type of palladium salt did not have significant impact on the nanoparticles size.

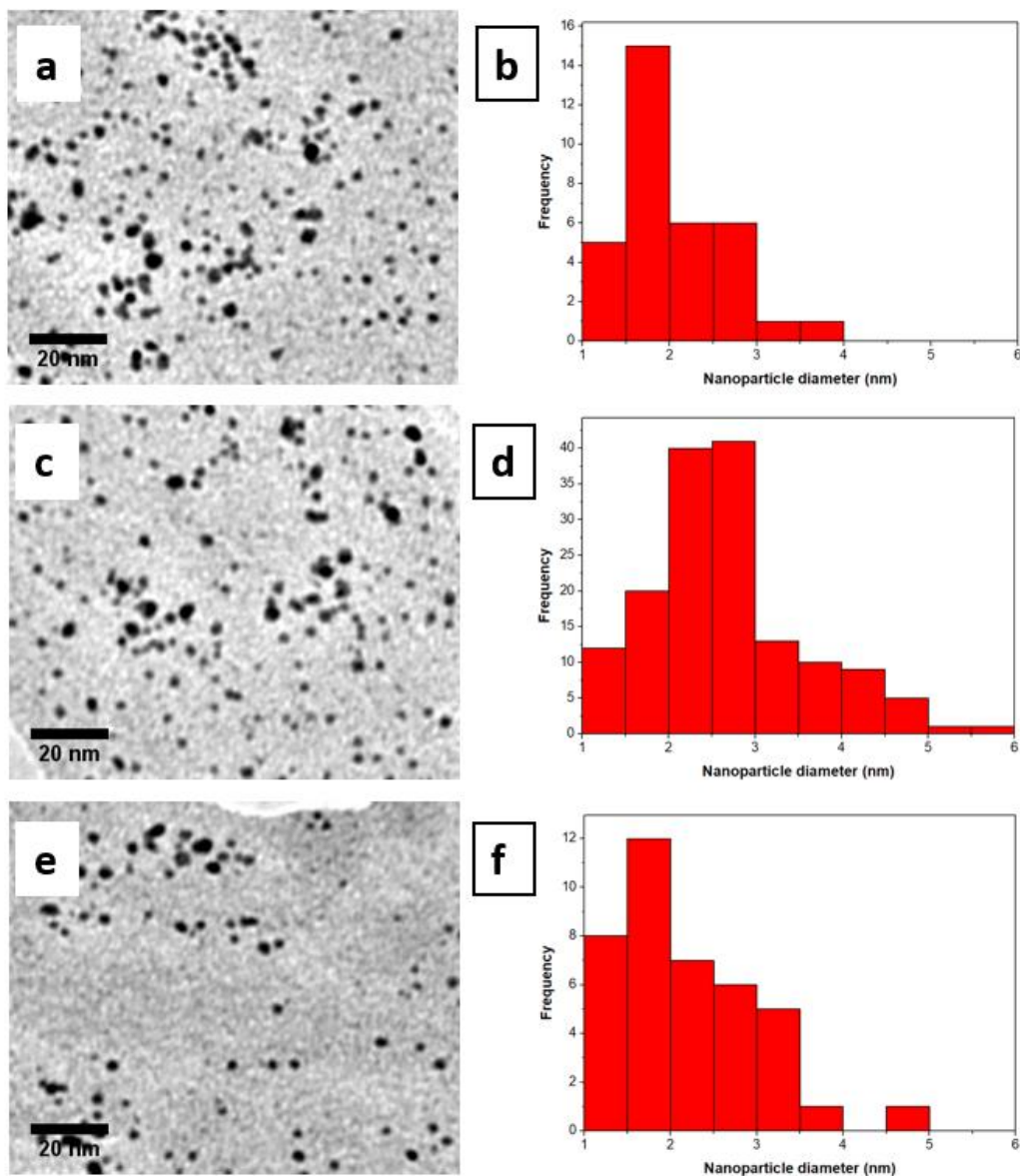


Figure 11. TEM image of palladium nanoparticles prepared using (a) Na_2PdCl_4 , (c) PdI_2 , and (e) $\text{Pd}(\text{TFA})_2$ as palladium salt. Size histogram of synthesized palladium nanoparticles prepared using (b) Na_2PdCl_4 , (d) PdI_2 , and (f) $\text{Pd}(\text{TFA})_2$.

3.3.7. Conclusion

$(\text{Pd}4)_1\text{-GFPuv}$, $(\text{A}6)_1\text{-GFPuv}$, $(\text{A}11)_1\text{-GFPuv}$, and $(\text{A}6,11)_1\text{-GFPuv}$ fusion proteins were successfully constructed using *E. coli* as expression host. A simple aqueous solution phase nanoparticle synthesis approach was exploited in a crude biological protein environment, and the

palladium nanoparticles obtained are similar to those synthesized. The effect of six parameters on nanoparticle size, morphology, and properties were investigated. Comparing to the other parameters, temperature change was found to be the parameter that can be used to prepare nanoparticle within broad range of diameter size from 2 to 10 nms.

3.4. References

- [1] R. Coppage, J.M. Slocik, M. Sethi, D.B. Pacardo, R.R. Naik, M.R. Knecht, Elucidation of peptide effects that control the activity of nanoparticles, *Angew. Chem. Int. Ed.* 49 (2010) 3767–3770.
- [2] A. Jakhmola, R. Bhandari, D.B. Pacardo, M.R. Knecht, Peptide template effects for the synthesis and catalytic application of Pd nanoparticle networks, *J. Mater. Chem.* 20 (2010) 1522–1531.
- [3] D.B. Pacardo, M. Sethi, S.E. Jones, R.R. Naik, M.R. Knecht, Biomimetic synthesis of Pd nanocatalysts for the Stille coupling reaction, *ACS Nano.* 3 (2009) 1288–1296.
- [4] I. Mosleh, M. Benamara, L. Greenlee, M.H. Beyzavi, R. Beitle, Recombinant peptide fusion proteins enable palladium nanoparticle growth, *Mater. Lett.* 252 (2019) 68–71. doi:10.1016/j.matlet.2019.05.080.
- [5] R.B. Pandey, H. Heinz, J. Feng, B.L. Farmer, J.M. Slocik, L.F. Drummy, R.R. Naik, Adsorption of peptides (A3, Flg, Pd2, Pd4) on gold and palladium surfaces by a coarse-grained Monte Carlo simulation, *Phys. Chem. Chem. Phys.* 11 (2009) 1989–2001. doi:10.1039/B816187A.
- [6] N.M. Bedford, H. Ramezani-Dakhel, J.M. Slocik, B.D. Briggs, Y. Ren, A.I. Frenkel, V. Petkov, H. Heinz, R.R. Naik, M.R. Knecht, Elucidation of peptide-directed palladium surface structure for biologically tunable nanocatalysts, *ACS Nano.* 9 (2015) 5082–5092.
- [7] R. Coppage, J.M. Slocik, H. Ramezani-Dakhel, N.M. Bedford, H. Heinz, R.R. Naik, M.R. Knecht, Exploiting Localized Surface Binding Effects to Enhance the Catalytic Reactivity of Peptide-Capped Nanoparticles, *J. Am. Chem. Soc.* 135 (2013) 11048–11054. doi:10.1021/ja402215t.
- [8] A. Mosleh, M. Ehteshamzadeh, R. Taherzadeh Mousavian, Fabrication of an r-Al₂Ti intermetallic matrix composite reinforced with α -Al₂O₃ ceramic by discontinuous mechanical milling for thermite reaction, *Int. J. Miner. Metall. Mater.* 21 (2014) 1037–1043. doi:10.1007/s12613-014-1006-6.
- [9] M.R. Roshan, T.R. Mousavian, H. Ebrahimkhani, A. Mosleh, Fabrication of Al-based composites reinforced with Al₂O₃-TiB₂ ceramic composite particulates using vortex-casting method, *J. Min. Metall. B Metall.* 49 (2013) 299–305. doi:10.2298/JMMB120701032R.
- [10] Permeability enhancement of Escherichia coli by single-walled carbon nanotube treatment - Mosleh - 2017 - *Biotechnology Progress* - Wiley Online Library, (n.d.). <https://onlinelibrary.wiley.com/doi/abs/10.1002/btpr.2443> (accessed April 1, 2019).
- [11] A.L. Isfahani, I. Mohammadpoor-Baltork, V. Mirkhani, A.R. Khosropour, M. Moghadam, S. Tangestaninejad, R. Kia, Palladium Nanoparticles Immobilized on Nano-Silica Triazine Dendritic Polymer (Pdnp-nSTDP): An Efficient and Reusable Catalyst for Suzuki–Miyaura Cross-Coupling and Heck Reactions, *Adv. Synth. Catal.* 355 (2013) 957–972. doi:10.1002/adsc.201200707.

- [12] N. Punna, K. Harada, N. Shibata, Stille cross-coupling of secondary and tertiary α -(trifluoromethyl)-benzyl chlorides with allylstannanes, *Chem. Commun.* 54 (2018) 7171–7174. doi:10.1039/C8CC03541E.
- [13] W. Zhang, Q. Qin, L. Dai, R. Qin, X. Zhao, X. Chen, D. Ou, J. Chen, T.T. Chuong, B. Wu, N. Zheng, Electrochemical Reduction of Carbon Dioxide to Methanol on Hierarchical Pd/SnO₂ Nanosheets with Abundant Pd–O–Sn Interfaces, *Angew. Chem. Int. Ed.* 57 (2018) 9475–9479. doi:10.1002/anie.201804142.
- [14] M. Bao, I.S. Amiin, T. Peng, W. Li, S. Liu, Z. Wang, Z. Pu, D. He, Y. Xiong, S. Mu, Surface Evolution of PtCu Alloy Shell over Pd Nanocrystals Leads to Superior Hydrogen Evolution and Oxygen Reduction Reactions, *ACS Energy Lett.* 3 (2018) 940–945. doi:10.1021/acsenergylett.8b00330.
- [15] P.G. Andersson, I.J. Munslow, *Modern Reduction Methods*, John Wiley & Sons, 2008.
- [16] R.W. Lodge, G.A. Rance, M.W. Fay, A.N. Khlobystov, Movement of palladium nanoparticles in hollow graphitised nanofibres: the role of migration and coalescence in nanocatalyst sintering during the Suzuki–Miyaura reaction, *Nanoscale.* 10 (2018) 19046–19051. doi:10.1039/C8NR05267K.
- [17] S.F. Tan, G. Bisht, U. Anand, M. Bosman, X.E. Yong, U. Mirsaidov, In Situ Kinetic and Thermodynamic Growth Control of Au–Pd Core–Shell Nanoparticles, *J. Am. Chem. Soc.* 140 (2018) 11680–11685. doi:10.1021/jacs.8b05217.
- [18] Y. Li, J. Cheng, J. Li, X. Zhu, T. He, R. Chen, Z. Tang, Tunable Chiroptical Properties from the Plasmonic Band to Metal–Ligand Charge Transfer Band of Cysteine-Capped Molybdenum Oxide Nanoparticles, *Angew. Chem. Int. Ed.* 57 (2018) 10236–10240. doi:10.1002/anie.201806093.
- [19] J.A. Dunkle, M.R. Bruno, F.W. Outten, P.A. Frantom, Structural Evidence for Dimer-Interface-Driven Regulation of the Type II Cysteine Desulfurase, SufS, *Biochemistry.* 58 (2019) 687–696. doi:10.1021/acs.biochem.8b01122.

Chapter 4. Recombinant peptide fusion proteins enable palladium nanoparticle growth

The following chapter has been published as “Featured Letter” in Materials Letters Journal (ISSN: 0167-577X). This chapter is presented as the verbatim reproduction of the published letter.

Recombinant peptide fusion proteins enable palladium nanoparticle growth

Imann Mosleh (1),

Mourad Benamara (2),

Lauren Greenlee (1),

M. Hassan Beyzavi (3),

Robert Beitle (1) *

(1) Ralph E. Martin Department of Chemical Engineering, University of Arkansas, Fayetteville, Arkansas 72701, USA.

(2) Institute for Nanoscale Materials Science and Engineering, University of Arkansas, Fayetteville, Arkansas 72701, USA.

(3) Department of Chemistry and Biochemistry, University of Arkansas, Fayetteville, Arkansas 72701, USA.

Corresponding Author

* Robert Beitle (rbeitle@uark.edu).

3202 Bell Engineering Center, University of Arkansas,

Fayetteville AR 72701 USA.

Abstract

The soluble fraction of bacterial lysates containing repeat units of a metal binding domain (Pd4) fused to the carrier protein Green Fluorescent Protein was used to direct palladium nanoparticle synthesis on the order of 2 nm. Characterization confirmed the synthesis of highly ordered materials, as evident by microscopy and elemental analysis, demonstrating the fact that crude bacterial lysates containing fusion peptides may be used in lieu of expensive, pure peptide.

Keywords Recombinant protein, Palladium nanoparticles, Pd4 peptide

4.1. Introduction.

Nanoparticles (NPs) often show unique physical and chemical properties due to their crystallinity, phase, morphology and structure. These properties are advantageous for applications in electronics, catalysis, composite design, drug delivery, and biopharmaceuticals [1–6]. Researchers have been inspired by biological systems that order structures in nature, resulting in NP fabrication employing short peptide sequences to direct the assembly, composition, and structure of inorganic NPs and hybrid bioinorganic NPs [7,8].

Rather than using peptides of a high degree of purity to direct NP formation, we tested the use of amino acid sequences that are biologically inhomogeneous in terms of purity and composition. Since recombinant sources can be one to two orders of magnitude less expensive when compared to chemically synthesized peptides, biologically produced sequences will be cost effective in the synthesis of NPs. We recently demonstrated this approach with the palladium (Pd) metal binding sequence Pd4 (TSNAVHPTLRHL) [9]. Extending this work to fully characterize Pd NPs created with crude *Escherichia coli* lysate containing (Pd4)₃-GFPuv is the subject of this report, where we show that highly ordered NPs can be created using crude lysate as a source of multimeric Pd4.

4.2. Experimental Methods

4.2.1. Fusion Protein Preparation

An arabinose inducible plasmid that codes for (Pd4)₃-GFPuv was recently constructed by Tejada Vaprio *et al.* [9]. Bacterial lysates were obtained from cells induced with arabinose and grown in LB medium containing 50 µg/mL ampicillin. Cells (15–20 g) were resuspended in 40 mL of deionized water and then lysed for 30 minutes on ice using a Q125 Sonicator at 40% amplitude with 10 secs. pulse and 5 secs. rest. After sonication the samples were centrifuged to

remove insoluble material. Total concentration of protein in a sample was determined using the DC Protein Assay (Bio-Rad, Hercules, CA).

4.2.2. Palladium Nanoparticle Synthesis

A method adapted from Pacardo *et al.* was followed to synthesize palladium nanoparticles at room temperature [3]. Synthesis mixtures (one milliliter total volume) contained 0.16 mg K_2PdCl_4 , 0.23 mg $(Pd_4)_3$ -GFPuv, and 1.5 mg $NaBH_4$. These amounts result in a ratio of Pd^{+2} to Pd_4 equal to 2 [3]. The reducing agent was added thirty minutes after the metal salt and lysate were mixed. Reduction of Pd^{2+} to Pd^0 was indicated by a color change (yellow to light brown).

The NP growth mechanism and size distribution analysis were investigated using TEM and HRTEM. Ten microliter samples of the reaction mixture were taken periodically and immediately placed on a 300 mesh standard lacey carbon grid. Measurements with an FEI Titan 80–300 determined NP size distribution and morphology. HRTEM images were used to determine the d-spacing of crystal lattices. Analysis of the images was performed using ImageJ software.

4.3. Results and Discussion.

Extracts of soluble protein contained approximately 10% $(Pd_4)_3$ -GFPuv, with SDS-PAGE (graphical abstract) indicating the heterogeneity of the lysate. Multiple bands from proteins of differing molecular weight and concentration were observed. Indeed, there are approximately fifteen distinct species in the lysate including $(Pd_4)_3$ -GFPuv. When reducing agent was added to a solution containing lysate and Pd salt, nanoparticles were formed.

TEM images shown in Figure 1 are representative of synthesized Pd NPs with average diameters ranging from 1.52 ± 0.61 to 2.37 ± 0.70 nm. TEM images of the synthesized Pd NPs indicated discrete and almost spherical particles (aspect ratio close to 1) with an absence of the formation of large aggregates. A representative EDX spectrum of the Pd NPs is shown in Figure 1g, with Pd peak located at 3.3 keV. All NP samples were evaluated with EDX and similar spectra were obtained. The peak of oxygen resulted, at least in part, from the organic materials (peptides and proteins) deposited on the grid. Lastly, the peaks of copper and carbon originated from the use of the lacey carbon grid that held the NPs.

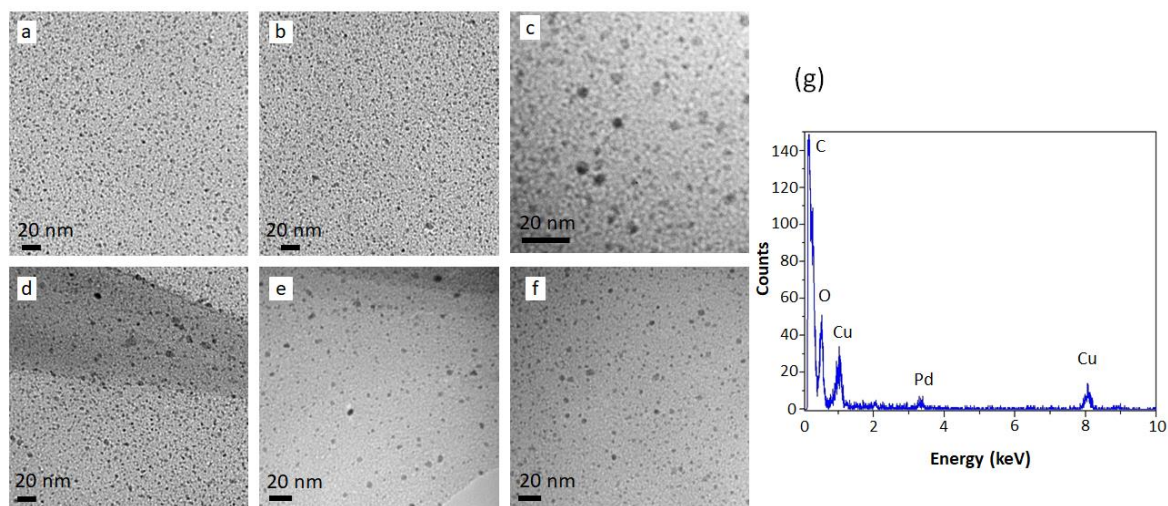


Figure 1. TEM of Pd NPs at (a) 10, (b) 20, (c) 40, (d) 80, (e) 120, and (f) 240 secs. Representative EDX spectrum (240 secs).

Areas for 150–300 individual NPs were obtained from each image and an effective size of $d = 2 \times \sqrt{\frac{A}{\pi}}$ was used to calculate the diameter, where A is measured area of the particle. Histograms of particle diameters for a given time may be found in the SI. A graph of the trajectory of average NP size was prepared to describe growth (Figure 2a). The average diameter of the NPs increased rapidly in the first few secs. as Pd atoms organized into clusters and smaller

NPs, with the rate of change in diameter decreasing at later times. Larger diameter NPs were the result of coalescence, Ostwald ripening and oriented attachment (OA) as observed in Figures 3b–d [10,11].

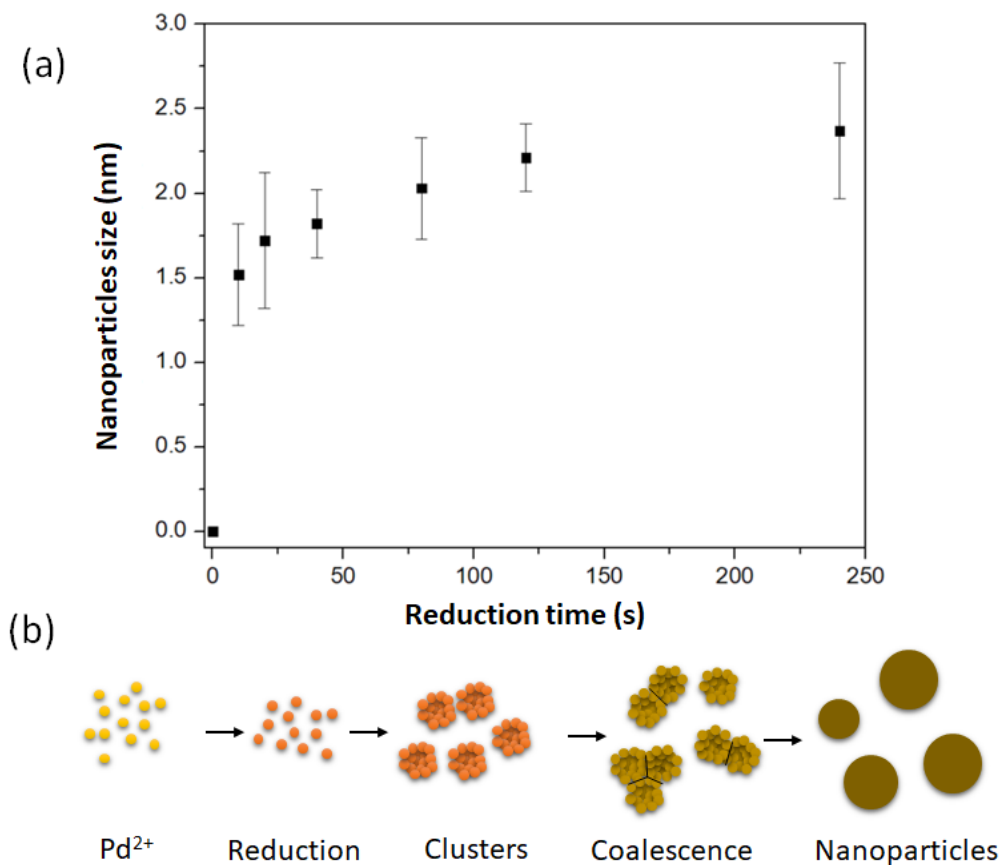


Figure 2. (a) Average NP diameter versus reaction time. Times correspond to times (a–f) identified in Figure 1. (b) Proposed schematic of NP growth.

Figure 3a is a HRTEM image of an individual Pd NP where lattice fringes are clearly visible. The measured spacing between fringes is 2.24 Å which corresponds well with the spacing between (111) plane of cubic Pd [12]. Fast Fourier Transformation (FFT) of the HRTEM data is represented in the inset of Figure 3a and it confirms the crystalline nature of this NP. HRTEM images (Figures 3b–d) showed NPs, obtained by means of coalescence (Figure 3b-d),

OA (Figure 3c-d), with particles in the process of changing shape and morphology to minimize total free energy [13]. In Figure 3b, adjacent NPs were likely in the process of rotation and alignment to fuse through the observed (111) facet along the long axis. In Figure 3c, alignment had taken place along a common crystallographic direction and OA was observed. Eventually, particles could adopt a configuration or shape like Figures 3a with an aspect ratio close to unity. In Figure 3d, two fused Pd particles are visible. The bottom one is imaged along $\langle 112 \rangle$ making both (111) and (022) planes visible. While a boundary is seen in Figure 3d, the lack of observed boundary in Figure 3a indicated Ostwald ripening at an advanced stage (small nanoparticle fused to larger nanoparticle).

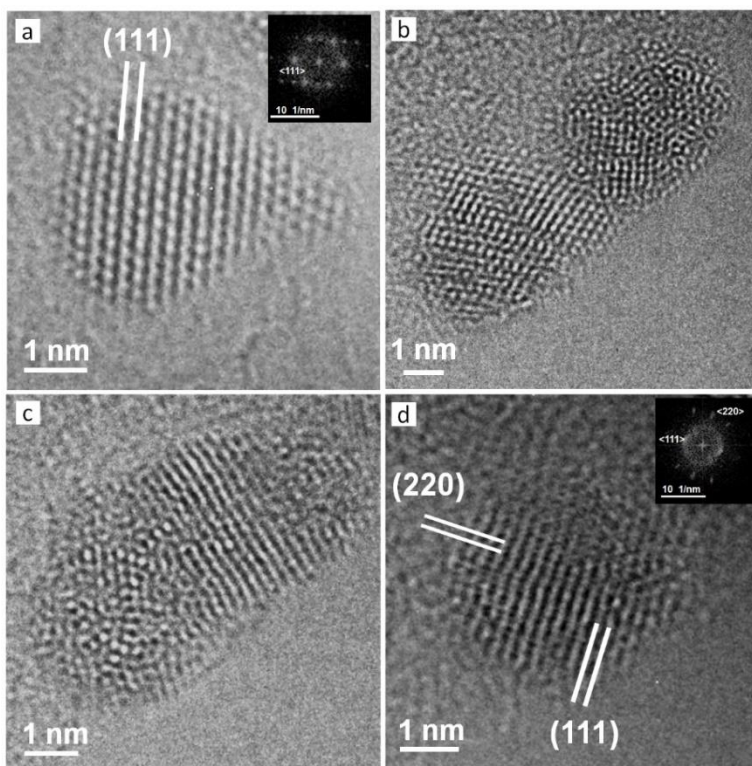


Figure 3. HRTEM and FFT analysis NPs (240 secs.) (a) The lattice planes (111) are observed. NPs in the process of (b) coalescence, (c) oriented attachment, and (d) formation of bicrystals with (111) and (220) planes identified, respectively.

When NPs are formed in the presence of Pd⁴, there are likely many independent nucleation sites due to the coordination of Pd⁺² by the peptide, in contrast to a peptide free environment where metal ions may easily associate prior to, and during, reduction. The former provides an ensemble containing a lower total free energy. Consequently, a greater number of minimum sized NPs survive after making the first clusters. These observations are consistent with literature that describe small NP growth, and unlike previous studies with fusion peptides, generate material two orders of magnitude smaller than previously reported [14-17]. Once a cluster achieves the minimum critical size at which a particle can survive dissolution, the NP is formed by simple growth and coalescence of smaller clusters.

4.4. Conclusion

In this study, highly ordered NPs using biological templates were prepared without the costly purification of a peptide. It represents a paradigm shift in the preparation of highly ordered materials because the heterogeneous nature of the synthesis did not preclude the formation of small nanoparticles. Future work includes the use of these nanoparticles in representative catalytic applications that include ammonia synthesis and the production of chemical intermediates of high value.

Acknowledgement. The authors appreciate the use of the Nano & Bio Materials Characterization Facility at the University of Arkansas. The authors thank Dr. Elmasheiti and R. Tejada Vaprio for their assistance. This work was funded by the Arkansas Bioscience Institute and the University of Arkansas.

4.5. References

- [1] M. Nathanson, K. Kanhaiya, J. Alan Pryor, J. Miao, H. Heinz, Atomic-Scale Structure and Stress Release Mechanism in Core–Shell Nanoparticles, *ACS Nano*. 12 (2018) 12296–12304. doi:10.1021/acsnano.8b06118.
- [2] A. Mosleh, M. Ehteshamzadeh, R. Taherzadeh Mousavian, Fabrication of an r-Al₂Ti intermetallic matrix composite reinforced with α -Al₂O₃ ceramic by discontinuous mechanical milling for thermite reaction, *Int. J. Miner. Metall. Mater.* 21 (2014) 1037–1043. doi:10.1007/s12613-014-1006-6.
- [3] D.B. Pacardo, M. Sethi, S.E. Jones, R.R. Naik, M.R. Knecht, Biomimetic Synthesis of Pd Nanocatalysts for the Stille Coupling Reaction, 3 (2009) 1288–1296. doi:10.1021/nm9002709.
- [4] A. Mosleh, H. Shahverdi, R. Poursalehi, Characterization of Al-CNT Composite Nanoparticles Synthesized by Electrical Explosion of Wire in Acetone, *Adv. Mater. Eng.* 35 (2016) 47-53. DOI: 10.18869/acadpub.jame.35.2.47.
- [5] M.R. Roshan, T.R. Mousavian, H. Ebrahimkhani, A. Mosleh, Fabrication of Al-based composites reinforced with Al₂O₃-TiB₂ ceramic composite particulates using vortex-casting method, *J. Min. Metall. B Metall.* 49 (2013) 299–305. doi:10.2298/JMMB120701032R.
- [6] A. Mosleh, A. Heintz, K. Lim, J. Kim, R. Beitle, Permeability enhancement of Escherichia coli by single-walled carbon nanotube treatment, *Biotechnol. Progr.* 33 (2017) 654–657. DOI: 10.1002/btpr.2443.
- [7] N.M. Bedford, A.R. Showalter, T.J. Woehl, Z.E. Hughes, S. Lee, B. Reinhart, S.P. Ertem, E.B. Coughlin, Y. Ren, T.R. Walsh, B.A. Bunker, Peptide-Directed PdAu Nanoscale Surface Segregation: Toward Controlled Bimetallic Architecture for Catalytic Materials *ACS Nano* 10 (2016) 8645–8659. doi:10.1021/acsnano.6b03963.
- [8] S. Chen, Z. Yang, A. Wang, K. Fang, J. Feng, Facile synthesis of bimetallic gold-palladium nanocrystals as effective and durable advanced catalysts for improved electrocatalytic performances of ethylene glycol and glycerol oxidation, *J. Colloid, Interf. Sci.* 509 (2018) 10-17. DOI: 10.1016/j.jcis.2017.08.063.
- [9] R. Tejada Vaprio, Theses and Dissertations, Peptide-directed Nanoparticle Synthesis With A Denovo Pd-binding Sequence Fused To A Reporter Protein, University of Arkansas (2017) 2393.
- [10] G. Collins, M. Schmidt, G.P. McGlacken, C. O'Dwyer, J.D. Holmes, Stability, Oxidation, and Shape Evolution of PVP-Capped Pd Nanocrystals, *J. Phys. Chem. C.* 118 (2014) 6522–6530. DOI: 10.1021/jp500716z.
- [11] C. Zhu, S. Liang, E. Song, Y. Zhou, W. Wang, F. Shan, Y. Shi, C. Hao, K. Yin, T. Zhang, J. Liu, H. Zheng, L. Sun, In-situ liquid cell transmission electron microscopy

investigation on oriented attachment of gold nanoparticles, *Nat. Commun.* 9 (2018) 421. doi:10.1038/s41467-018-02925-6.

[12] P. Grammatikopoulos, C. Cassidy, V. Singh, M. Sowwan, Coalescence-induced crystallisation wave in Pd nanoparticles, *Sci. Rep.* 4 (2014) 5779. DOI: 10.1038/srep05779.

[13] G. Wang, E.R. Batista, P. Yang, Ligand induced shape transformation of thorium dioxide nanocrystals, *Phys. Chem. Chem. Phys.* 20 (2018) 17563–17573. doi:10.1039/C8CP00240A.

[14] N.T. Thanh, N. Maclean, S. Mahiddine, Mechanisms of Nucleation and Growth of Nanoparticles in Solution, *Chem. Rev.* 114 (2014) 7610–7630. DOI: 10.1021/cr400544s.

[15] T.T. Olmez, E. Yuca, E. Eyupoglu, H.B. Catalak, O. Sahin, U.O. Safak, Autonomous Synthesis of Fluorescent Silica Biodots Using Engineered Fusion Proteins, *ACS Omega*, 3 (2018) 585-594. DOI: 10.1021/acsomega.7b01769.

[16] W.D. Marnier, A.S. Shaikh, S.J. Muller, J.D. Keasling, Enzyme immobilization via silaffin-mediated autoencapsulation in a biosilica support, *Biotechnol. Prog.* 25 (2009) 417–423. doi:10.1002/btpr.136.

[17] D.H. Nam, K. Won, Y.H. Kim, B.I. Sang, A novel route for immobilization of proteins to silica particles incorporating silaffin domains, *Biotechnol. Prog.* 25 (2009) 1643–1649. doi:10.1002/btpr.261.

4.6. Supporting Information

Recombinant peptide fusion proteins enable palladium nanoparticle growth

Imann Mosleh^a, *Mourad Benamara*^b, *Lauren Greenlee*^a, *M. Hassan Beyzavi*^c, *Robert Beitle*^{a,*}

^a Ralph E. Martin Department of Chemical Engineering, University of Arkansas, Fayetteville, Arkansas 72701, USA

^b Institute for Nanoscale Materials Science and Engineering, University of Arkansas, Fayetteville, Arkansas 72701, USA

^c Department of Chemistry and Biochemistry, University of Arkansas, Fayetteville, Arkansas 72701, USA

Corresponding Author

* Robert Beitle (rbeitle@uark.edu)

Address: 3202 Bell Engineering Center, University of Arkansas, Fayetteville AR 72701 USA.

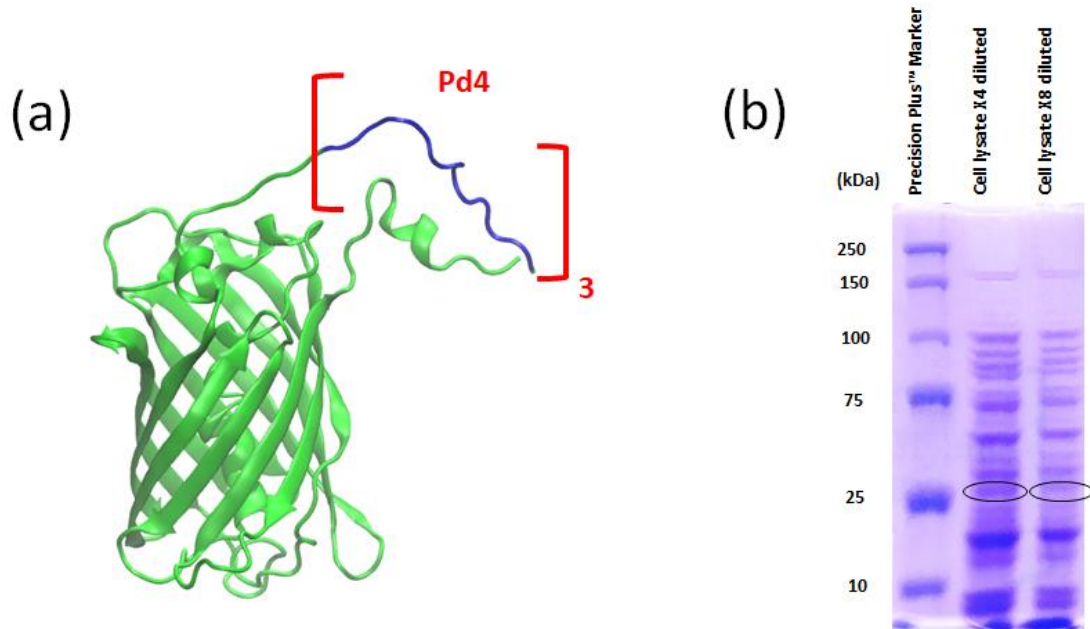


Figure S1. Strategy of fusion peptide directed NP formation. (a) Illustration of $(Pd4)_3$ -GFPuv, where the N-terminus extension of the reporter protein has three copies of Pd4. (b) The fusion protein $(Pd4)_3$ -GFPuv is contained in a bacterial lysate, as indicated by SDS-PAGE (lanes contain MW markers and two dilutions of extract, respectively, with $(Pd4)_3$ -GFPuv circled).

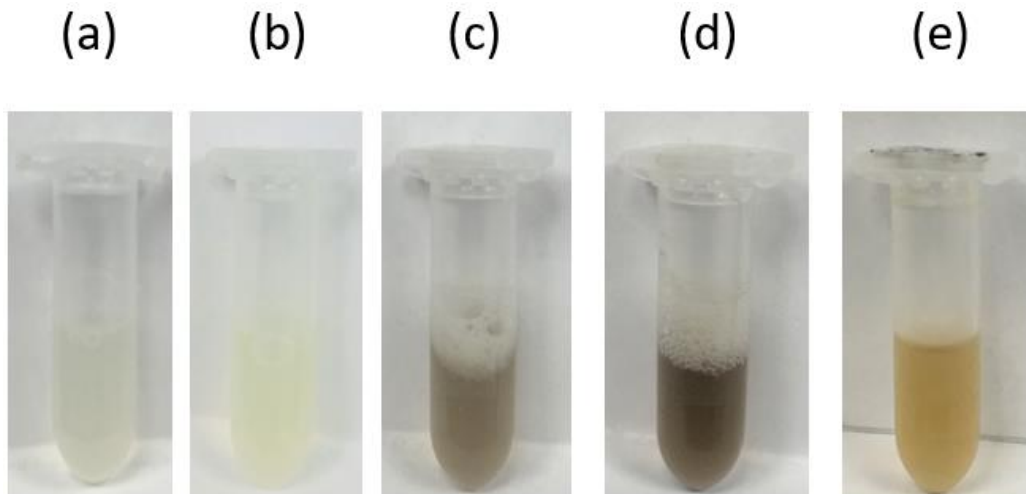


Figure S2. The control tubes presenting each step of nanoparticle formation. (a) reaction mixture of water and lysate containing (Pd4)₃-GFP protein before adding K₂PdCl₄ and NaBH₄ (b) reaction mixture before adding NaBH₄ (c) reaction mixture 10 secs. after adding NaBH₄ (d) reaction mixture 10 mins. after adding NaBH₄ (e) reaction mixture of water and lysate containing only GFP protein 10 mins. after adding NaBH₄.

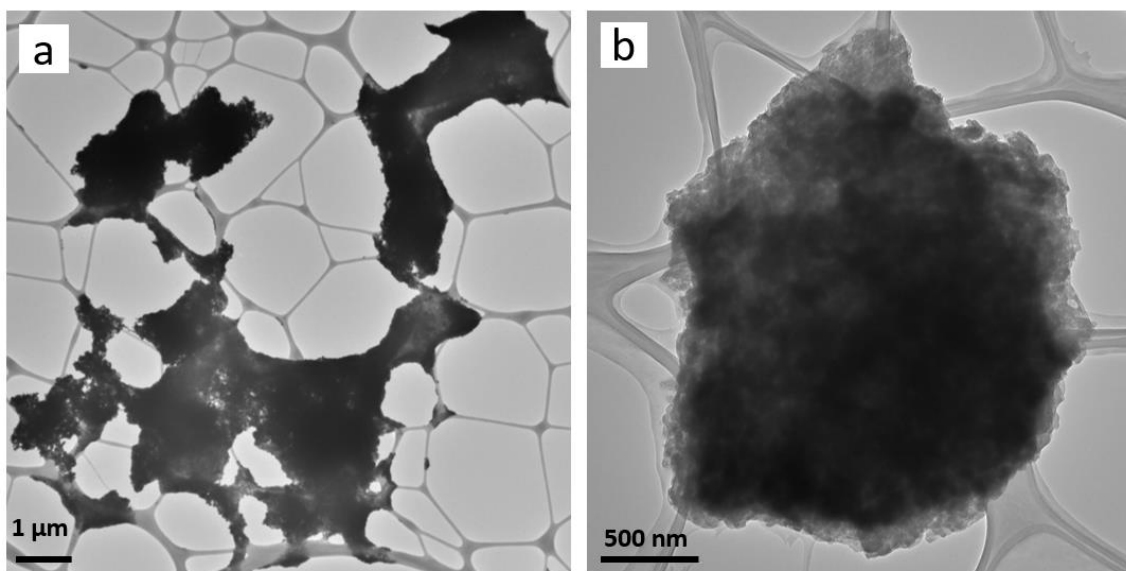


Figure S3. TEM of synthesized particles (a) using lysate without (Pd4)₃-GFPuv protein and (b) lysate containing GFPuv protein.

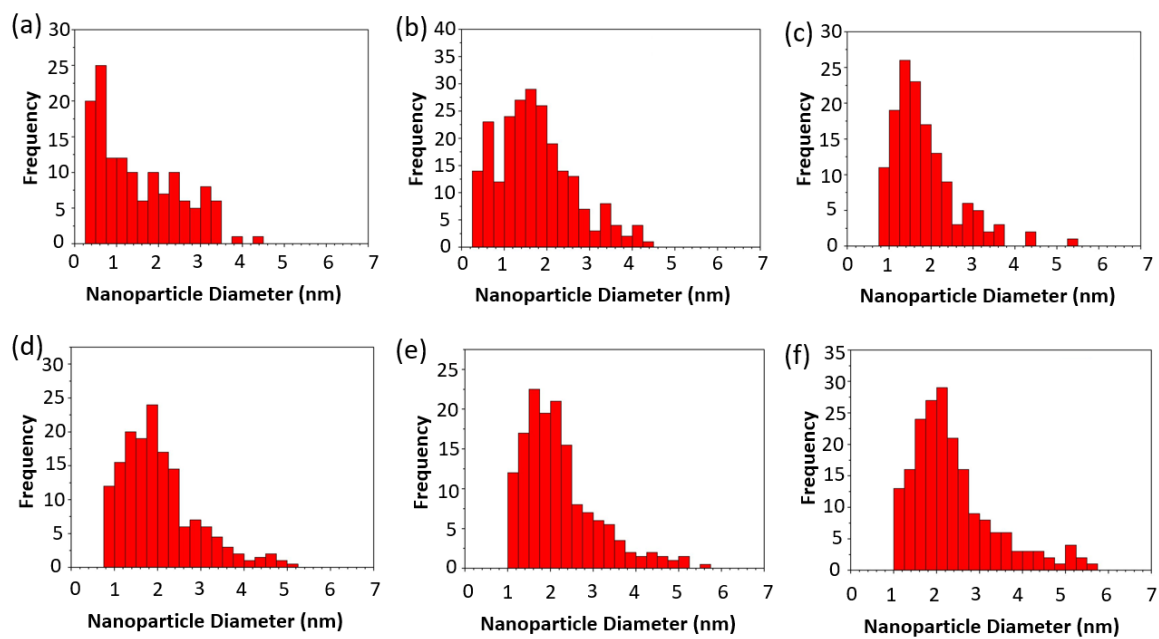


Figure S4. Diameter analysis of NPs. Size histograms of synthesized Pd NPs correspond to times (a–f) identified in the caption of Figure 1 in the main manuscript.

Chapter 5. Recombinant peptide fusion protein-templated palladium nanoparticles for Suzuki-Miyaura coupling and Stille coupling reactions

The following chapter will be submitted to the Journal of American Chemical Society (ISSN: 0002-7863). This chapter is presented in manuscript form.

Recombinant peptide fusion protein-templated palladium nanoparticles for Suzuki-Miyaura coupling and Stille coupling reactions.

Imann Mosleh¹,

Rita Tejada Vaprio¹,

Rudra Palash Mukherjee¹,

McKinzie Fruchtl²,

Nicholas Bedford³,

Hamidreza Shahsavari⁴,

Lauren Greenlee¹,

M. Hassan Beyzavi^{4*},

Robert Beitle^{1*}

(1) Ralph E. Martin Department of Chemical Engineering, University of Arkansas, Fayetteville, Arkansas 72701, USA.

(2) Boston Mountain Biotech, LLC, 700 W Research Center Blvd, Fayetteville, AR 72701, USA.

(3) Materials and Manufacturing Directorate, Air Force Research Laboratory, 5135 Pearson Road, Building 10, Wright-Patterson AFB, OH 45433, USA.

(4) Department of Chemistry and Biochemistry, University of Arkansas, Fayetteville, Arkansas 72701, USA.

***corresponding authors**

beyzavi@uark.edu

Department of Chemistry and Biochemistry,

University of Arkansas,

Fayetteville AR 72701

(479) 575-2083

rbeitle@uark.edu

3202 Bell Engineering Center

University of Arkansas

Fayetteville AR 72701

(479) 575-4951

Abstract

Although peptide-enabled synthesis of nanostructures has garnered considerable interest for use in catalytic applications, it has so far been achieved mostly via Fmoc based solid phase peptide synthesis. Consequently, the potential of longer peptides in nanoparticle synthesis have not been explored largely due to the complexities and economic constraints of this chemical synthesis route. This study examines the potential of a 45-amino acid long peptide expressed as fusion to Green Fluorescence Protein (GFPuv) in *Escherichia coli* for use in palladium nanoparticle synthesis. Fed-batch fermentation with *E. coli* harboring an arabinose-inducible plasmid produced a peptide containing three copies of Pd4 peptide fused to N-terminus of GFPuv ((Pd4)₃-GFPuv). Using the intrinsic fluorescence of GFPuv, expression and enrichment of the fusion product was easily monitored. Crude lysate, desalted lysate and an ion-exchange enriched fraction containing (Pd4)₃-GFPuv were used to test the hypothesis that high purity of the biologic material used as the nanoparticle synthesis template may not be necessary. Nanoparticles were characterized using transmission electron microscope (TEM), energy-dispersive X-ray spectroscopy (EDS). Results demonstrate that palladium nanoparticles can be synthesized using the soluble cell extract containing (Pd4)₃-GFPuv without extensive purification or cleavage steps – a highly attractive prospect from both scientific and economic standpoints.

Keywords: Palladium nanoparticles, Peptides, Bio-templated synthesis

5.1. Introduction

Nanoparticles (NPs) receive much attention due to their unique chemical, physical, and mechanical properties arising from their crystallinity, phase, morphology, and structure. These properties which are distinct from those of bulk materials enable them for a diverse set of applications, including catalysis, composite design, drug delivery, and biopharmaceuticals [1–10]. Since NPs properties are highly depended on their morphology and size, the approach toward NPs synthesis has becomes an important research subject for nanoscience experts. Various methods have been developed employing bottom-up approach in solution phase with the main backbone of dendritic architectures and surface capping ligands. On the other hand, bounding nanoparticles to specific size and shape were achieved using hollow structures, metal-coordination complexes, and organic molecular cages. Unfortunately, these methods were either expensive or unable to eliminate the challenge toward property-controllable synthesis of nanoparticles with narrow size distribution. Recently, researchers have been mimicing biological systems that order structures in nature, resulting in using short peptide sequences for NP synthesis in order to direct the assembly, composition, and structure as well as control the growth and properties of inorganic NPs and hybrid bioinorganic NPs [11].

The singular roadblock to widespread development and commercialization of peptide-directed NP synthesis platforms is the high cost of chemically-synthesized peptides. For example, it would be cost prohibitive to manufacture precious NPs such as platinum or palladium, where the metals are valued at \$200 - \$2,000 per gram when the peptide costs normally exceed \$10,000 per gram. Such a differential is even more exacerbating for a nonprecious nanoparticle or when the peptide length grows to incorporate multiple functional domains. Technical challenges to both chemical and recombinant peptide synthesis approaches

have slowed deployment in scale-up applications. Chemical approaches to building peptides have length constraints, and recombinant approaches suffer from purification issues after expression [12].

Any proposed method for the cost-effective production of peptide(s) for nanoparticle synthesis must recognize the necessity of expression with a high degree of fidelity while providing a minimalist approach to peptide purification. We hypothesized that peptides capable of tuning nanoparticle morphology can direct synthesis in an environment that contains remnants of the fermentation process. The degree of purity with respect to the concentration and the nature of contaminating material (proteins, DNA, RNA, medium components) has not, to our knowledge, been extensively explored because in contrast to most biochemical engineering applications, the purity requirement of the peptide for nanoparticle synthesis may be less stringent. Indeed, it is conceivable that simply concentrating the peptide may be the only purification step necessary for nanoparticle synthesis. Additionally, the use of a reporter protein that may easily be tracked through the fermentation and recovery process is desirable from the standpoint of bioprocessing.

In this work, we describe the successful synthesis of Pd NPs using a peptide fused to Green Fluorescent Protein (GFPuv) and demonstrate that partially purified material is capable of controlling both composition and morphology. The peptide used to illustrate nanoparticle synthesis, commonly referred to as Pd4 (TSNAVHPTLRHL) has been described previously to non-covalently bind to Pd [13]. This peptide was derived from M13 phage display adsorption on bulk polycrystalline palladium and has histidine residues at its 6th and 11th position in the peptide structure [13,14]. The peptide can anchor to the surface of palladium nanoparticle surfaces through histidine residues. Our construction provides three N-terminal copies of Pd4

separated from GFPuv by an additional methionine for optional cyanogen bromide cleavage, with this construction referred to as (Pd4)₃-GFPuv throughout the paper [15]. Pd NPs were synthesized and characterized by several physical and chemical techniques that include transmission electron microscopy (TEM), UV-visible spectroscopy, energy-dispersive X-ray spectroscopy (EDS). It showed that highly ordered NPs can be prepared using crude lysate as a source of multimeric Pd4. Furthermore, the catalytic activity of (Pd4)₃-GFPuv fusion protein-templated Pd NPs were investigated using two major cross-coupling reaction. The Suzuki-Miyaura coupling and Stille coupling reactions have become the most efficient ways to construct molecules with different sizes through carbon-carbon bond coupling. These reactions have been widely used for complex pharmaceutical compounds as well as natural products [16,17]. In addition, the ability of prepared fusion protein-templated Pd NPs were successfully studied toward anticancer drug construction. The synthesized NPs also showed high performance in green environment and their catalytic activities did not suffer significant loss after cycling test.

5.2. Experimental

The metal-binding peptide called Pd4 was designed and synthesized by Integrated DNA Technologies (Coralville, IA). Potassium tetrachloropalladate (II) was used as a Pd precursor and was purchased from Sigma Aldrich (St. Louis, MO, USA). The chemical in this study were of analytical grade.

5.2.1. Preparation of strain used to express (Pd4)₃-GFPuv

In order to construct (Pd4)₃-GFPuv fusion protein, a plasmid carrying DNA fragment encoding three copies of Pd4 was designed according to the codon preference of *Escherichia*

coli. The fragment containing multiple cloning sites for gene fusion followed by Pd4 was synthesized (Figure 12). Subsequently, the fragment was cloned into the *EcoRI* and *NcoI* sites of pBAD myc- His B introduced at the 5' end of the (Pd4)₃ using primer *Forward 1* along with GFPuv in the 3' end with the primer *Reverse 1*, respectively. Afterward, the (Pd4)₃ overlap region was introduced in the 5' end of GFPuv using the primer *Forward 2* and *Reverse 2*, a stretch that contained both a His₆ tag and an *EcoRI* restriction site. The two polymerase chain reaction (PCR) products were finally spliced together in a third PCR using the *Forward 1* and *Reverse 2* primers (Table 18). The PCR product of the third step, and plasmid pBAD (synthesized by Invitrogen) were double digested using *EcoRI-HF*® and *NcoI-HF*® restriction enzymes from New England Biolabs. Both products were recovered using a two-tier 1.2% agarose FlashGel cassette and Recovery buffer. Finally, ligation of the digested PCR product and the digested pBAD occurred overnight using T4 DNA Ligase enzyme and T4 DNA Ligase Reaction buffer (New England Biolabs) at 14°C [18].

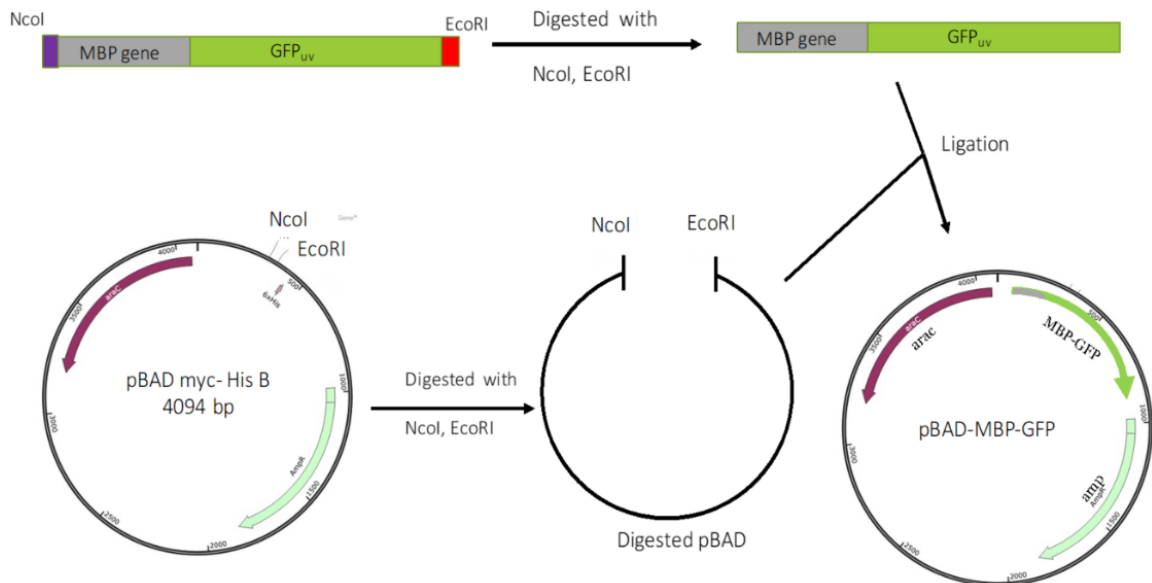


Figure 12. Overview of plasmid construction. A synthetic gene was constructed using SOE PCR, which was added to the commercially available expression vector pBAD myc-HisB [18].

Table 18. List of primers used for plasmid construction.

Primer	Sequence
Forward 1	5'-GACGGTAGAACCATGGGTA CTTCCAATGCCGTCCA-3'
Reverse 1	5'-GTGAAAAGTTCTTCTCCTTTACTCATTAAAGTGACGCAAGGTCGG-3'
Forward 2	5'-CCGACCTTGCGTCACTTAATGAGTAAAGGAGAAGAACTTTTCAC-3'
Reverse 2	5'-TGCGAATTCTTAATGGTGATGGTGATGGTGTTTGTAGAGCTCATC-3'

10-Beta *E. coli* competent cells were transformed with the plasmid using heat shock [19]. Cells were plated on LB agar media containing 50 µg/mL ampicillin and 2 mg/mL arabinose. The plates were incubated overnight at 37°C and the product was checked for green fluorescence using UV light.

5.2.2. Expression of the recombinant protein

The expression plasmids of GFPuv and (Pd4)₃-GFPuv were introduced in *E. coli* BL21 DE3, and the transformed cells were grown in Lysogeny Broth (LB) media at 37°C. Fermentation steps contained 50µg/mL ampicillin to serve as a selection method. The prepared inoculum for the fed batch fermentation in a shake flask was added to LB media in an Applikon bioreactor and the growth process was performed at 37°C and pH of 6.8. After six hours of cultivation, the culture was fed with 500 g/L sterilized glucose solution. Subsequently, the cell culture was induced with 10 mM arabinose when an optical density of 600 nm (OD₆₀₀) was reached to 0.4. Ultimately, the fermentation was stopped after four hours, and the harvested cells were collected by centrifugation at 5000×g at 4 °C for 45 minutes.

5.2.3. Lysate preparation

Thawed cells (5 – 10 g) were resuspended in 40 mL of deionized water and lysed ultrasonically for 20 minutes followed by centrifugation to remove insoluble material at 8000×g for 45 minutes at 4 °C. The supernatants containing soluble His-tagged protein were decanted to avoid any insoluble materials for fusion protein purification.

5.2.4. Enrichment

The decanted lysate was filtered through a 3.5 kDa MWCO dialysis membrane (Spectrum Laboratories, Rancho Dominguez, CA) to obtain clarified soluble fusion protein prior to purification. A gravity-flow HiTrap DEAE FF column containing HisPur Cobalt resin (GE Healthcare, Pittsburgh, PA, USA) was equilibrated with 25 mM Tris-HCl buffer, pH 8.0 (IEX DEAE Buffer A). The clarified supernatants containing soluble N-terminal His-tagged proteins were then loaded onto a gravity-flow HiTrap DEAE FF column containing HisPur Cobalt resin (GE Healthcare, Pittsburgh, PA, USA). Fusion proteins were processed using an ÄKTA FPLC System (Amersham Biosciences, Little Chalfont, UK). Following this, the column was developed with a stepwise elution of 25 mM Tris-HCl (pH 8.0) containing 1 M NaCl (IEX DEAE Buffer B). Subsequently, the target proteins were collected, and UV light was employed to verify the fluorescent green emission of target protein. The purity of the fusion proteins was determined by sodium dodecyl sulfate-polyacrylamide gel electrophoresis (SDS PAGE) followed by staining with Coomassie brilliant blue (CBB) R-250. The protein concentration was measured using the Bradford method (Bio-Rad Protein assay kit, Bio-Rad, Hercules, CA, USA), with bovine serum albumin (BSA) as the standard.

5.2.5. Nanoparticle synthesis and characterization

Pacardo *et al.* method was adapted and followed for palladium nanoparticles (Pd NPs) synthesis in this work [14]. 0.23 mg (Pd4)₃-GFPuv was added to an aqueous solution (on milliliter total volume) containing 0.16 mg of K₂PdCl₄ so that each peptide was dissolved with 2 equivalents of K₂PdCl₄ and the mixture was stirred for thirty minutes at 800 rpm at 25 °C. After Pd complexation, 1.5 mg NaBH₄ was added to the prepared mixture. Reduction of Pd²⁺ to Pd⁰ and formation of NPs was indicated by color change (yellow to light brown) [19]. The solution was mixed at 200 rpm for an hour.

The NP morphology and size distribution analysis were investigated using transmission electron microscopy (TEM). A ten microliter drop of the reaction mixture containing NPs were taken and immediately placed on a 300 mesh standard lacey carbon grid. An FEI Titan 80–300 was used to measure and determine NP size distribution and morphology. Analysis of the images was performed using ImageJ software.

5.3. Results and Discussion

In order to investigate the ability of recombinant Pd4 in NP synthesis, an expression vector for (Pd4)₃-GFPuv encoding gene was constructed [18]. Electrophoresis results using a single-tier 1.2% agarose Lonza's FlashGel™ cassette confirmed that DNA product from PCR steps were of the correct size (936 bp) as expected for the recombinant gene (Figure 13a). This gene was recovered, digested, ligated with the pBAD vector, and transformed into 10-Beta *E. coli* competent cells. Transformants produced green fluorescence under UV light when plated on LB agar and LB media containing 10 mM arabinose and 50 µg/mL ampicillin (Figure 13b). Subsequently, Fed-batch fermentation was performed to achieve high harvested cell density with

a typical run having a terminal optical density (OD_{600}) of 22 and a yield of 75 g cell pellet (wet cell weight).

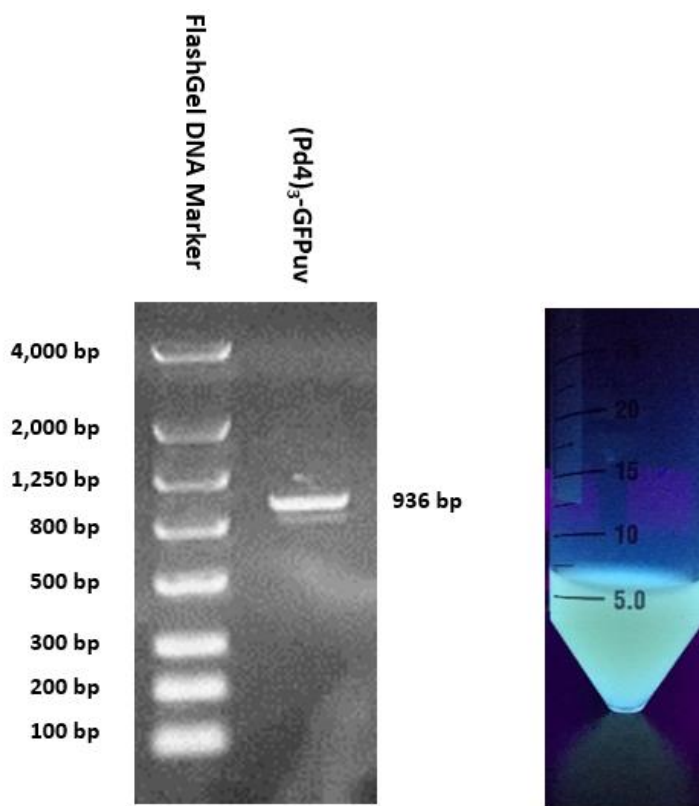


Figure 13. Gel electrophoresis indicating successful gene construction. a. The final (936 bp) fragment constructed after the third round of PCR was analyzed on a gel to insure correct size. Lane 1, DNA standard. Lane 2, PCR product of step 3. b. (Pd4)₃-GFPuv fusion protein under UV light.

Clarified lysate obtained from fed-batch fermentation were used to obtain fractions that were enriched in (Pd4)₃-GFPuv by removal of undesired *E. coli* host-cell proteins. A final gradient incorporating five steps was used for the single column enrichment process of (Pd4)₃-GFPuv. Figure 14a is a representative chromatogram of the intracellular lysate, with peaks eluting due to increasing NaCl concentration. Fluorometric measurements confirmed that a single peak had high fluorescent intensity and were further checked using SDS-PAGE analysis. As shown in Figure 14b, the purified band with 31.5 kDa molar mass belongs to (Pd4)₃-GFPuv.

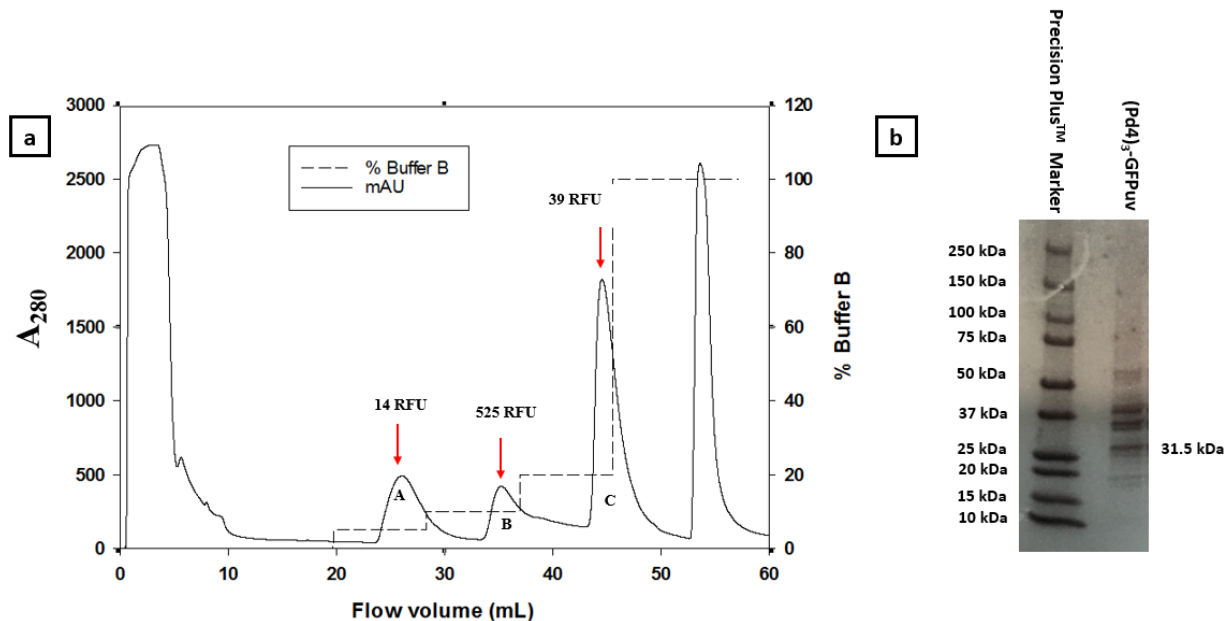


Figure 14. a. Ion exchange chromatography for enrichment of $(Pd4)_3$ -GFPuv. Samples were fractionated using ion exchange chromatography. Peak B had highest $(Pd4)_3$ -GFPuv, indicated by a RFU (relative fluorescent units) of 525. b. SDS-PAGE electrophoresis of ion exchange fraction. Calculated molecular weight of $(Pd4)_3$ -GFPuv is 31.5 kDa. Lane 1, protein standard. Lane 2, sample.

The NP synthesis process were performed using *E. coli* lysate containing $(Pd4)_3$ -GFPuv, the purified fraction of $(Pd4)_3$ -GFPuv, the *E. coli* lysate containing GFPuv, and control experiment without $(Pd4)_3$ -GFPuv fusion protein. As shown in Figure 15a-b, obtained particles were neither discrete nor consistent in the absence of Pd4 peptide. It could be argued that Pd4 sequence is required to obtain uniform NPs as agglomeration, non-uniformity, and irregularity of particles occurred due to lack of nucleation site needed to anchor to the NPs in the absence of Pd4 sequence. On the other hand, discrete and uniformed NPs were successfully synthesized using the crude lysate contained $(Pd4)_3$ -GFPuv protein obtained from fed-batch fermentation. Although there are approximately fifteen different species in the lysate, spherical Pd NPs with an average size of $2.4 \text{ nm} \pm 0.7 \text{ nm}$ were formed when the reducing agent was added to the solution

of lysate and Pd salt (Figure 15c). The results were consistent with our previous study [19].

Discrete and uniform Pd NPs with aspect ratio close to unity were synthesized using purified and enriched (Pd4)₃-GFPuv fusion protein. The average diameter of Pd NPs was 2.6 ± 0.7 nm and no formation of large aggregates was observed (Figure 15d).

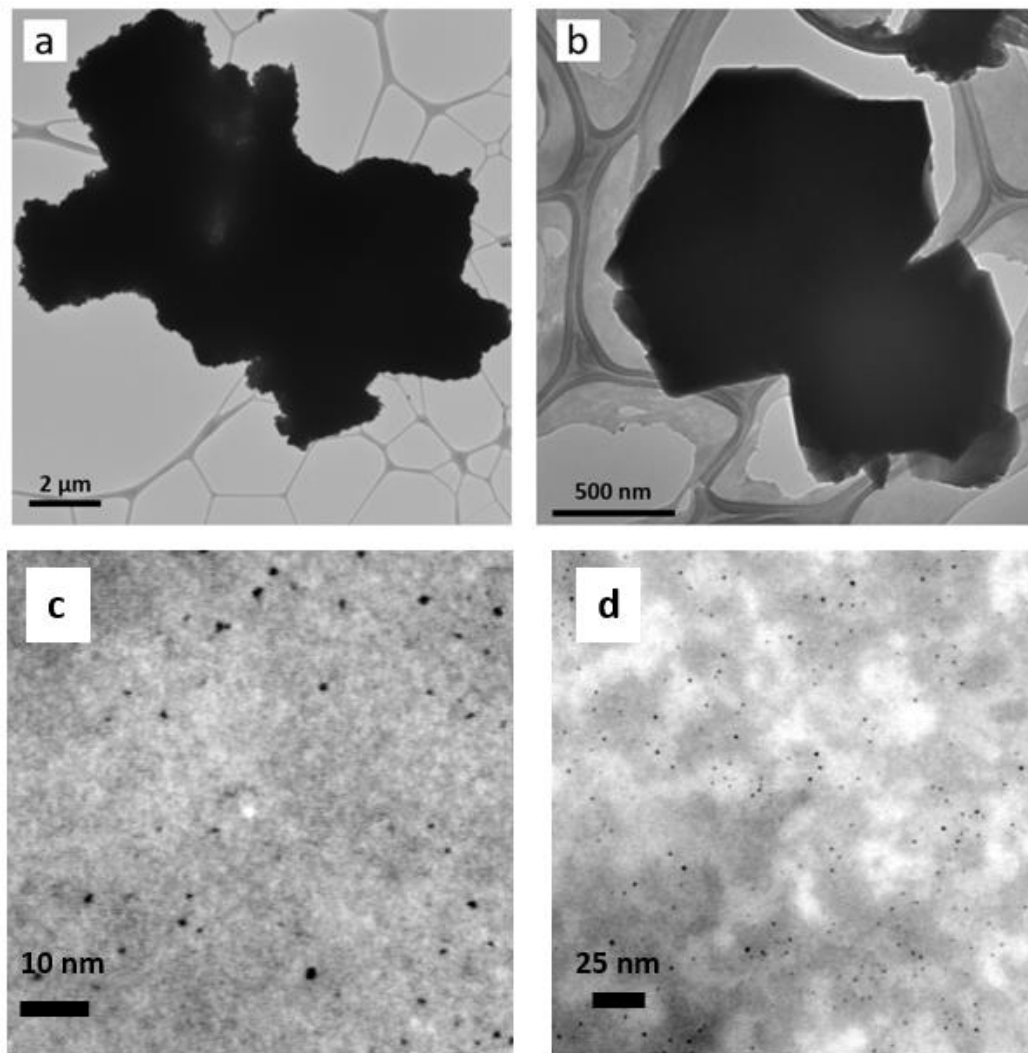


Figure 15. Transmission Electron Microscopy of particles derived from extracts devoid of Pd4. Large particles were obtained in the presence of (a) lysate, and (b) lysate containing GFPuv. Ultrafine NPs obtained in presence of (c) lysate containing (Pd4)₃-GFPuv, and (d) purified (Pd4)₃-GFPuv.

X-ray photoelectron spectroscopy spectrum of (Pd4)₃-GFPuv fusion protein templated Pd NPs indicated that sodium chloride was also present and accompanied the Pd NPs (Figure 16a). Typically, sodium chloride concentration in LB is estimated to be within the range of 5-10 mg/g. Since neither sonication nor centrifugation would affect salt concentration in the soluble fraction of the lysate, the presence of sodium chloride (NaCl) is not surprising. Also, the nanoparticles were obtained after lyophilizing the mixture resulting in powder containing 1.2% of palladium confirmed by Inductively Coupled Plasma Atomic Emission Spectroscopy (ICP-AES) (See SI for the details). The Pd3d spectrum shows the characteristic peaks of 3d_{3/2,5/2} doublets (Figure 16b). The peaks at the binding energy (BE) around 341.2 eV (Pd 3d_{3/2}) and 335.3 eV (Pd 3d_{5/2}) are attributed to Pd⁰ species and the peaks around BE of 343.7 eV (Pd 3d_{3/2}) and 337.6 eV (Pd 3d_{5/2}) are related to Pd^{II} species, which probably result from the reoxidation of Pd⁰ [20]. In addition, X-ray diffraction pattern of crude lysate and Pd NPs synthesized using crude lysate confirmed the NaCl content in the catalyst (Figure 16c).

SEM analysis of (Pd4)₃-GFPuv fusion protein templated Pd NPs indicated that sodium chloride was also present and accompanied the Pd NPs (Figure 17a and b). However, NaCl content was eliminated from Pd NPs prepared using purified (Pd4)₃-GFPuv fusion protein as confirmed by Energy-dispersive X-ray spectroscopy analysis (Figure 17c). Based on representative EDX spectrum of the Pd NPs prepared using enriched (Pd4)₃-GFPuv fusion protein, Pd peak was detected at 3.3 keV. Also, the peak of oxygen resulted, at least in part, from the organic materials (fusion proteins) deposited on the grid. Lastly, the peaks of copper and carbon originated from the use of the lacey carbon grid that held the NPs (Figure 17c).

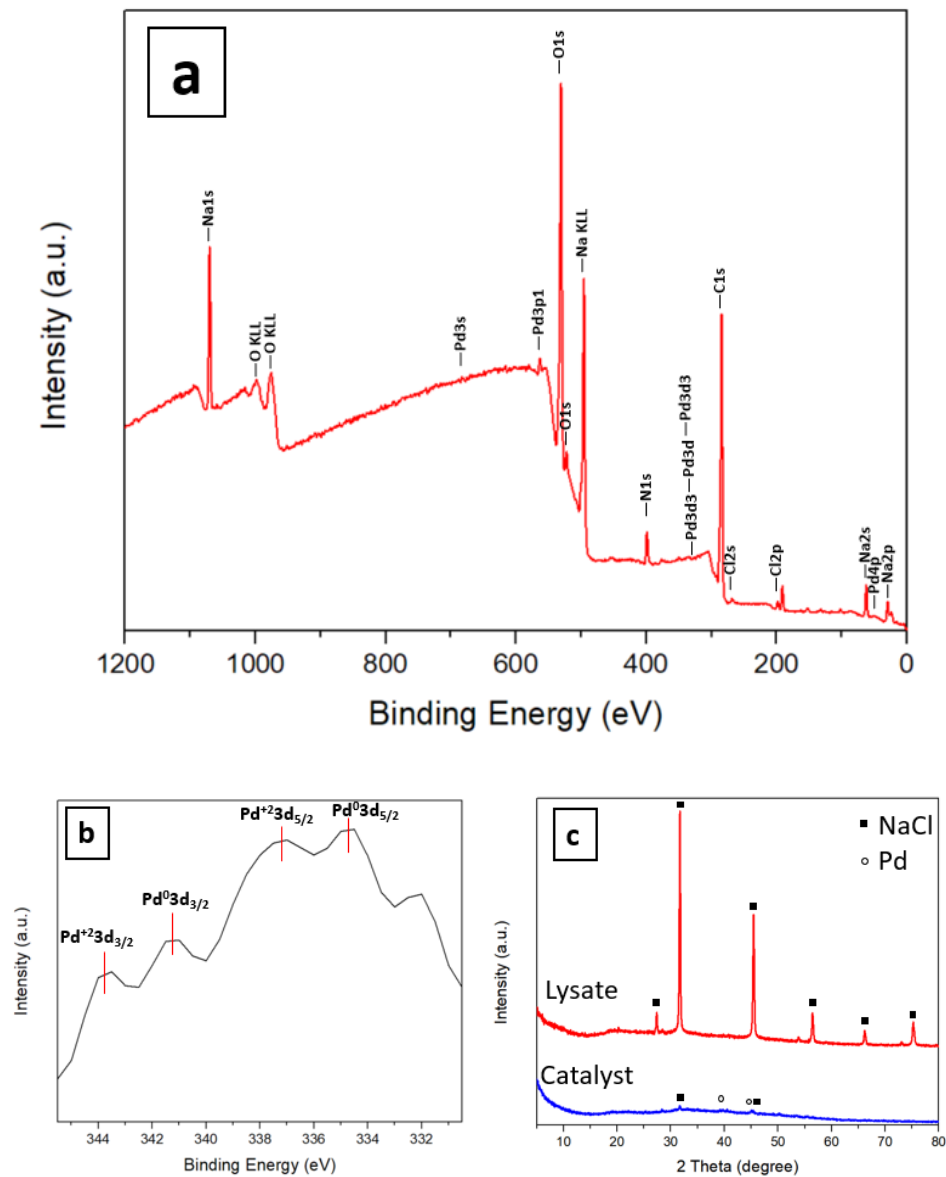


Figure 16. XPS spectrum of (a) $(Pd_4)_3$ -GFPuv fusion protein templated Pd NPs and (b) Pd3d XPS spectrum of Pd NPs. (c) XRD pattern of $(Pd_4)_3$ -GFPuv fusion protein templated Pd NPs using as catalyst.

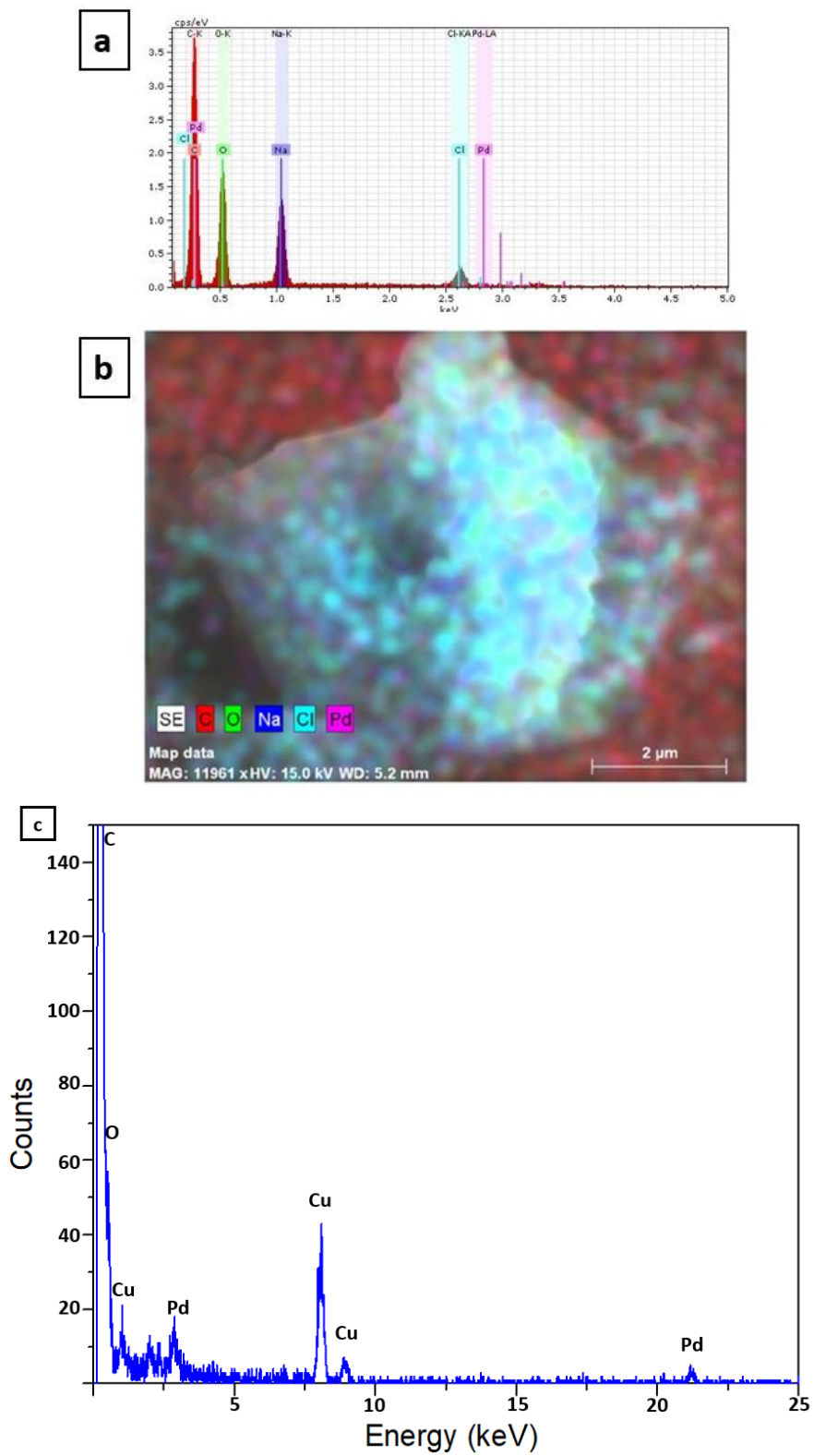


Figure 17. Elemental analysis of prepared nanoparticles from cell lysate. (a) SEM

spectrum prepared nanoparticles in cell lysate and (b) SEM image analysis of the spectrum. (c) EDX spectrum of the Pd NPs prepared using enriched (Pd4)₃-GFPuv fusion protein.

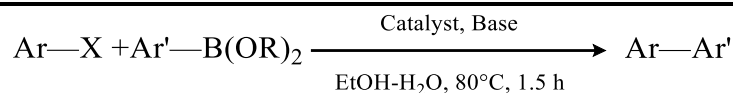
5.3.1. Application as catalyst in coupling reactions

5.3.1.1. Suzuki-Miyaura coupling

The (Pd4)₃-GFPuv fusion protein-templated Pd NPs described above were employed to the Suzuki-Miyaura coupling reaction of aryl halides with phenylboronic acid. The coupling reaction of iodobenzene and phenyl boronic acid was selected as model.

Table 19 shows the effect of catalyst and the base determined by biphenyl yield. The reaction did not take place in the absence of base showing that it is needed to activate the boronic acid via boosting the polarization of organic ligands thus accelerating the transmetallation step (entry 1). The reaction did not occur in the absence of catalyst or (Pd4)₃-GFPuv fusion protein (entries 2 and 3) while excellent catalytic activities were observed when (Pd4)₃-GFPuv fusion protein-templated Pd NPs was used (entries 4-7). It exhibits the important role of Pd NPs for driving the Suzuki-Miyaura coupling reaction. The catalytic performance of different loadings of fusion protein-templated Pd indicated that employing the catalyst containing 5 mmol% Pd NPs and 0.15 mmol of K₂CO₃ resulted in 77% yield of the biphenyl product under the given conditions (entry 4). However, by increasing the base content to 0.3 mmol, the biphenyl product in yield of 97% was obtained (entry 5). Moreover, the yield of reaction using catalysts containing 2 mmol% and 1 mmol% Pd were 94% and 71%, respectively after four hours while the other reaction conditions were as given (entries 6 and 7).

Table 19. Catalyst survey for Suzuki-Miyaura coupling reaction of iodobenzene and phenylboronic acid ^a.



Entry	Parameters	Yield ^b (%)
1	No K ₂ CO ₃	—
2	No Catalyst	—
3	(Pd ₄) ₃ -GFPuv fusion protein	—
4	(Pd ₄) ₃ -GFPuv fusion protein-templated Pd NPs	77 ^c
5	(Pd ₄) ₃ -GFPuv fusion protein-templated Pd NPs	97
6	(Pd ₄) ₃ -GFPuv fusion protein-templated Pd NPs	94 ^d
7	(Pd ₄) ₃ -GFPuv fusion protein-templated Pd NPs	71 ^e

^a Reaction conditions: iodobenzene (0.1 mmol), phenylboronic acid (1.2 mmol), K₂CO₃ (0.3 mmol) and Pd NPs (0.005 μmol) were mixed in 0.5 mL of water and 0.5 mL of ethanol and refluxed under N₂ after 90 min. ^b Yield were determined by HPLC. ^c The amount of K₂CO₃ is equivalent to 0.15 mmol, and other reaction conditions were as above. ^d The amount of catalyst is equivalent to 0.002 μmol Pd and yield was measured after 4 hours. ^e The amount of catalyst is equivalent to 0.001 μmol Pd and yield was measured after 4 hours.

The other reaction conditions including solvent, base, and temperature were also evaluated using the model coupling reaction (Table 20). The reaction did not result in high yield when KOtBu, K₂HPO₄, and KH₂PO₄ (entries 1-3) were used as base while the reaction proceeded with excellent catalytic activity in the presence of K₂CO₃ (entry 4). Although DMF and toluene could hinder the reaction (entries 5 and 6), high catalytic activities were achieved when THF and EtOH were used as solvent (entries 4 and 7). Using THF as solvent, the reaction did not occur at 40 °C even after 48 h (entry 8) while the yield of 69% of biphenyl was achieved when EtOH was used with the same reaction conditions (entry 9). The catalytic performance of reaction under different temperatures indicated that by increasing the temperature, higher yields could be obtained. Indeed, the Suzuki-Miyaura coupling reaction can be proceeded with high

yield of biphenyl when water is present. Presence of EtOH in water-contained solvents was observed to boost the catalytic performance of the reaction compared to those that THF was present (entries 9-12 and 14). Green solvent of EtOH and water with the ratio of one to one was found to be the best solvent for Suzuki-Miyaura coupling reaction (entries 13, 14, and 15).

Table 20. Optimized condition via coupling reaction of iodobenzene and phenylboronic acid. Solvent, base, and temperature.

$\text{Ar-X} + \text{Ar'-B(OR)}_2 \xrightarrow[\text{Solvent, Temperature, Time}]{\text{Catalyst, Base}} \text{Ar-Ar'}$					
Entry	Solvent	Base (mmol)	Time (h)	Temperature (°C)	Yield ^b (%)
1	THF	KOtBu	3.0	80	56
2	THF	K ₂ HPO ₄	3.0	80	63
3	THF	KH ₂ PO ₄	3.0	80	61
4	THF	K ₂ CO ₃	3.0	80	96
5	DMF	K ₂ CO ₃	3.0	80	49
6	Toluene	K ₂ CO ₃	3.0	80	51
7	EtOH	K ₂ CO ₃	1.5	80	98
8	THF	K ₂ CO ₃	48.0	40	0
9	EtOH	K ₂ CO ₃	48.0	40	69
10	EtOH: H ₂ O (1:1)	K ₂ CO ₃	8.0	60	81
11	THF: H ₂ O (1:1)	K ₂ CO ₃	8.0	60	43
12	THF: H ₂ O (1:1)	K ₂ CO ₃	4.0	80	95
13	EtOH: H ₂ O (3:1)	K ₂ CO ₃	1.5	80	98
14	EtOH: H ₂ O (1:1)	K ₂ CO ₃	1.5	80	97
15	EtOH: H ₂ O (1:3)	K ₂ CO ₃	3.5	80	82

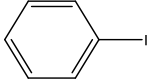
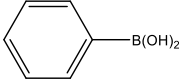
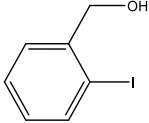
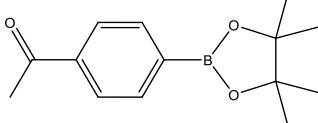
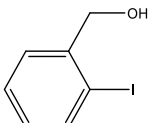
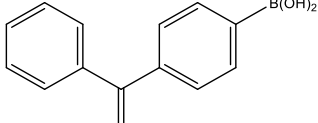
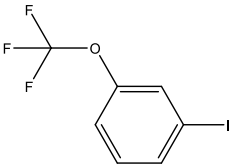
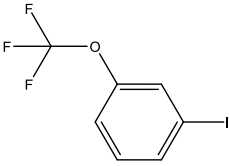
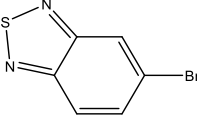
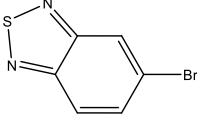
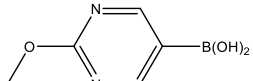
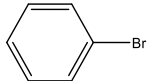
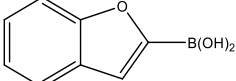
^a Reaction conditions: iodobenzene (0.1 mmol), phenylboronic acid (1.2 mmol), base (0.3 mmol) and Pd NPs (0.005 μmol) were mixed in solvent and refluxed under N₂. ^b Yield were determined by HPLC.

5.3.1.2. General applicability using Suzuki-Miyaura coupling reaction

A wide variety of aryl halides and phenylboronic acids was chosen to study the feasibility of (Pd4)₃-GFPuv fusion protein-templated Pd NPs as catalyst and the substrate scope of Suzuki-Miyaura coupling reactions (Table 21). Different aryl halide groups such as iodobenzene (entry 1), electron donating groups (entry 2 and 3), electron withdrawing groups (entry 4 and 5), bromobenzene (entry 6), and heterocycle compounds (entry 7 and 8) as well as different boronic acids were participated in the substrate scope results in high to excellent yields (Table 21).

Different aryl iodides bearing electron-rich and electron-deficient groups involved and reacted satisfactory with phenylboronic acids bearing electron-rich ($\text{—CH}_2\text{OH}$) as well as electron-deficient (—CHO , —COCH_3) substituents (Table 21. entries 1-5). In addition, aryl bromides known as low reactive substrates showed high to excellent yields even though heteroaryl boronic acids and heterocycle substituents were participated in Suzuki-Miyaura coupling reaction, respectively. It was also obtained that different substituents such as $\text{—CH}_2\text{OH}$, —CHO , —COCH_3 , and $\text{CF}_3\text{O—}$ remained intact during these transformations. Thus, (Pd4)₃-GFPuv fusion protein-templated Pd NPs was determined to be an efficient, inexpensive, and green catalyst for the Suzuki-Miyaura coupling reaction.

Table 21. Substrate scope for Suzuki-Miyaura coupling reaction ^a

$\text{Ar-X} + \text{Ar'-B(OR)}_2 \xrightarrow[\text{EtOH-H}_2\text{O, Reflux}]{\text{Catalyst, Base}} \text{Ar-Ar'}$					
Entry	Ar—X	Ar'—R	Time (h)	Yield ^b (%)	TOF
1			1.5	97	12,933
2			2	86	8,600
3			6	83	2,766
4			2	88	8,800
5			2.5	94	7,520
6			15	82	1,093
7			16	69	920
8			4	95	4,750

^a Reaction conditions: Aryl halide (0.1 mmol), arylboronic acid (1.2 mmol), K₂CO₃ (0.3 mmol) and Pd NPs (0.005 μmol) were mixed in 0.5 mL of water and 0.5 mL of ethanol and refluxed under N₂ under 80 °C.

5.3.1.3. Stille coupling

For the Stille coupling reaction, the coupling reaction of iodobenzene and phenyltin trichloride was selected as model and the mixture of EtOH and water with the ratio of one to one was chosen as the solvent since the aim of this work is to explore the catalytic ability of (Pd4)₃-GFPuv fusion protein-templated Pd NPs in green environment.

Table 22. Catalyst survey for Stille coupling reaction of iodobenzene and phenylboronic acid ^a.

$$\text{Ar-X} + \text{Ar}'\text{-SnCl}_3 \xrightarrow[\text{EtOH-H}_2\text{O, Reflux}]{\text{Catalyst, Base}} \text{Ar-Ar}'$$

Entry	Parameters	Yield ^b (%)
1	No K ₃ PO ₄	—
2	No Catalyst	—
3	(Pd4) ₃ -GFPuv fusion protein	—
4	(Pd4) ₃ -GFPuv fusion protein-templated Pd NPs	54 ^c
5	(Pd4) ₃ -GFPuv fusion protein-templated Pd NPs	96
6	(Pd4) ₃ -GFPuv fusion protein-templated Pd NPs	88 ^d
7	(Pd4) ₃ -GFPuv fusion protein-templated Pd NPs	64 ^e

^a Reaction conditions: iodobenzene (0.1 mmol), phenyltin trichloride (1.2 mmol), K₃PO₄ (0.3 mmol) and Pd NPs (0.005 μmol) were mixed in 0.5 mL of water and 0.5 mL of ethanol and refluxed under N₂ after 6 hours. ^b Yield were determined by HPLC. ^c The amount of K₃PO₄ is equivalent to 0.15 mmol, and other reaction conditions were as above. ^d The amount of catalyst is equivalent to 0.002 μmol Pd and yield was measured after 20 hours. ^e The amount of catalyst is equivalent to 0.001 μmol Pd and yield was measured after 20 hours.

As indicated in Table 22, in the Stille reaction, the presence of both base and catalyst containing Pd NPs is required for driving the Stille coupling as the reaction did not occur in their absence (entries 1-3). In contrast, excellent catalytic activities were obtained when (Pd4)₃-GFPuv fusion protein-templated Pd NPs was used (entries 4-7). The catalytic performance of different

loadings of fusion protein-templated Pd and base content indicated that biphenyl product can be obtained with when 1 mmol% Pd NPs and 0.15 mmol of K₂CO₃ were employed (entries 4, 6, and 7), although by increasing the Pd NPs loading to 5 mmol% and base content to 0.3 mmol, the biphenyl product in yield of 96% was obtained (entry 5).

Table 23. Optimized condition via coupling reaction of iodobenzene and phenyltin trichloride. Solvent, base, and temperature.

$$\text{Ar-X} + \text{Ar'-SnCl}_3 \xrightarrow[\text{EtOH-H}_2\text{O, Reflux}]{\text{Catalyst, Base}} \text{Ar-Ar'}$$

Entry	Pd (mmol %)	Base (mmol)	Time (h)	Temperature (°C)	Yield ^b (%)
1	5	KOH	6.0	80	72
2	5	K ₂ CO ₃	6.0	80	34
3	5	CsF	6.0	80	36
4	5	K ₃ PO ₄	6.0	80	96
5	5	K ₃ PO ₄	48.0	40	58
6	5	K ₃ PO ₄	24.0	60	74
7	10	K ₃ PO ₄	6.0	80	96
8	2	K ₃ PO ₄	16.0	80	88
9	1	K ₃ PO ₄	16.0	80	64

Reaction conditions: iodobenzene (0.1 mmol), phenyltin trichloride (1.2 mmol), base (0.3 mmol) and Pd NPs were mixed in 0.5 mL of water and 0.5 mL of ethanol and refluxed under N₂. ^b Yield were determined by HPLC.

In order to explore the optimized condition for Stille coupling reaction, the model reaction was used and other reaction conditions including base, temperature, and catalyst loading were evaluated (

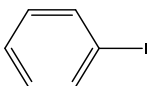
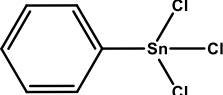
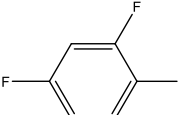
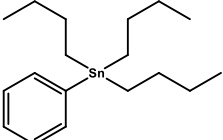
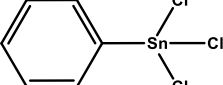
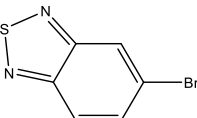
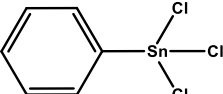
Table 23). A series of bases were explored for the base study and it was found that in the presence of K_3PO_4 excellent catalytic activity of 96% yield of biphenyl was achieved (entries 1-4). The temperature study of the reaction under showed that higher yields could be obtained in higher temperature. Although 74% yield of biphenyl was proceeded at 60 °C, the reaction was performed for 24 h. In contrast, employing 80 °C, 96% yield of biphenyl was achieved after 6 h. (entries 4-6). Furthermore, increasing the amount of catalyst did not alter the yield of biphenyl while lower catalytic activities were observed when 2 mmol% and 1 mmol% of Pd was present in the reaction (entries 7-9).

5.3.1.4. General applicability using Stille coupling reaction

A series of aryl halides, phenyltin trichloride, and phenyl tributyltin were chosen to investigate the substrate scope of Stille coupling reactions using $(Pd_4)_3$ -GFPuv fusion protein-templated Pd NPs as catalyst (Table 24). Different aryl halides bearing electron-withdrawing groups reacted efficiently with phenyltin trichloride and phenyl tributyltin. Furthermore, the coupling of heterocycle compound with phenyltin trichloride showed high yield through the reaction. This high catalytic activity is of high importance since heterocycles are known as low-reactive substrates (Table 24). It was also obtained that during transformations through Stille coupling, different substituents such as $-CH_2OH$, $-F$, and $-CHO$ remained intact indicating that $(Pd_4)_3$ -GFPuv fusion protein-templated Pd NPs are efficient, green, and inexpensive catalysts for the Stille coupling reaction.

Table 24. Substrate scope for Stille coupling reaction ^a

$$\text{Ar-X} + \text{Ar}'\text{-SnY}_3 \xrightarrow[\text{EtOH-H}_2\text{O, Reflux}]{\text{Catalyst, Base}} \text{Ar-Ar}'$$

Entry	Ar—X	Ar'—R	Time (h)	Yield ^b (%)	TOF
1			5.75	96	3,324
2			18	72	800
3			12	86	1,433
4			40	93	465

^a Reaction conditions: Aryl halide (0.1 mmol), arylboronic acid (1.2 mmol), K₃PO₄ (0.3 mmol) and Pd NPs (0.005 μmol) were mixed in 0.5 mL of water and 0.5 mL of ethanol and refluxed under N₂ under 80 °C.

5.3.2. Stability and recyclability

Since environmental protection concerns as well as cost-effective approaches for appropriate catalyst used in chemical reactions are of high importance, employing a catalyst with aforementioned characteristics is highly desired. The heterogenous catalysts including (Pd₄)₃-GFPuv fusion protein-templated Pd NPs due to their remarkable stability and recyclability in chemical and separation processes are desired candidates for industries. Taking the model reaction of iodobenzene and phenylboronic acid for Suzuki-Miyaura coupling and iodobenzene

and phenyltin trichloride for Stille coupling, the reusability of (Pd₄)₃-GFPuv fusion protein-templated Pd NPs catalyst was investigated. The catalyst was reused for five times and the catalytic activity decrease of about 13% and 18% after five cycles was achieved in Suzuki-Miyaura coupling and Stille coupling reactions study, respectively (Figure 18).

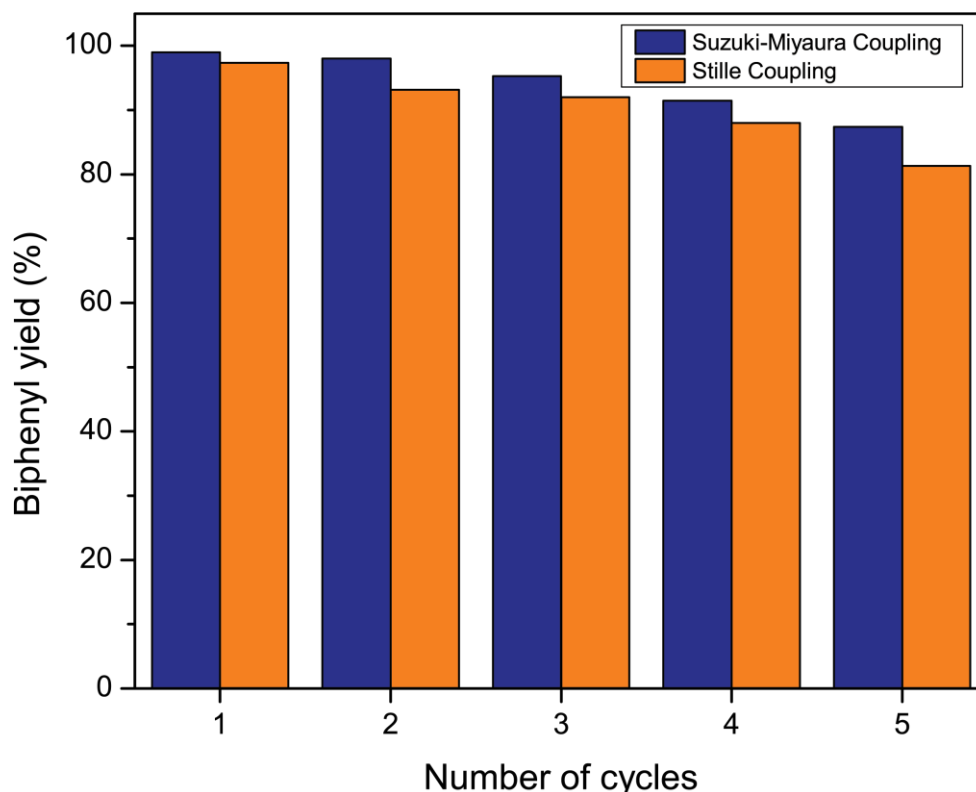


Figure 18. Recyclability of (Pd₄)₃-GFPuv fusion protein-templated Pd NPs catalyst using the model reaction of iodobenzene and phenylboronic acid.

No aggregation or morphological changes were observed in used catalyst after five cycles and the Pd NPs remained spherical and uniformed without any aggregation. The average size of nanoparticles remained almost unchanged (2.2 ± 0.7 nm in Suzuki-Miyaura coupling and $2.1 \pm$

0.8 nm in Stille coupling) confirming excellent stability and recyclability of the as-prepared catalyst (Figure 19).

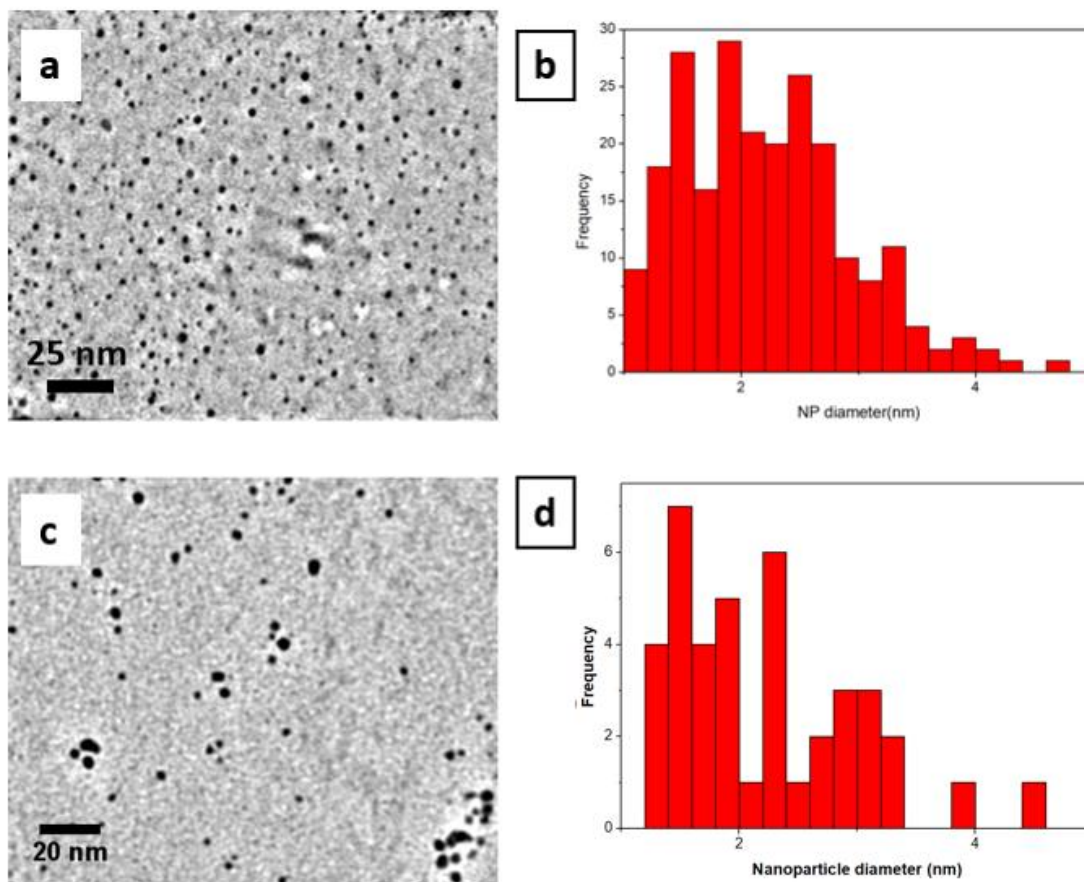


Figure 19. (a) TEM image, and (b) particle size distribution of $(\text{Pd}_4)_3\text{-GFPuv}$ fusion protein-templated Pd NPs catalyst after five cycles for Suzuki-Miyaura coupling. (c) TEM image, and (d) particle size distribution of $(\text{Pd}_4)_3\text{-GFPuv}$ fusion protein-templated Pd NPs catalyst after five cycles for Stille coupling.

5.3.3. Kinetic study of coupling reactions

In order to understand the kinetics of the coupling reactions enabled by $(\text{Pd}_4)_3\text{-GFPuv}$ fusion protein-templated Pd NPs, coupling reactions rates should be determined. As stated previously, the coupling reaction of iodobenzene and phenylboronic acid and the coupling reaction of iodobenzene and phenyltin trichloride was selected as model reactions for Suzuki-Miyaura coupling and Stille coupling, respectively. To determine the reaction rates as well as the

efficiency of the (Pd₄)₃-GFPuv fusion protein-templated Pd NPs, the turnover frequency (TOF) of both reactions were determined. Employing the reaction conditions, the ratio of starting materials to the amount of catalyst remained constant as taken aliquot for analysis was removed from the reaction mixture containing all reaction elements. An aliquot was extracted from the reaction vial at 5 min and 15 min intervals from Suzuki-Miyaura coupling and Stille coupling reaction vials, respectively, until the completion of reactions.

5.3.3.1. Suzuki-Miyaura coupling reaction rate study

The Suzuki-Miyaura coupling reaction yields employing model reaction condition (iodobenzene (0.1 mmol), phenylboronic acid (1.2 mmol), base (0.3 mmol) and Pd NPs (0.005 μ mol)) are plotted in Figure 20. The average TOF of the reaction can be determined after the completion of the reaction after 90 mins. From this analysis, a TOF value of $14,117 \pm 113$ mol biphenyl. (mol Pd. h)⁻¹ was determined for the model reaction system.

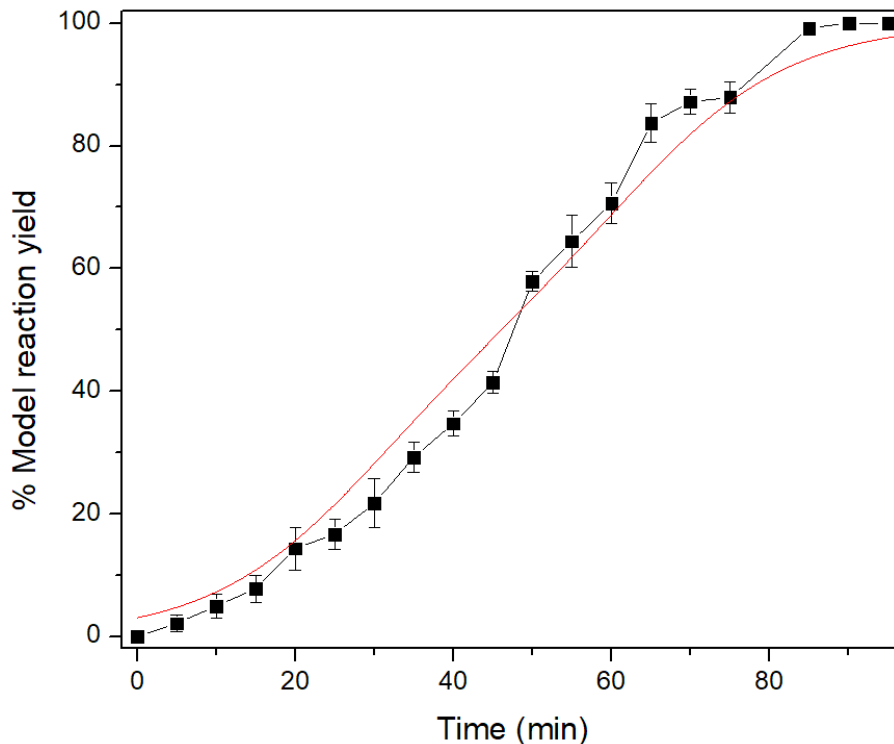


Figure 20. TOF determination for the Suzuki-Miyaura coupling model reaction. The concentration of each starting materials (iodobenzene and phenylboronic acid) as well as the product (biphenyl) was determined based on the reaction yields for 5 min intervals. To further analyze the rate of the reaction over time, the fractional conversion of the reaction which is define as

$$f_A = \frac{[n_A]_{reacted}}{[n_A]_{fed}} \quad (3)$$

Where f_A is fractional conversion, $n_{A_{reacted}}$ is mole reacted starting material and $n_{A_{fed}}$ is mole fed starting material was determined based on the conversion of iodobenzene. Also, the model reaction yield data points were polynomial fitted resulted in an equation given as

$$Y(t) = 127 - 123.3/(1 + t/56)^3 \quad (4)$$

Where $Y(t)$ is the model reaction yield and t is time. The first derivation of Equation (4) was resulted in the conversion rate of iodobenzene. As shown in Figure 21, the rate of the Suzuki-Miyaura coupling model reaction for iodobenzene was higher at the start of the reaction while it decreased over time and in the last two intervals, the reaction was proceeded with almost the same rate. On the other hand, the biphenyl production rate was high at the beginning while it decreased as the reaction was near the completion.

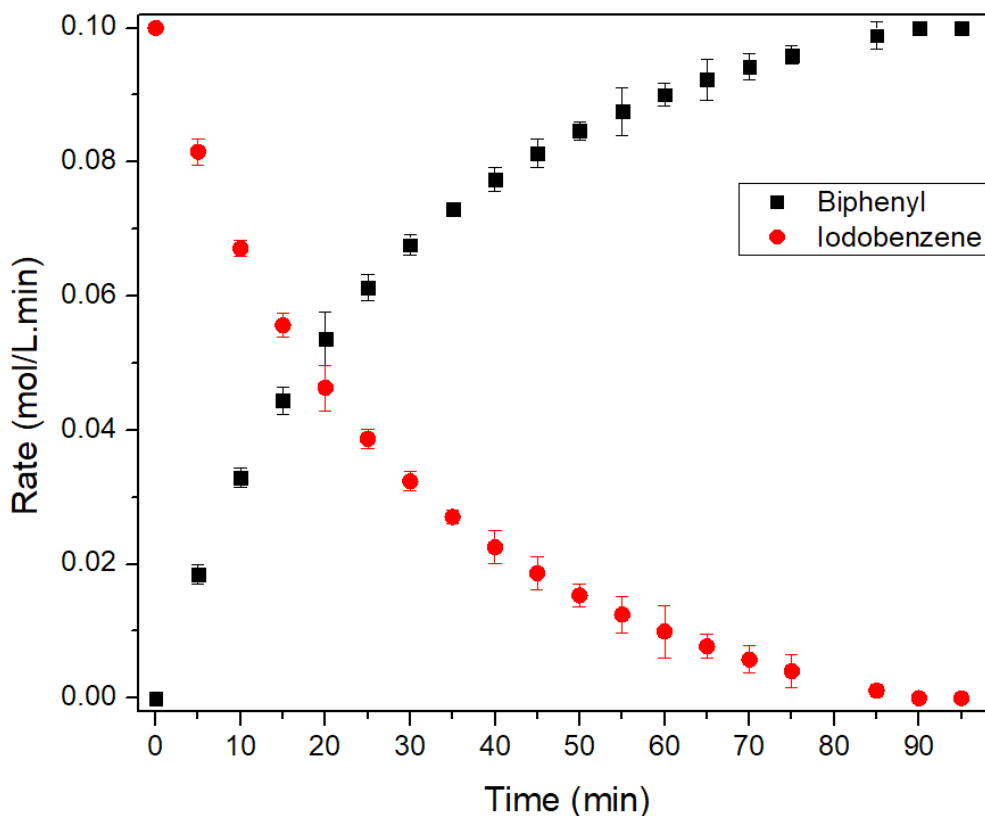


Figure 21. Reaction rate determination for the Suzuki-Miyaura coupling.

5.3.3.2. Stille coupling reaction rate study

The Stille coupling model reaction yields are plotted in Figure 22. The reaction was proceeded employing the optimized conditions and 0.005 μmol of Pd NPs were used. Comparing to the Suzuki-Miyaura coupling reaction, the reaction was completed in six hours and a TOF

value of $3,324 \pm 83 \text{ mol biphenyl. (mol Pd. h)}^{-1}$ was determined for the model reaction system. This value is slightly larger than those reported for similar systems using chemically synthesized peptides for palladium direction confirming that unpurified $(\text{Pd}_4)_3\text{-GFPuv}$ fusion protein-templated Pd NPs can show high reactivity[13,14]. It is important the note that, the amount of base used in this work was four times less than the similar systems [13,14].

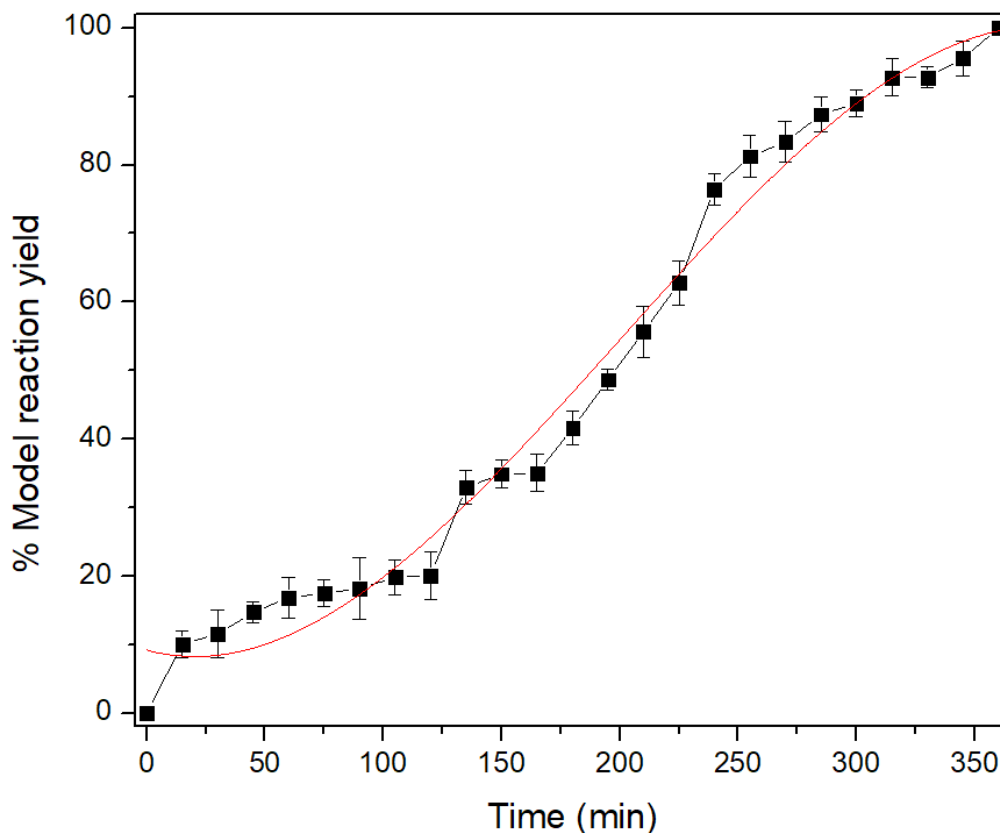


Figure 22. TOF determination for the Stille coupling model reaction.

Similar to Suzuki-Miyaura coupling reaction rate study, the concentration of reactants and the product was determined based on the reaction yields. The samples were taken every 15 min and their fractional conversion were analyzed based on the conversion of iodobenzene. The polynomial fit of the model reaction yield data points was polynomial fitted resulted in an equation given as

$$Y(t) = 112 - 100 / \left[(1 + t/217) \right]^3 \quad (5)$$

The rate of iodobenzene the Stille coupling reaction can be determined by the derivation of Equation $Y(t) = 112 - 100 / \left[(1 + t/217) \right]^3$ (5). Stille coupling model reaction rate analysis exhibited that the reaction rate followed the same behavior as Suzuki-Miyaura coupling model reaction. The rate of the reaction decreased over time and the reaction continued with almost the same rate at the last time intervals.

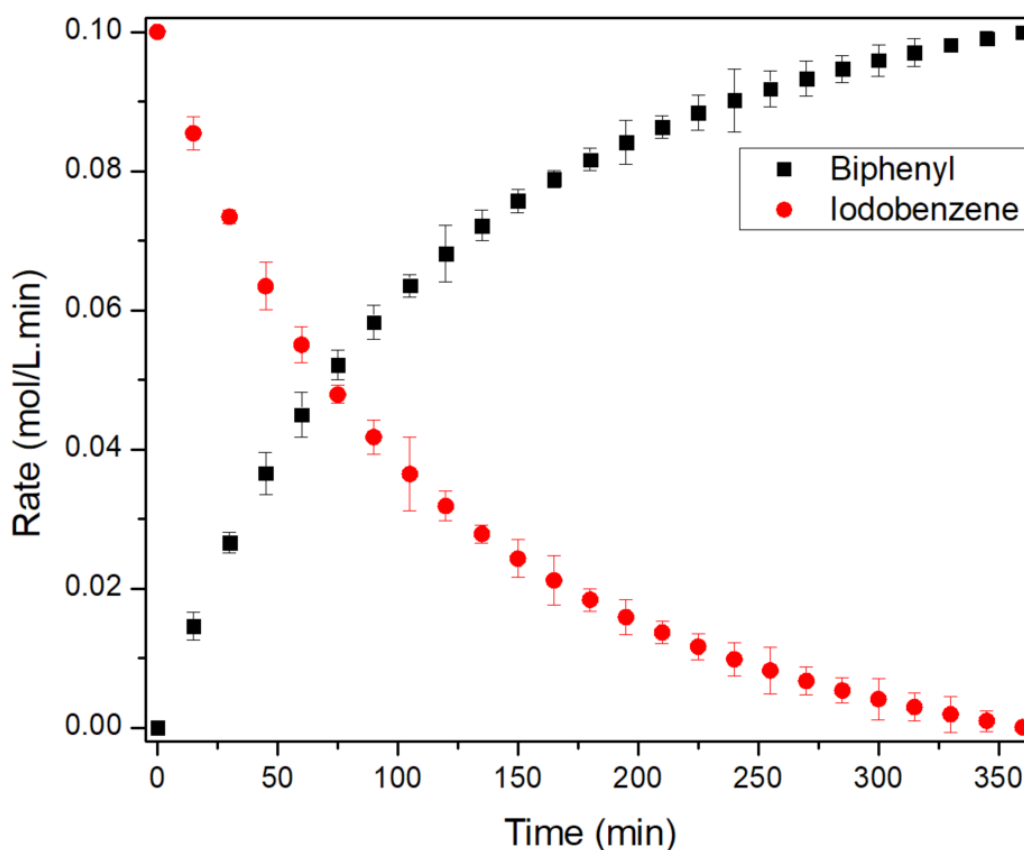


Figure 23. Stille coupling model reaction rate analysis.

5.3.4. Fusion protein-templated Pd NPs for anticancer drug precursor synthesis

For the extension of the ability of (Pd₄)₃-GFPuv fusion protein-templated Pd NPs as catalyst, the synthesis of Lapatinib precursor was performed. Lapatinib (Tykerb) is an oral active

drug used for the treatment of patients with advanced breast cancer [21,22]. The key step in Lapatinib synthesis is to employ Suzuki-Miyaura reaction for coupling of 5-formyl-2-furanylboronic acid and iodoquinazoline (Figure 24) [21]. A method adapted from Mahboobi *et al.* was followed to synthesize Lapatinib precursor [22]. Employing (Pd4)₃-GFPuv fusion protein-templated Pd NPs as catalyst, the precursor was obtained in a good yield which confirmed that the catalyst is a suitable candidate causing no conflict with the substituents of the drug precursor. As shown in Figure 24, different substituents such as halo (F and Cl), ether, amin, and formyl as well as heterocycles such as furan and benzodiazine scaffolds remained intact during coupling process. This achievement can be considered as a remarkable applicability of this protocol.

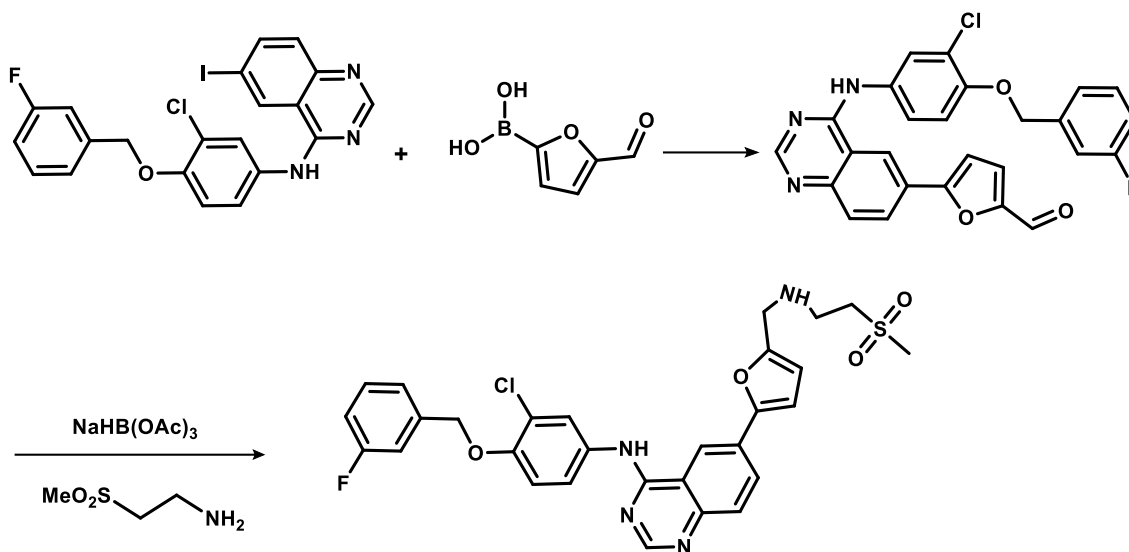


Figure 24. Lapatinib route of synthesis

This work was based on the hypothesis that recombinant route for peptide synthesis can be a viable alternate to solid phase peptide synthesis in terms of producing peptides capable of enabling nanoparticle morphology. In the current work, we demonstrate that recombinantly synthesized (Pd4)₃-GFPuv peptide is capable of directing palladium nanoparticle synthesis

without extensive peptide purification and as a fusion protein. Nucleation and growth of palladium nanoparticles occurred when Pd^{2+} was reduced to Pd^0 . As demonstrated in this work, nucleation and growth process of nanoparticles using recombinant peptide expressed in *E. coli* occurred in the presence of other soluble proteins (primarily *E. coli* host cell proteins) and other remnants such as salt, and media components from the upstream fermentation process.

Previously reported results with chemically synthesized, pure Pd4 peptide have demonstrated that during nucleation and growth, metallic cations interact with free electrons of the imidazole side chain of histidine moieties present in the peptide sequence [23]. Results obtained in this work indicated that nucleation was not compromised by either the heterogeneous nature of the mixture or histidine moieties randomly distributed throughout GFPuv or other proteins in the mixture.

Along with our demonstration of nanoparticle synthesis in the aforementioned environments, we also present a preliminary economic analysis [24]. Our basis for the cost estimate (Table 6) and process scheme uses data from two commercial platforms / products: recombinant human insulin (unit cost \$42/ gram final product) and an Enbrel®-like monoclonal antibody (Mab) (unit cost \$908/ gram). Each product is produced in the kilogram per year range, with a detailed breakdown of the fixed capital investment, total capital investment, and manufacturing costs obtained from [24]. Analyses presented in this reference describe plants capable of producing 18,000 kg/y and 6.5 g/y of insulin and Mab, respectively. The analyses demonstrate economy of scale, with each process starting from a host cell and ending with protein (polypeptide).

Importantly, we note that the two aforementioned products require absolute purity as they are pharmaceuticals. In contrast, we envision that nanoparticle synthesis may not require the

same level of purity. It is thus reasonable to conclude that the unit operations and cost to produce Pd4 or (Pd4)_n-GFPuv on the kilogram per year scale would not exceed that of insulin or Mab. More likely, the cost per gram will be at least two or one order of magnitude, respectively, less when compared to the Mab or insulin due to the reduction / elimination of bio separation process steps (Table 6). In other words, a recombinant approach to provide Pd4 or a similar construct appears to be attractive from both a scientific and economic standpoint.

5.4. Conclusion

To conclude, a facile aqueous solution phase nanoparticle synthesis method was exploited in a heterogeneous biological protein environment, and the palladium nanoparticles obtained are similar to those synthesized in prior work via chemically-synthesized Pd4 peptide. The prepared NPs could be utilized for Suzuki-Miyaura as well as Stille coupling reactions in green solvents. Compared to chemically-synthesized Pd4 peptide-directed Pd NPs, recombinant fusion protein-directed Pd NPs exhibits good catalytic activity (TOF of 12933 h⁻¹ and 3324 h⁻¹ for the Suzuki-Miyaura and Stille coupling model reactions, respectively) with very good stability (5 cycles) for both Suzuki-Miyaura and Stille coupling reactions. Also, recombinant fusion protein-directed Pd NPs were successfully used to prepare different substrates as well as Lapatinib precursor, an anti-cancer drug. Results demonstrated the potential for successful economic viability of both peptide synthesis and subsequent nanoparticle synthesis, where the biological peptide synthesis approach is expected to result in a three order of magnitude decrease in cost. The purity of peptide was found to have not large impact on catalytic performance of Pd NPs. Recombinant fusion protein-directed Pd NPs catalyst not only extends the catalytic

application of peptide-templated catalyst, but also provides a cost-effective approach to design heterogenous catalysts for substrates and precursors synthesis.

5.5. References

- [1] M.B. Dickerson, K.H. Sandhage, R.R. Naik, Protein- and peptide-directed syntheses of inorganic materials, *Chem. Rev.* 108 (2008) 4935–4978.
- [2] M. Sarikaya, C. Tamerler, A.K.-Y. Jen, K. Schulten, F. Baneyx, Molecular biomimetics: nanotechnology through biology, *Nat. Mater.* 2 (2003) 577.
- [3] B.D. Briggs, M.R. Knecht, Nanotechnology Meets Biology: Peptide-based Methods for the Fabrication of Functional Materials, *J. Phys. Chem. Lett.* 3 (2012) 405–418. doi:10.1021/jz2016473.
- [4] R. Schreiber, J. Do, E.-M. Roller, T. Zhang, V.J. Schüller, P.C. Nickels, J. Feldmann, T. Liedl, Hierarchical assembly of metal nanoparticles, quantum dots and organic dyes using DNA origami scaffolds, *Nat. Nanotechnol.* 9 (2014) 74–78. doi:10.1038/nnano.2013.253.
- [5] R. Coppage, J.M. Slocik, H. Ramezani-Dakhel, N.M. Bedford, H. Heinz, R.R. Naik, M.R. Knecht, Exploiting Localized Surface Binding Effects to Enhance the Catalytic Reactivity of Peptide-Capped Nanoparticles, *J. Am. Chem. Soc.* 135 (2013) 11048–11054. doi:10.1021/ja402215t.
- [6] A. Mosleh, M. Ehteshamzadeh, R. Taherzadeh Mousavian, Fabrication of an r-Al₂Ti intermetallic matrix composite reinforced with α -Al₂O₃ ceramic by discontinuous mechanical milling for thermite reaction, *Int. J. Miner. Metall. Mater.* 21 (2014) 1037–1043. doi:10.1007/s12613-014-1006-6.
- [7] A. Mosleh, H. Shahverdi, R. Poursalehi, Characterization of Al-CNT Composite Nanoparticles Synthesized by Electrical Explosion of Wire in Acetone, *J. Adv. Mater. Eng. Esteghlal.* 35 (2016) 47–53. doi:10.18869/acadpub.jame.35.2.47.
- [8] A. Mosleh, A. Heintz, K.-T. Lim, J.-W. Kim, R. Beitle, Permeability enhancement of Escherichia coli by single-walled carbon nanotube treatment, *Biotechnol. Prog.* 33 (2017) 654–657. doi:10.1002/btpr.2443.
- [9] M.R. Roshan, T.R. Mousavian, H. Ebrahimkhani, A. Mosleh, Fabrication of Al-based composites reinforced with Al₂O₃-TiB₂ ceramic composite particulates using vortex-casting method, *J. Min. Metall. B Metall.* 49 (2013) 299–305. doi:10.2298/JMMB120701032R.
- [10] G.M. Whitesides, B. Grzybowski, Self-Assembly at All Scales, *Science.* 295 (2002) 2418–2421. doi:10.1126/science.1070821.
- [11] N.M. Bedford, A.R. Showalter, T.J. Woehl, Z.E. Hughes, S. Lee, B. Reinhart, S.P. Ertem, E.B. Coughlin, Y. Ren, T.R. Walsh, Peptide-directed PdAu nanoscale surface segregation: toward controlled bimetallic architecture for catalytic materials, *ACS Nano.* 10 (2016) 8645–8659.

- [12] M. Fruchtl, J. Sakon, R. Beitle, Alternate carbohydrate and nontraditional inducer leads to increased productivity of a collagen binding domain fusion protein via fed-batch fermentation, *J. Biotechnol.* 226 (2016) 65–73. doi:10.1016/j.jbiotec.2016.03.016.
- [13] R. Coppage, J.M. Slocik, M. Sethi, D.B. Pacardo, R.R. Naik, M.R. Knecht, Elucidation of peptide effects that control the activity of nanoparticles, *Angew. Chem. Int. Ed.* 49 (2010) 3767–3770.
- [14] D.B. Pacardo, M. Sethi, S.E. Jones, R.R. Naik, M.R. Knecht, Biomimetic synthesis of Pd nanocatalysts for the Stille coupling reaction, *Acs Nano.* 3 (2009) 1288–1296.
- [15] R.P. Mukherjee, R. Beitle, S. Jayanthi, T.K.S. Kumar, D.S. McNabb, Production of an anti-Candida peptide via fed batch and ion exchange chromatography, *Biotechnol. Prog.* 32 (2016) 865–871.
- [16] W. Fu, Y. Cao, Q. Feng, W.R. Smith, P. Dong, M. Ye, J. Shen, Pd–Co nanoalloys nested on CuO nanosheets for efficient electrocatalytic N₂ reduction and room-temperature Suzuki–Miyaura coupling reaction, *Nanoscale.* 11 (2019) 1379–1385. doi:10.1039/C8NR08724E.
- [17] A. Biffis, P. Centomo, A. Del Zotto, M. Zecca, Pd Metal Catalysts for Cross-Couplings and Related Reactions in the 21st Century: A Critical Review, *Chem. Rev.* 118 (2018) 2249–2295. doi:10.1021/acs.chemrev.7b00443.
- [18] R. Tejada Vaprio, Peptide-directed Nanoparticle Synthesis With A Denovo Pd-binding Sequence Fused To A Reporter Protein, Theses Diss. (2017). <https://scholarworks.uark.edu/etd/2393>.
- [19] I. Mosleh, M. Benamara, L. Greenlee, M.H. Beyzavi, R. Beitle, Recombinant peptide fusion proteins enable palladium nanoparticle growth, *Mater. Lett.* 252 (2019) 68–71. doi:10.1016/j.matlet.2019.05.080.
- [20] D. Han, Z. Bao, H. Xing, Y. Yang, Q. Ren, Z. Zhang, Fabrication of plasmonic Au–Pd alloy nanoparticles for photocatalytic Suzuki–Miyaura reactions under ambient conditions, *Nanoscale.* 9 (2017) 6026–6032. doi:10.1039/C7NR01950E.
- [21] G. Erickson, J. Guo, M. McClure, M. Mitchell, M.-C. Salaun, A. Whitehead, Synthesis of Lapatinib via direct regioselective arylation of furfural, *Tetrahedron Lett.* 55 (2014) 6007–6010. doi:10.1016/j.tetlet.2014.09.039.
- [22] S. Mahboobi, A. Sellmer, M. Winkler, E. Eichhorn, H. Pongratz, T. Ciossek, T. Baer, T. Maier, T. Beckers, Novel Chimeric Histone Deacetylase Inhibitors: A Series of Lapatinib Hybrides as Potent Inhibitors of Epidermal Growth Factor Receptor (EGFR), Human Epidermal Growth Factor Receptor 2 (HER2), and Histone Deacetylase Activity, *J. Med. Chem.* 53 (2010) 8546–8555. doi:10.1021/jm100665z.

[23] N.M. Bedford, H. Ramezani-Dakhel, J.M. Slocik, B.D. Briggs, Y. Ren, A.I. Frenkel, V. Petkov, H. Heinz, R.R. Naik, M.R. Knecht, Elucidation of peptide-directed palladium surface structure for biologically tunable nanocatalysts, *ACS Nano*. 9 (2015) 5082–5092.

[24] R.G.A. HARRISON, T.G. Day, R.G. Harrison, P. Todd, S.R. Rudge, S.R. Rudge, T.L.S.R. Rudge, P.W. Todd, D. Petrides, *Bioseparations Science and Engineering*, Oxford University Press, 2003.

5.5. Supporting Information

Recombinant peptide fusion protein-templated palladium nanoparticles for Suzuki-Miyaura coupling and Stille coupling reactions.

Imann Mosleh¹,

Rita Tejada Vaprio¹,

Rudra Palash Mukherjee¹,

McKinzie Frucht²,

Nicholas Bedford³,

Hamidreza Shahsavari⁴,

Lauren Greenlee¹,

M. Hassan Beyzavi^{4*},

Robert Beitle^{1*}

(1) Ralph E. Martin Department of Chemical Engineering, University of Arkansas, Fayetteville, Arkansas 72701, USA.

(2) Boston Mountain Biotech, LLC, 700 W Research Center Blvd, Fayetteville, AR 72701, USA.

(3) Materials and Manufacturing Directorate, Air Force Research Laboratory, 5135 Pearson Road, Building 10, Wright-Patterson AFB, OH 45433, USA.

(4) Department of Chemistry and Biochemistry, University of Arkansas, Fayetteville, Arkansas 72701, USA.

Inductively coupled plasma mass spectroscopy (ICP-MS)

To study the amount of palladium, an aliquot of (Pd4)₃-GFPuv fusion protein-templated Pd NPs catalyst containing palladium was added to one mL of 2% nitric acid solution. A catalyst solution of containing approximately 50 parts per billion (ppb) palladium were prepared and analyzed using ICP-MS. The palladium standard for ICP-MS was purchased from SIGMA-ALDRICH[®] was used to make 5 ppm, 2 ppm, and 50 ppb standards for this analysis. As shown in Fig S1, the 46 ppb Pd content of the catalyst from the aliquot was confirmed. A fraction containing 5 mmol% was taken for coupling reactions.

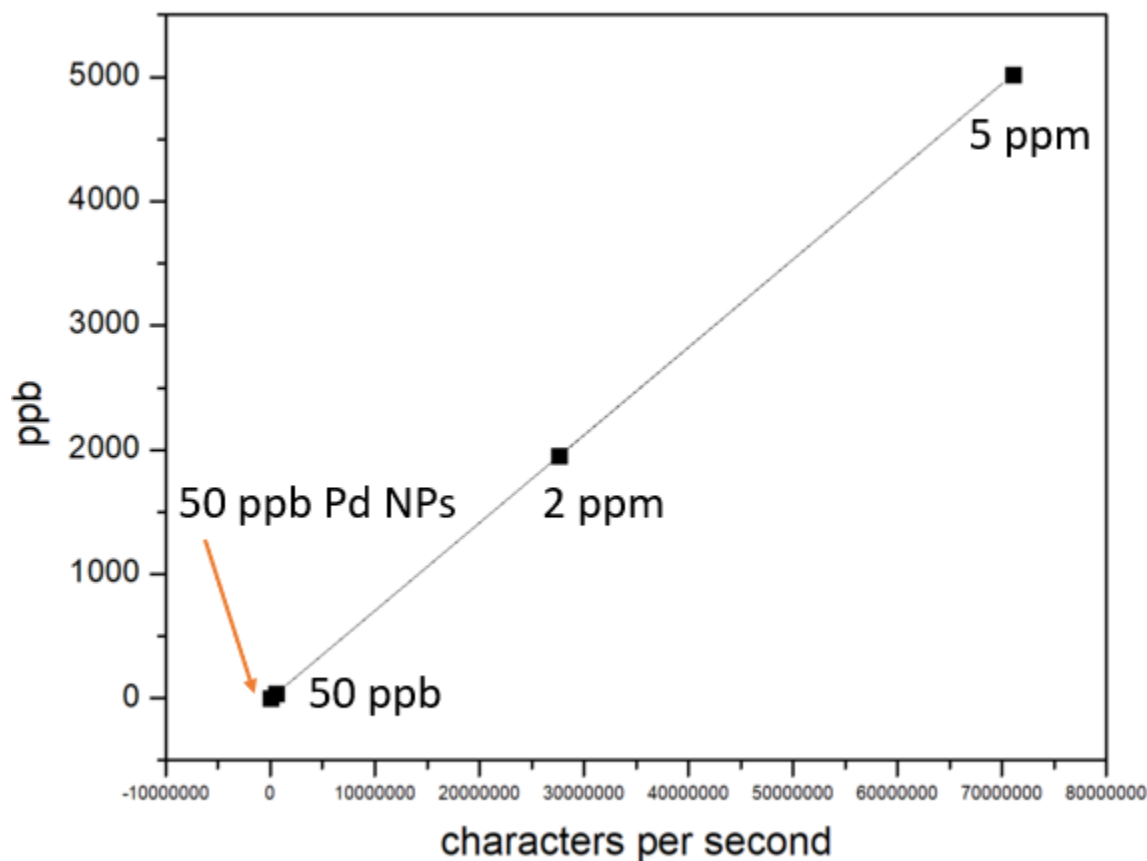
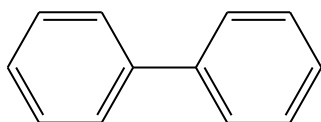


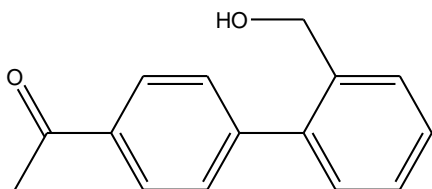
Fig S1. Inductively Coupled Plasma Atomic Emission Spectroscopy (ICP-AES) of the catalyst

A Procedures for Catalytic Processes and Compound Characterization

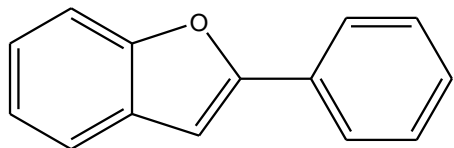
General procedure for the Suzuki-Miyaura cross coupling: To a stirred solution of iodo benzene (0.1 mmol, 1.0 equiv.), boronic acid (0.12 mmol, 1.2 equiv.) and catalyst (1 mmol%) in 1 ml of EtOH and deionized water (1:1), K_2CO_3 (0.3 mmol, 3 equiv.) was added at 80 °C. The reaction mixture was stirred for 90 minutes. The biphenyls were obtained using TELOS thin-layer chromatography plates as white solids.



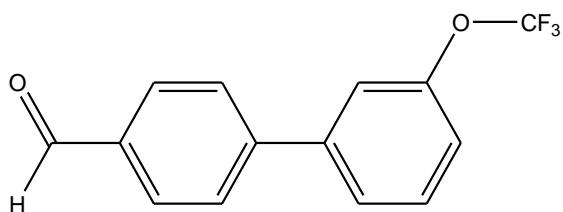
LC-MS m/z Calcd. for $[M]^+$ 154.08; Found 154.02. 1H NMR (400 MHz, $CDCl_3$) δ 7.36 (t, $J = 7.3$ Hz, Ar-H, 1H), 7.45 (t, $J = 7.6$ Hz, Ar-H, 2H), 7.61 (d, $J = 7.7$ Hz, Ar-H, 2H). $^{13}C\{^1H\}$ NMR (101 MHz, $CDCl_3$) δ 127.3 (C_{Ar}), 127.4 (C_{Ar}), 128.9 (C_{Ar}), 141.4 (C_{Ar}).



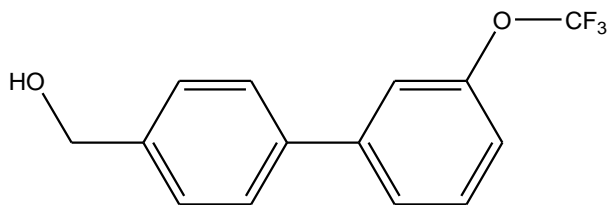
1H NMR (400 MHz, $CDCl_3$) δ 2.64 (s, CH_3 , 3H), 4.60 (s, CH_2 , 2H), 7.28 (dd, $J = 1.3, 7.5$ Hz, Ar-H, 1H), 7.35 – 7.45 (m, Ar-H, 2H), 7.49 (d, $J = 8.3$ Hz, Ar-H, 2H), 7.58 (d, $J = 7.4$ Hz, Ar-H, 1H), 8.01 (d, $J = 8.3$ Hz, Ar-H, 2H). $^{13}C\{^1H\}$ NMR (101 MHz, $CDCl_3$) δ 26.8 (CH_3), 63.1 (CH_2), 128.0 (C_{Ar}), 128.4 (C_{Ar}), 128.5 (C_{Ar}), 128.9 (C_{Ar}), 129.6 (C_{Ar}), 129.9 (C_{Ar}), 136.1 (C_{Ar}), 138.0 (C_{Ar}), 140.4 (C_{Ar}), 145.8 (C_{Ar}), 198.0 ($C=O$).



HR ESI-MS(+) m/z Calcd. for $[M+H]^+$ 195.0804; Found 195.0798. ^1H NMR (400 MHz, CDCl_3) δ 7.04 (s, Ar-H, 1H), 7.24 (td, $J = 1.1, 7.4$ Hz, Ar-H, 1H), 7.29 (td, $J = 1.6, 7.9$ Hz, Ar-H, 1H), 7.36 (t, $J = 7.4$ Hz, Ar-H, 1H), 7.46 (t, $J = 7.6$ Hz, Ar-H, 2H), 7.53 (d, $J = 7.8$ Hz, Ar-H, 1H), 7.59 (d, $J = 7.6$ Hz, Ar-H, 1H), 7.88 (d, $J = 7.3$ Hz, Ar-H, 2H). $^{13}\text{C}\{^1\text{H}\}$ NMR (101 MHz, CDCl_3) δ 101.4 (C_{Ar}), 111.3 (C_{Ar}), 121.0 (C_{Ar}), 123.1 (C_{Ar}), 124.4 (C_{Ar}), 125.1 (C_{Ar}), 128.7 (C_{Ar}), 128.9 (C_{Ar}), 129.4 (C_{Ar}), 130.6 (C_{Ar}), 155.2 (C_{Ar}), 155.9 (C_{Ar}).

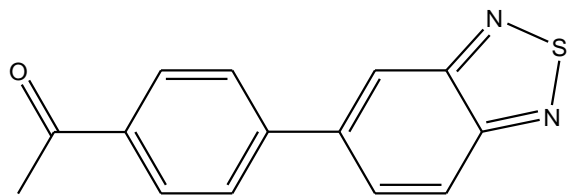


^1H NMR (400 MHz, CDCl_3) δ 7.28 (d, $J = 8.2$ Hz, Ar-H, 1H), 7.48 (s, Ar-H, 1H), 7.51 (t, $J = 7.9$ Hz, Ar-H, 1H), 7.57 (d, $J = 7.8$ Hz, Ar-H, 1H), 7.74 (d, $J = 8.2$ Hz, Ar-H, 2H), 7.98 (d, $J = 8.2$ Hz, Ar-H, 2H), 10.08 (s, CHO, 1H). $^{13}\text{C}\{^1\text{H}\}$ (101 MHz, CDCl_3) δ 120.1 (C_{Ar}), 120.9 (C_{Ar}), 125.9 (C_{Ar}), 127.9 (C_{Ar}), 130.5 (C_{Ar}), 130.6 (C_{Ar}), 135.9 (C_{Ar}), 141.8 (C_{Ar}), 145.2 (C_{Ar}), 191.9 (C=O). $^{19}\text{F}\{^1\text{H}\}$ NMR (377 MHz, CDCl_3) δ -58.0 (CF_3).

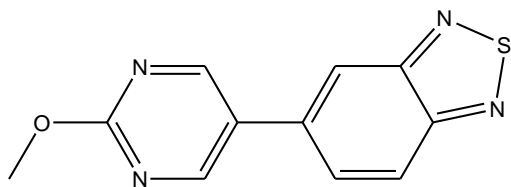


HR ESI-MS(+) m/z Calcd. for $[M+H-H_2O]^+$ 251.0678; Found 251.0679. ^1H NMR (400 MHz, CDCl_3) δ 4.75 (s, CH_2 , 2H), 7.20 (d, $J = 7.9$ Hz, Ar-H, 1H), 7.43 – 7.49 (m, Ar-H, 4H), 7.52 (d, $J = 7.8$ Hz, Ar-H, 1H), 7.57 (d, $J = 8.1$ Hz, Ar-H, 2H). $^{13}\text{C}\{^1\text{H}\}$ NMR (101 MHz, CDCl_3) δ 65.1

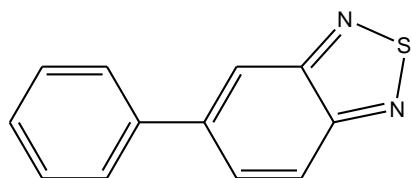
(CH₂), 119.7 (C_{Ar}), 119.8 (C_{Ar}), 125.5 (C_{Ar}), 127.4 (C_{Ar}), 127.7 (C_{Ar}), 130.2 (C_{Ar}), 139.1 (C_{Ar}), 140.9 (C_{Ar}), 143.1 (C_{Ar}). ¹⁹F{¹H} NMR (377 MHz, CDCl₃) δ -57.9 (CF₃).



HR ESI-MS(+) m/z Calcd. for [M+H]⁺ 255.0587; Found 255.0593. ¹H NMR (400 MHz, CDCl₃) δ 2.64 (s, CH₃, 3H), 7.81 (d, *J* = 8.4 Hz, Ar-H, 2H), 7.91 (dd, *J* = 1.7, 9.1 Hz, Ar-H, 1H), 8.09 – 8.12 (m, Ar-H, 3H), 8.23 (d, *J* = 1.7 Hz, Ar-H, 1H). ¹³C{¹H} NMR (101 MHz, CDCl₃) δ 26.9 (CH₃), 119.5 (C_{Ar}), 122.0 (C_{Ar}), 127.9 (C_{Ar}), 129.3 (C_{Ar}), 129.8 (C_{Ar}), 136.9 (C_{Ar}), 141.3 (C_{Ar}), 144.3 (C_{Ar}), 154.6 (C_{Ar}), 155.4 (C_{Ar}), 197.7 (C=O).

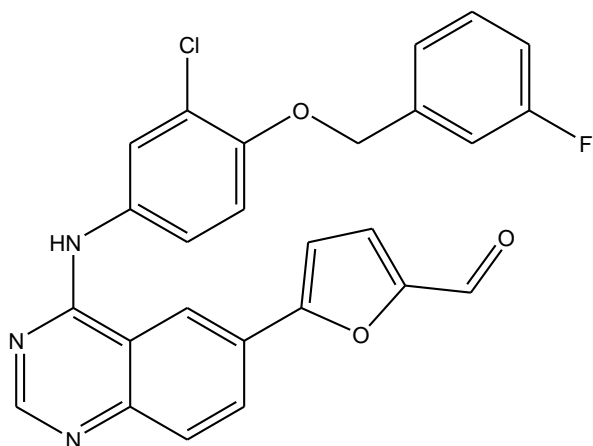


HR ESI-MS(+) m/z Calcd. for [M+H]⁺ 245.0492; Found 245.0491. ¹H NMR (400 MHz, CDCl₃) δ 4.11 (s, CH₃, 3H), 7.79 (dd, *J* = 1.7, 9.1 Hz, Ar-H, 1H), 8.14 (d, *J* = 9.1 Hz, Ar-H, 1H), 8.16 (d, *J* = 1.7 Hz, Ar-H, 1H), 8.86 (s, Ar-H, 2H). ¹³C{¹H} NMR (101 MHz, CDCl₃) δ 55.5 (CH₃), 118.6 (C_{Ar}), 122.7 (C_{Ar}), 126.5 (C_{Ar}), 127.1 (C_{Ar}), 128.9 (C_{Ar}), 129.0 (C_{Ar}), 135.5 (C_{Ar}), 155.3 (C_{Ar}), 157.9 (C_{Ar}).

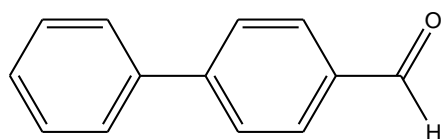


HR ESI-MS(+) m/z Calcd. for [M+H]⁺ 213.0481; Found 213.0477. ¹H NMR (400 MHz, CDCl₃) δ 7.44 (t, *J* = 7.3 Hz, Ar-H, 1H), 7.52 (t, *J* = 7.4 Hz, Ar-H, 2H), 7.71 (d, *J* = 7.3 Hz, Ar-H, 2H),

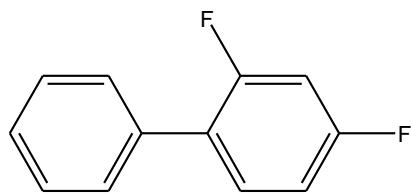
7.89 (dd, $J = 1.7, 9.1$ Hz, Ar-H, 1H), 8.06 (d, $J = 9.1$ Hz, Ar-H, 1H), 8.1.17 (d, $J = 1.7$ Hz, Ar-H, 1H). $^{13}\text{C}\{^1\text{H}\}$ NMR (101 MHz, CDCl_3) δ 118.7 (C_{Ar}), 121.6 (C_{Ar}), 124.4 (C_{Ar}), 127.7 (C_{Ar}), 128.5 (C_{Ar}), 129.2 (C_{Ar}), 130.4 (C_{Ar}), 139.7 (C_{Ar}), 142.4 (C_{Ar}).



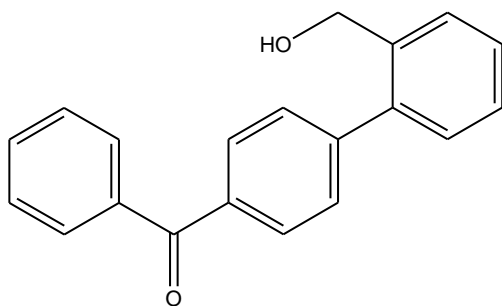
HR ESI-MS(+) m/z Calcd. for $[\text{M}+\text{H}]^+$ 474.1015; Found 474.1023. ^1H NMR (400 MHz, Acetone) δ 5.30 (s, CH_2 , 2H), 7.12 (dt, $J = 2.5, 8.6$ Hz, Ar-H, 1H), 7.25 (d, $J = 9.0$ Hz, Ar-H, 1H), 7.32 (d, $J = 3.7$ Hz, Ar-H, 1H), 7.35 (s, Ar-H, 1H), 7.38 (d, $J = 7.7$ Hz, Ar-H, 1H), 7.42 – 7.53 (m, Ar-H, 1H), 7.62 (d, $J = 3.7$ Hz, Ar-H, 1H), 7.76 – 7.80 (m, Ar-H, 1H), 7.91 (d, $J = 8.8$ Hz, Ar-H, 1H), 8.12 (dd, $J = 2.6, 4.4$ Hz, Ar-H, 1H), 8.32 (dd, $J = 1.8, 8.8$ Hz, Ar-H, 1H), 8.65 (s, Ar-H, 1H), 8.92 (d, $J = 1.6$ Hz, Ar-H, 1H), 9.55 (s, NH, 1H), 9.70 (s, CHO, 1H). $^{19}\text{F}\{^1\text{H}\}$ NMR (377 MHz, CDCl_3) δ -114.9 (F).



HR ESI-MS(+) m/z Calcd. for $[\text{M}+\text{H}]^+$ 183.0804; Found 183.0799. ^1H NMR (400 MHz, CDCl_3) δ 7.42 (t, $J = 7.6$ Hz, Ar-H, 1H), 7.49 (t, $J = 7.4$ Hz, Ar-H, 2H), 7.65 (d, $J = 7.4$ Hz, Ar-H, 2H), 7.76 (d, $J = 8.2$ Hz, Ar-H, 2H), 7.96 (d, $J = 8.2$ Hz, Ar-H, 2H), 10.07 (s, CHO, 1H). $^{13}\text{C}\{^1\text{H}\}$ NMR (101 MHz, CDCl_3) δ 127.5 (C_{Ar}), 127.9 (C_{Ar}), 128.6 (C_{Ar}), 129.2 (C_{Ar}), 130.4 (C_{Ar}), 135.4 (C_{Ar}), 139.8 (C_{Ar}), 147.4 (C_{Ar}), 192.1 (C=O).

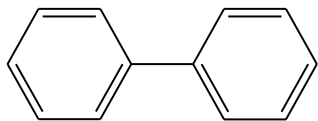


LC-MS m/z Calcd. for $[M]^+$ 190.06; Found 190.02. ^1H NMR (400 MHz, CDCl_3) δ 6.86 – 7.00 (m, Ar-H, 2H), 7.35 – 7.54 (m, Ar-H, 6H). $^{13}\text{C}\{^1\text{H}\}$ NMR (101 MHz, CDCl_3) δ 104.5 (dd, $J = 25, 27$ Hz, C_{Ar}), 111.6 (dd, $J = 4, 21$ Hz, C_{Ar}), 125.5 (dd, $J = 4, 14$ Hz, C_{Ar}), 127.9 (C_{Ar}), 128.7 (C_{Ar}), 129.0 (d, $J = 3$ Hz, C_{Ar}), 131.6 (dd, $J = 5, 9$ Hz, C_{Ar}), 135.1 (d, $J = 1$ Hz, C_{Ar}), 159.8 (dd, $J = 12, 251$ Hz, C-F), 162.4 (dd, $J = 12, 249$ Hz, C-F). $^{19}\text{F}\{^1\text{H}\}$ NMR (377 MHz, CDCl_3) δ -113.9 (d, $J = 9$ Hz, F), -111.8 (d, $J = 9$ Hz, F).

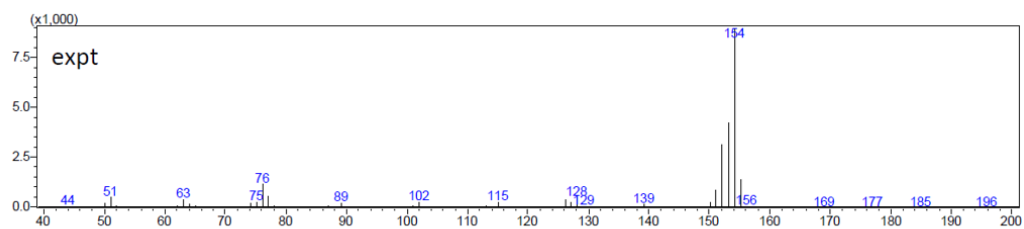


HR ESI-MS(+) m/z Calcd. for $[M+H]^+$ 289.1223; Found 289.1226. ^1H NMR (400 MHz, CDCl_3) δ 4.65 (s, CH_2 , 2H), 7.33 (dd, $J = 1.3, 7.4$ Hz, Ar-H, 1H), 7.40 (td, $J = 1.5, 7.5$ Hz, Ar-H, 1H), 7.45 (td, $J = 1.4, 7.3$ Hz, Ar-H, 1H), 7.50 – 7.54 (m, Ar-H, 4H), 7.56 – 7.65 (m, 2H), 7.77 – 7.97 (m, 4H).

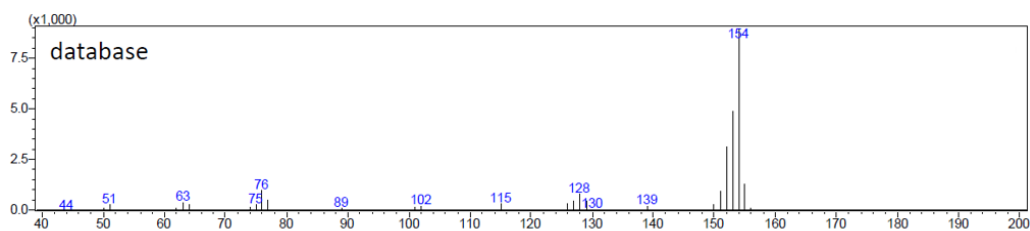
GC mass spectrometry spectra of the compounds

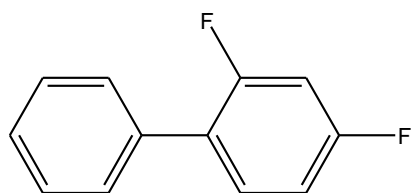


a) Experimental LC-MS

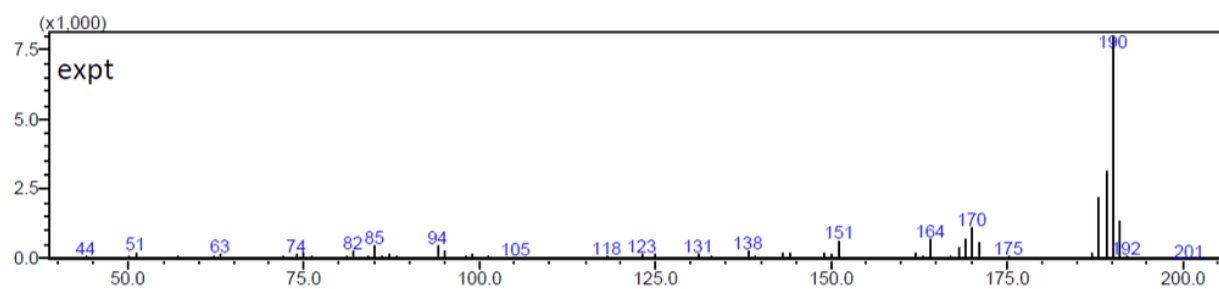


b) Calculated LC-MS

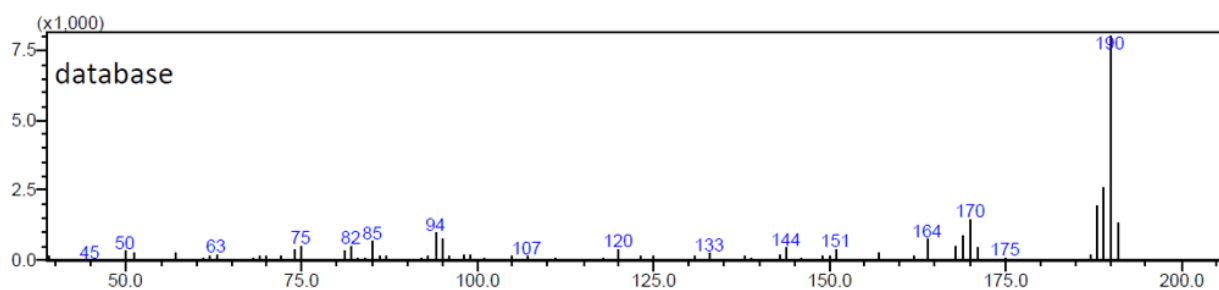




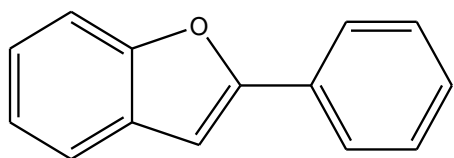
a) Experimental LC-MS



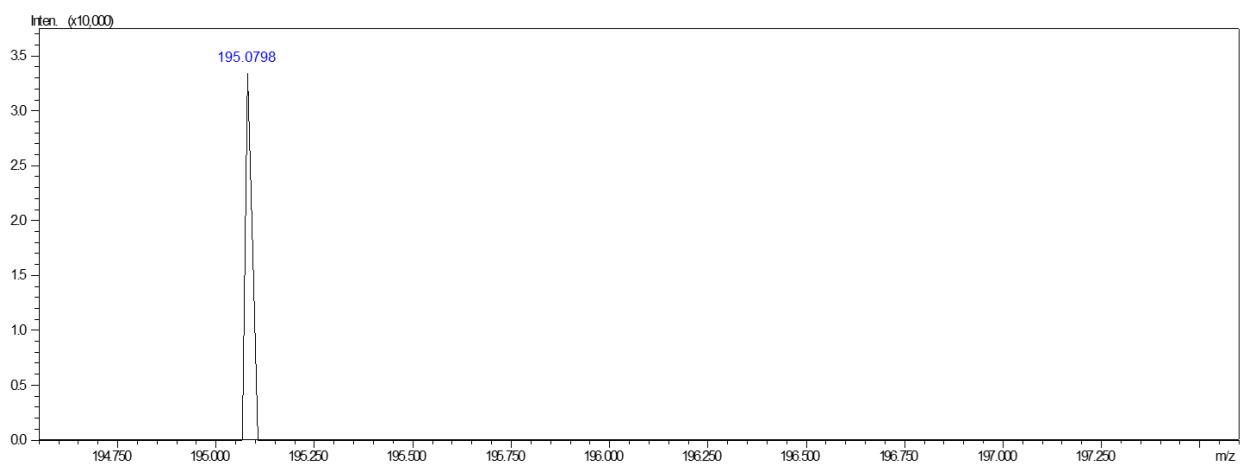
b) Calculated LC-MS



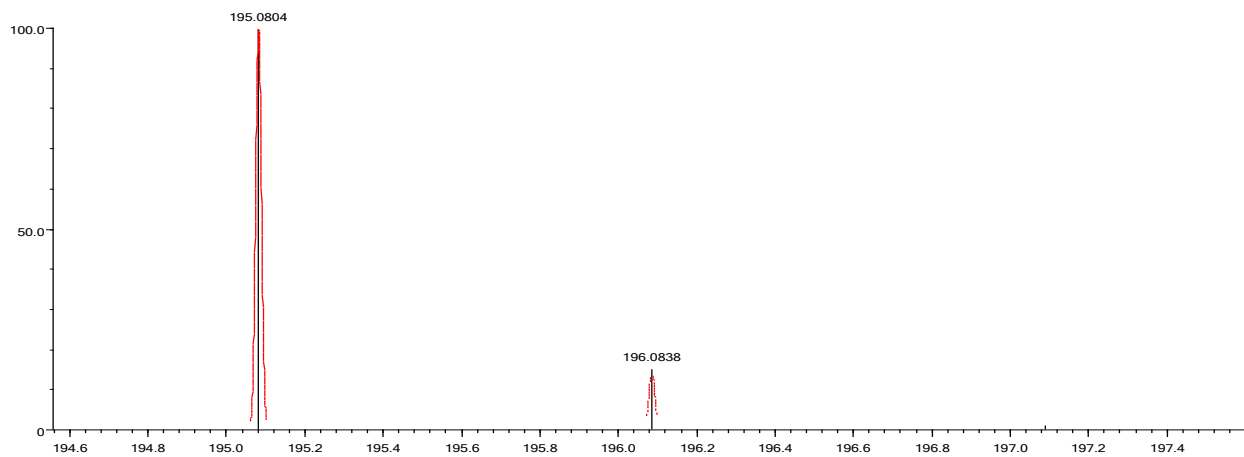
ESI high resolution mass spectrometry spectra of the compounds

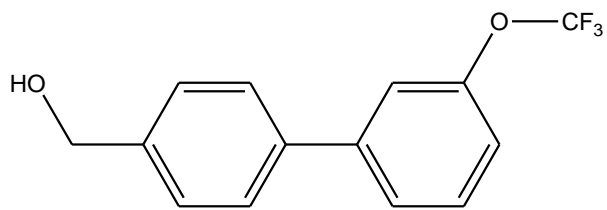


c) Experimental HR ESI-MS

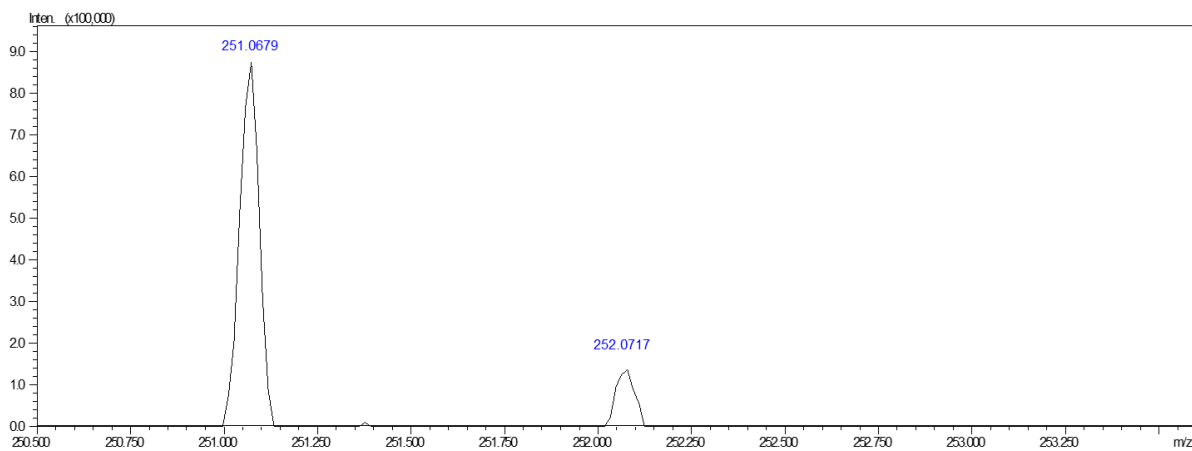


d) Calculated HR ESI-MS

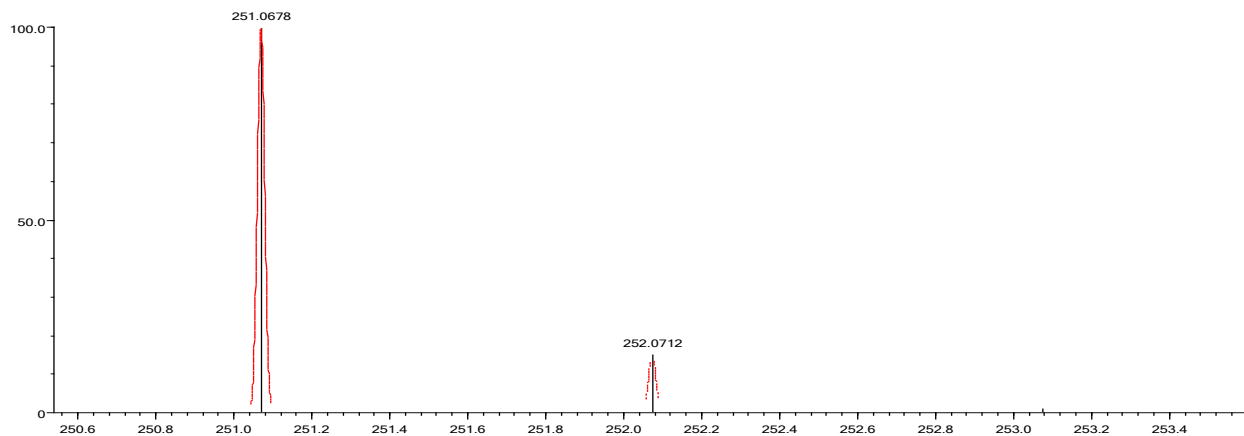


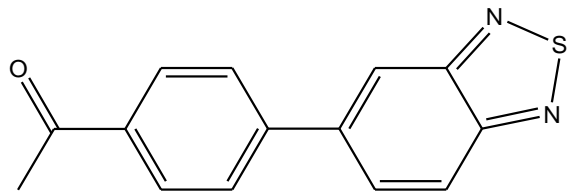


a) Experimental HR ESI-MS

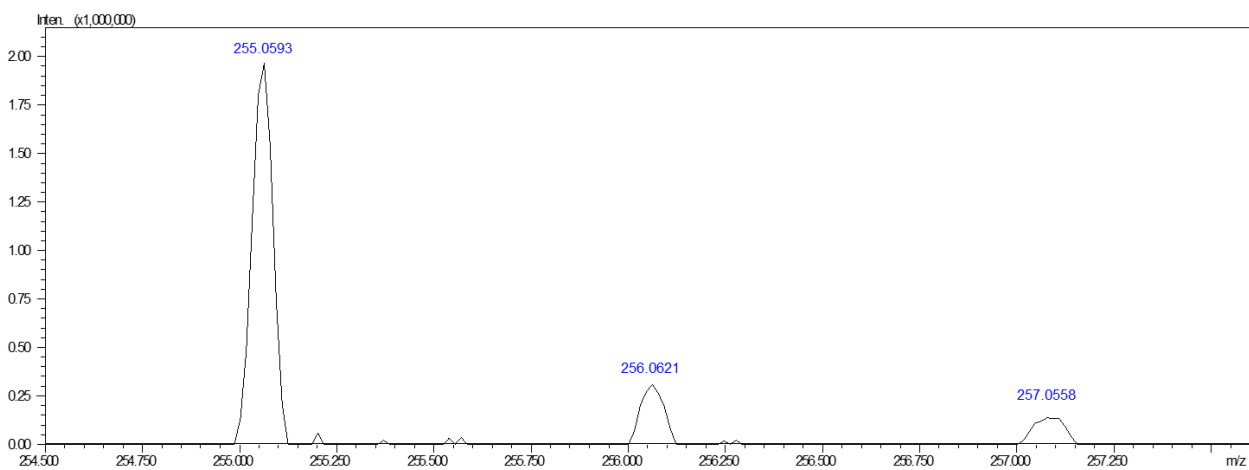


b) Calculated HR ESI-MS

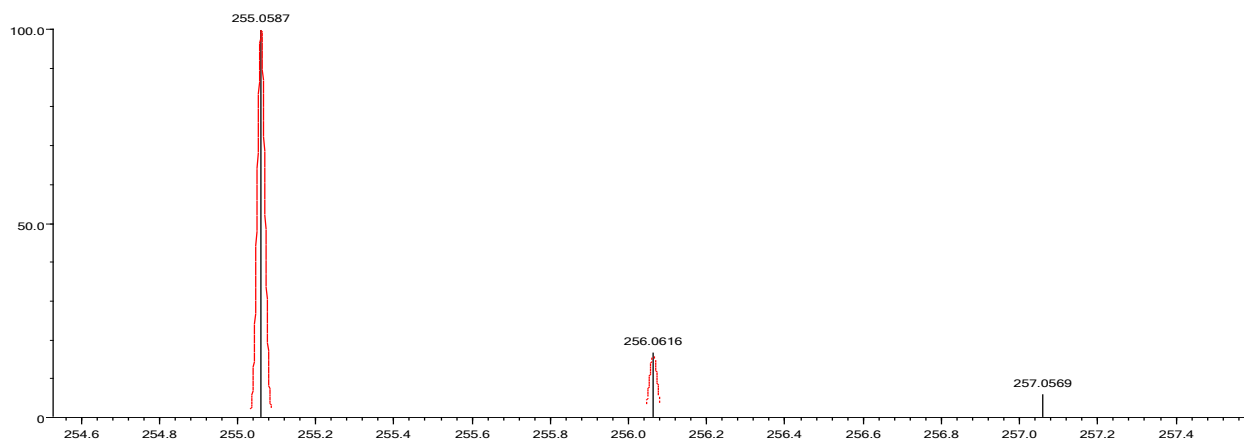


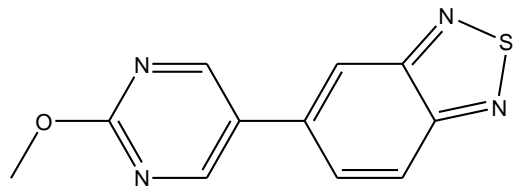


a) Experimental HR ESI-MS

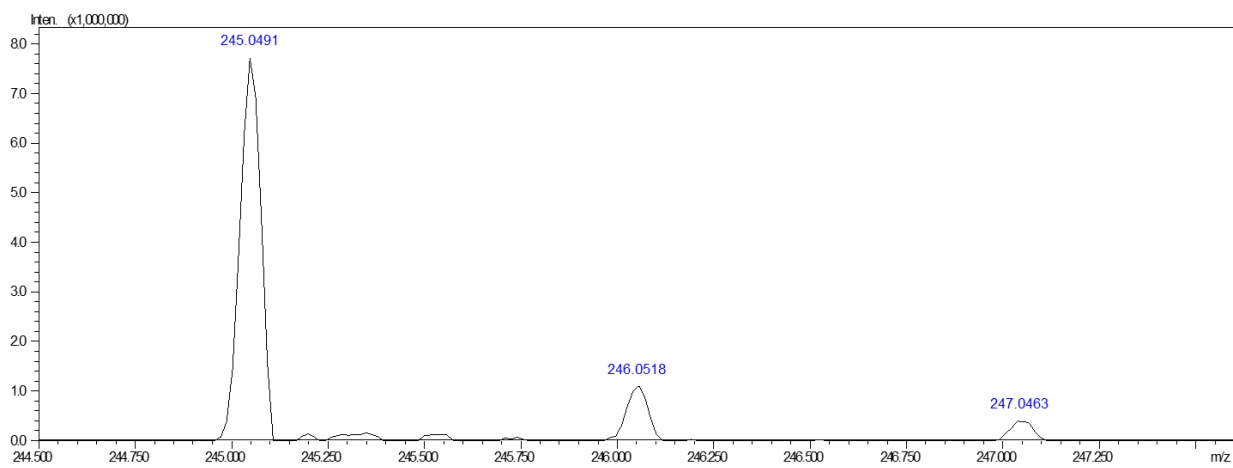


b) Calculated HR ESI-MS

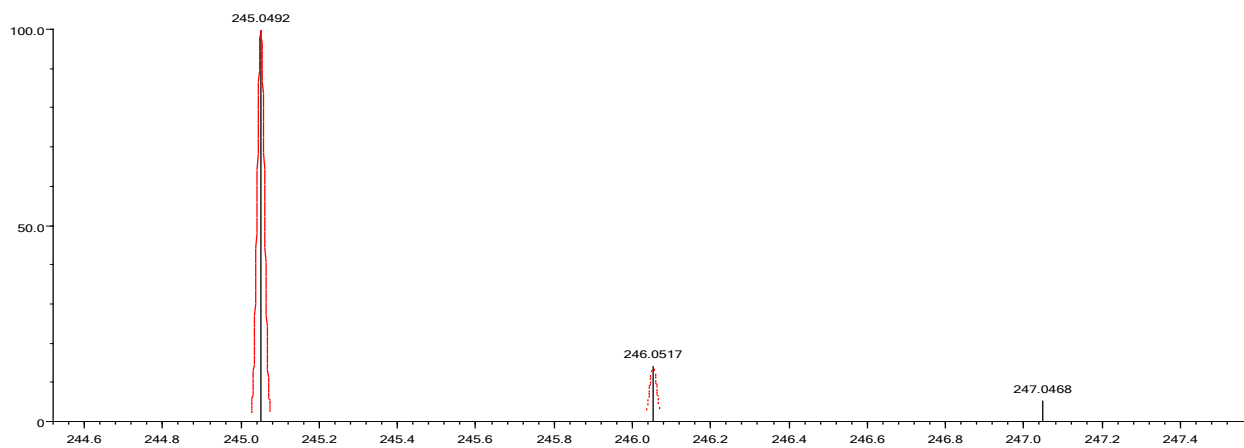


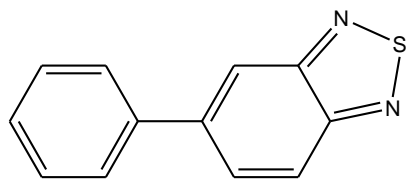


a) Experimental HR ESI-MS

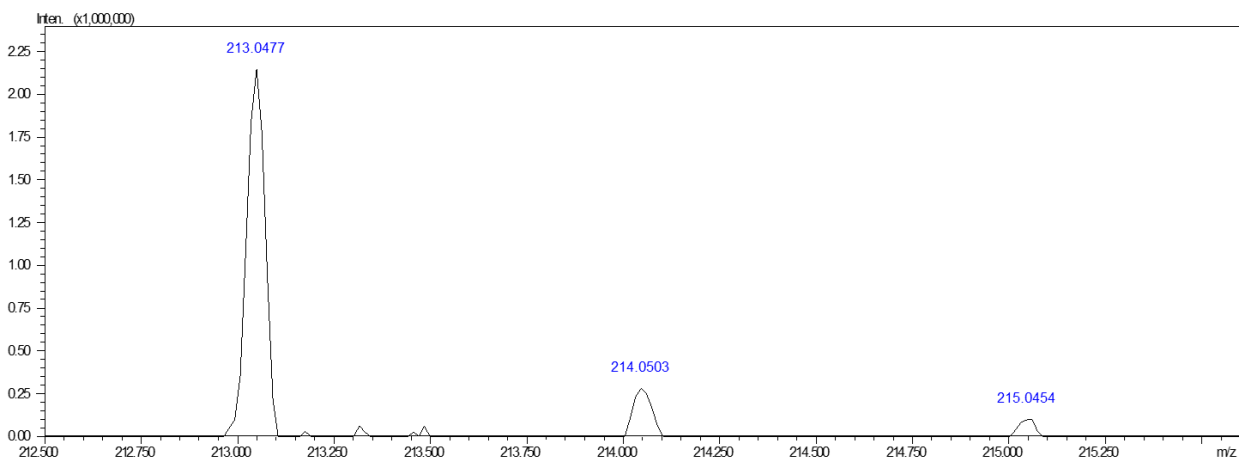


b) Calculated HR ESI-MS

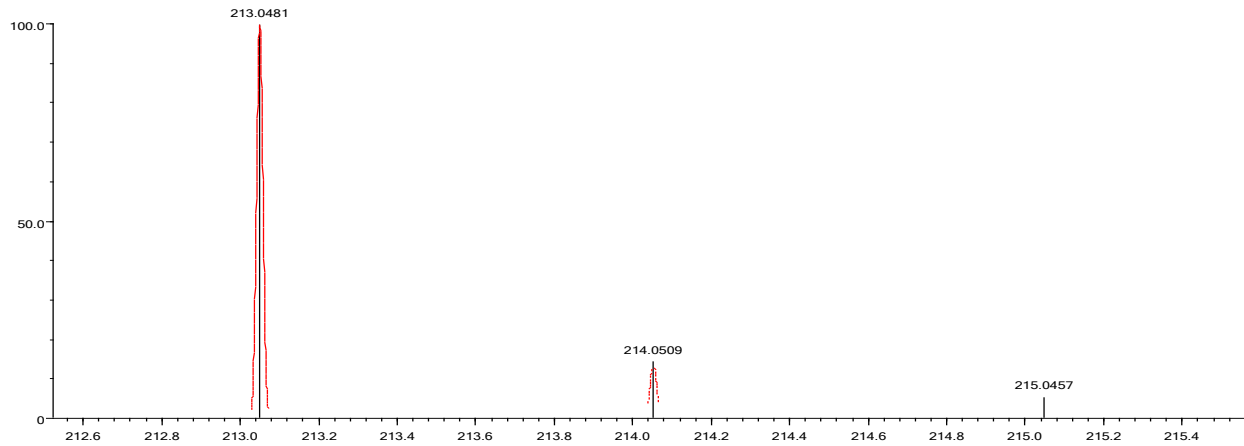


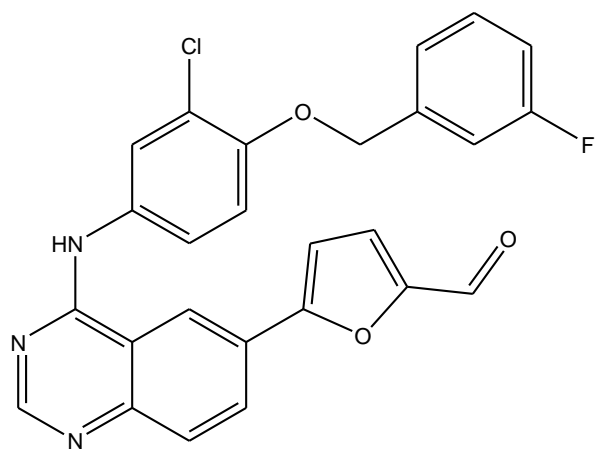


a) Experimental HR ESI-MS

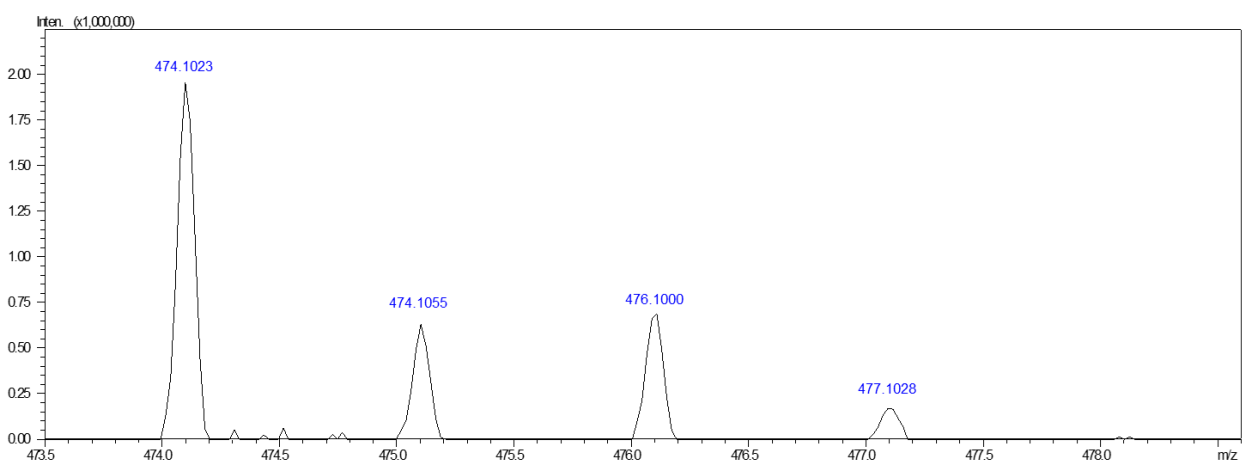


b) Calculated HR ESI-MS

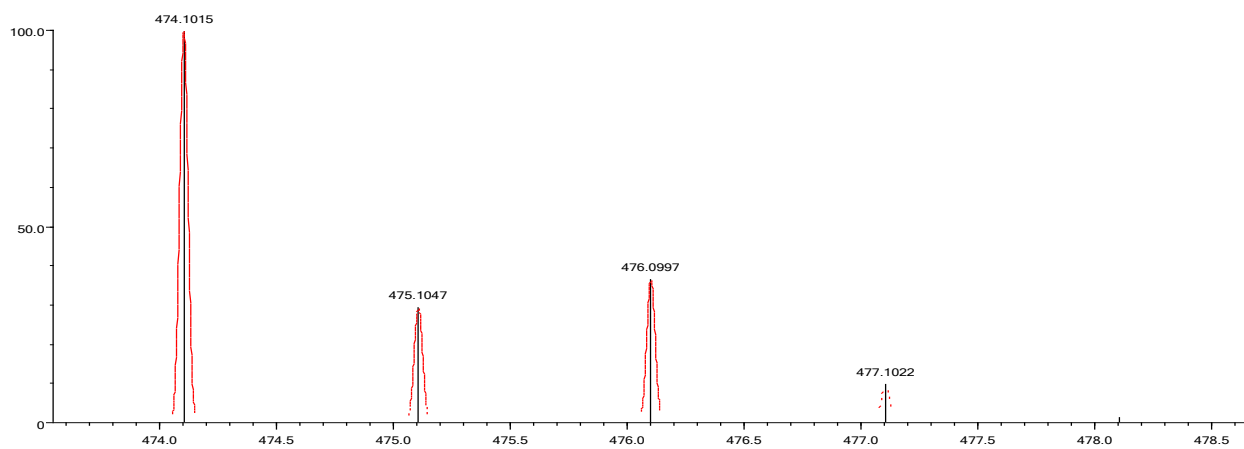


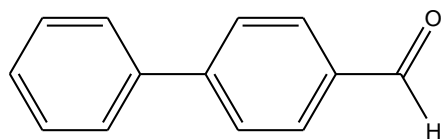


a) Experimental HR ESI-MS

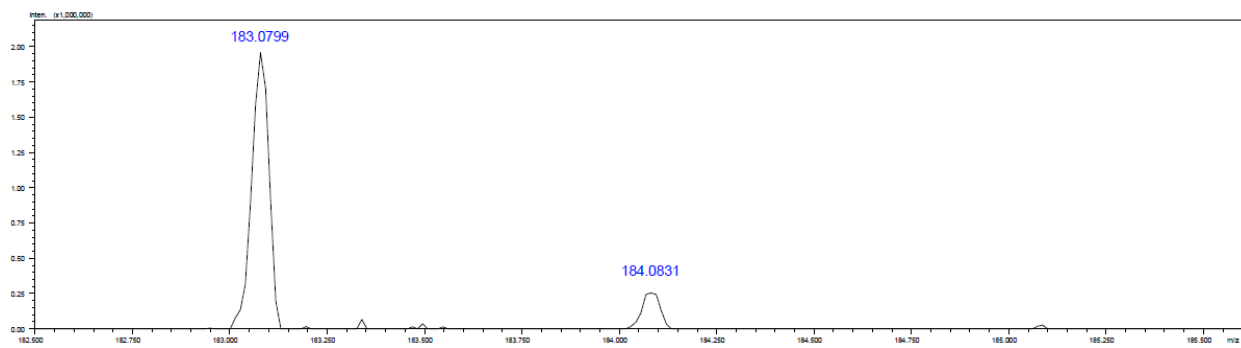


b) Calculated HR ESI-MS

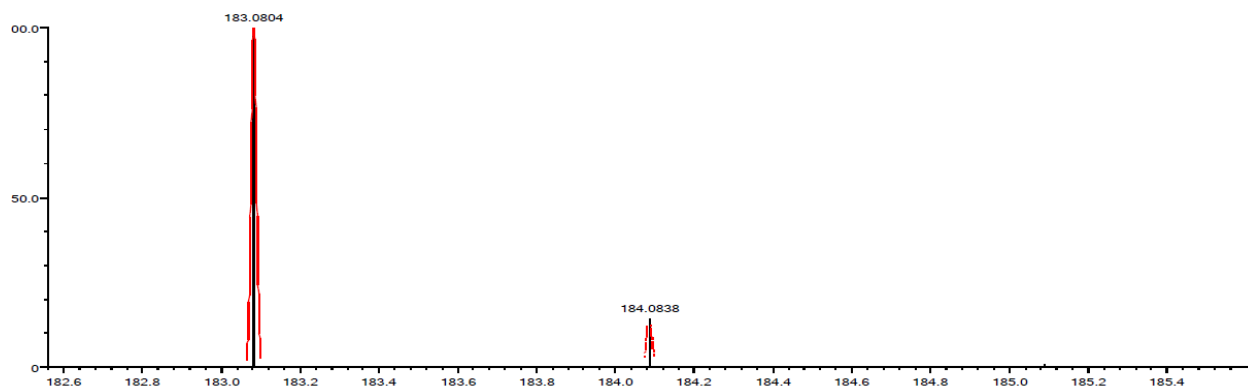


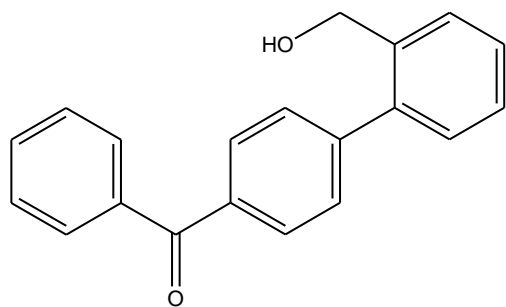


a) Experimental HR ESI-MS

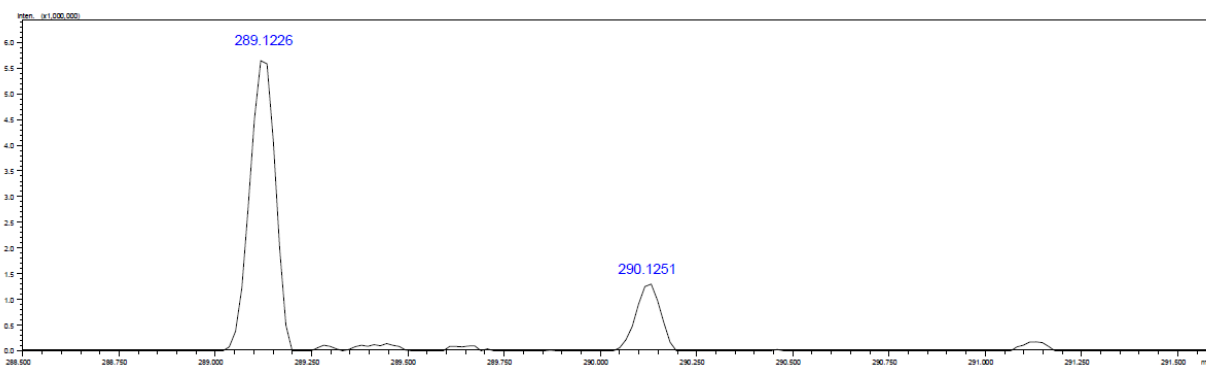


b) Calculated HR ESI-MS

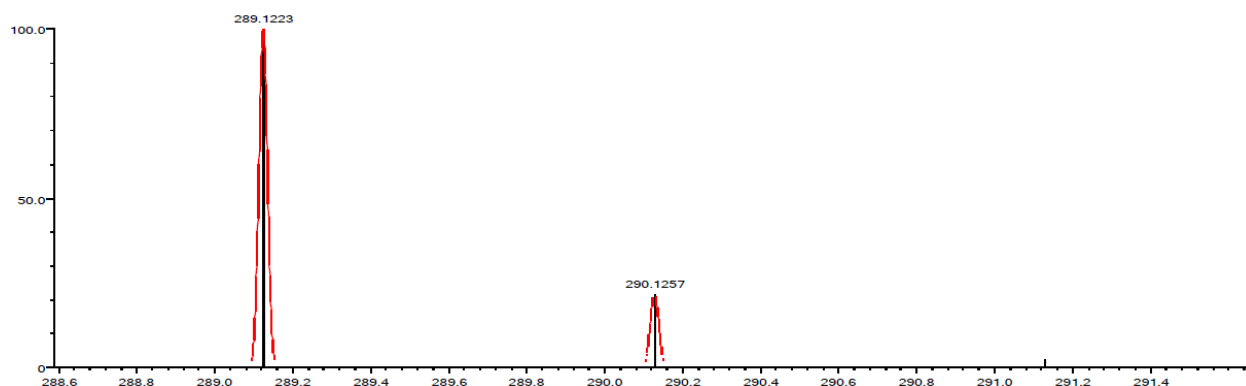




a) Experimental HR ESI-MS



b) Calculated HR ESI-MS



NMR spectra of the compounds

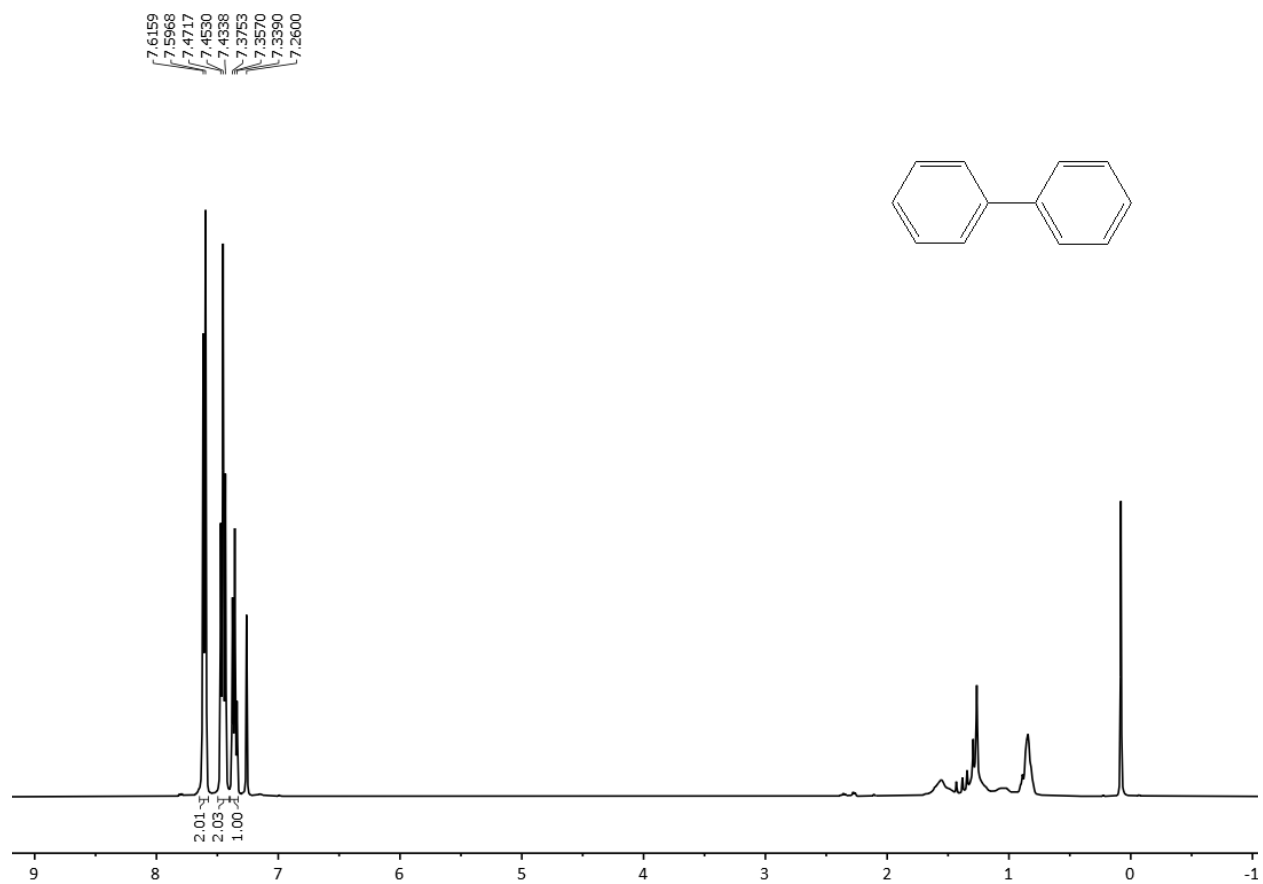


Fig S2. ^1H NMR (400 MHz, CDCl_3) spectrum.

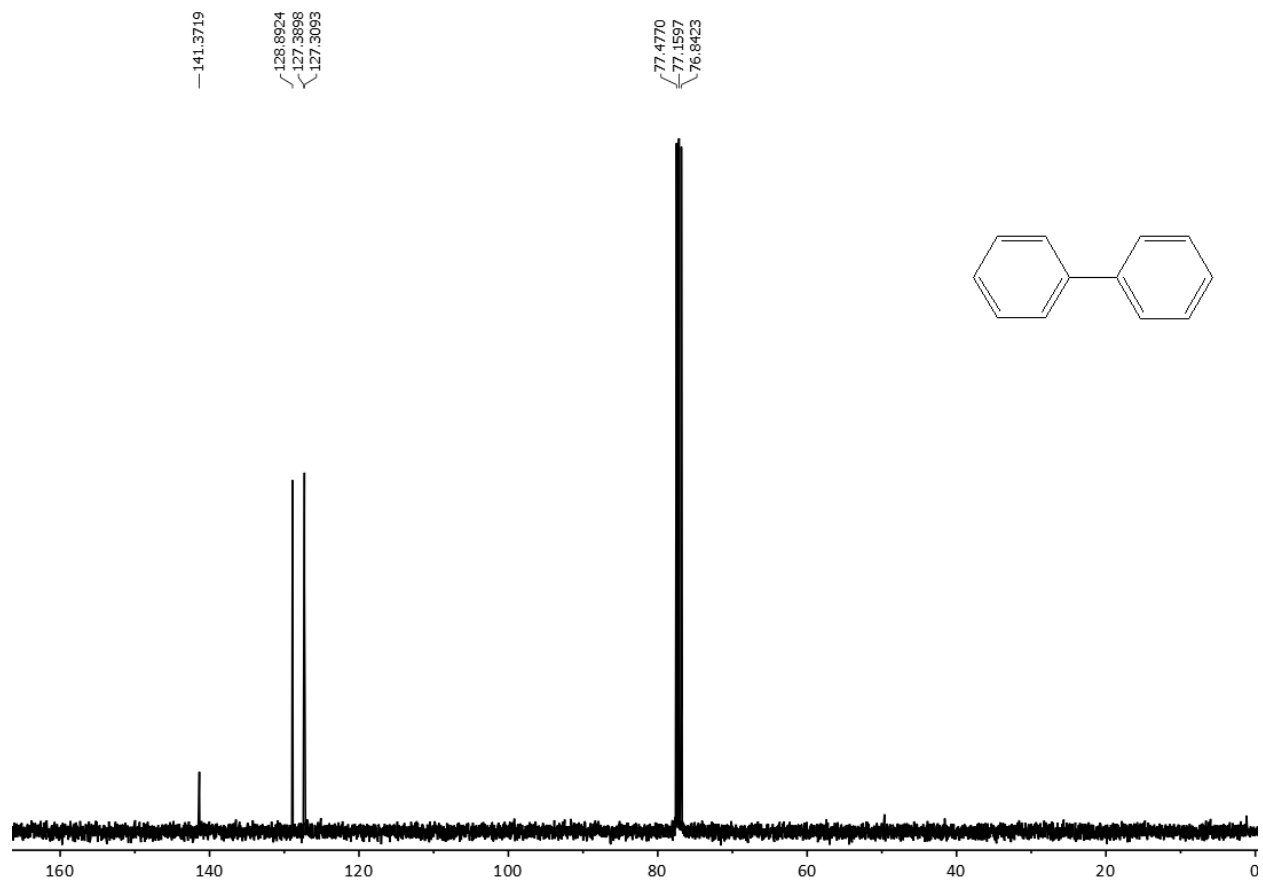


Fig S3. ^{13}C NMR (400 MHz, CDCl_3) spectrum.

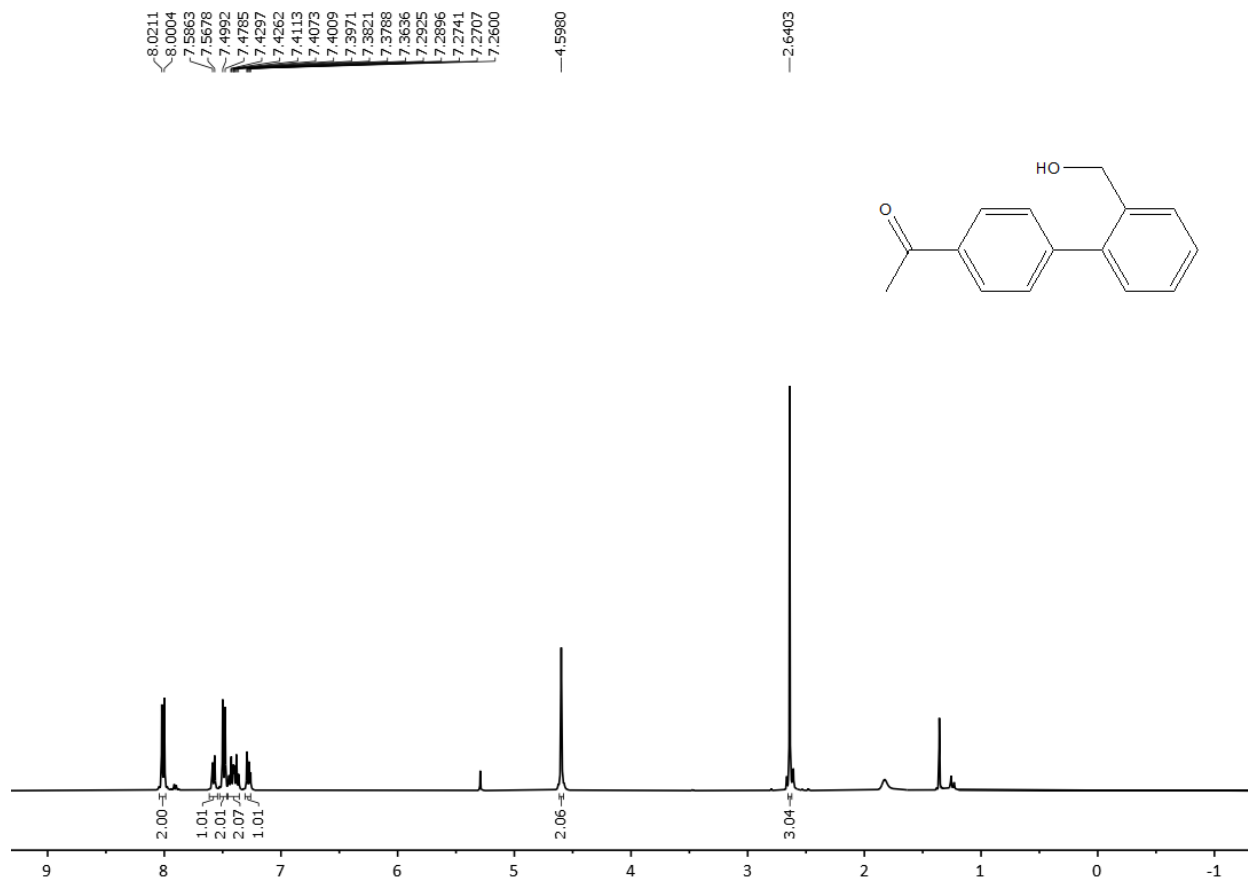


Fig S4. ¹H NMR (400 MHz, CDCl₃) spectrum.

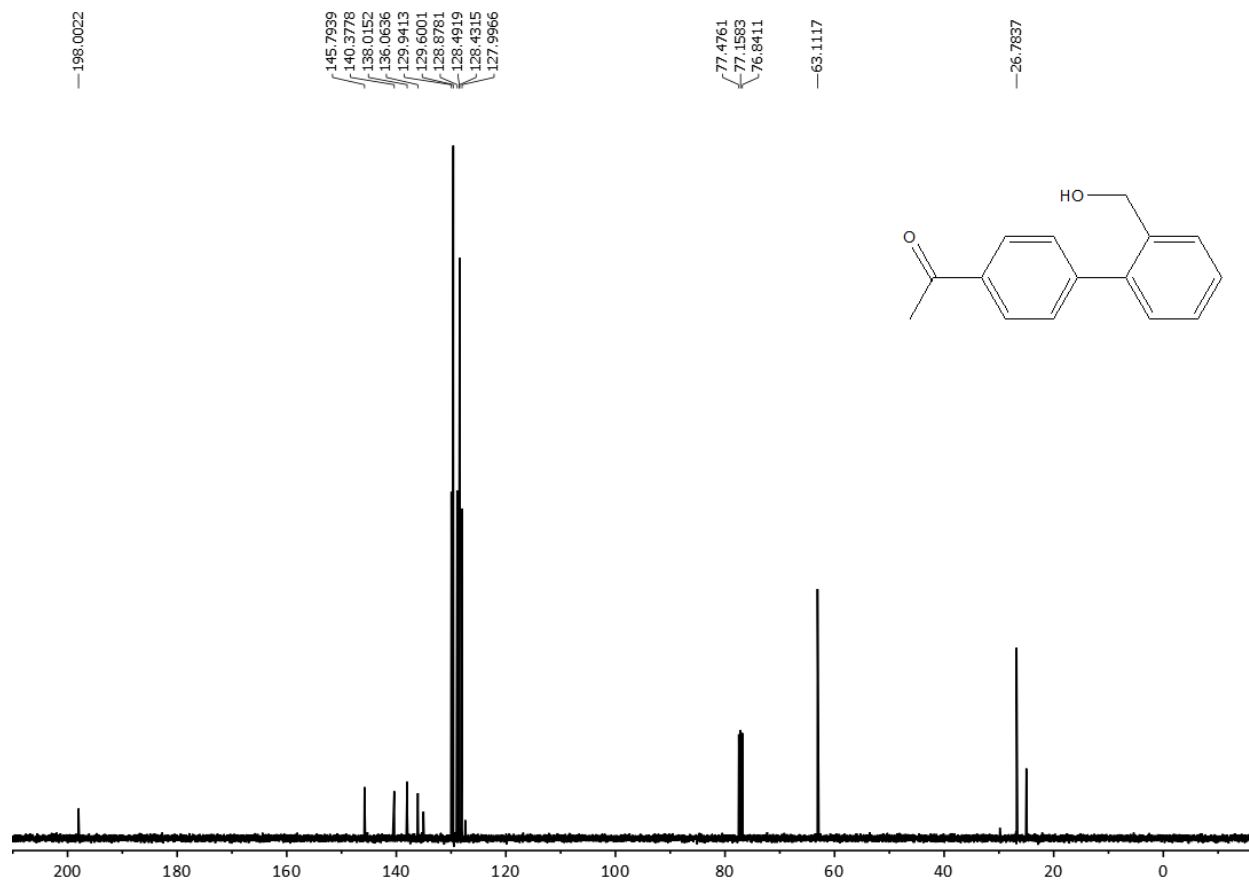


Fig S5. ^{13}C NMR (400 MHz, CDCl_3) spectrum.

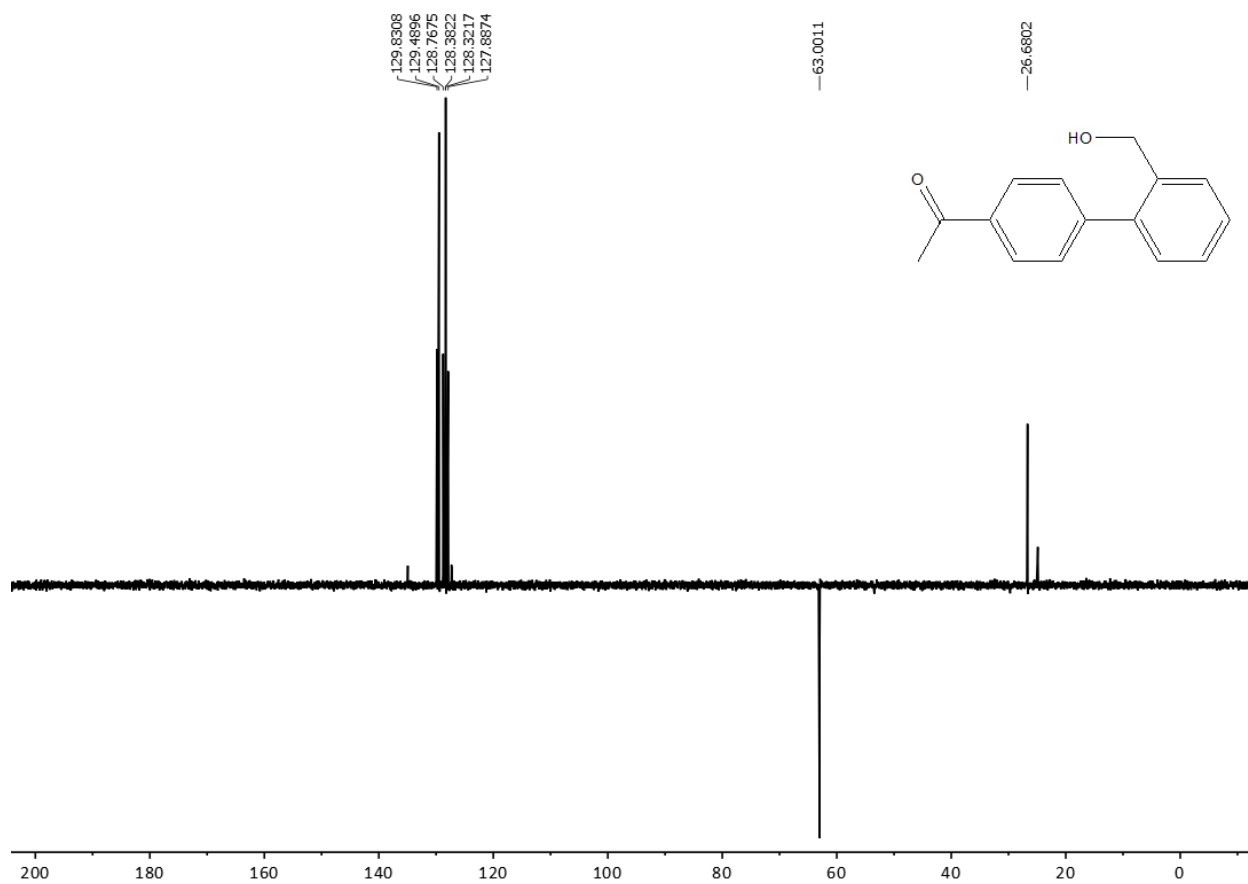


Fig S6. DEPT 135 NMR (400 MHz, CDCl_3) spectrum.

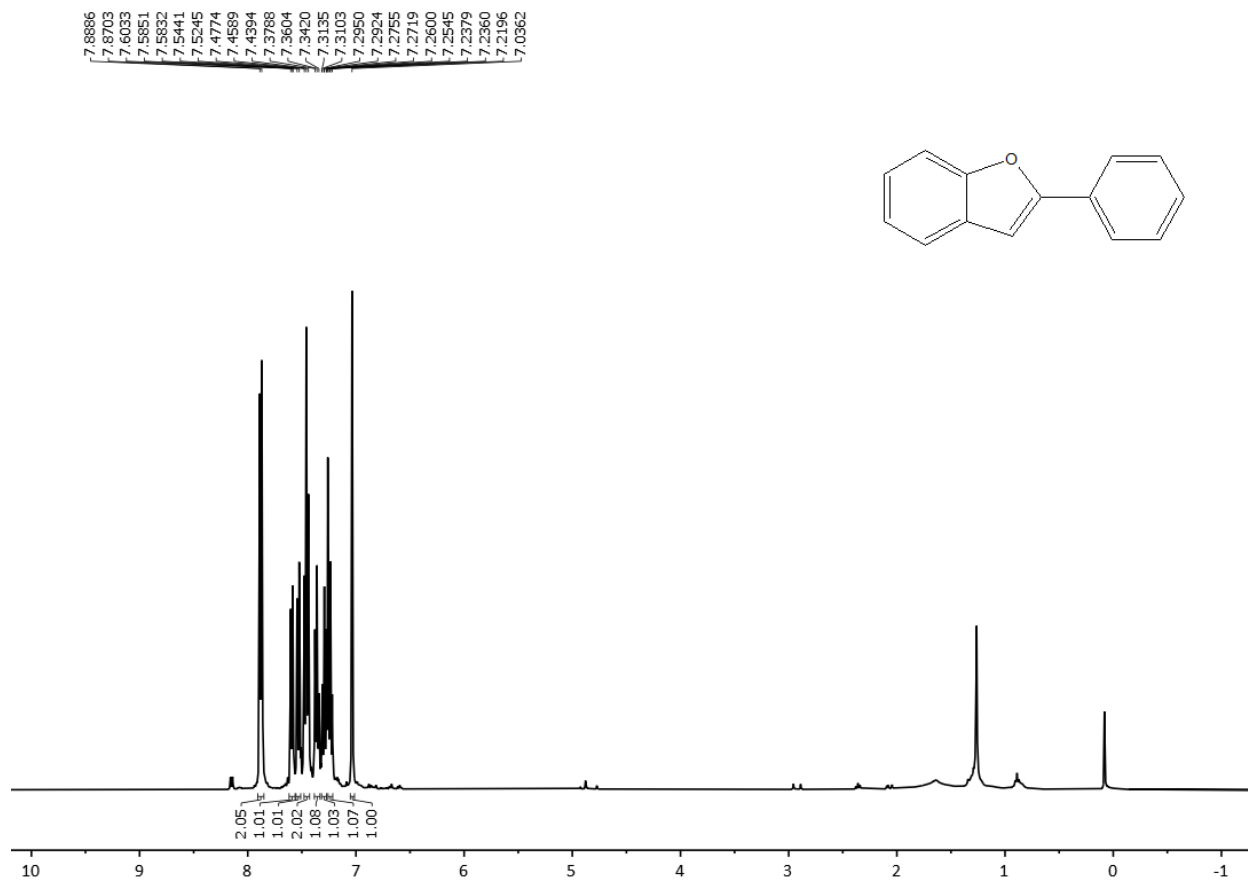


Fig S7. ^1H NMR (400 MHz, CDCl_3) spectrum.

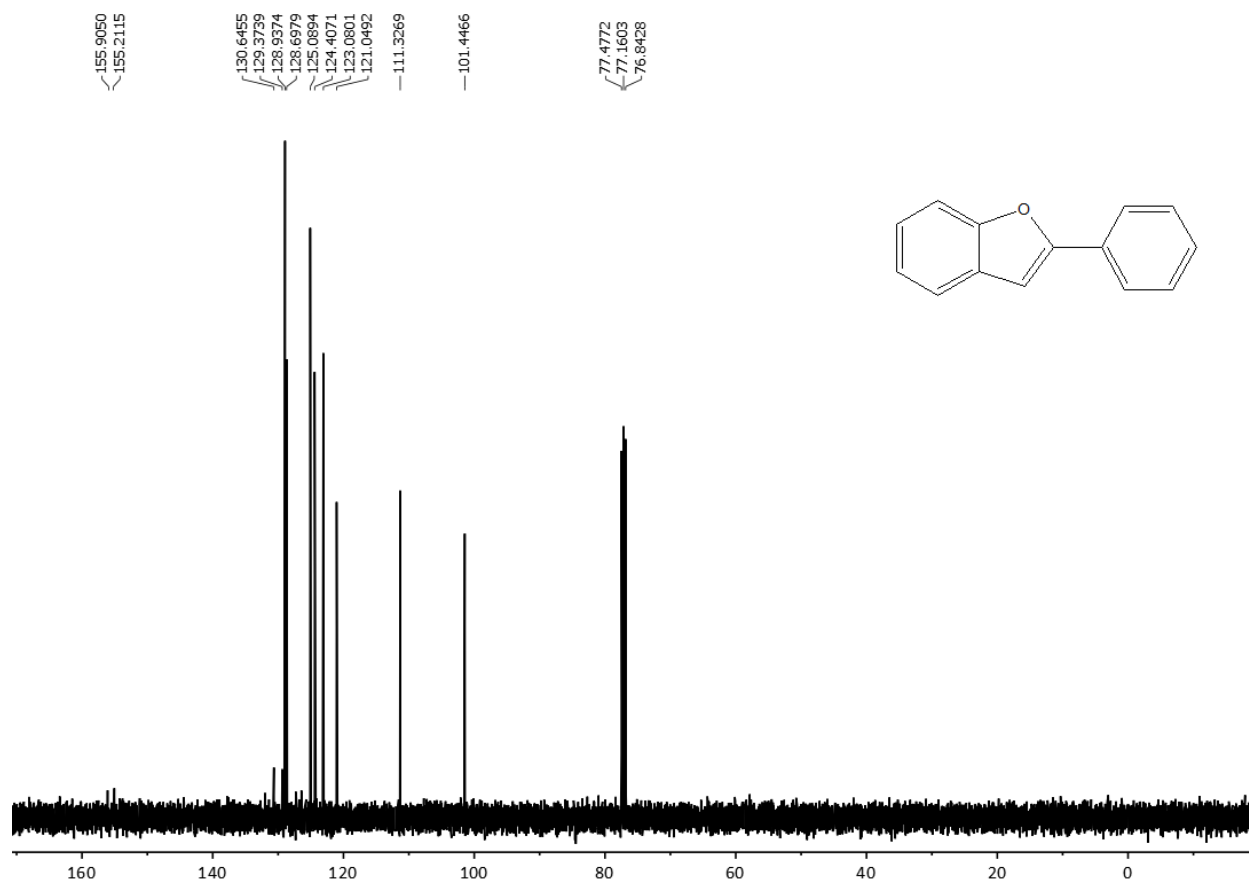


Fig S8. ^{13}C NMR (400 MHz, CDCl_3) spectrum.

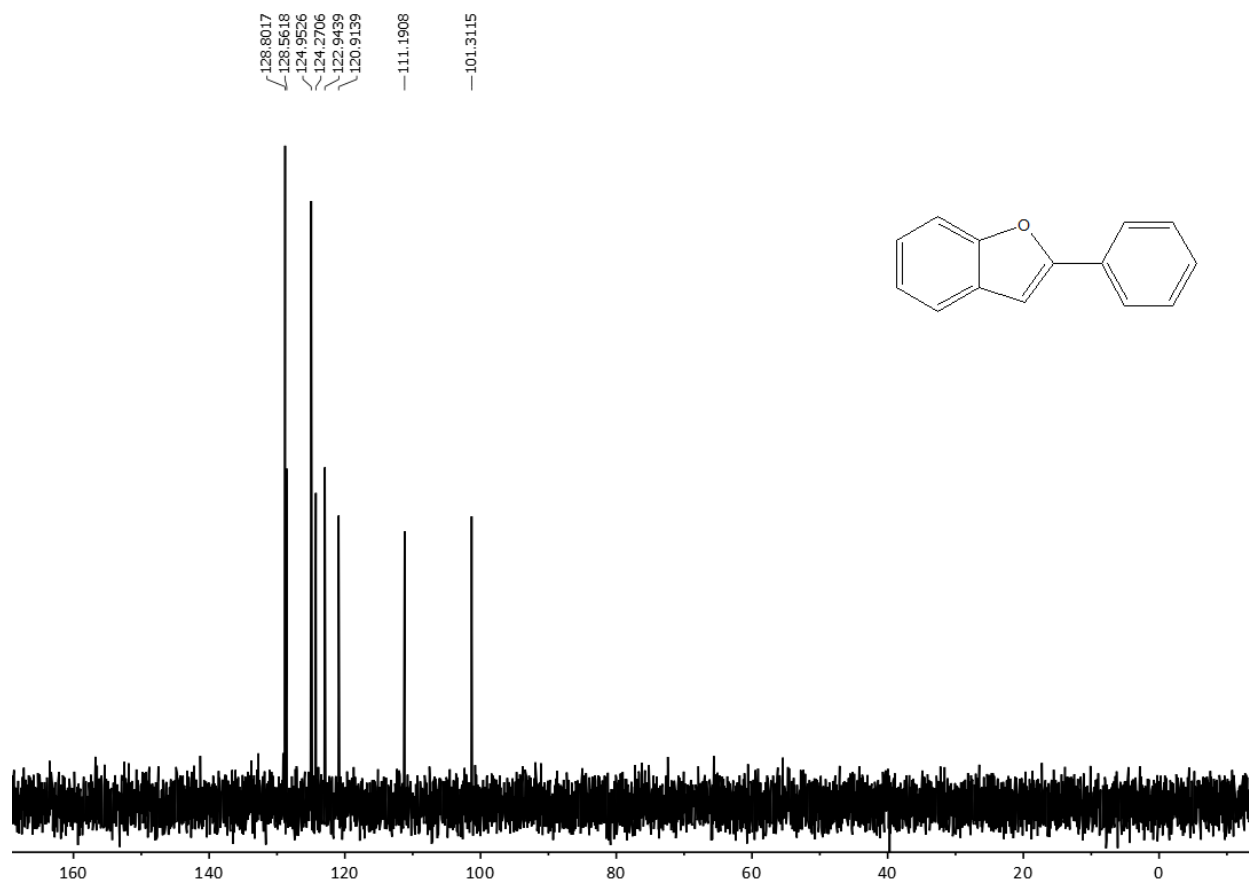


Fig S9. DEPT 135 NMR (400 MHz, CDCl_3) spectrum.

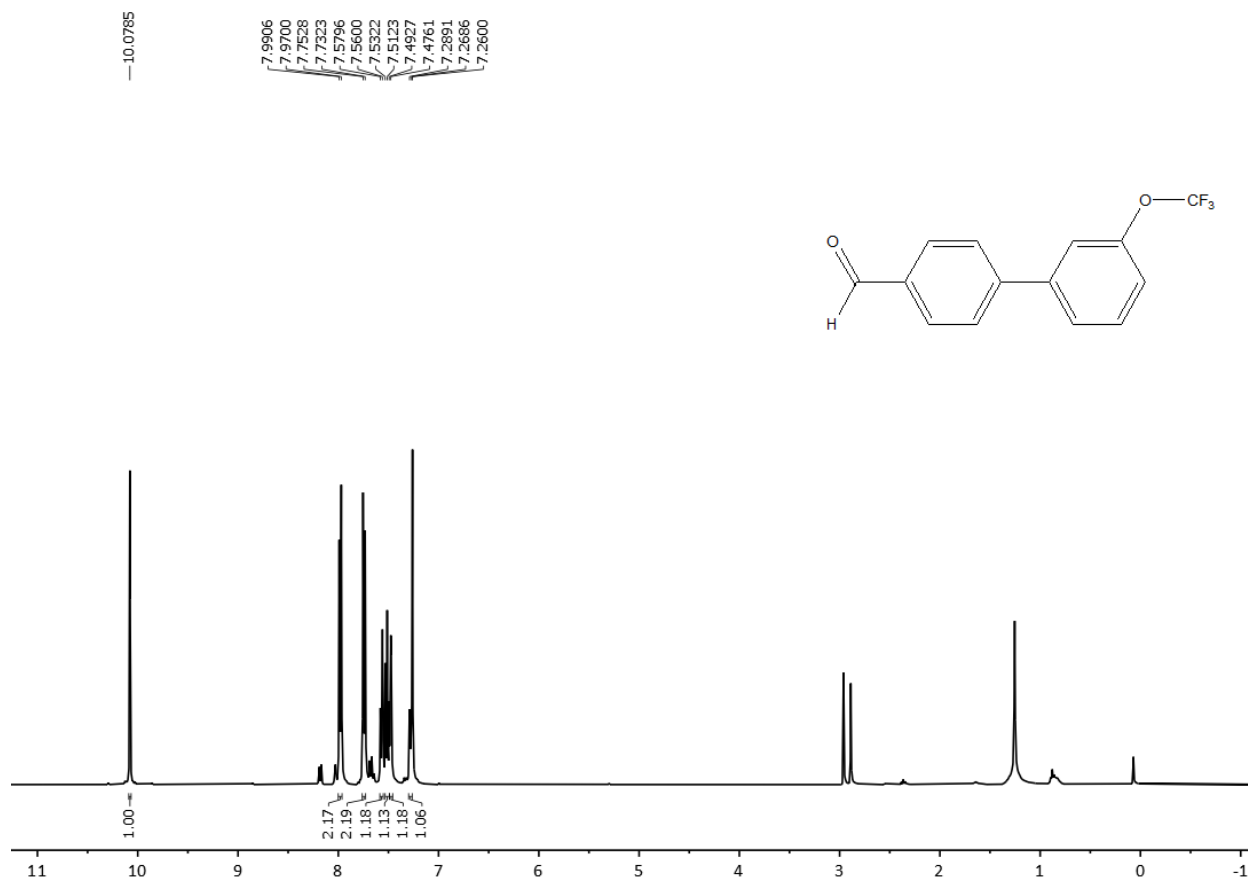


Fig S10. ¹H NMR (400 MHz, CDCl₃) spectrum.

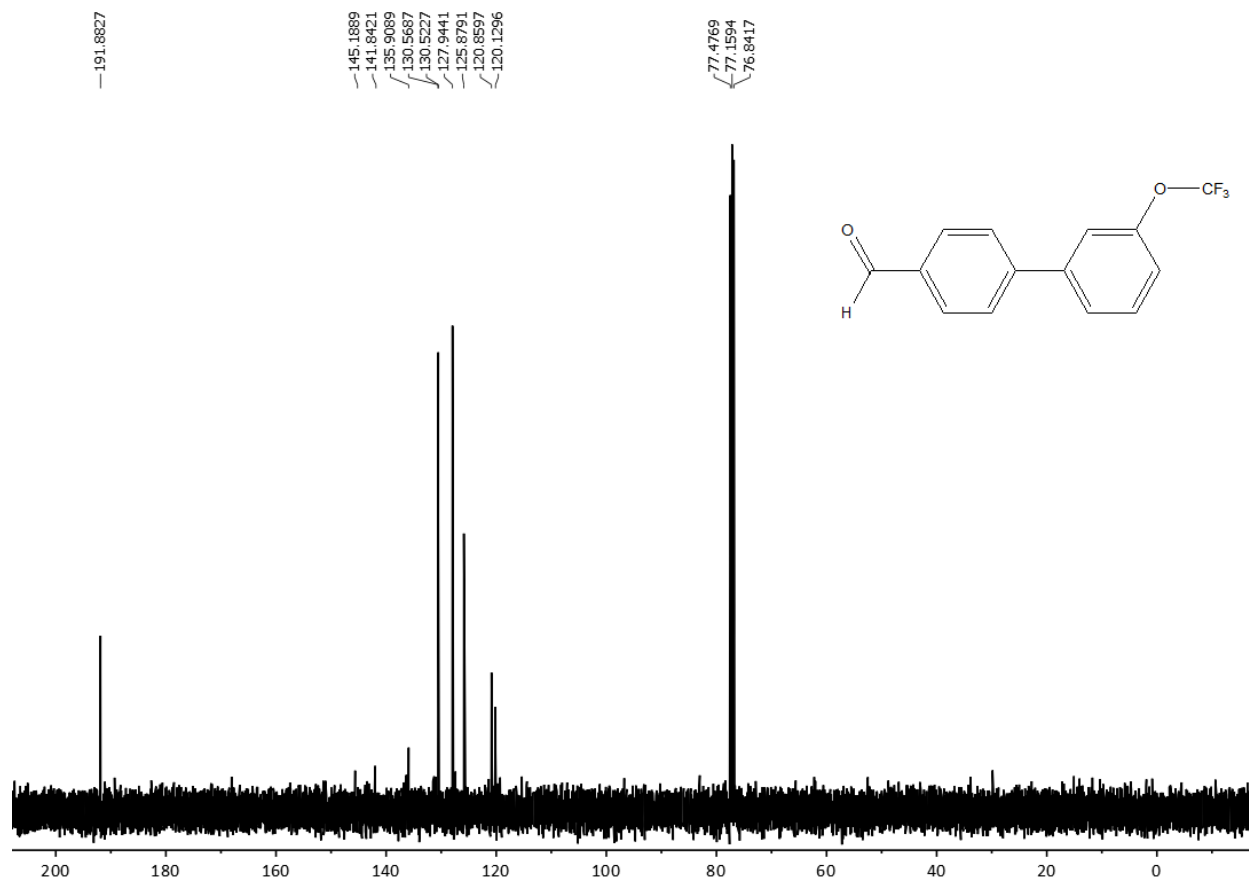


Fig S11. ^{13}C NMR (400 MHz, CDCl_3) spectrum.

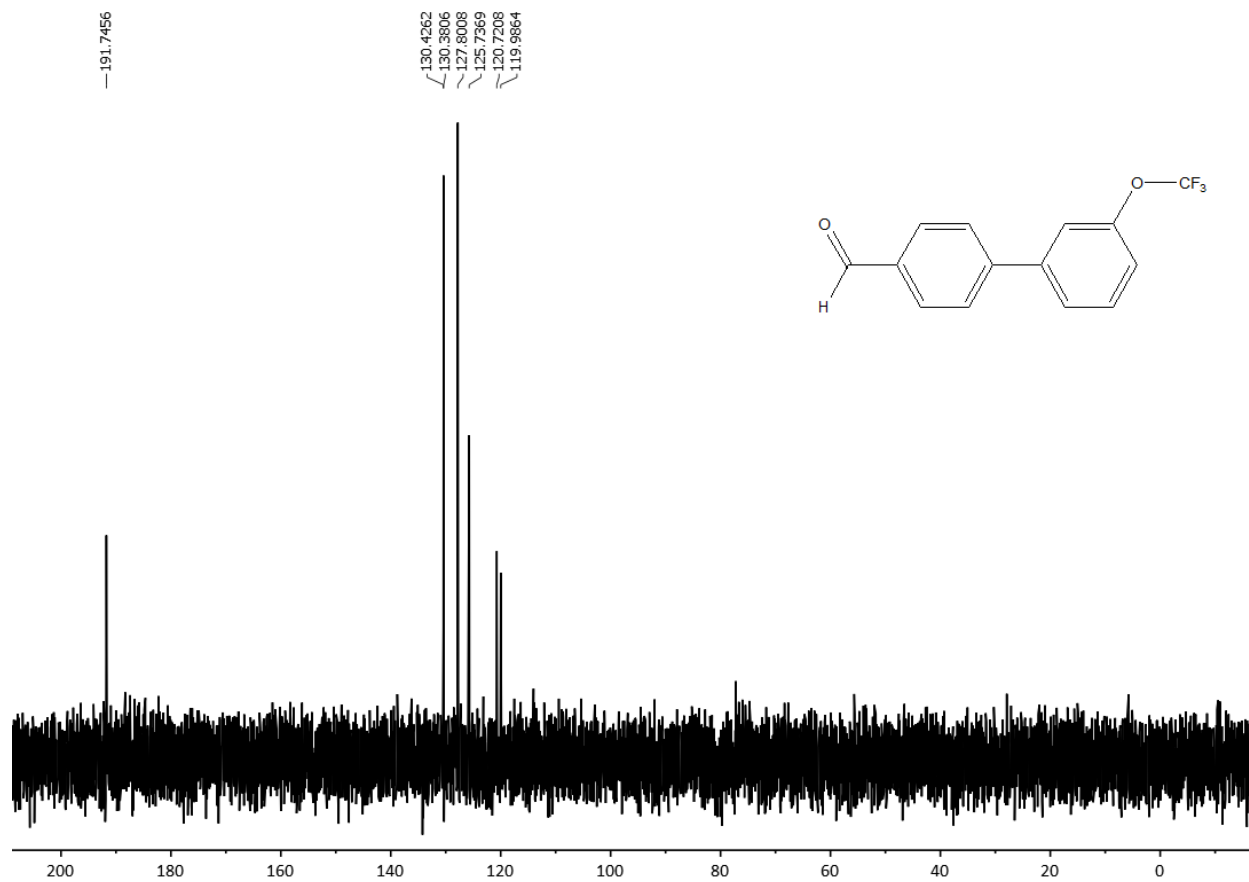


Fig S12. DEPT 135 NMR (400 MHz, CDCl_3) spectrum.

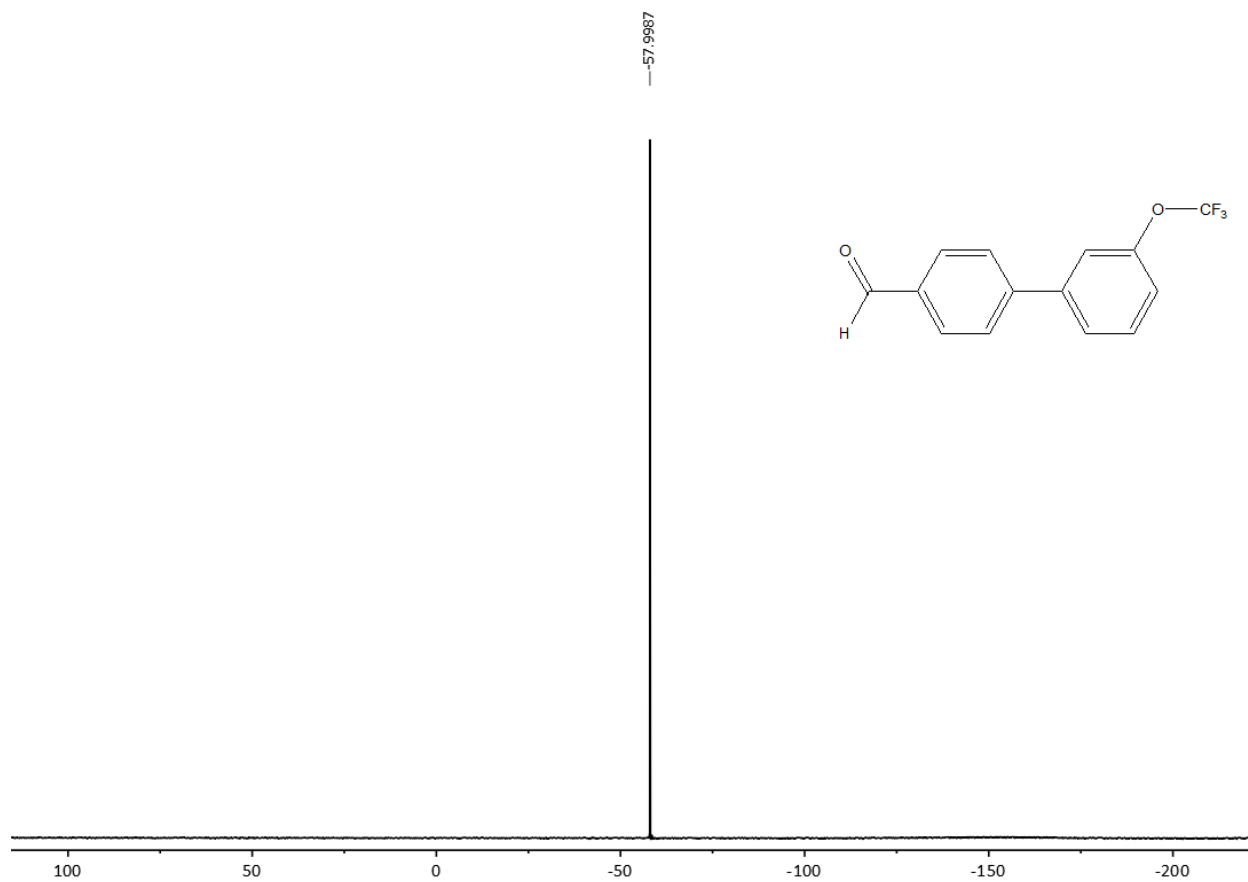


Fig S13. ^{19}F NMR (400 MHz, CDCl_3) spectrum.

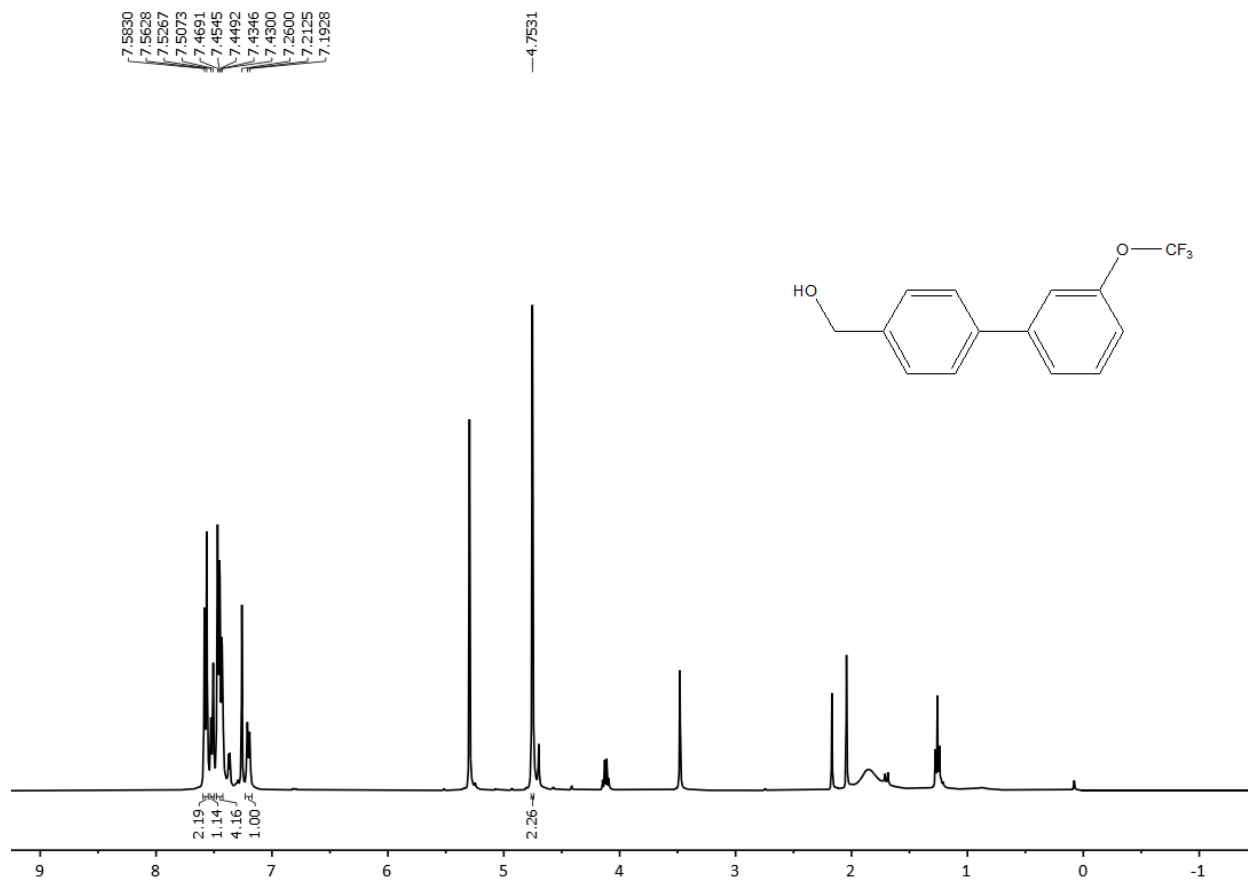


Fig S14. ^1H NMR (400 MHz, CDCl_3) spectrum.

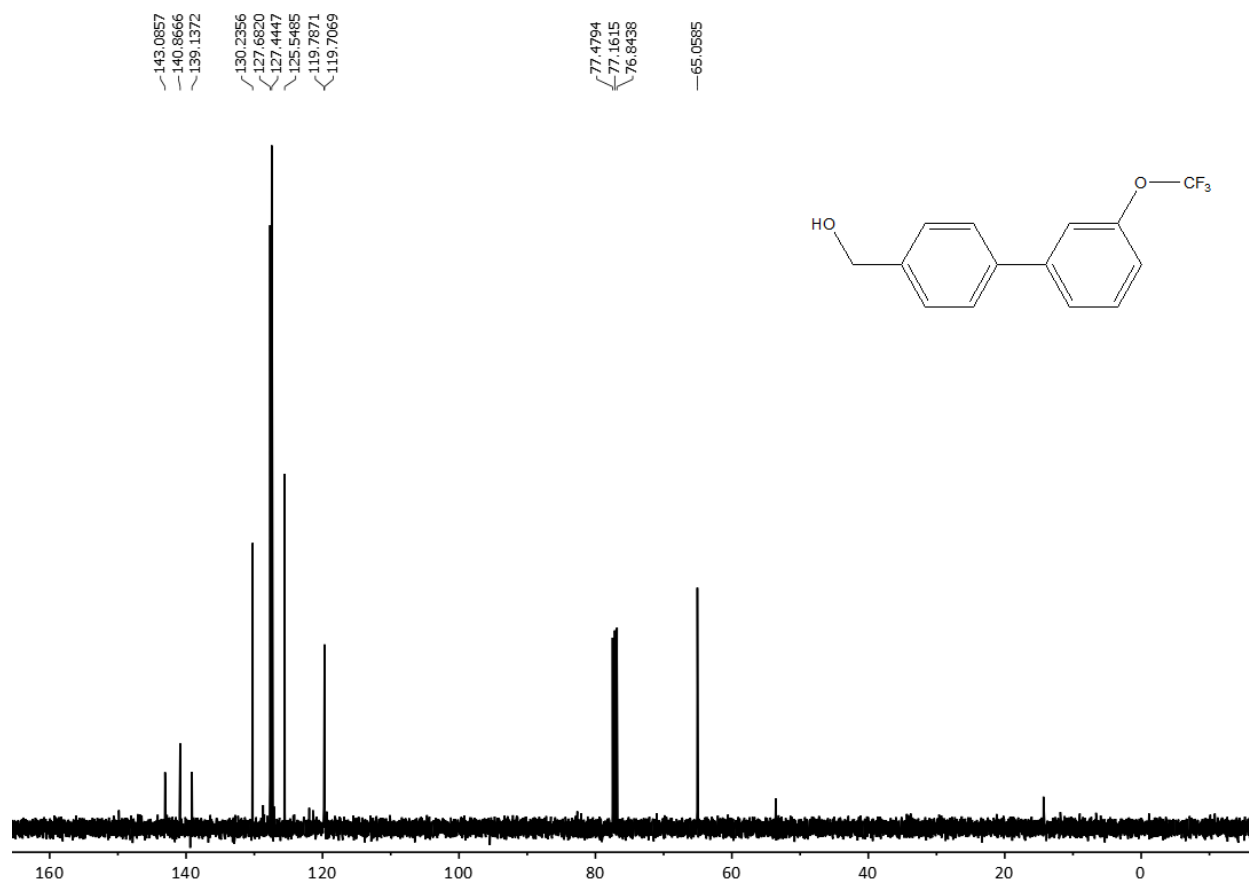


Fig S15. ^{13}C NMR (400 MHz, CDCl_3) spectrum.

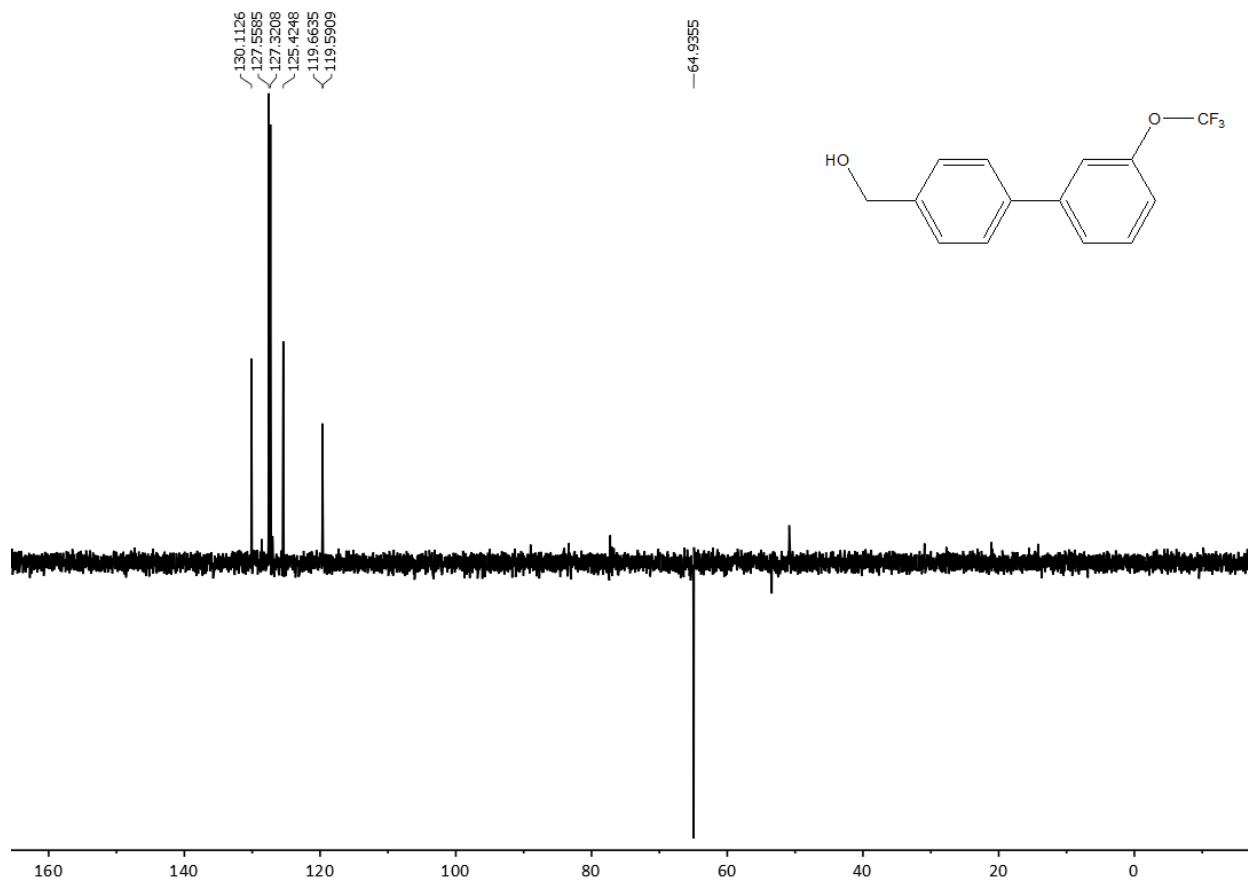


Fig S16. DEPT 135 NMR (400 MHz, CDCl₃) spectrum.

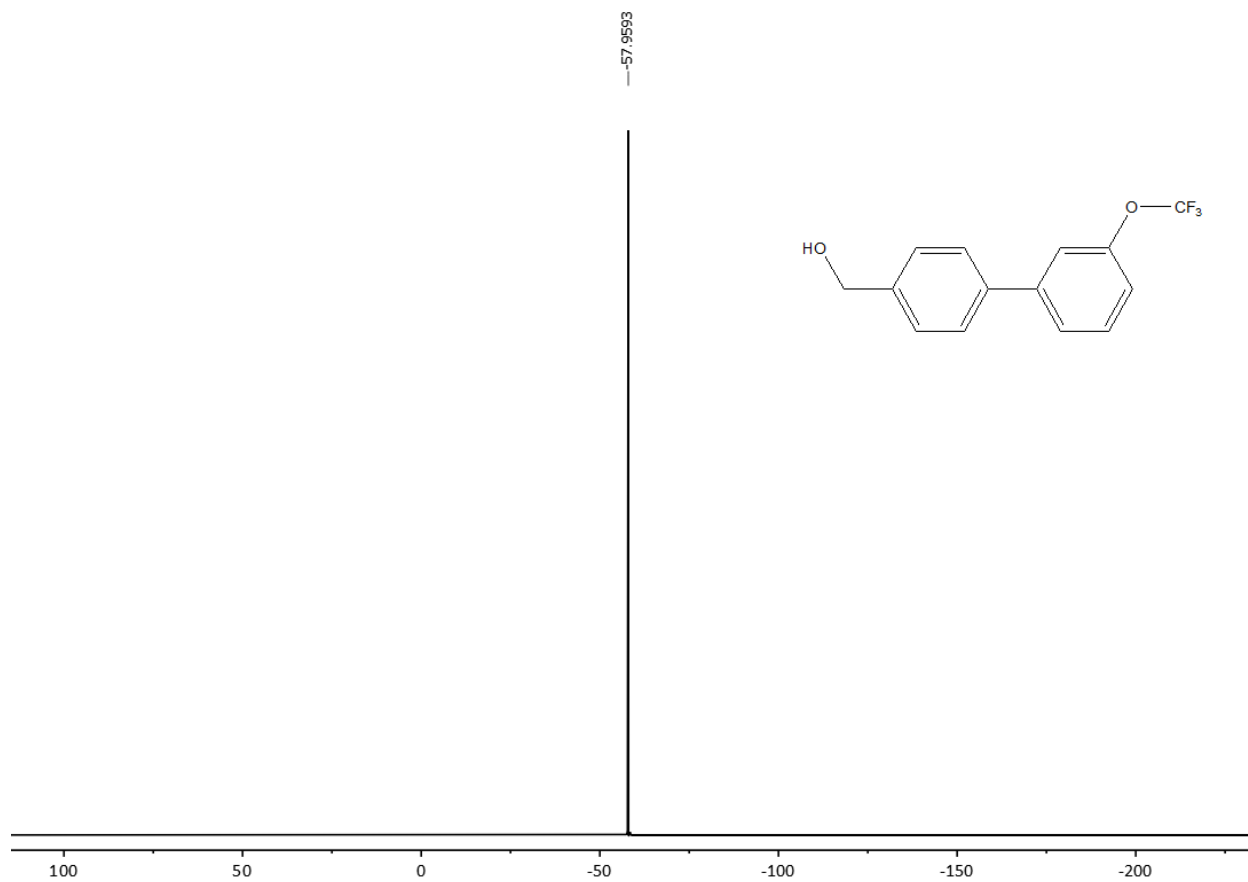


Fig S17. ^{19}F NMR (400 MHz, CDCl_3) spectrum.

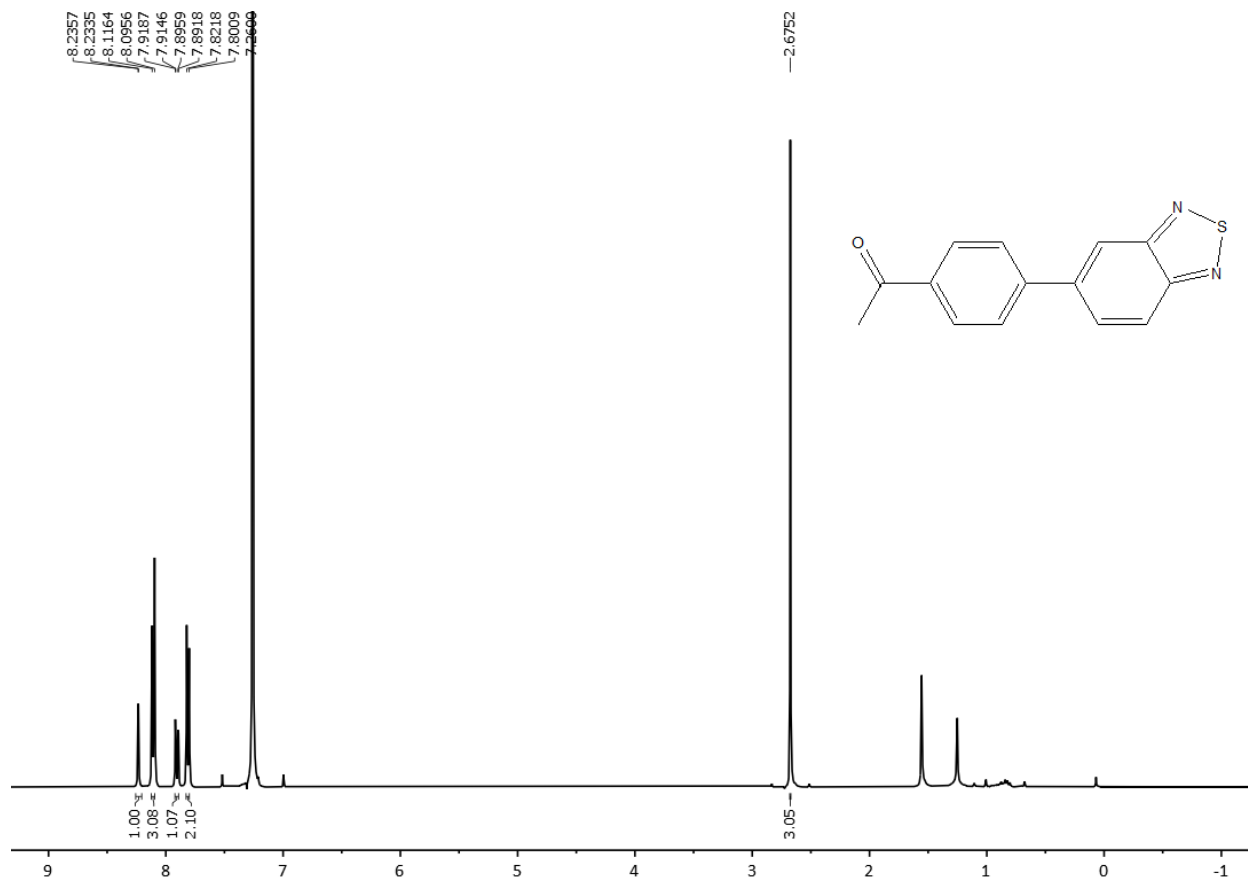


Fig S18. ^1H NMR (400 MHz, CDCl_3) spectrum.

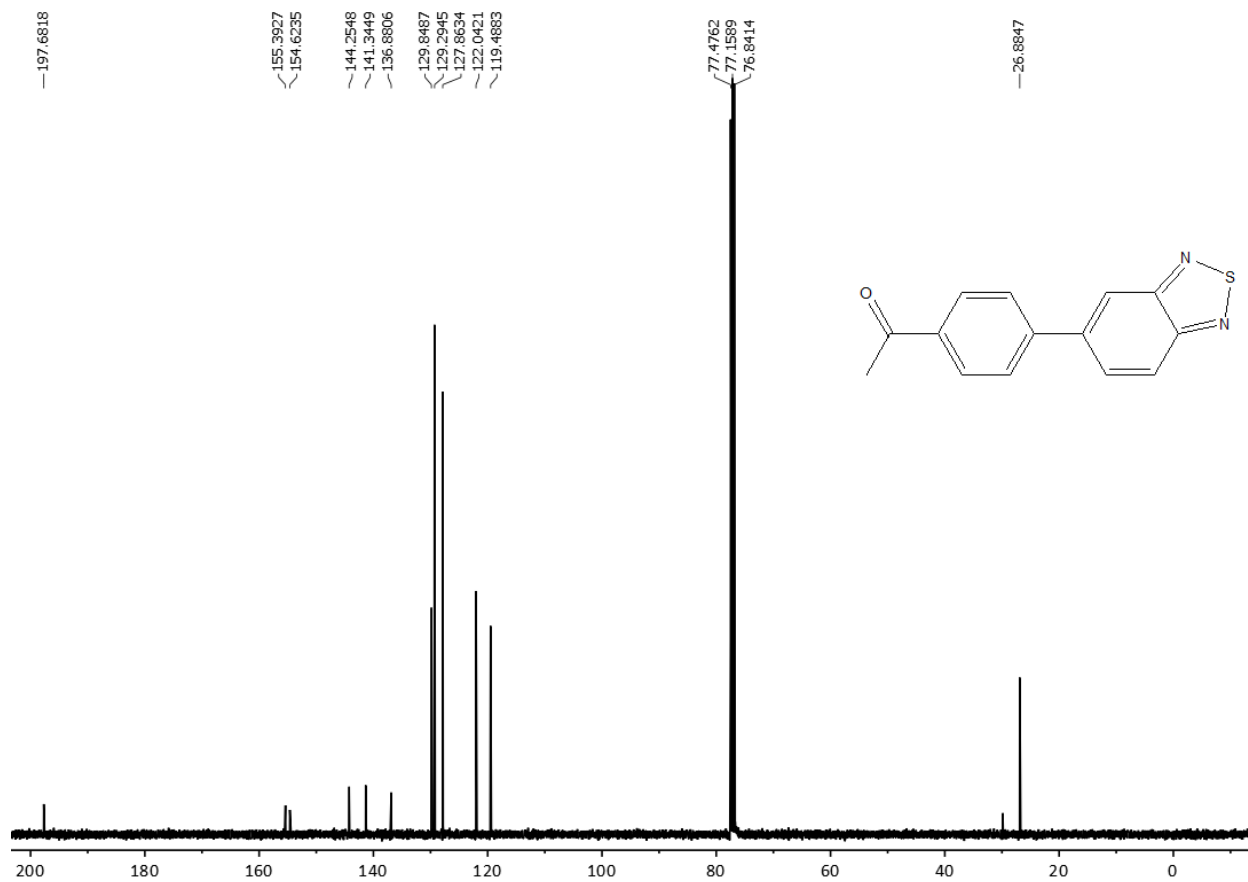


Fig S19. ^{13}C NMR (400 MHz, CDCl_3) spectrum.

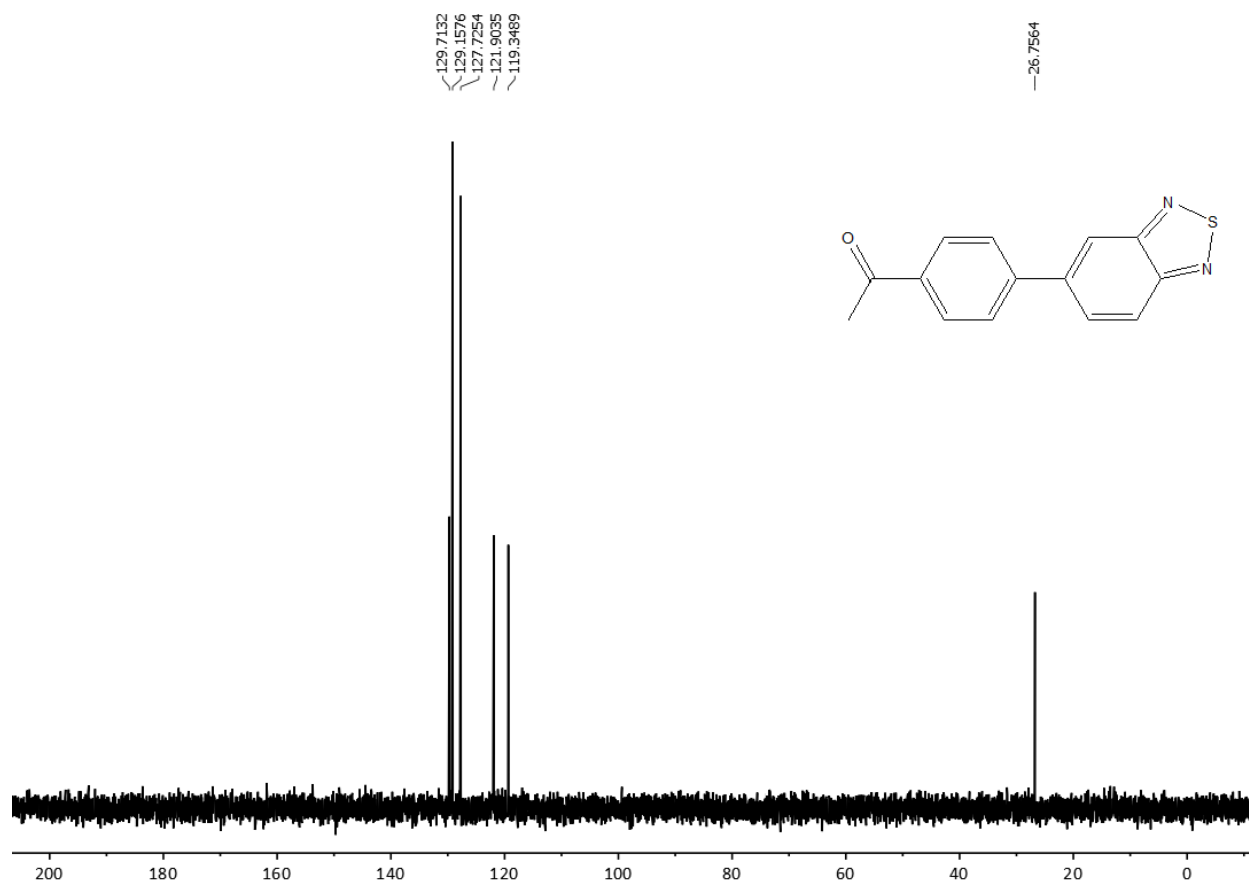


Fig S20. DEPT 135 NMR (400 MHz, CDCl₃) spectrum.

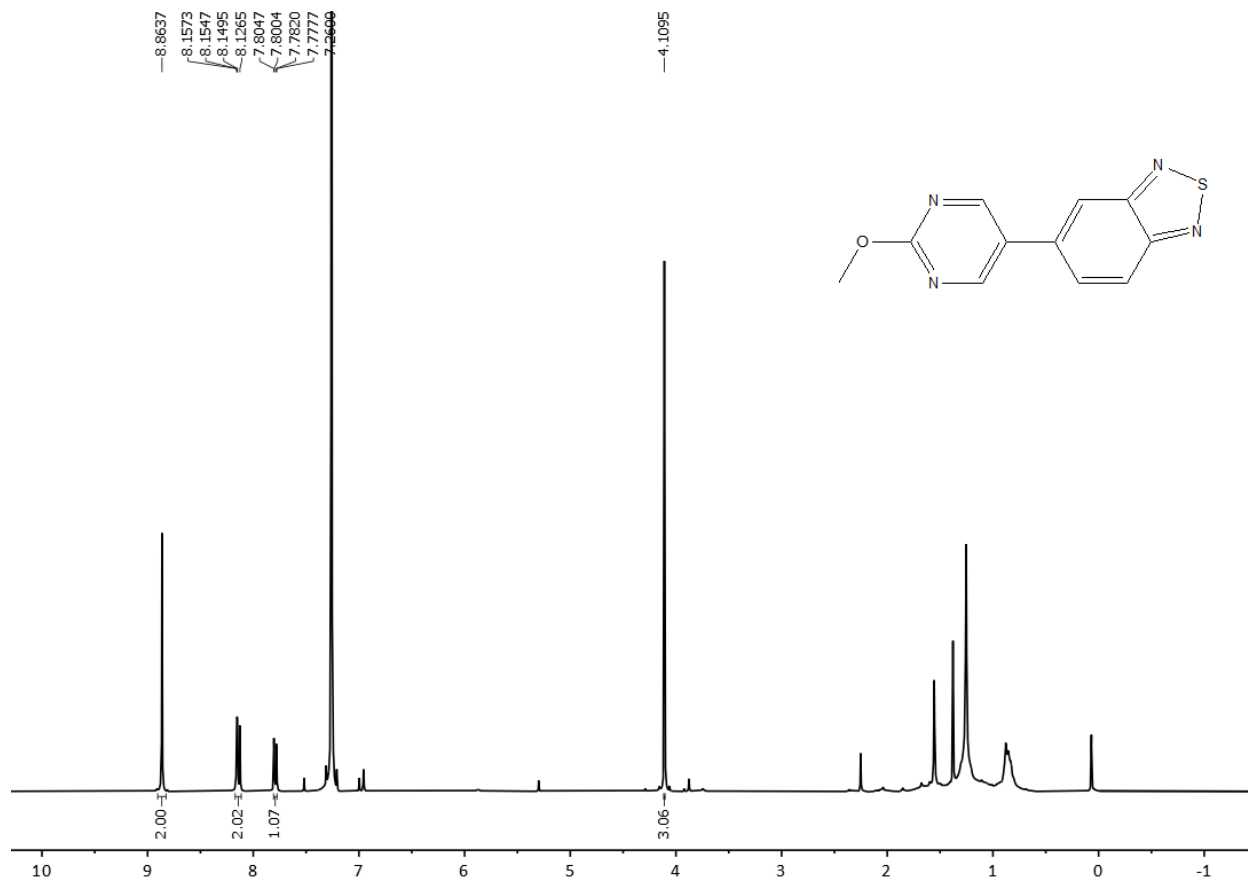


Fig S21. ¹H NMR (400 MHz, CDCl₃) spectrum.

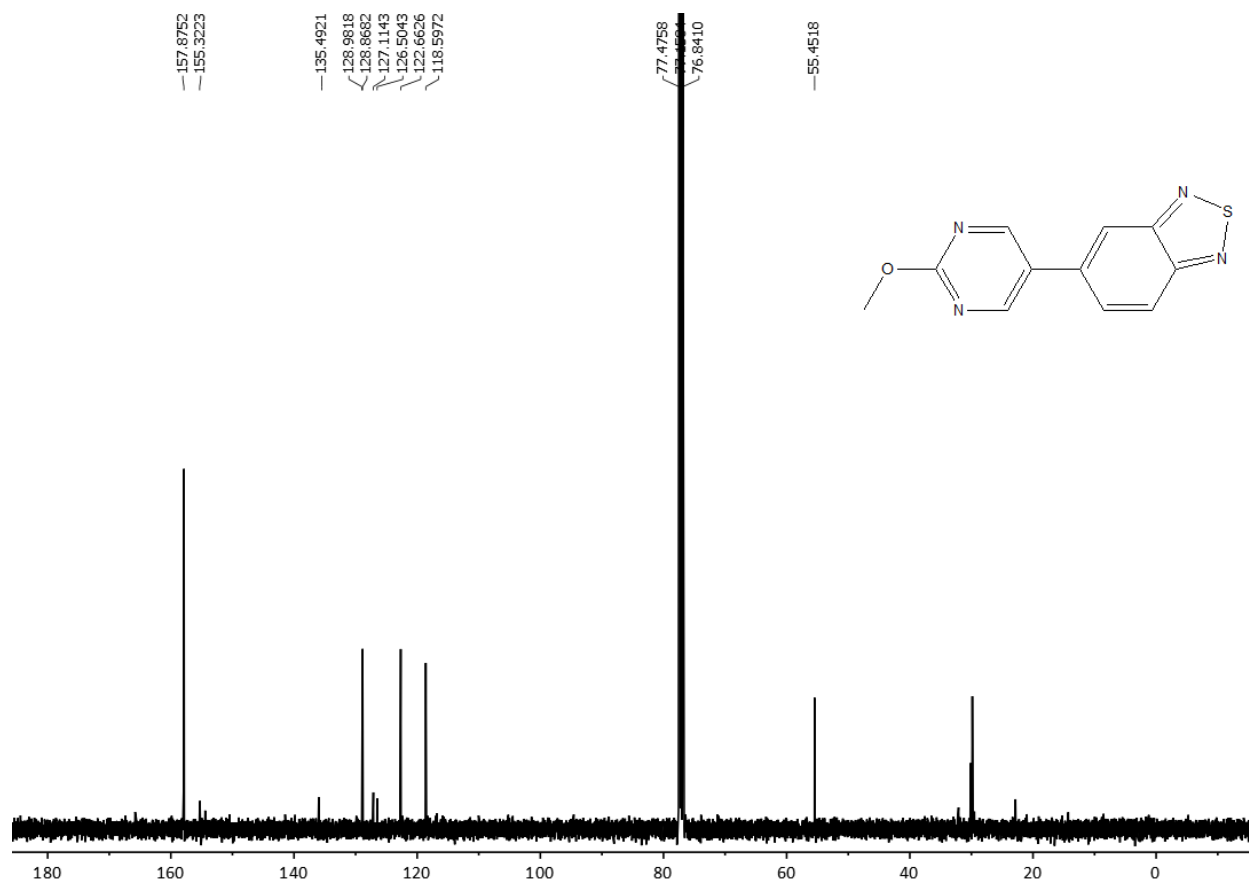


Fig S22. ^{13}C NMR (400 MHz, CDCl_3) spectrum.

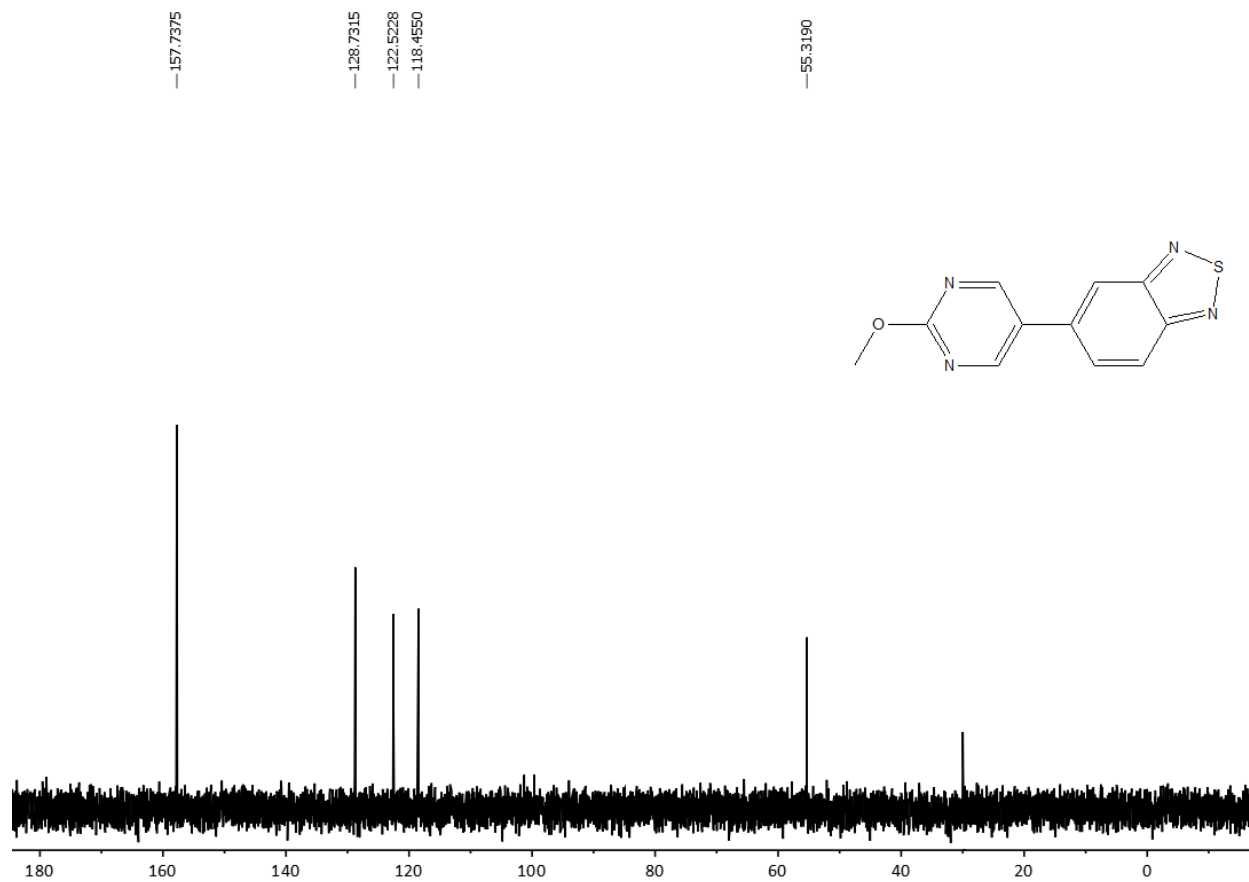


Fig S23. DEPT 135 NMR (400 MHz, CDCl₃) spectrum.

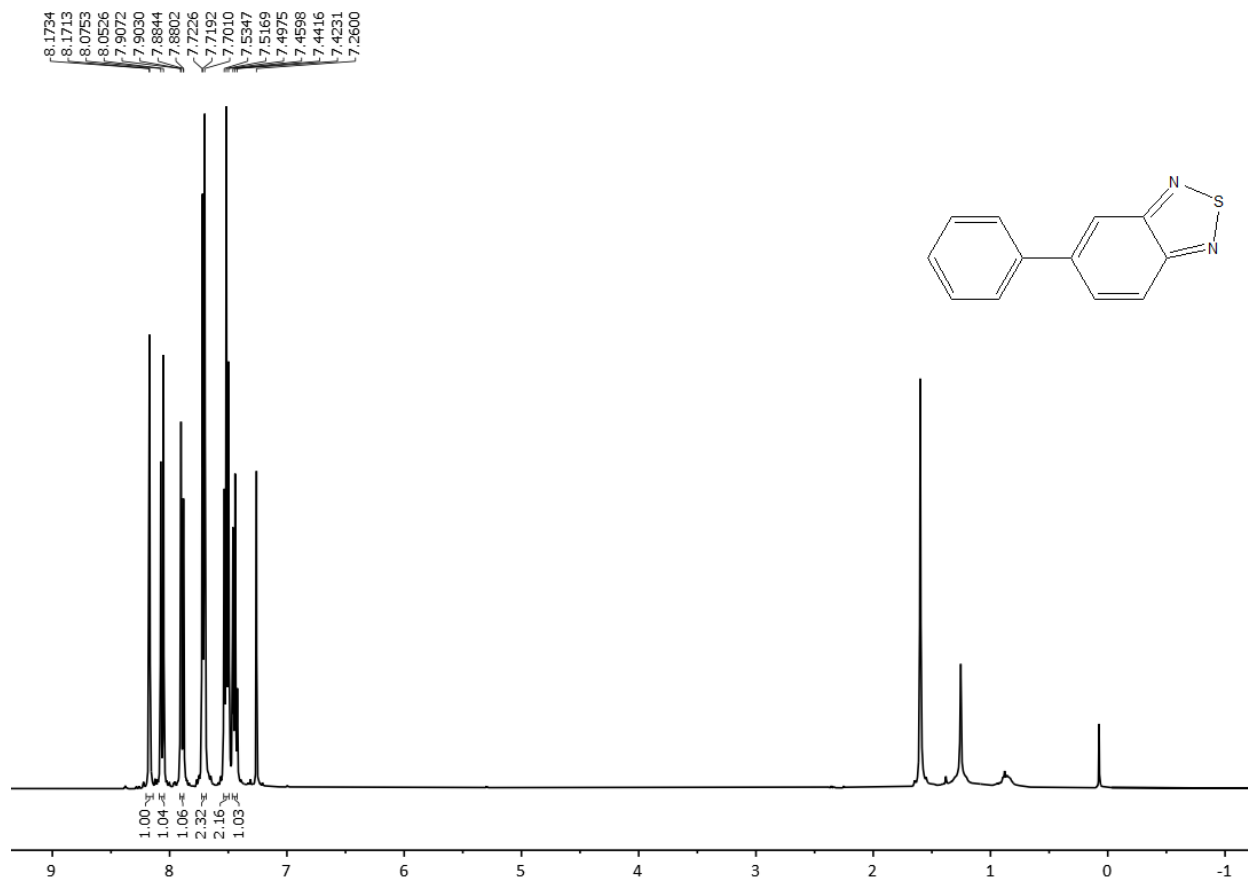


Fig S24. ¹H NMR (400 MHz, CDCl₃) spectrum.

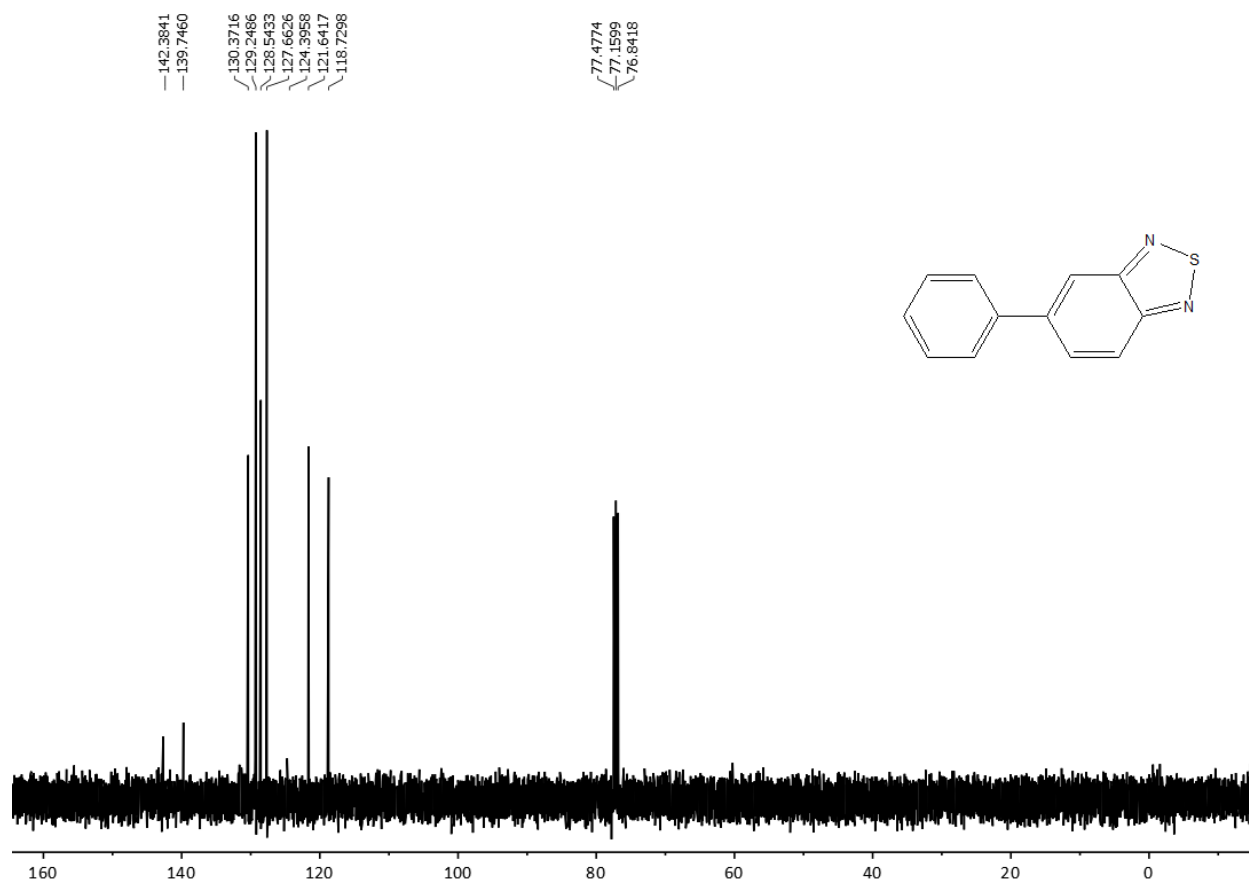


Fig S25. ^{13}C NMR (400 MHz, CDCl_3) spectrum.

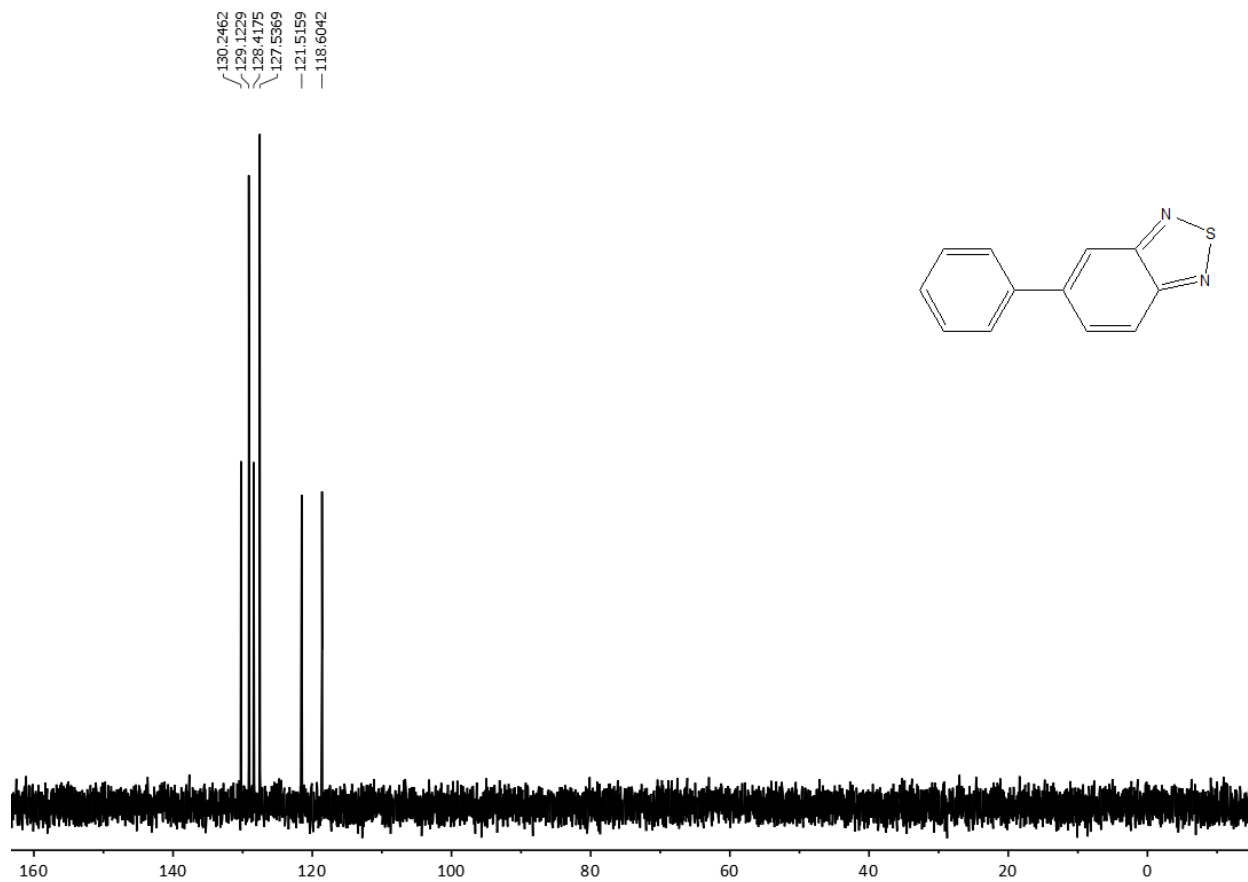


Fig S26. DEPT 135 NMR (400 MHz, CDCl₃) spectrum.

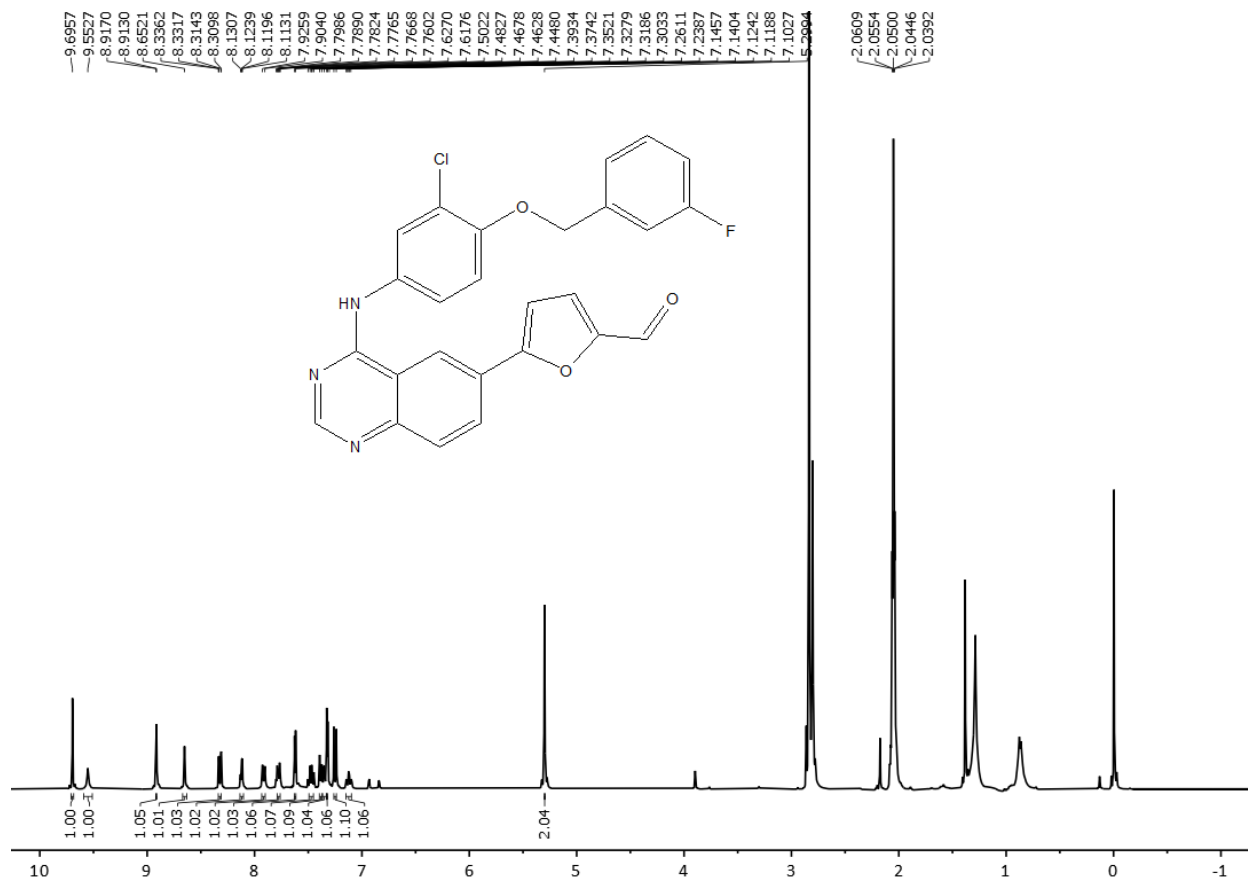


Fig S27. ¹H NMR (400 MHz, Acetone) spectrum.

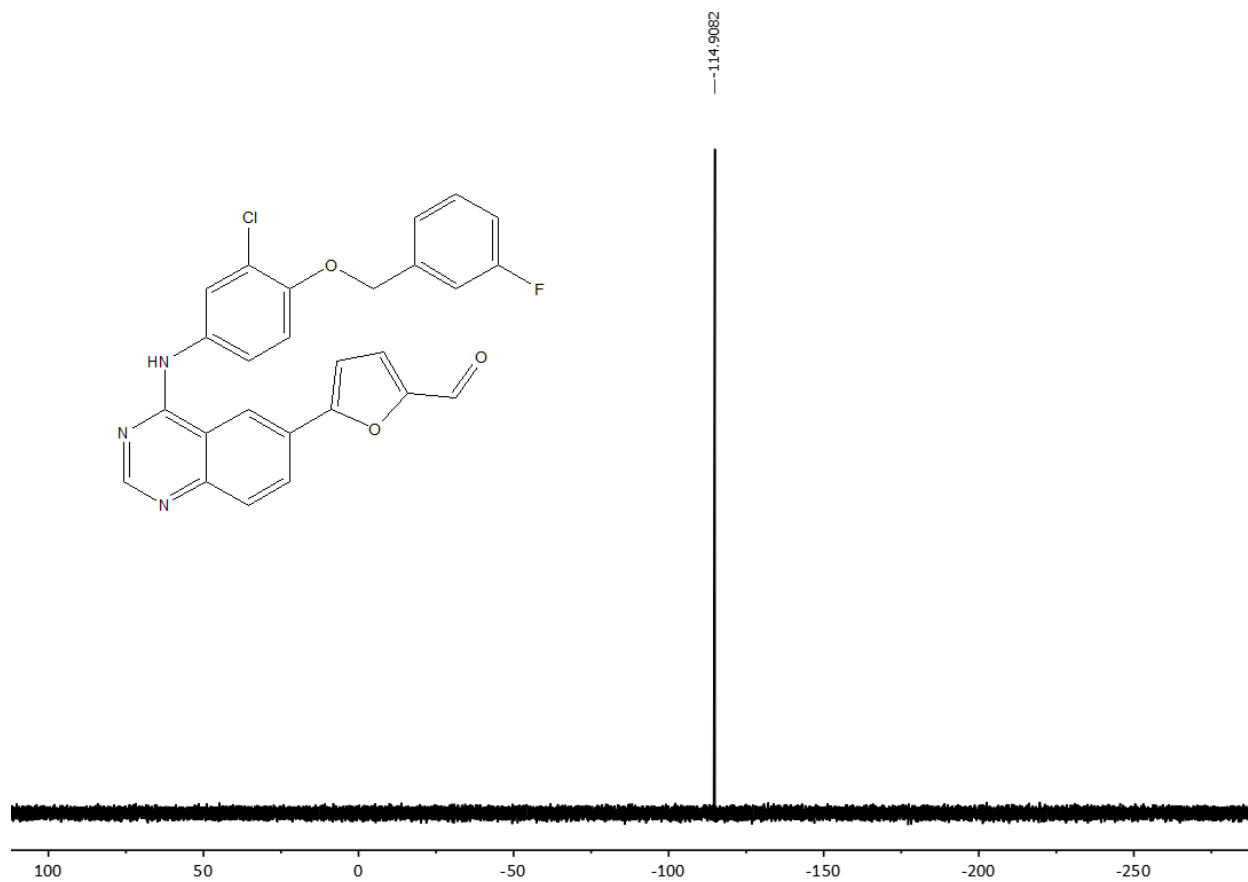


Fig S28. ^{19}F NMR (400 MHz, Acetone) spectrum.

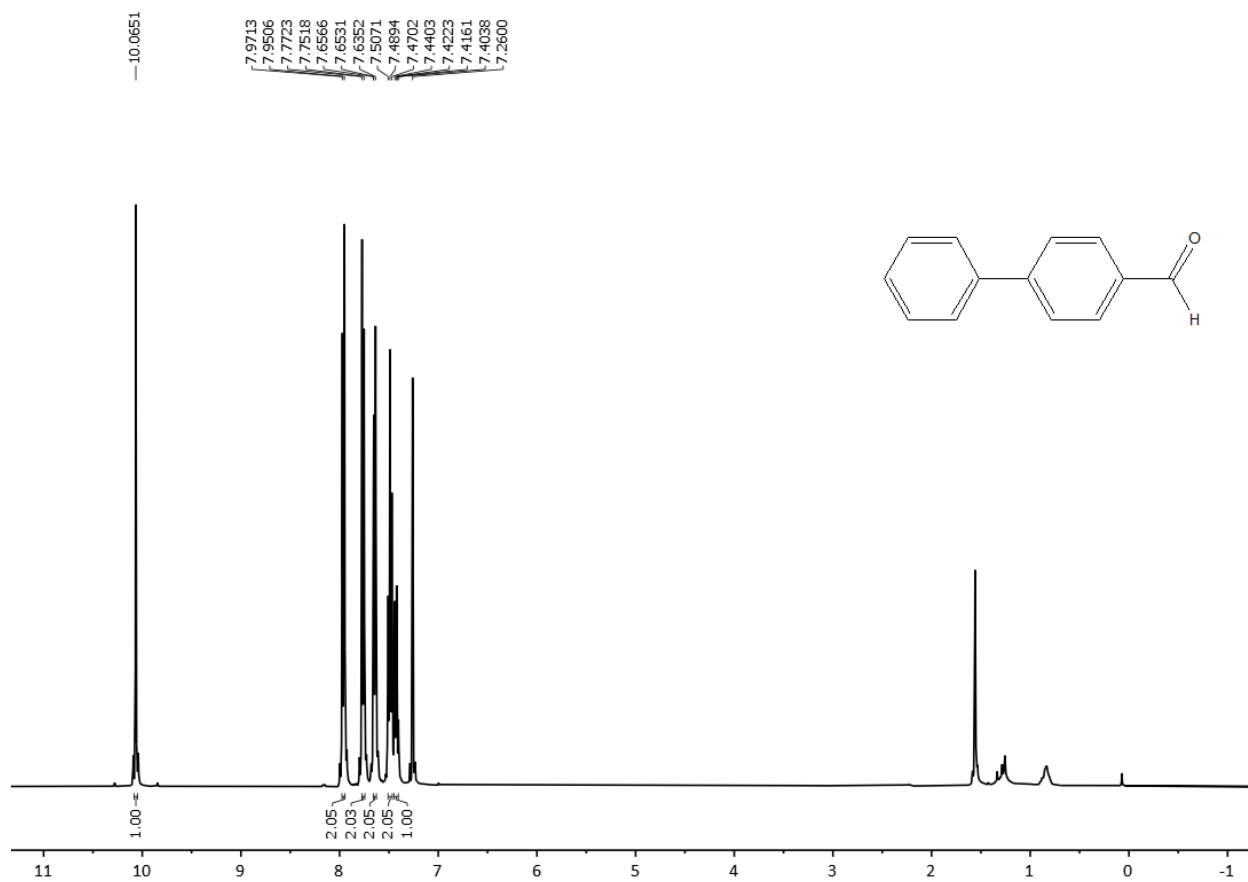


Fig S29. ^1H NMR (400 MHz, CDCl_3) spectrum.

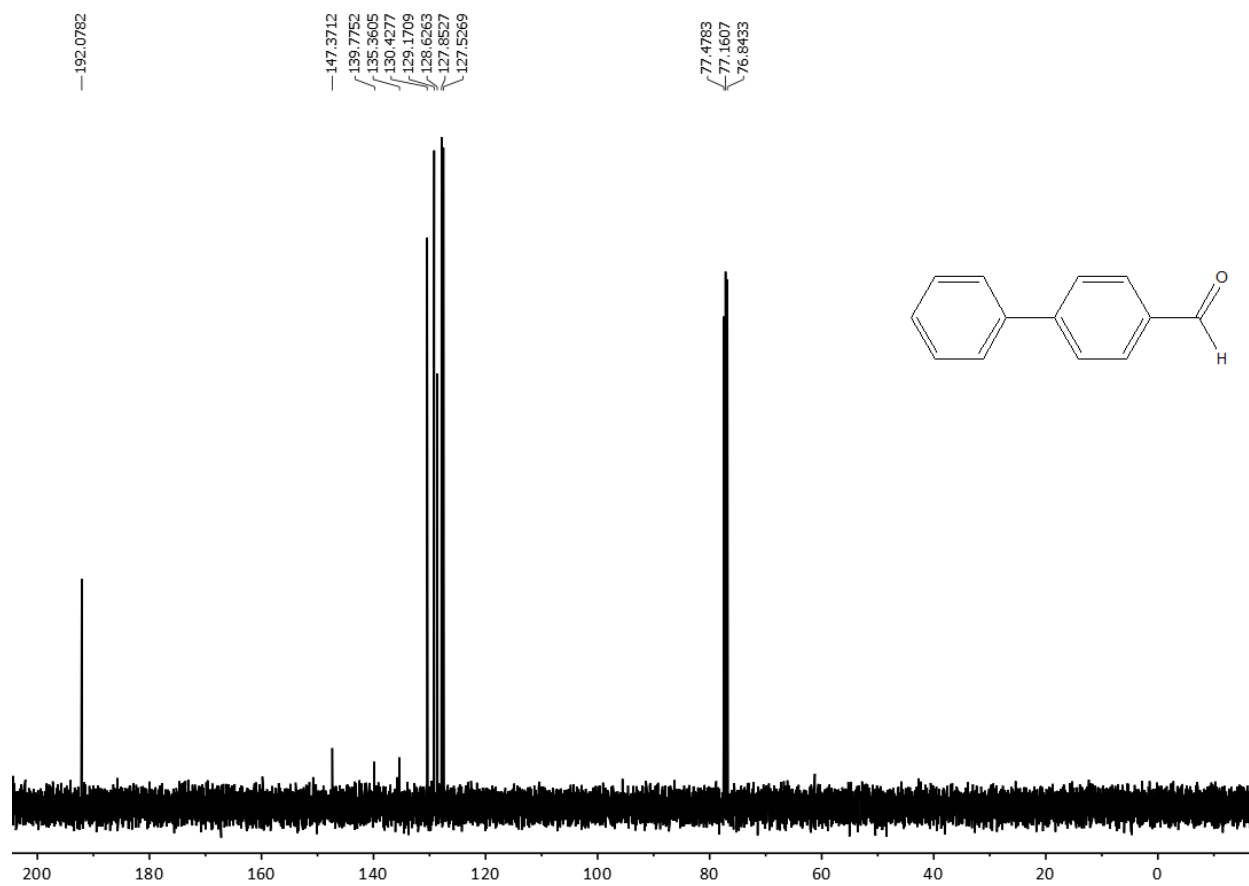


Fig S30. ^{13}C NMR (400 MHz, CDCl_3) spectrum.

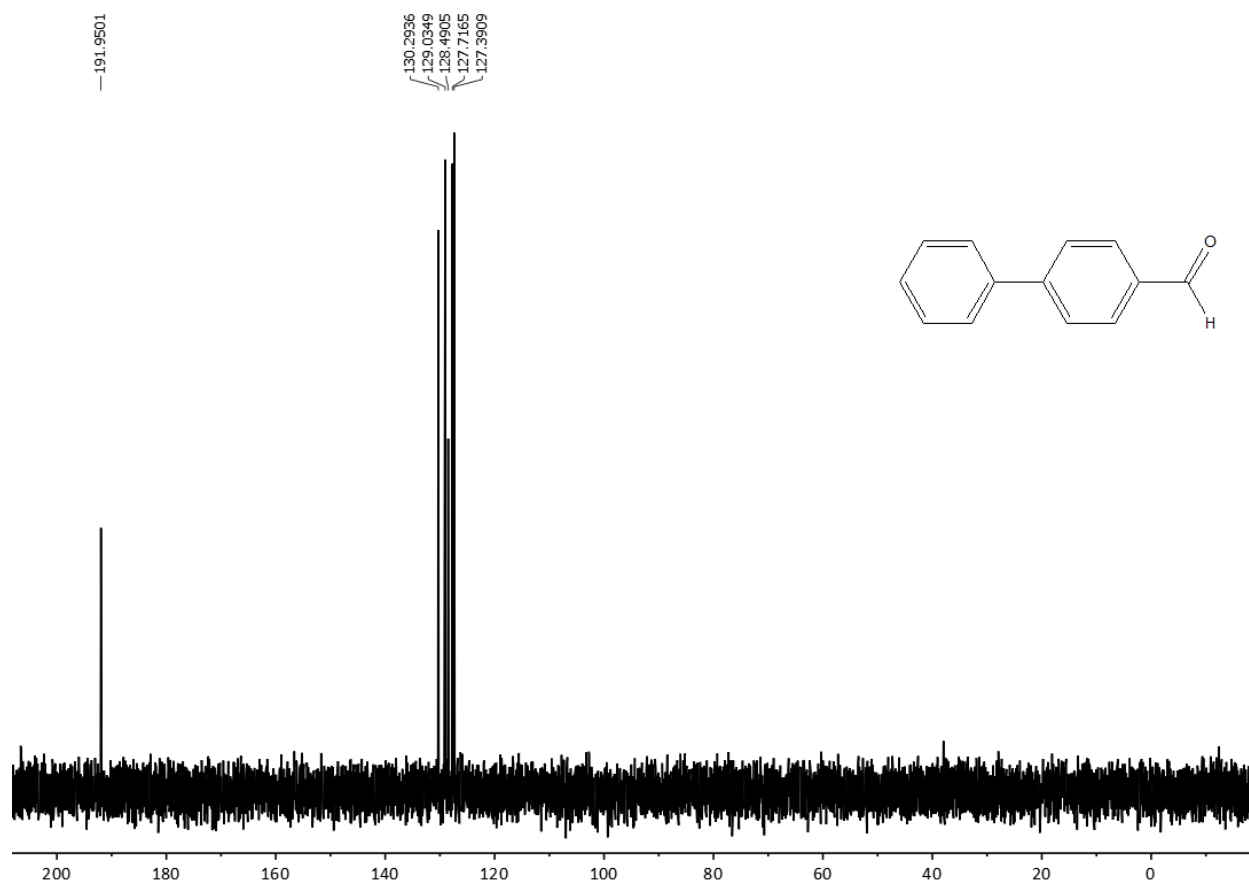


Fig S31. DEPT 135 NMR (400 MHz, CDCl₃) spectrum.

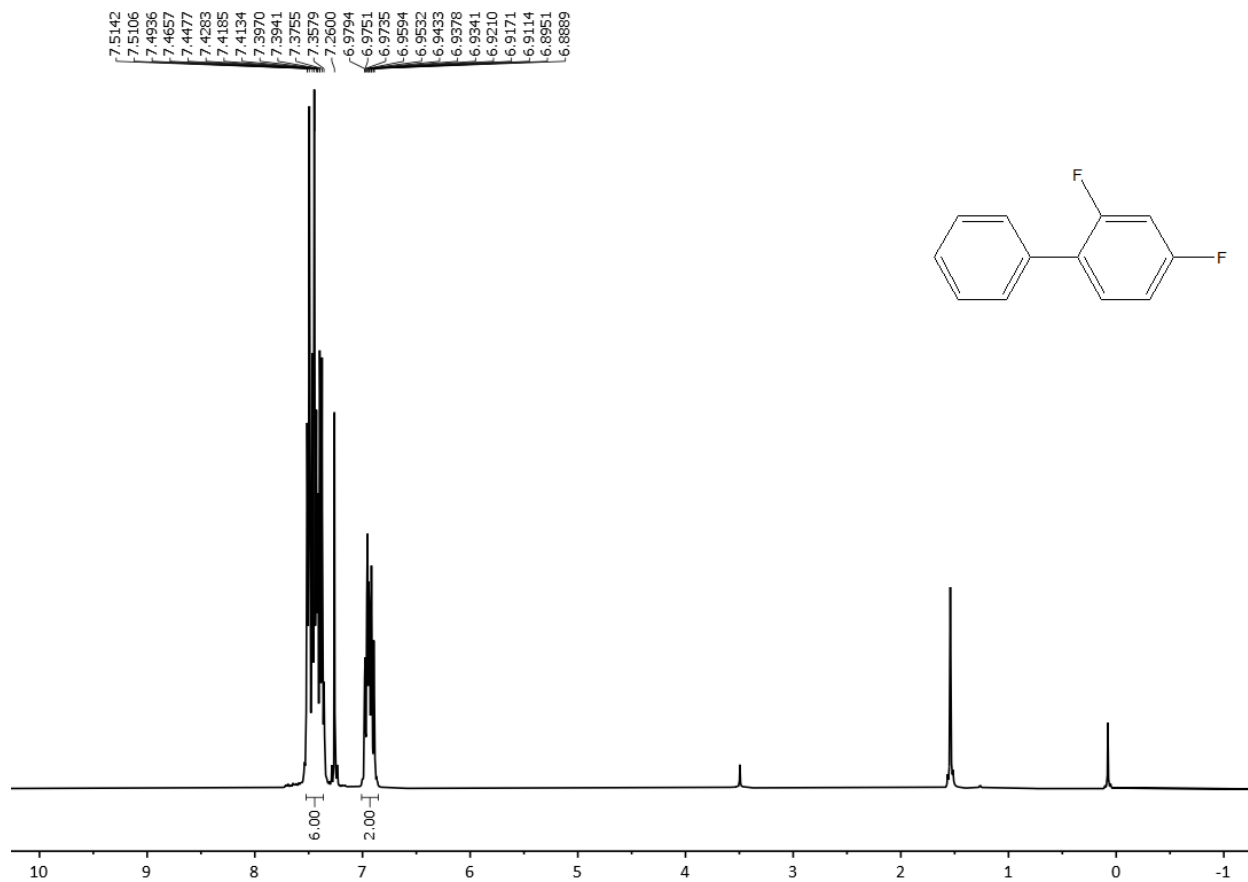


Fig S32. ^1H NMR (400 MHz, CDCl_3) spectrum.

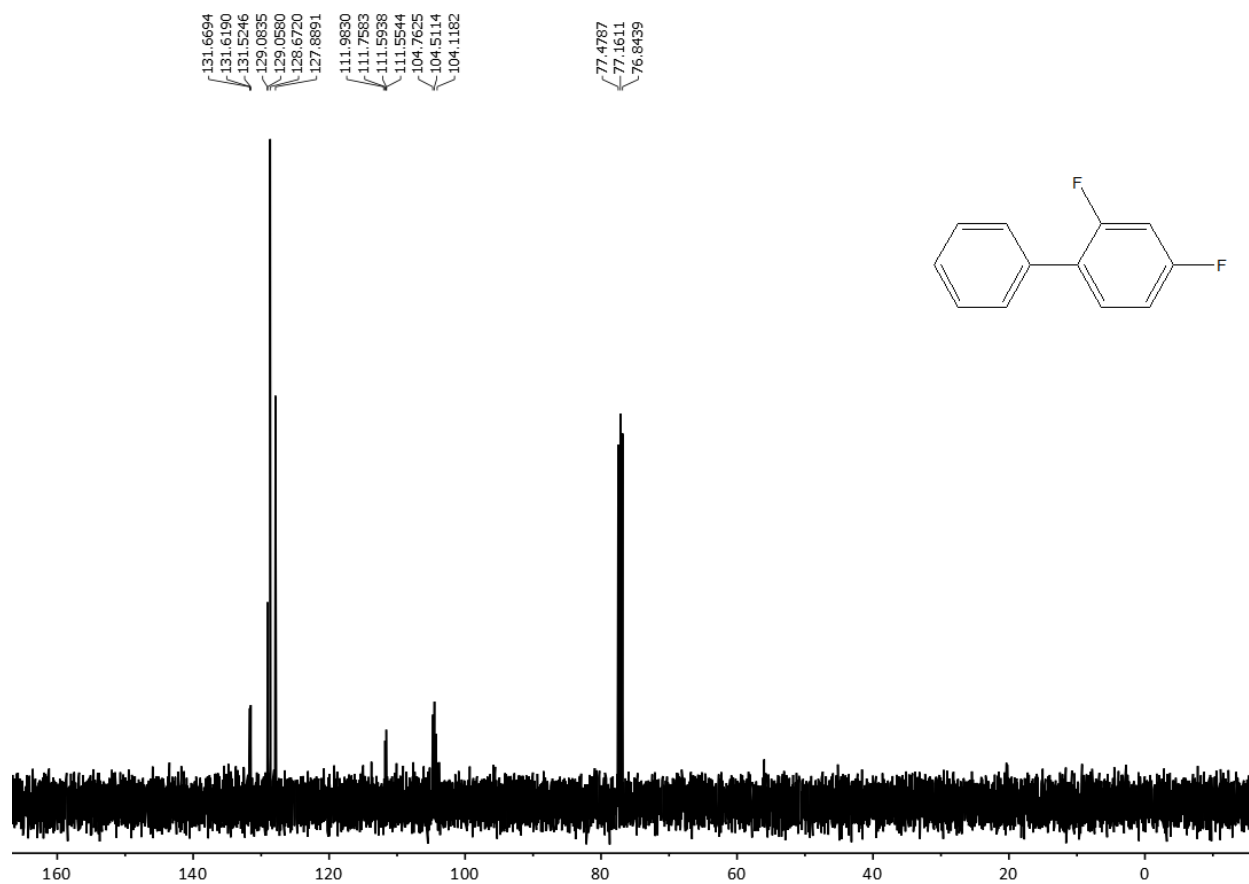


Fig S33. ^{13}C NMR (400 MHz, CDCl_3) spectrum.

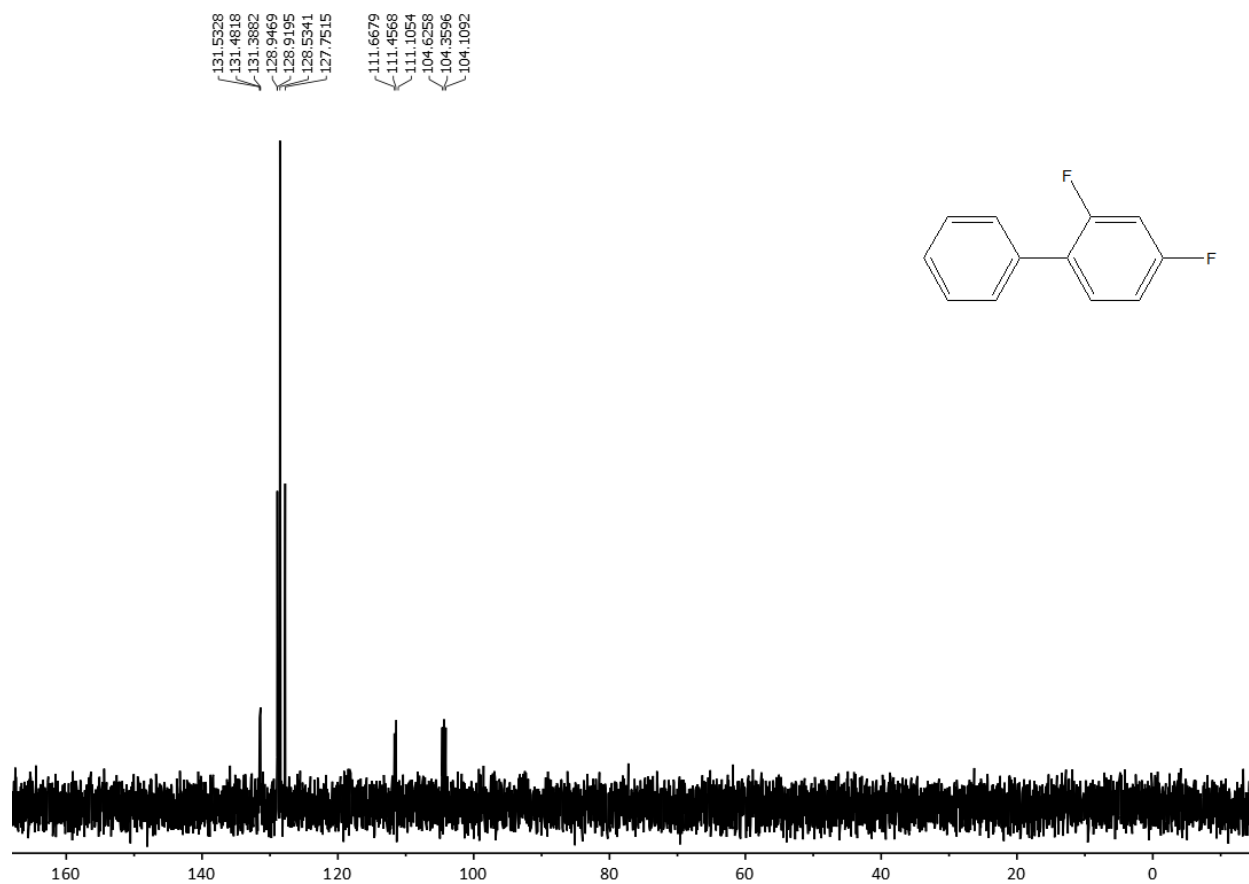


Fig S34. DEPT 135 NMR (400 MHz, CDCl_3) spectrum.

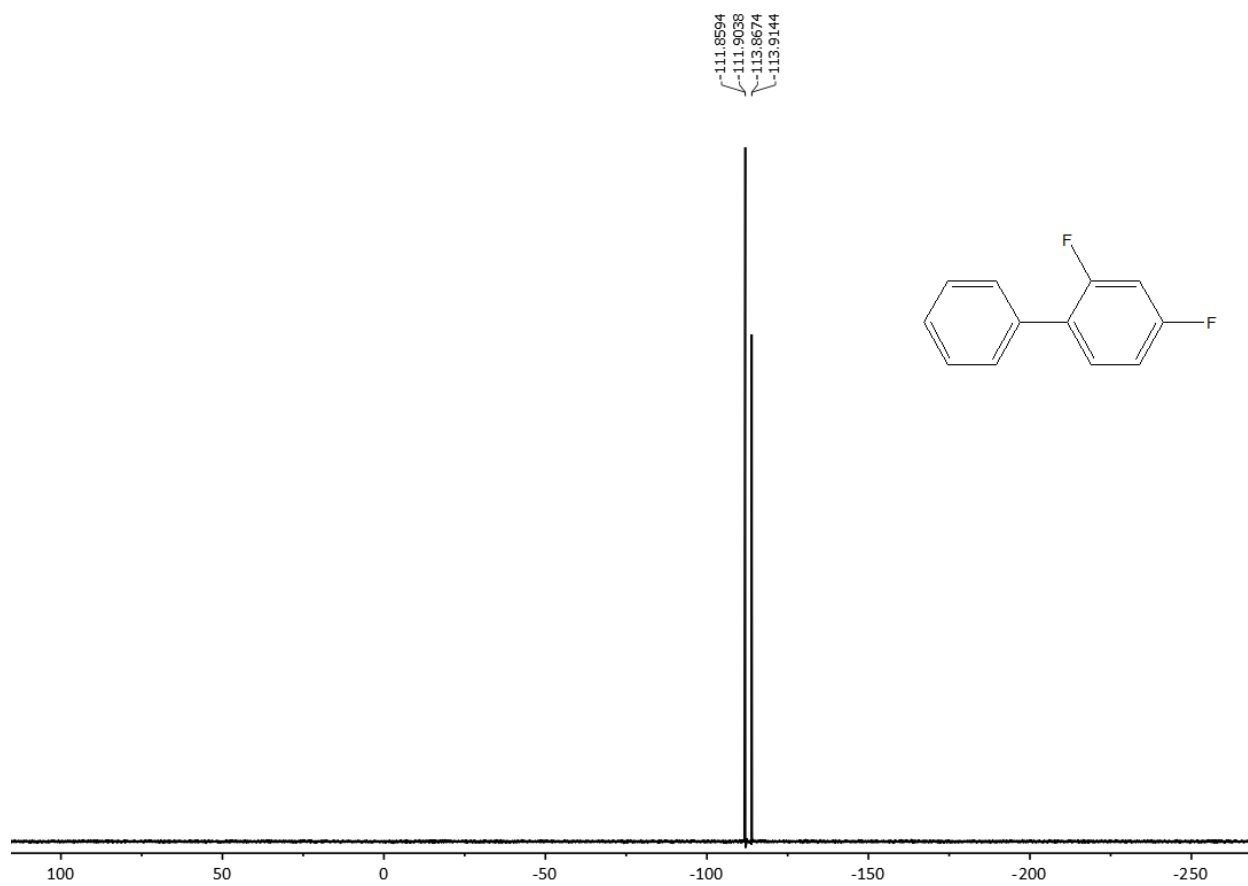


Fig S35. ^{19}F NMR (400 MHz, Acetone) spectrum.

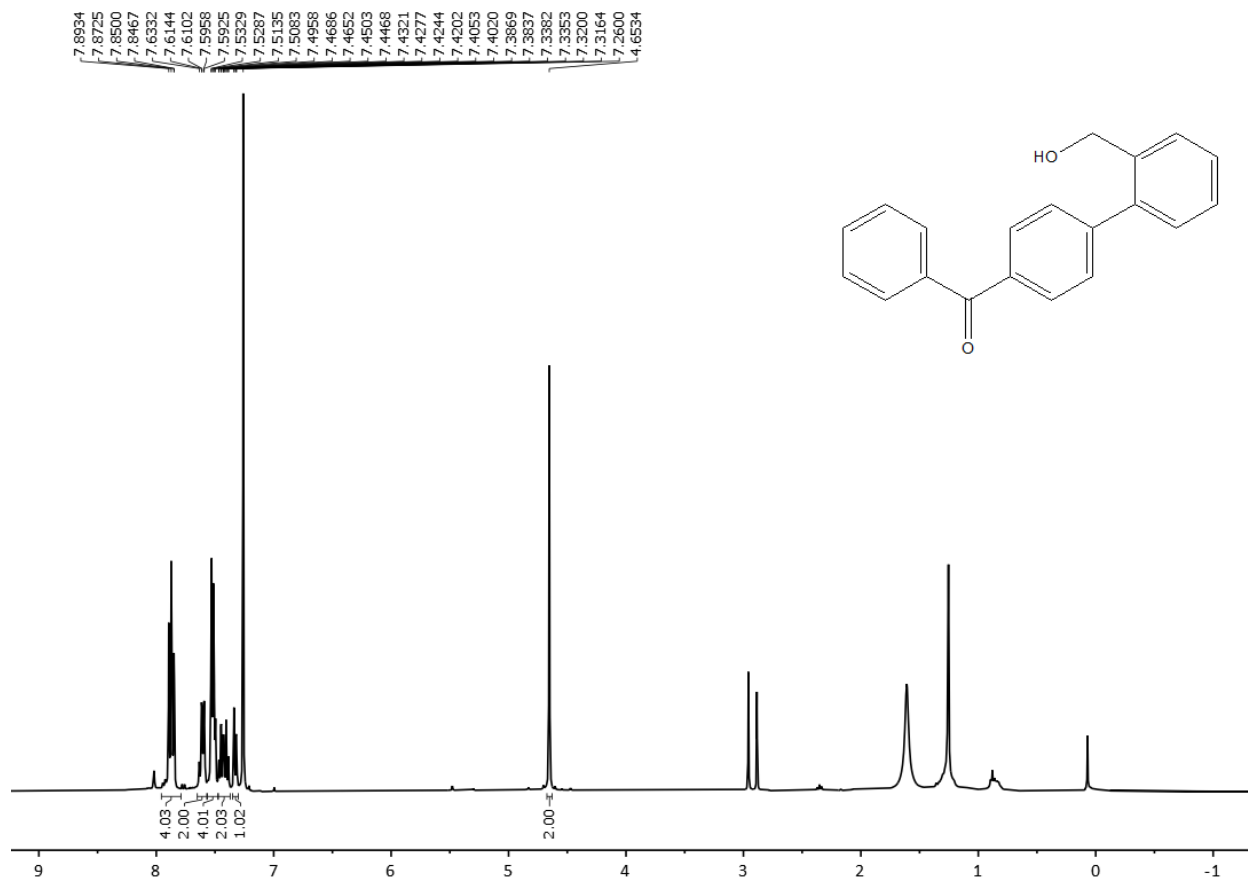


Fig S36. ¹H NMR (400 MHz, CDCl₃) spectrum.

Chapter 6. Summary and future works

6.1. Summary

As the fabrication of nanoparticles with controllable properties gains momentum in a broad range of application, especially, in catalysis fields like pharmaceuticals, the development of a cost-effective nanoparticle synthesis platform is highly desired. The recombinant production of fusion proteins capable in precious nanoparticle direction using *E. coli* host was demonstrated in this work. GFPuv reporter protein was used to enable the recombinant production of small peptides—containing 12-45 amino acids in their structures— as well as process monitoring through microbiological production steps. Recombinant fusion protein synthesis using four different peptide types has been demonstrated. A facile aqueous solution phase nanoparticle synthesis method was exploited in a heterogeneous biological protein environment, and the palladium nanoparticles similar to those synthesized in prior work via chemically-synthesized Pd4 peptide were obtained.

The nucleation and growth mechanism of recombinant protein-directed palladium nanoparticles has been elucidated. Data showed nanoparticles were obtained by means of coalescence, Ostwald ripening, and oriented attachment. The presence of peptide in enhancing independent nucleation sites due to the coordination of Pd⁺² by the peptide has been demonstrated to be the main cause of survival of ultrafine nanoparticles with minimum critical sizes in the environment.

The recombinant fusion protein synthesis of palladium nanoparticles has been shown to be a cost-effective approach toward catalytic applications. The use of fusion protein-directed palladium nanoparticles in Suzuki-Miyaura coupling reaction was investigated. The capability of fusion protein-directed palladium nanoparticles in coupling of different types of aryl halide

groups such as electron-donating, electron-withdrawing, and heterocycles with different boronic acids in green environment has been demonstrated. Moreover, the use of fusion protein-directed palladium nanoparticles in Stille coupling reaction demonstrated that different aryl iodides involved and reacted satisfactory with stannane substituents to synthesize coupling products. The high catalytic activity of fusion protein-directed palladium nanoparticles in low reactive substrate coupling has also been demonstrated. It was determined that fusion protein-directed palladium nanoparticles were efficient, inexpensive, and green catalysts for the Suzuki-Miyaura and Stille coupling reactions. These nanoparticles environment were demonstrated to show slightly higher reactivity comparing to chemically prepared peptide-directed ones. Furthermore, nanoparticles were successfully recycled for five times showing excellent yield.

The use of fusion protein-directed palladium nanoparticles the synthesis of Lapatinib precursor—an anti-breast cancer drug— was demonstrated. In addition, different substituents of Lapatinib precursor remained intact during coupling process confirming the high ability of synthesized fusion protein-directed palladium nanoparticles as catalyst in coupling reactions.

6.2. Future work

6.2.1. Fusion protein purification

Although the palladium nanoparticles studied in this work were obtained from the heterogenous environment, investigation of the effect of purification of fusion proteins on catalytic activity of palladium nanoparticles is highly needed. As the crude materials may disable the catalytic sites on the surface of the palladium nanoparticles, purification of fusion proteins is expected to lead in palladium nanoparticles with higher catalytic activities.

6.2.2. Coupling product purification

Prepared fusion protein-directed palladium nanoparticles can potentially be used to synthesize small molecules for pharmaceutical application. In this regard, developing an ultrafiltration process for the separation of small molecular weight products is required. As the pharmaceutical products can be contaminated by palladium, it is certainly needed to minimize the palladium content of the products in order to employ them in pharmaceutical industries.

6.2.3. Fabrication of precious and non-precious nanoparticles

There are many other nanoparticles including gold, silver, platinum, nickel, iron, cobalt, and copper that have many industrial applications such as catalysis, ammonia synthesis, and pharmaceuticals. Investigation of their synthesis employing bottom-up approach using fusion proteins is expected to result in a dramatic and competitive decrease in cost as compared to available counterparts.

Appendix (I)



Office of Research Compliance

July 12, 2019

MEMORANDUM

TO: Drs. Josh Sakon and Bob Beitle

FROM: Ines Pinto, Biosafety Committee Chair

RE: Protocol Modification

PROTOCOL #: 18013

PROTOCOL TITLE: Fracture Healing System Using Lesion Seeking Peptides

APPROVED PROJECT PERIOD: Start Date August 17, 2017 Expiration Date August 16, 2020

The Institutional Biosafety Committee (IBC) has approved your request, dated July 12, 2019, to modify Protocol # 18013, "Fracture Healing System Using Lesion Seeking Peptides" to add laboratory personnel.

The IBC appreciates your assistance and cooperation in complying with University and Federal guidelines for research involving hazardous biological materials.

1424 W. Martin Luther King, Jr. • Fayetteville, AR 72701
Voice (479) 575-4572 • Fax (479) 575-6527

The University of Arkansas is an equal opportunity/affirmative action institution.

Appendix (II)

Table 1. Nucleotide sequence used for construction of rGFPuv genes for fusion proteins

Fusion Protein	Sequence
GFPuv	RKGEEFTGVVPILVELDGDVNGHKFSVRGEGEGDATNGKLTCLKFIC TTGKLPVPWPTLVTTLTYGVQCFARYPDHMKQHDFFKSAMPEGYV QERTISFKDDGTYKTRAEVKFEGDTLVNRIELKGIDFKEDGNILGHK LECNFNSHNVYITADKQKNGIKANFKIRHNVEDGSVQLADHYQQN TPIGDGPVLLPDNHYLSTQSVLSIDPNEKRDHMLLEFVTAAGITHG MDELYK
Pd4-GFPuv	MTSNAVHPTLRHLARARKGEEFTGVVPILVELDGDVNGHKFSVRG EGEDATNGKLTCLKFICTTGKLPVPWPTLVTTLTYGVQCFARYPDHM KQHDFFKSAMPEGYVQERTISFKDDGTYKTRAEVKFEGDTLVNRIEL KGIDFKEDGNILGHKLECNFNSHNVYITADKQKNGIKANFKIRHNVED GSVQLADHYQQNTPIGDGPVLLPDNHYLSTQSVLSIDPNEKRDHML LEFVTAAGITHGMDELYKGLE
A6-GFPuv	MTSNAVAPTLRHLARARKGEEFTGVVPILVELDGDVNGHKFSVRG EGEDATNGKLTCLKFICTTGKLPVPWPTLVTTLTYGVQCFARYPDHM KQHDFFKSAMPEGYVQERTISFKDDGTYKTRAEVKFEGDTLVNRIEL KGIDFKEDGNILGHKLECNFNSHNVYITADKQKNGIKANFKIRHNVED GSVQLADHYQQNTPIGDGPVLLPDNHYLSTQSVLSIDPNEKRDHML LEFVTAAGITHGMDELYKGLE

A11-GFP _{uv}	<p>MTSNAVHPTLRALARARKGEELFTGVVPILVELDGDVNGHKFSVRG</p> <p>EGEGDATNGKLTCLKFICTTGKLPVPWPTLVTTLTYGVQCFARYPDHM</p> <p>KQHDFFKSAMPEGYVQERTISFKDDGTYKTRAEVKFEGDTLVNRIEL</p> <p>KGIDFKEDGNILGHKLECNFNHNVYITADKQKNGIKANFKIRHNVED</p> <p>GSVQLADHYQQNTPIGDGPVLLPDNHYLSTQSVLSIDPNEKRDHML</p> <p>LEFVTAAGITHGMDELYKGLE</p>
A6,11-GFP _{uv}	<p>MTSNAVAPTLRALARARKGEELFTGVVPILVELDGDVNGHKFSVRG</p> <p>EGEGDATNGKLTCLKFICTTGKLPVPWPTLVTTLTYGVQCFARYPDHM</p> <p>KQHDFFKSAMPEGYVQERTISFKDDGTYKTRAEVKFEGDTLVNRIEL</p> <p>KGIDFKEDGNILGHKLECNFNHNVYITADKQKNGIKANFKIRHNVED</p> <p>GSVQLADHYQQNTPIGDGPVLLPDNHYLSTQSVLSIDPNEKRDHML</p> <p>LEFVTAAGITHGMDELYKGLE</p>

Appendix (III)

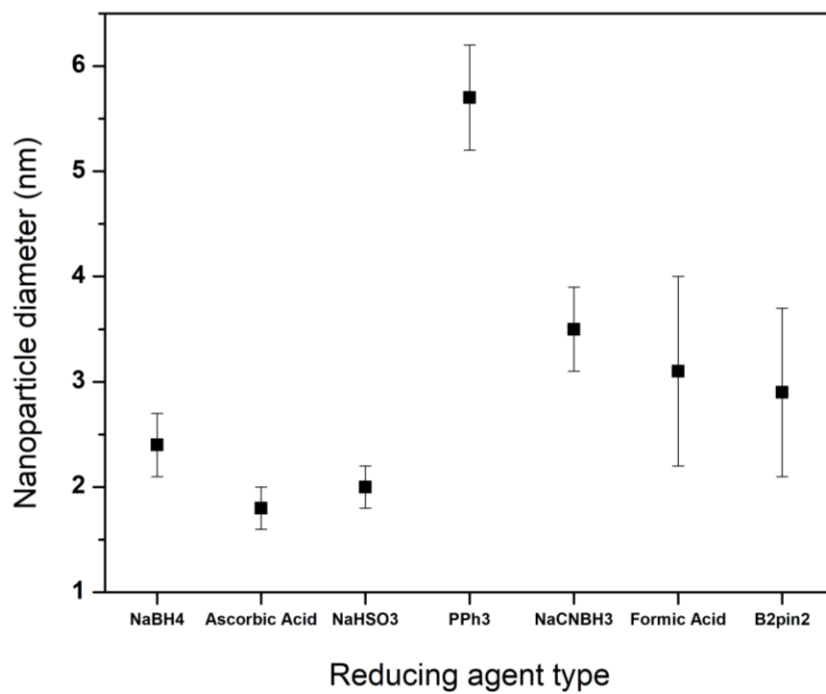


Figure 4. Effect of reducing agent type on NP diameter size.

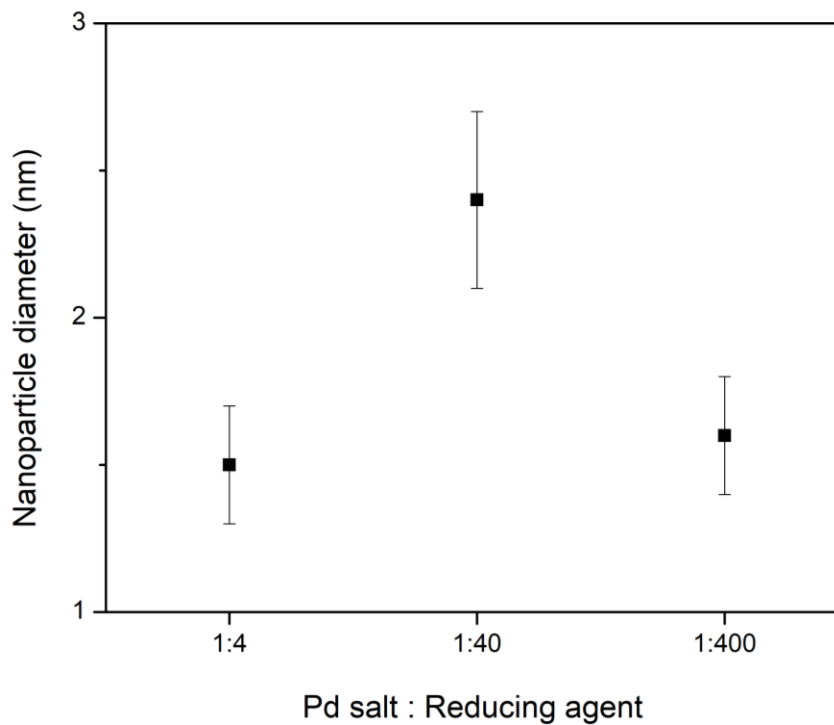


Figure 5. Effect of salt to reducing agent ratio on NP diameter size.

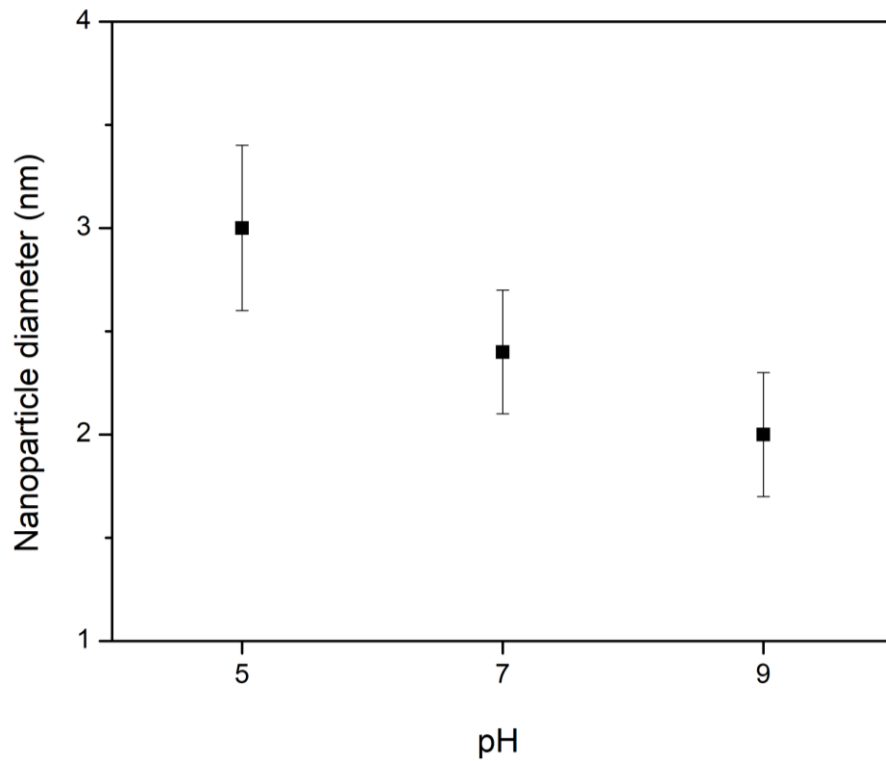


Figure 6. Effect of pH on NP diameter size.

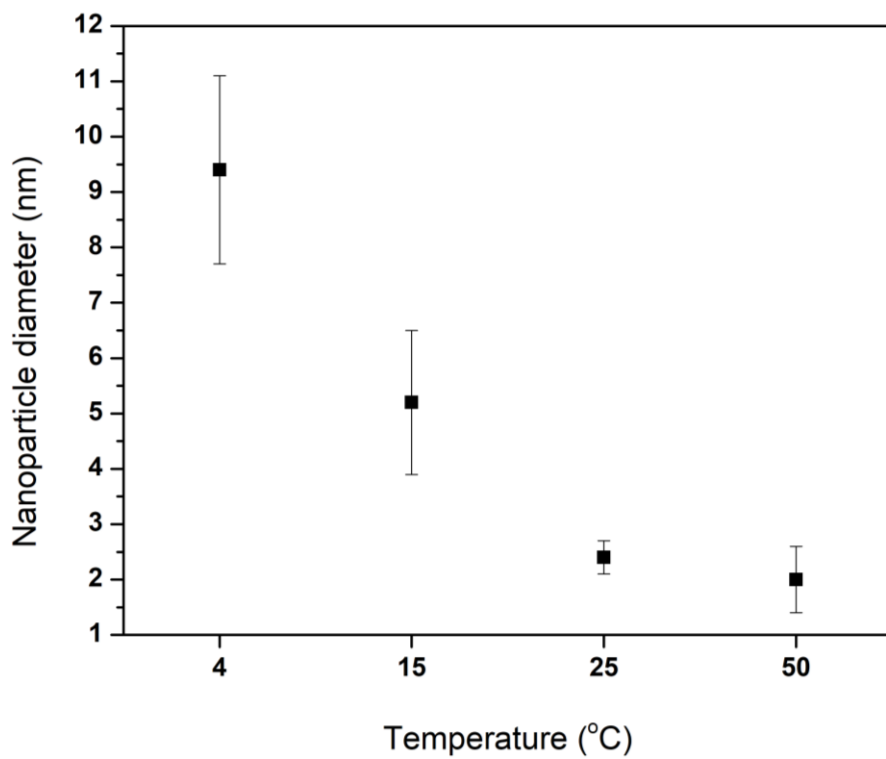


Figure 7. Effect of temperature on NP diameter size.

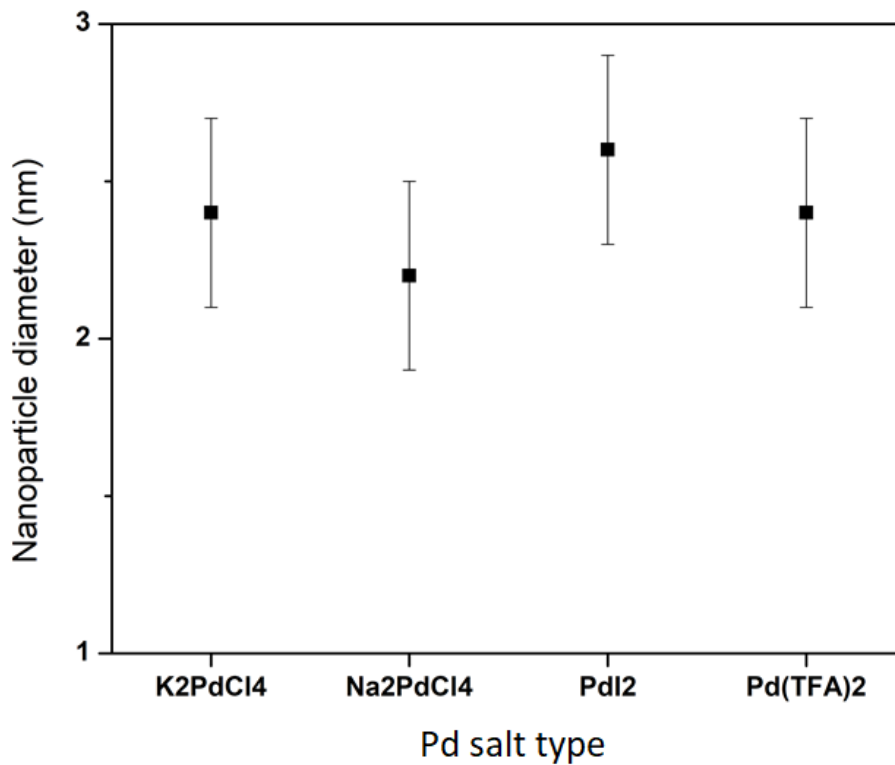


Figure 8. Effect of Pd salt on NP diameter size.

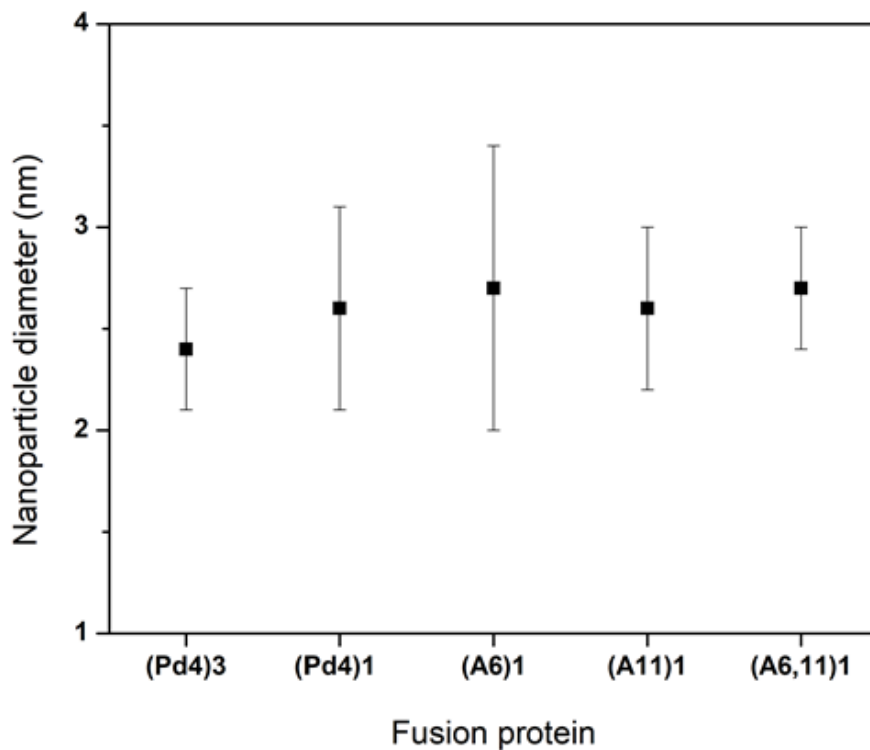


Figure 9. Effect fusion protein on NP diameter size.

Appendix (IV)

Cost analysis

Cost for 500 mL of LB media containing cells = \$2.

Volume of lysate containing desired fusion protein deriving from 500 mL of LB media = 20 mL

Cost for K_2PdCl_4 per gram (Sigma-Aldrich) = \$64.50.

As synthesis mixtures (one milliliter total volume) contain 0.16 mg K_2PdCl_4 , 0.23 mg fusion protein (230 μ L of lysate), and 1.5 mg $NaBH_4$, the cost analysis would be as follows:

- \$0.01032 for K_2PdCl_4 , \$0.023 for lysate containing fusion protein resulting in \$0.03332 for 0.16 mg of Pd nanoparticles with average diameter of 2.4 nm.
- Subsequently, the cost of Pd nanoparticles synthesis per gram would be \$207.50.

In contrast, the price of commercially available Pd nanoparticles with average diameter of 25 nm (Sigma-Aldrich) is \$1394 per gram. As the atoms on the surface area of the nanoparticles can be abstracted during catalytic reactions, the analysis was performed based on the available surface area of the nanoparticles. The surface area of a sphere can be determined using the following equation:

$$A = 4\pi r^2$$

Where A is the surface area and r is the radius of a spherical particle. By a simple calculation it can be found that one gram of nanoparticle with average diameter of 2.4 nm has 108.5 times more surface area comparing to the nanoparticle with the average diameter of 25 nm. In other

words, 9.2 mg of nanoparticle with average diameter of 2.4 nm have the same functionality as one gram of nanoparticles with average diameter of 25 nm. The final cost of 9.2 mg of Pd nanoparticles ($d=2.4$ nm) is \$1.91 with is three orders of magnitude cheaper than the commercially available one.